

TALLINN UNIVERSITY OF TECHNOLOGY  
DOCTORAL THESIS  
38/2019

# **Research and Development of Computational–Intelligence–Based Safety Systems for Ground Vehicles**

ANDREI AKSJONOV



TALLINN UNIVERSITY OF TECHNOLOGY

School of Engineering

Department of Electrical Power Engineering and Mechatronics

This dissertation was accepted for the defence of the degree 26/04/2019

**Supervisor:** Senior Lecturer Valery Vodovozov  
Department of Electric Power Engineering and Mechatronics  
Tallinn University of Technology, Estonia

**Co-supervisor:** Prof Eduard Petlenkov  
Department of Computer Systems: Centre for Intelligent Systems  
Tallinn University of Technology, Estonia

**Opponents:** PD Dr.-Ing. habil. Valentin Ivanov  
Automotive Engineering Group  
Technische Universität Ilmenau, Germany

Prof Alessandro Corrêa Victorino  
Department of Mechanical Engineering  
Federal University of Minas Gerais, Brazil

**Defence of the thesis:** 27/06/2019, Tallinn

**Declaration:**

Hereby I declare that this doctoral thesis, my original investigation and achievement, submitted for the doctoral degree at Tallinn University of Technology has not been submitted for doctoral or equivalent academic degree.

Andrei Aksjonov



European Union  
European Regional  
Development Fund



Investing  
in your future

-----  
signature

Copyright: Andrei Aksjonov, 2019

ISSN 2585-6898 (publication)

ISBN 978-9949-83-456-3 (publication)

ISSN 2585-6901 (PDF)

ISBN 978-9949-83-457-0 (PDF)

TALLINNA TEHNIKAÜLIKOOL  
DOKTORITÖÖ  
38/2019

**Tehisintellekti meetoditel põhinevate  
ohutussüsteemide uurimine ja arendamine  
maapealsete sõidukite jaoks**

ANDREI AKSJONOV





# Contents

List of Publications .....	7
Author’s Contribution to the Publications .....	8
Introduction .....	9
Abbreviations .....	12
Terms .....	13
Symbols .....	15
1 Literature review .....	16
1.1 Road safety.....	16
1.1.1 Antilock braking system and driver distraction safety correlation .....	17
1.2 Antilock braking system .....	17
1.2.1 Problem definition .....	17
1.2.2 Literature review.....	18
1.3 Driver distraction .....	20
1.3.1 Problem definition .....	20
1.3.2 Literature review.....	21
1.4 Summary .....	23
2 Control method for blended antilock braking system .....	24
2.1 Control method description.....	25
2.1.1 States observation .....	27
2.1.2 Fuzzy logic controller.....	28
2.1.3 Torque blending strategy .....	31
2.2 Experimental verification .....	32
2.2.1 Vehicle modelling and parameterization .....	32
2.2.2 Tire model .....	33
2.2.3 Hardware–in–the–loop test bed .....	33
2.2.4 Experimental results .....	35
2.3 Summary .....	37
3 Method for driver distraction detection and evaluation .....	38
3.1 Method description.....	38
3.1.1 Driver model .....	39
3.1.2 Error calculation .....	40
3.1.3 Driver distraction evaluation.....	41
3.2 Experimental verification .....	44
3.2.1 Participants .....	44
3.2.2 Apparatus .....	44
3.2.3 Procedure .....	46
3.2.4 Experimental results .....	46
3.3 Summary .....	51
4 Conclusions and future works.....	52
4.1 Conclusions .....	52
4.2 Future works .....	53
List of Figures .....	55
List of Tables .....	56

References .....	57
Acknowledgements.....	63
Abstract.....	64
Lühikokkuvõte.....	66
Appendix 1 .....	69
Appendix 2 .....	191
Appendix 3 .....	195
Curriculum vitae.....	196
Elulookirjeldus.....	197

## List of Publications

The list of main author's publications, on the basis of which the thesis has been prepared:

- I **Aksjonov, A.**, Augsborg, K., & Vodovozov, V. (2016). Design and Simulation of the Robust ABS and ESP Fuzzy Logic Controller on the Complex Braking Maneuvers. *Applied Sciences*, 6(12), 1–18. doi: 10.3390/app6120382
- II **Aksjonov, A.**, Nedoma, P., Vodovozov, V., Petlenkov, E., & Herrmann M. (2017). A Method of Driver Distraction Evaluation Using Fuzzy Logic. Phone usage as a driver's secondary activity: Case study. *Proceedings of the 26<sup>th</sup> IEEE International Conference on Information, Communication and Automation Technologies (ICAT2017)* (pp. 23–28). Sarajevo: IEEE. doi: 10.1109/ICAT.2017.8171599
- III **Aksjonov, A.**, Nedoma, P., Vodovozov, V., & Petlenkov, E. (2018). Driver Distraction Detection and Evaluation with Artificial Neural Network and Fuzzy Logic. In-vehicle information system as a driver's secondary activity: Case study. *Proceedings of the 15<sup>th</sup> IEEE International Workshop on Advanced Motion Control (AMC2018)* (pp. 523–528). Tokyo: IEEE. doi: 10.1109/AMC.2019.8371148
- IV **Aksjonov, A.**, Nedoma, P., Vodovozov, V., Petlenkov, E., & Herrmann, M. (2018). A Novel Driver Performance Model Based on Machine Learning. *Proceedings of the 15<sup>th</sup> IFAC Symposium on Control in Transportation Systems (CTS 2018)* (pp. 267–272). Savona: IFAC. doi: 10.1016/j.ifacol.2018.07.044
- V **Aksjonov, A.**, Nedoma, P., Vodovozov, V., & Petlenkov, E. (2018). An Enhancement of the Driver Distraction Detection and Evaluation Method Based on Computational Intelligence Algorithms. *Proceedings of the 16<sup>th</sup> IEEE International Conference on Industrial Informatics (INDIN'2018)* (pp. 201–206). Porto: IEEE. doi: 10.1109/INDIN.2018.8472045
- VI **Aksjonov, A.**, Nedoma, P., Vodovozov, V., Petlenkov, E., & Herrmann, M. (2018). Detection and Evaluation of Driver Distraction Using Machine Learning and Fuzzy Logic. *IEEE Transactions on Intelligent Transportation Systems*, Early Access. doi: 10.1109/TITS.2018.2857222
- VII **Aksjonov, A.**, Vodovozov, V., Augsborg, K., & Petlenkov, E. (2018). Design of Regenerative Anti-Lock Braking System Controller for 4 In-Wheel-Motor Drive Electric Vehicle with Road Surface Estimation. *International Journal of Automotive Technology*, 19(4), 727–742. doi: 10.1007/s12239-018-0070-8
- VIII **Aksjonov, A.**, Nedoma, P., Vodovozov, V., & Petlenkov, E. (2018). A Method for Detection and Evaluation of Driver Distraction Induced by In-Vehicle Information Systems. *Proceedings of the 44<sup>th</sup> Annual Conference of the IEEE Industrial Electronics Society (IECON'18)* (pp. 4513–4518). Washington: IEEE. doi: 10.1109/IECON.2018.8591252
- IX **Aksjonov, A.**, Vodovozov, V., Augsborg, K., & Petlenkov, E. (2019). Blended Antilock Braking System Control Method for All-Wheel Drive Electric Sport Utility Vehicle. *Proceedings of the 13th International Conference of the IMACS TC1 Committee (ELECTRIMACS 2019)*. Salerno: Springer.
- X **Aksjonov, A.**, Ricciardi, V., Vodovozov, V., Augsborg, K., & Petlenkov, E. (–) Hardware-in-the-Loop Test of a Fuzzy-Logic-Based Control Method for Antilock Braking System on All-Wheel Drive Electric Vehicle. *In review*.

Copies of these articles are included in Appendix .

## Author's Contribution to the Publications

Contribution to the papers in this thesis are:

- I Andrei Aksjonov is the main author of the paper. He reviewed the literature, designed the controller, parametrized vehicle model in Automotive Simulation Models™ (i.e. a dSPACE software), and conducted the simulation experiments.
- II Andrei Aksjonov is the main author of the paper. He developed the evaluation method and interpreted it in MATLAB™ (i.e. a MathWorks, Inc. software). He also contributed to data collection procedure and experiment procedure design.
- III Andrei Aksjonov is the main author of the paper. He reviewed the literature, developed and realised the detection and evaluation method in MATLAB™ environment. He participated in planning of data collection procedure.
- IV Andrei Aksjonov is the main author of the paper. He reviewed the literature, developed and realised the driver model in MATLAB™ environment.
- V Andrei Aksjonov is the main author of the paper. He reviewed the literature and re-designed the driver distraction detection and evaluation method.
- VI Andrei Aksjonov is the main author of the paper. He was responsible for literature review and method design in MATLAB™.
- VII Andrei Aksjonov is the main author of the paper. He was responsible for literature review, vehicle parametrization in Automotive Simulation Models™, control method design and programming. He also performed the simulation study.
- VIII Andrei Aksjonov is the main author of the paper. He reviewed the literature, designed and programmed the prediction models, and assisted in data collection.
- IX Andrei Aksjonov is the main author of the paper. He reviewed the literature, designed and programmed the blended antilock braking system control method. He also accompanied in vehicle model parametrization and hardware-in-the-loop experimental validation.
- X Andrei Aksjonov is the main author of the paper. He was responsible for literature review, control method design and programming. He also assisted in vehicle model parametrization in IPG CarMaker™ (i.e. an IPG Automotive software), and hardware-in-the-loop experimental study.

## Introduction

Although modern cars are constantly being improved with advanced driver assistance systems and in-vehicle information systems, mortality on public roads do not tend to decrease as some experts predicted. Contrariwise, the number of traffic accidents with dramatic outcomes remains unacceptably high with 1.35 million people dying worldwide annually. Not to mention significant effects on global economy due to the financial harm from traffic accidents, it results in the 8<sup>th</sup> leading cause of death for people of all age, and the 1<sup>st</sup> leading cause of death for children and young adults of the age of 5 – 29 (The International Traffic Safety Data and Analysis Group, 2018), (World Health Organization, 2018).

The ground vehicle safety systems' improvement is mainly obstructed with outdated technology and deficiencies in infrastructure (Post, Motor-vehicle safety, 2014). A part of it is occupied by lack of intelligent control algorithms and methods, because most of the known problems in vehicle safety control are complex and ill-defined that require several aspects to be considered simultaneously. To some degree the set point oriented control systems (i.e. based on proportional-integral-derivative, sliding mode control,  $H_\infty$ , etc.) often perform poorly or are not applicable at all in such complex and dynamic disciplines as vehicle safety due to fundamental lack of robustness to varying environmental conditions and human factor that always appear in transportation systems. Nevertheless, research over the past decade shows a rapid development of computational-intelligence-based control methods that brings up scientist into a new era in controlling uncertain systems with lack of precise information. The computational intelligence algorithms provide a rich and meaningful addition to standard logic for the purpose of engineering control due to its capability to approximate qualitative aspect of human reasoning and decision-making process (Jang, Sun, & Mizutani, 1997), (Passino & Yurkovich, 1998), (Castillo O. , 2012).

The purpose of this research is to increase safety of the ground vehicles by providing their high robustness to heavily changing environmental and human factors. New intelligent vehicle safety management will result in the effective antilock braking system with retained steerability, maximal braking force and energy recuperation of electric and hybrid cars, what in turn decreases braking distance, fuel consumption and consequent emissions. New intelligent safety function will essentially reduce the driver distraction influence on driving quality, safety, humans' life protection, and traffic accidents. Therefore, this research is an influential on ground vehicle safety systems, which are characterised by complicated human-machine-environment interaction, where two fundamentally distinct safety systems, namely antilock braking system and driver distraction detection and evaluation, are investigated simultaneously and designed applying the same solutions, specifically computational intelligence algorithms. Lastly, the research will help to achieve the European Union's "Vision Zero" objective (i.e. "to reduce road deaths to almost zero by 2050") by advancing ground vehicle safety systems (Communication from the Commission to the European Parliament, the Council, the European Economic and Social Committee and the Committee of the Regions, 2018). The developed concepts and solutions will also contribute to European Union's sustainable development goals, Goal 3. Target 3.6: "By 2020, the halved number of global deaths and injuries from road traffic accidents".

Up to now, management of such multi-input, multi-output human-machine systems as vehicles met various challenges due to their essential complexity. Solutions of the car

safety problems, the environmental safety problems, and the human safety problems are conflicted with each other, what often results in impossibility for their combined implementation. The main idea of the presented research is to merge these three groups of problems together via the development of the universal methodology based on such novel computational intelligence tools as fuzzy logic, machine learning, artificial neural networks, and neuro–fuzzy systems. The first issue, which may be resolved by the offered method, is to arrange the intelligent road surface recognition aiming to maximize the antilock braking system force at full steerability, thus guaranteeing the overall vehicle safety. On the other hand, by prioritizing the usage of the electric motors along with introducing the blended braking and considering the battery state–of–charge, the amount of recuperated energy can be raised considerably, hence ensuring the environmental safety. At the same time, by predicting driver performance in multiple distractive situations, the driver behaviour can be continuously identified with high precision, thus enabling the human safety.

Hence, the following tasks are set:

1. Expansion of the artificial intelligent approach towards the safety in the automotive sector.
2. Comparative study of the neuro–fuzzy and traditional binary logic approaches in view of their robustness to heavily changing environmental and human factors.
3. Research and development of a **method for an antilock braking system management** aiming to recognize the road surface and to enable maximal force during emergency braking manoeuvres.
4. Research and development of a **torque blending strategy** for an antilock braking system, which enables maximal amount of recuperated energy during emergency braking manoeuvres.
5. Research and development of a novel **driver distraction detection and evaluation methodology** fitting the accurate distraction measurement and evaluation of various secondary tasks.
6. Investigation and analysis of the model–based methods suitability for driver modelling, and development of a novel **method for driver performance prediction**.
7. Experimental validation of the designed methods.

The theoretical novelty achieved during the research are as follows:

1. Fuzzy logic **control method for antilock braking system** management with road surface recognition, which maintains vehicle steerability and decreases braking distance on heavily changeable surfaces.
2. **Torque blending strategy** for the antilock braking system, which ensures remarkable energy recuperation capability at actively varying surfaces and vehicle states.
3. **Driver distraction detection and evaluation methodology** based on the fuzzy logic and machine learning combination, which allows for accurate detection and precise measurement of driver distraction.
4. **Research environment** including the library of driver models, flexible algorithms, and simulation tools intended for high quality **prediction of driver performance** on different road segments.

The practical value obtained during the research are:

1. The **antilock braking system** with intelligent road surface estimation providing **braking distance decrease by 12% and 41%** in comparison to the conventional electro–hydraulic braking systems and the antilock–free braking systems, respectively.
2. The **blended braking** module ensuring energy **recuperation extension up to 10% (17 kJ)** thanks to the new blending control strategy.
3. The **experimental setup** including the instruments for advanced experimental **investigation of driver distraction**.
4. The **software for analysis of driver distraction** including recommendations on safe and intuitive human–machine interface installation in ground vehicle cockpit.

The results of the research are approbated via scientific publications, conferences, symposiums, and workshops presentations. In total, during the Ph.D. studies the author contributed to 22 publications related to the research and development of the ground vehicle safety systems applying computational intelligence methods. Among them, five works are the peer–reviewed journal publications, the rest are published in highly ranked international conference or workshop proceedings. The dissertation is based on ten main scientific publications attached to this edition, including four journals and six conference papers presented at different IEEE international conferences and workshops.

The dissertation is logically divided into four chapters. Chapter 1 discusses the state–of–the–art in development of computation–intelligence–based safety systems for ground vehicles. The problem statement is also considered here. Chapter 2 is dedicated to the description of the fuzzy–logic–based control method for blended antilock braking system and to experimental verification in hardware–in–the–loop research environment. Chapter 3 describes the method for driver distraction detection and evaluation together with experimental verification in multiple driver–in–the–loop tests. Finally, the dissertation is concluded in Chapter 4, where the future work is also proposed. Each chapter is divided to clearly numbered and labelled subchapters and is summarized with a brief conclusion.

## Abbreviations

3D	Three-dimensional
ABS	Antilock braking system
ANN	Artificial neural network
CAN	Controller area network
CI	Computational intelligence
DD	Driver distraction
DIL	Driver-in-the-loop
EHB	Electro-hydraulic brake
EV	Electric vehicle
FB	Friction braking
FLC	Fuzzy logic controller
HIL	Hardware-in-the-loop
HMI	Human-machine interface
IVIS	In-vehicle information systems
$k$ -NN	$k$ -nearest neighbour
MF	Membership function
ML	Machine learning
MISO	Multi-input, single-output
PID	Proportional-integral-derivative
RB	Regenerative braking
SMC	Sliding mode control
SRM	Switched reluctance motor
ST	Secondary task
SUV	Sport utility vehicle
SVM	Support vector machine
UOD	Universe of discourse

## Terms

Artificial neural network	A mathematical model composed of a large number of processing elements organized into layer.
Auditory distraction mode	Driver distraction caused by “taking ears off the road”.
Biomechanical distraction mode	Driver distraction caused by “taking hands off the road”.
Boolean <sup>1</sup> logic	Binary–type logic where any variable may have two values only: true or false.
Brake blending	A process of utilizing dual braking system approach. True for the regenerative braking system used in electric or hybrid vehicles.
Classification	A mathematical method to assign the input to one of the classes.
Classifier	A mathematical model conducting classification analysis.
Cognitive distraction mode	Driver distraction caused by “taking mind off the road”.
Control surface	A plot, which virtually presents how the controller output depends on the inputs.
Crisp	A collection of objects of any kind. In fuzzy set theory, it can be considered as a specific type of the fuzzy set with a membership function having the value of unity for the elements of the crisp set and zero for others.
Defuzzification	A process of converting a fuzzy set into a crisp output.
Driver	A person responsible for vehicle lateral and longitudinal control.
Driver distraction	An activity performed by a driver that diverts attention away from primary activity potentially leading to safe driving performance degradation. It appears due to some event, activity, object, or person within or outside the vehicle, which compels or induces the driver’s shifting attention away from the primary task.
Fuzzification	A process of converting crisp inputs into fuzzy sets.
Fuzzy logic	A system of logic operators defined by calculus of interaction that attempts to construct a model for the various modes of human reasoning, which are approximated rather than exact.
Fuzzy logic controller	A control and regulation system which implies the methodology of fuzzy logic.
Fuzzy rule	A rule of the “ <i>If &lt;antecedent1&gt; and/or &lt;antecedent2&gt; ... Then &lt;consequence&gt;</i> ” structure.
Fuzzy set	A set of ordered pairs, consisting of an element of the universe of discourse and the membership degree. The theory was firstly introduced by professor Lotfi Zadeh <sup>2</sup> in 1965.

<sup>1</sup> George Boole (1815 – 1864) – an English mathematician, philosopher and logician.

<sup>2</sup> Lotfi Aliasker Zadeh (1921 – 2017) – mathematician, computer scientist, electrical engineer, artificial intelligence researcher and professor emeritus of computer science.

Fuzzy singleton	A fuzzy set with a membership function that is unity in a particular point on the universe of discourse and zero everywhere else.
Inference mechanism (engine)	A process of mapping fuzzy inputs into fuzzy outputs by applying the pertinent rules from the rule base.
Linguistic variable	A variable with a linguistic value that is a word or a word sentence.
Machine learning	An adaptive mathematical mechanism that enables computer to learn from experience, learn by example, or learn by analogy.
Membership degree	Also called “degree of certainty”. A number between 0 and 1 characterizing the degree to which the element of the universe belongs to the fuzzy set.
Membership function	A function which corresponds to a real number between 0 and 1 for any generic element of the universe of discourse.
Modus ponens	Valid argument form in logic (If–Then form).
PID controller	A controller that consists of three parts: proportional to the input, integral of the input and input derivative. Can be also realized as PI–controller or PD–controller.
Plant	A controlled or regulated object or system.
Prediction	An operation applied to novel input to forecast the future output.
Pre–process	Training set simplification and dimensional reduction.
Primary task (activity)	A task needed to drive a vehicle correctly.
Regression	Estimation of relationship among variables, where the outputs are the real numbers.
Robustness	The ability of the system to withstand or overcome changes without changing its initial configuration.
Rule base	A block of fuzzy logic controller containing fuzzy rules, which has a linguistic description of the desired behaviour of the plant.
Secondary task (activity)	All other tasks not related to the primary ones.
Sugeno’s <sup>3</sup> type inference	A type of fuzzy inference engines, in which the consequent part of each rule is a linear combination of the inputs.
Training set	A subset of data used to learn the hyperparameters.
Universe of discourse	The range of values for an input or output. The set which contains all the elements considered in the problem.
Visual distraction mode	Driver distraction caused by “taking eyes off the road”.

---

<sup>3</sup> Michio Sugeno (1940) – Japanese scientist, mathematician engineer and inventor.

## Symbols

$a_{vx}$	Longitudinal acceleration of vehicle
$a_{sw}$	Acceleration of steering wheel
$a_{swp}$	Predicted acceleration of steering wheel
$a_{swr}$	Resultative acceleration of steering wheel
$c_r$	Radius of road curve
$c_d$	Direction of road curve
$DD$	Level of driver distraction
$F_x$	Longitudinal force of tire
$F_y$	Lateral force of tire
$F_z$	Vertical force of tire
$g$	Gravitational acceleration
$i_j$	Phase current of switch reluctance motor
$J_W$	Moment of inertia of wheel
$k_b$	Friction braking coefficient
$L$	Phase bulk inductance of switch reluctance motor
$m_v$	Mass of vehicle
$p_b$	Line pressure of brake
$r_w$	Radius of tire
$T_b$	Braking torque of wheel
$T_d$	Driving torque of wheel
$T_{FB}$	Friction braking torque
$T_{RB}$	Regenerative braking torque
$v_l$	Speed limit
$v_{vx}$	Longitudinal velocity of vehicle
$v_{wx}$	Longitudinal velocity of wheel
$\Delta v$	Real vehicle speed deviation
$\Delta v_p$	Predicted vehicle speed deviation
$\Delta v_r$	Resultative vehicle speed deviation
$\Delta x$	Real lane keeping offset
$\Delta x_p$	Predicted lane keeping offset
$\Delta x_r$	Resultative lane keeping offset
$\theta$	Rotor aligned position of switch reluctance motor
$\lambda$	Longitudinal slip of wheel
$\lambda_{opt}$	Optimal longitudinal slip of wheel
$\mu$	Tire–road adhesion coefficient
$\mu^*$	Estimated road surface
$u$	Output of fuzzy logic controller
$\omega_w$	Angular speed of wheel

# 1 Literature review

This Chapter opens the dissertation with literature overview of related works in the area of development of the CI-based safety systems for ground vehicles. The focus is addressed to ABS control and DD detection methods. The problem of systems' complexity and states' imprecision are also stressed here.

The Chapter is divided to three subchapters. In Road safety, the concept of vehicle–environment–human interaction is introduced and their correlation. The ABS safety concern and related works are described in Antilock braking system. Problem statement and literature review of recent developments in DD detection and evaluation are provided in Driver distraction subchapter. Finally, the Chapter conclusion is delivered in Summary.

## 1.1 Road safety

Road safety is one of the most important and complex parts of the intelligent transportation systems. Mary Ward<sup>4</sup> became the world's first recorded victim of automobile accident in 1869. Since then, the number of road victims only grows each year. The first ground vehicle eventually was equipped with all four–wheel hydraulic brakes only in 1922. Until now, for instance, the brakes are the key elements of every ground vehicle. However, with intensive population grow and consequent increase of number of passenger vehicles on the roads, braking system can hardly be accepted as enough for vehicle safety (Post, Motor–vehicle safety, 2014).

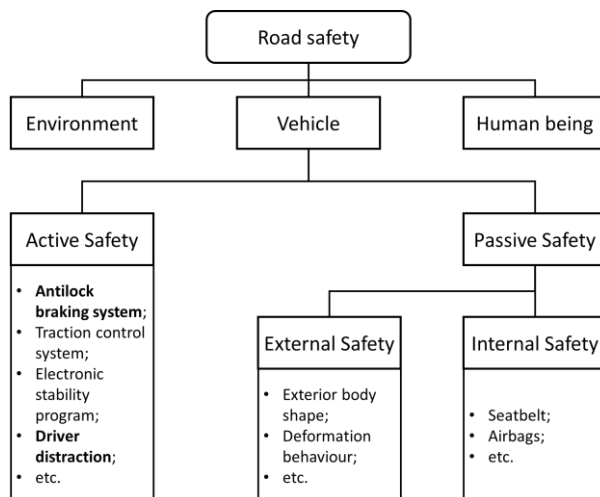


Figure 1. Road safety concept and influencing variables (adapted from (Post, Motor–vehicle safety, 2014)).

Road safety roughly depends on three main influencing factors: environment (e.g. weather, road surface, traffic condition, etc.), vehicle (e.g. equipment, components wear, etc.), and human being (e.g. driving skills, health conditions, etc.) (Figure 1). Vehicle involves active and passive safety systems. The first ones tend to “actively” prevent

---

<sup>4</sup> Mary Ward (née King, 1827 – 1869) – an Anglo–Irish naturalist, astronomer, microscopist, author, and artist.

accidents in the first place, while the second – to reduce the severity of accidents, when they do occur (Post, Motor–vehicle safety, 2014). Most of the modern ground vehicle safety systems are designed, yet, without consideration of vehicle–environment or vehicle–human interaction. It makes them, on one hand, simple, but, on the other hand, limited in functionality.

Within past decades, to advance vehicle safety systems, different environment–vehicle–human interaction concepts were developed by the researchers all over the world. Most of the impressive solutions have been achieved applying CI–based methods (Ivanov V. , 2015). Burying in mind only safety functions that are related to the present dissertation (i.e. ABS and DD detection) and revisiting Figure 1, the new concepts of safety systems are rudimentary summarized in Figure 2.

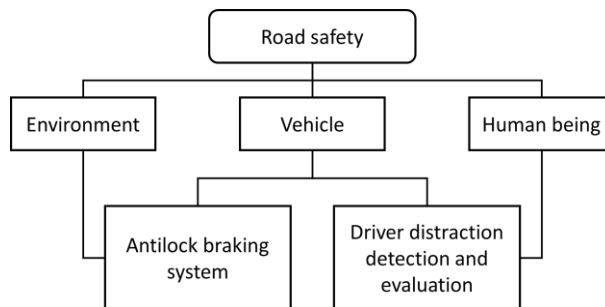


Figure 2. Road safety concept and influencing variables of the studied safety systems.

### 1.1.1 Antilock braking system and driver distraction safety correlation

Despite fundamental functionality and aim disparity, there is a clear correlation between ABS and DD safety systems. On one hand, drivers’ mistakes caused by DD often lead a vehicle to exit the road or late recognition of probable collision. In this occasion, rapid vehicle deceleration with presumed latera controllability is critical, when the ABS plays a great role. On the other hand, emergency braking with help of ABS may lead to additional distraction created by safety system functionality. The unusual ABS operation may lead to changes in road user behaviour (Ashenbrenner, Biehl, & Wurm, 1987). This distraction may result in additional mistakes delivered by the driver. As a consequence, driver behaviour may cause to ABS functionality burden or even vehicle deceleration failure and following vehicle occupants’ and other traffic participants’ life danger.

## 1.2 Antilock braking system

In this subchapter, the state–of–the–art on advancements in ABS control methods is reported. The focus is addressed to CI–based approaches that involve more complex solutions, where vehicle–environment interaction is considered. First, the problem statement is delivered, then the previously proposed solutions are analysed.

### 1.2.1 Problem definition

The ABS introduction to ground vehicles was motivated from aerospace industry and for the first time used on a volume–production ground vehicle in 1978. Nowadays, the ABS is an obligatory system in almost every country in the world (Post, Car braking systems, 2014). To understand the complexity of the safety problem and the aim of an ABS, it is necessary to understand the safety concern caused by the vehicle’s wheels lockage during braking manoeuvres.

An exhaustive braking torque applied to the wheels during emergency braking leads to wheel lockage, i.e. the condition when the wheel of a moving vehicle is no longer rotating. This action, in its turn, arouses vehicle control degradation and significant reduction of braking force. As a result, the vehicle goes into a slip or/and leaves the road. Therefore, an ABS (as it comes from its name “antilock”) aims at wheel lockage avoidance by means of braking torque reduction resulting in steerability maintenance and braking force minimization (Koch–Dücker & Papert, 2014).

The main problem of an ABS enhancement is its dependence on highly changing environmental and vehicle condition factors (Ivanov & Shyrokau, 2010). Precisely, how fast will the wheels lock highly depends on numerous factors: condition of the tire (e.g. worn or new, pressure, etc.) and on surface of the road (e.g. dry, wet, icy, etc.) or road–tire friction coefficient, etc. This latter has a dramatic impact on vehicle deceleration force, what negatively influences vehicle stability and braking distance. Therefore, to increase the efficiency of an ABS, intensively changing and hardly predictable environmental factors, namely road surface, must be take into consideration (Pacejka, 2012), (Koch–Dücker & Papert, 2014).

### **1.2.2 Literature review**

Traditional control algorithms that are characterized with good robustness to noise and nonlinearities are actively applied in conventional and electric vehicles braking system control. For instance, SMC (Regolin, Incremona, & Ferrara, 2017), model predictive control (Jacquet, et al., 2008), nonlinear PID (Tanelli, Astolfi, & Savaresi, 2006), linear matrix inequality (Başlamışli, Köse, & Anlaş, 2007), and other robust control methods were recently developed for ABS. Unfortunately, those approaches always require complex mathematical modeling and reference slip input, which is in reality vague due to dynamically changing environmental conditions.

The CI algorithms, especially fuzzy logic, are also widely used in ABS control methods for both FB and RB (Ivanov V. , 2015). The CI method unlike conventional control algorithms are successfully applied to highly nonlinear and complex plans, which are described by ill-defined or lack of precise information. Some of the first patents, where fuzzy logic was applied to ABS control were issued to the Nissan Motor Co., Ltd. for conventional FB (USA Patent No. 4 842 342, 1989) and to the Ford Motor Company for RB (USA Patent No. 5 358 317, 1994).

Simple FLCs with set point regulation were developed for different vehicle types, including EV with on–board motor powertrain. The optimal FLC designed to maintain the wheel slip to a desired level on various road surfaces outperformed FLC and PI controllers (Mirzaei, Moallem, Dehkordi, & Fahimi, 2006). The self–learning fuzzy SMC capable to automatically generate and reduce fuzzy rules was proposed for ABS to hold wheel slip at 20% for any road surface (Lin & Hsu, 2003). Later, the authors improved the control method by introducing the self–organized function–link fuzzy cerebellar model articulation controller (Lin & Li, 2013). A combination of SMC and FLC, where the latter serves as parameters optimization, was designed for RB, in which motor torque is taken full advantage of (Guo, Jian, & Lin, 2014). A control method for a hybrid EV with four separate wheel drives, where fuzzy logic is applied as a vehicle speed estimator reading the motor current and wheel speeds, was developed in (Pusca, Ait–Amirat, Berthon, & Kauffmann, 2004). Fuzzy logic accompanied with genetic algorithm is a strong tool for PID controller self–tuning for varying road surfaces (Sharkawy, 2010). Those methods, however, have strong limitation, because they hold only one reference wheel slip (i.e. 15–20%) on different road surfaces, what is optimal only for dry asphalt. This limitation

does not allow for adaptation to highly changing environment, because braking with an optimal slip for dry road on icy one will lead to more than 50% of efficiency losses (Koch–Dücker & Papert, 2014).

As the reference slip regulation does not solve a problem of efficient ABS performance on varying road conditions, the following logical extension in the discipline was to develop road recognition methods. As a result, it was assumed that the road conditions can be inferred by observing the slip ratio resulting from a given braking force, where an FLC was designed for an ABS (Mauer, 1995). In (Ivanov, Algin, & Shyrokau, 2006), the fuzzy logic together with statistical regularities were combined for road and environmental properties identification and adaptive, self–learning control strategy. A genetic algorithm crossed with FLC was exploited to obtain optimal braking torque distribution between RB and FB (Kim, Kim, Hwang, & Kim, 2007). An FLC–based ABS and traction control system successfully demonstrated that the FLC adjusts a vehicle at changing environment (Khatun, Bingham, Schofield, & Mellor, 2003).

The fuzzy slip controller guaranteed the highest traction or braking force on each wheel on every road condition by individually controlling slip ratio of each wheel (Jalali, Uchida, McPhee, & Lambert, 2012). The FLC and PID merging resulted in torque control method for various drive–slip conditions involving abrupt change in road–tire friction conditions. The CI algorithm compensated sudden changes in the road friction (Li, et al., 2012). A quasi–SMC and fuzzy–neuro–system–based control method for nonlinear discrete–time system verified in the experiment on ABS test bed was described in (Perić, et al., 2016). Intelligent FLC also copes with more complex braking manoeuvre than straight road with even road surface. For example, via fuzzy logic road identification method it finds optimal wheel slip and ensures wheels lockage avoidance on split– $\mu$  road profiles (i.e. two halves of the roads have different surfaces) (Aly, 2010).

The FLC was used to tune and switch gains of an SMC. The controller coped well with normal and emergency braking cases under changing environmental conditions and vehicle initial states. Moreover, the controller showed significant advantage over traditional PID and conventional SMC (Peng, Jia, He, Yu, & Lv, 2018). Another control method obtains information about the type of the road by means of fuzzy logic and controls brake pressure using one more FLC. Accordingly, the method was able to provide optimal slip by interacting with the surrounding environment (Cabrera, Ortiz, Castillo, & Simon, 2005). A decade later, the authors enhanced the control method with another CI algorithm, ANN, where FLC served as optimal slip generator for identified road surface. Finally, additional FLC determined braking pressure in the braking circuit (Castillo, Cabrera, & Guer, 2016).

An FLC–based life–extending control achieved significant improvement in service life by the trade–off between satisfactory dynamic performance and safe operation, where the FLC predicts the wear rate of the brake pads/disc and modifies its control strategy on–line to keep safe ABS operation (El–Garhy, El–Sheikh, & El–Saify, 2013). A braking torque distribution strategy for an all–wheel drive EV with single electric motor, based on estimation of the tire–road friction coefficient using the fuzzy logic estimation approach was delivered in (Paul, Velenis, Cao, & Dobo, 2017). The goal was to maximize regenerative power during deceleration for a given vehicle speed and deceleration demand on changing road surfaces. Furthermore, the friction coefficient realised with FLC did not rely on any specific tire model. Some works used the knowledge–based methodology to overcome the complexity of tire–road friction coefficient estimation (Xu, Xu, Zheng, Zhang, & Zahid, 2016). An FLC–based control method is capable of maximizing

adhesion force even without road surface information and vehicle speed signal (Chen, Yang, Du, & Wang, 2010).

The related works' analyses prove CI-based control methods' potential in new advanced ground vehicle safety systems concepts development via vehicle-environment interaction. Despite mentioned, it is missing today any relatively simple approach for connecting environment together with vehicle to obtain highly efficient ABS functionality (i.e. fast deceleration with presumed lateral control) on varying road surfaces, which is also capable to enhance energy recuperation for EV via advanced torque blending strategy, and which avoids set-point-based control. Therefore, the blended ABS control method described here aims at filling this gap in advanced ABS design for ground vehicle by using CI algorithms for providing simple interaction between vehicle and environment with supreme energy recuperation capability for fully and hybrid EVs. Hence, the method enables safety of occupants, vehicle, and environment concurrently.

### **1.3 Driver distraction**

The state-of-the-art in improvements of DD detection is delivered in this subchapter. The attention is paid to CI-based methods that involve more complex solutions, where human-vehicle-environment interaction is important. The DD problem is stated next, then, the recent advancements are discussed.

#### **1.3.1 Problem definition**

Rapid development of IVIS noticeably improves road transportation. These systems allow drivers for enjoying their favourite music, listening to the news and even for remaining in touch with their family members, friends, and colleagues while driving a car. What is more, IVIS, such as navigation, vehicle state, etc. appreciably improves road safety and efficiency, vehicle maintenance cost and time spent on transportation. Though, driver's interaction with IVIS contributes to a newly arose problem of DD. The relevance of the problem is justified with tremendous number of people (i.e. 3450) killed on the roads due to the distracted driving in 2016 in the USA alone (National Traffic Law Center, 2017). In EU, 20% of all fatalities on the roads are caused by DD (European Union, 2017). Unfortunately, the statistics promise no improvement in the nearest future.

The main uncertainty in DD remains the driver her-/himself, who is often guilty for multitasking. Driving already demands high concentration and prudence, and performing ST in parallel only increases the cognitive and biomechanical loads. In addition, it is well known that "*humans are limited in their ability to divide attention between competing tasks*" (Regan, Young, & Lee, Introduction, 2009). There are different factors influencing DD, and most of them depend only on driver (i.e. current state, drowsy or inebriated, curiosity and boredom, etc.), yet, the results (i.e. traffic accidents) are always dramatic. Hence, the complexity of DD hazard is enhanced by human-vehicle interaction, what makes the problem much challenging (Regan, Young, & Lee, Introduction, 2009).

To this aim, various public and governmental road safety foundations and ground vehicle manufacturers work together to solve safety threat caused by DD. The first ones tend to establish road safety policies. Vehicle manufacturers are mainly focused on vehicle cockpit and HMI technology design to decrease driver's workload and reduce or even entirely eliminate IVIS-induced DD (Young, Regan, & Lee, 2009). Counting on every human uniqueness, preferences, and values it is severe for the vehicle manufacturers to design mass production vehicles according to each individual needs. Thus, considering dynamically changing environmental and human factors DD remains serious matter for

its detection and mitigation, because it appears to be that “*distraction is inevitable consequence of being human*” (Regan, Young, & Lee, Introduction, 2009).

### 1.3.2 Literature review

As there are different sources of distraction (Regan, Young, Lee, & Gordon, 2009), there are also different modes of DD: auditory, biomechanical, cognitive, and visual. In most of the cases DD is composed of more than one if not all modes of DD at the same time (Westin, Dougherty, Depcik, Hausmann, & Sprouse III, 2013). Furthermore, there are four main attributes to measure DD: behaviour (e.g. eye and head movement), physiological (e.g. electrocardio– and electroencephalographical measure), performance–based (e.g. vehicle lateral and longitudinal performance), and subjective (e.g. survey and expert evaluation) (Arun , Sundaraj , & Murugappan , 2012), (Papantoniou, Papadimitriou, & Yannis, 2017). The most progressive results in DD detection have been achieved by applying CI, including ML, which are discussed below.

The subjective measures for DD evaluation were used for very long time and are still used today. Among the most popular ones is the workload identification analysis NASA<sup>5</sup> Task Load Index (Hart & Staveland, 1988), which was applied in DD studies in (Kim & Son, 2011) and (Horberry, Anderson, Regan, Triggs, & Brown, 2006). In (Rajesh, Srinath, Sasikumar, & Subin, 2016), the questionnaire was used to analyse influence of human factors, driver space, and driving conditions on perception of mobile phone use while driving as a distractive activity. The main problem of subjective measures is that they depend on human examiner’ or evaluator’ opinions.

Different kinds of ML algorithms were explored for DD detection by measuring driver’s gaze, head, and body part movement, what appears to be the most popular among existing measures. Gradient boosting machine in cooperation with 3D convolutional ANN was used in driver drowsiness detection system (Huynh, Park, & Kim, 2017). Random forest classifier (Lex, Langhans, Lee, & Reimer, 2016) and convolutional ANN (Choi, Hong, & Kim, 2016) were useful for driver glance region prediction. The dynamic Bayesian<sup>6</sup> network outperformed logic regression, static Bayesian network, and SVM in visual DD detection (Azman, Ibrahim, Meng, & Edirisinghe, 2014). A semi–supervised extreme learning machine was combined with SVM for DD detection from eye and head movement (Liu, Yang, Huang, Yeo, & Lin, 2016). Real time IVIS–induced DD state monitoring is possible with classifier based on Mahalanobis<sup>7</sup> distance calculation algorithm (Jiménez, Bergasa, Nuevo, Hernández, & Daza, 2012). The fuzzy expert system is also useful in driver face monitoring for level of human fatigue estimation (Sigari, Fathy, & Soryani, 2013). Different classifiers (i.e. SVM,  $k$ –NN, and graph–regularized extreme learning machine) were designed for DD detection using driver’s behavioural measures (Jiao, et al., 2014). Another impressive solution was proposed by combining SVM with linear discriminate analysis and principle component analysis (Jo, Lee, Jung, Park, & Kim, 2011). Drowsy driving prediction is performed with the probabilistic restricted Coulomb<sup>8</sup> energy ANN (Matsuo & Khiat, 2012). By monitoring body parts of a driver via video camera mounted inside of a vehicle, DD induced by different STs is recognizable with kernel SVM algorithm (Billah, Rahman, Ahmad, & Swamy, 2018). Seven drivers gaze zone classifier applying different architectures of a convolutional ANN was studied in (Vora,

---

<sup>5</sup> The National Aeronautics and Space Administration (Washington, DC, USA).

<sup>6</sup> Thomas Bayes (1701 – 1761) – an English statistician, philosopher, and Presbyterian minister.

<sup>7</sup> Prasanta Chandra Mahalanobis (1893 – 1972) – an Indian scientist and applied statistician.

<sup>8</sup> Charles–Augustin de Coulomb (1736 – 1806) – a French military engineer and physicist.

Rangesh, & Trivedi , 2018). The main disadvantage of the methods is that they always require one or multiple cameras to be mounted inside of a vehicle, what negatively affects system's cost and complexity. Furthermore, behavioural measures only guarantee visual DD detection, whereas cognitive and auditory DD remain unrecognized. Lastly, some systems require a driver to wear additional devices, such as gaze-tracking goggles, what is considered as distraction itself and for some individuals is not always feasible.

Another DD measurement mode is psychological, where human's brain activity, heart rate, skin conductivity, temperature, etc. are tracked. The brain activity measured by electroencephalographic signals was used for online early detection of DD (Wang, Zhang, Wu, Darvas, & Chaovalitwongse, 2014). The same brain activity signals were exploited in DD detection applying numerous ML techniques, namely decision tree, random forest,  $k$ -NN, SVM, and naïve Bayes (Alizadeh & Dehzangi, 2016). Logistic-regression-based ML algorithm was applied for drowsy driving recognition from heart rate electrocardiogram signals (Babaeian, Bhardwaj, Esquivel, & Mozumdar, 2016). Electrocardiogram-signals-based driver inattention identification method using deep convolutional ANN was proposed (Taherisadr, Asnani, Galster, & Dehzangi, 2018). The psychological measures appear to be very efficient, because they track drive's conditions, which are not externally observable, and what the human itself is not able to recognize. However, those methods always involve expansive devices worn by the driver, what makes them unsatisfactory for practical use. Again, those devices may cause distraction as well.

Popular measures are extracted from vehicle performance, because they directly reflect ST or driver's fatigue impact on vehicle safe operation. In addition, those measures do not need additional devices, because most of the vital signals can be obtained directly from vehicle CAN-bus. Multiple STs were studied on DD detection using in-vehicle signals with classifier built with ANN and Gaussian<sup>9</sup> mixture model combination (Im, Lee, Yang, Kim, & You, 2014). The ANN-based DD classifier from CAN-bus information was incorporated with forward collision warning framework (Iranmanesh, Mahjoub, Kazemi, & Fallah, 2018). Driver behaviour was reproduced from the global positioning system, and Gaussian mixture model was used to capture the sequence of driving characteristics and classify distracted or non-distracted driving (Yang, Chang, & Hou, 2010). Extreme learning machine algorithm (Martínez, del Campo, Echanobe, & Basterretxea, 2015) and SVM (Ersal, Fuller, Tsimhoni, Stein, & Fathy, 2010) were also efficient in classifying distractive or attentive driving through performance-based measures. In (Tango & Botta, 2013), the SVM-based DD classifier outperformed other ML algorithms such as feedforward and layer-recurrent ANNs, and neuro-fuzzy system. Visual-manual SVM-based DD detection using kinematic signals from the vehicle CAN-bus and nonlinear autoregressive exogenous algorithm for vehicle speed prediction was developed in (Li, Bao, Kolmanovsky, & Yin, 2018). In (Miyajima & Takeda, 2016), the on-road driver-performance-based data were collected, which were used for predicting the driver behaviour and detecting risky driver frustration.

Ultimately, performance-based, psychological, behavioural, and even subjective measures can be combined. Steering wheel angle and lane position accompanied with head movement tracking data are utilized in DD detection with random forest and hidden Markov model (Schwarz, Brown, Lee, Gaspar, & Kang, 2016). Driver eye movement crossed with driving performance were used in real-time cognitive DD detection with

---

<sup>9</sup> Carl Friedrich Gauss (1777 – 1855) – German mathematician and physicist.

SVM (Liang, Reyes, & Lee, 2007) and Bayesian network (Liang, Lee, & Reyes, 2007). Online DD detection by observing driving data and head tracking with long short-term memory ML recurrent ANN was presented in (Wöllmer, et al., 2011). The SVM recursive feature elimination algorithm was built for cognitive DD detection at stop-controlled intersections and speed-limited highways using eye movement and vehicle operation data (Liao, et al., 2016). The features from different sources (i.e. audio, colour video, depth map, hearth rate, steering wheel and pedals positions) were fused for fatigue and DD assessment applying hidden Markov models and SVM with Bayesian network for data fusion (Craye, Rashwan, Kamel, & Karray, 2016). Human psychological stats, such as electrodermal, electrocardio, and brain activities were combined with capacitive touch and position detection sensors signals for human stress level monitoring (Mühlbacher-Karrer, et al., 2017). There the cellular ANN outperformed other designed classifiers based on SVM with radial basis function, naïve Bayes, decision tree, and ANN.

The accuracy of DD detection is very high for most of the previously developed methods. Nevertheless, they all have a common disadvantage: they are classifiers based on ML techniques mainly with only two possible outputs, i.e. distracted or non-distracted. This is not suitable for different HMI technologies for accurate IVIS comparative analysis and consequent vehicle cockpit design. Therefore, the method described here is developed to be capable of not only precisely detecting DD, but also measuring its influence on safe vehicle operation. Therefore, the method assures vehicle occupants and vehicle safety simultaneously.

## **1.4 Summary**

In this Chapter, the existing problem and concept solutions in ground vehicle safety systems are introduced. More deeply, the problems of state-of-the-art on control methods for ABS and DD detection are discussed. Theoretical background of both safety systems is reviewed with special attention dedicated to CI-based solutions. The advantage of the methods developed by the author described in this dissertation next is also briefly highlighted with respect to other related works.



The friction braking coefficient  $k_b$  depends on brake disc friction area, mechanical efficiency of brake components and braking factor. Tire deformation due to small impact is neglected. Thus, both  $k_b$  and  $r_w$  are assumed as constants.

In EV, the FB torque is accompanied with the RB torque  $T_{RB}$ . The RB torque of the SRM for saturated phase is found as (Ehsani, Gao, Gay, & Emadi, 2005):

$$T_{RB}^j = \int_0^{i_j} \frac{\partial L(\theta, i_j)}{\partial \theta} i_j di_j, \quad (2.3)$$

where  $T_{RB}$  – regenerative braking torque, N·m,  
 $j$  – phase number of SRM,  
 $i_j$  – phase current of SRM, A,  
 $L$  – phase bulk inductance of SRM, H,  
 $\theta$  – rotor aligned position of SRM, °.

The sum of all phase torques is the output torque of an SRM:

$$T_{RB} = \sum_{j=1}^N T_{RB}^j(i_j, \theta), \quad (2.4)$$

where  $N$  – total number of phases of SRM.

Consequently, a converter controls torque by acting on the phase current  $i_j$  (Ehsani, Gao, Gay, & Emadi, 2005). Pertinent sensors measure  $p_b$  and  $i_j$  (Zabler, 2014), which are approximately proportional to  $T_{FB}$  and  $T_{RB}$ , respectively. Hence, for the simplicity, the FLCs corrective variables are expressed as regenerative and friction torques directly. At last, total braking torque  $T_b$  is a summation of the torques generated by the RB and FB actuators.

## 2.1 Control method description

The main task of the ABS is to decrease braking distance with presumed lateral control. Moreover, for the EV, the ABS must also feature energy recuperation from vehicle deceleration manoeuvres. The main task is fulfilled by keeping the wheel slip rate for various tire–road friction coefficients as close as possible to, but not exceeding its optimal value. Additional requirement for the EVs is contented by prioritizing the usage of electric drive actuators. Friction braking torque is added in series, when regenerative torque is not enough to achieve maximum braking potential on a given road surface.

The blended ABS control method depicted in Figure 4 is identical for each wheel of the electric SUV with four on–board motor powertrain. It requires integrated signals transmitted from the vehicle CAN–bus. The method is composed of three main steps. First, the vehicle CAN–bus transmits signals required for states observation and torque blending. The signals are vehicle longitudinal deceleration  $a_{vx}$ , angular speed of the wheel  $\omega_w$ , and state–of–charge of the battery SOC.

The wheel longitudinal slip of each wheel is estimated from  $a_{vx}$  and  $\omega_w$ . The wheel slip serves as a first input of the FLCs. Although vehicle body deceleration rate does not provide friction coefficient directly, the variable can still be utilized for road recognition. The latter is used as the second input of the FLCs (I).

During the first step of heavy braking, a driver requests maximum braking torque from the actuators by slamming on a brake pedal. At this moment, the peak deceleration value

of the vehicle is measured. Therefore, this peak deceleration rate is mapped to an appropriate road surface, on which the same acceleration peak is achievable. This maximum  $a_{vx}$  is maintained by the FLC via holding the optimal wheel slip during the braking process. The road recognition is expressed as  $\mu^*$  (VII).

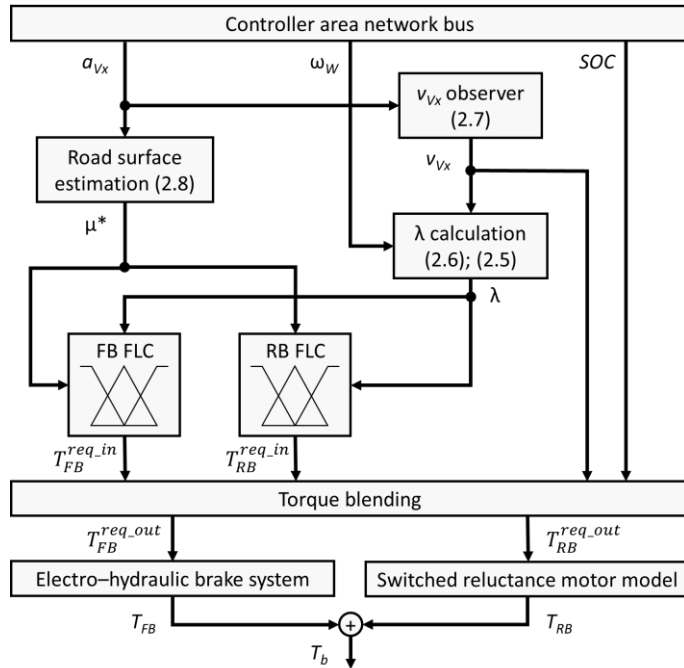


Figure 4. Block scheme of the blended antilock braking system control method for a single wheel: RB FLC – regenerative braking fuzzy logic controller; FB FLC – friction braking fuzzy logic controller. The symbols' description is introduced in Symbols.

In addition, during the deceleration,  $\mu^*$  is reset to zero with a fixed frequency. While the variable is reset, the ABS is turned off allowing maximum requested braking torque on the wheels. During this period, the peak  $a_{vx}$  is measured again. Hence, if the road surface remains unchanged, the same maximum reached  $a_{vx}$  is measured as in the previous step. Though, if the road surface changes, the value of  $\mu^*$  is updated according to the road profile. The reset principle, which is essential in road detection, is described with more details in (VII).

The road recognition principle is proved to be very efficient in combination with CI methods, such as FLC, because the CI algorithms, unlike conventional control methods (e.g. PID, SMC,  $H_\infty$ , etc.), successfully deal with stochastic and ill-defined data. To this aim, the control method does not require knowledge of vehicle peak decelerations and optimal wheel slip on every possible road surface. It is enough to know the tire specifications on most common ones, like dry, damp, wet, and icy. According to their tendency, an artificial decision-making system based on fuzzy logic is derived (I), (VII).

When the road is neither damp nor wet (i.e. partly true and partly false to any degree simultaneously), the optimal slip must be held also somewhere between two optimal rates. For example, when the control method detects maximum  $a_{vx}$  somewhere between damp and dry to any degree of certainty, it is not efficient to hold the wheel slip neither

for damp nor for dry road precisely. The optimal slip is somewhere between the optimal ones for those two surfaces. Hence, the FLC inferences these data in *modus ponens* form (**If** premise **Then** consequence) well understandable for human (Negnevitsky, 2005), for instance, with following fuzzy rule as: **If** the road surface value is between damp and dry, **And** wheel slip ratio is high for dry road, **Then** decrease torque to reach wheel slip to optimal between damp and dry road (X).

Second, the estimated variables, namely wheel slip ratio  $\lambda$  and road surface recognition  $\mu^*$ , enter the FLC blocks that are designed for the FB and RB actuators separately. Taking into consideration the input values, the FLCs calculate required RB and FB torques,  $T_{RB}^{req\_in}$  and  $T_{FB}^{req\_in}$ , to be directed to the Torque blending block. The FLCs obtain MISO forms.

Finally, the control method decides, how much torque to request from the actuators (i.e. EHB and SRM). This decision is made thanks to torque blending strategy, which also simultaneously considers vehicle speed and battery's state-of-charge.

### 2.1.1 States observation

The FLCs require two variables: longitudinal wheel slip and road surface derived from the deceleration rate of the vehicle body. In case of braking, the longitudinal wheel slip  $\lambda$  expressed in percentage is calculated as (Kiencke & Nielsen, 2005):

$$\lambda = \frac{v_{Vx} - v_{Wx}}{v_{Vx}} \cdot 100\%, \quad (2.5)$$

where  $\lambda$  – longitudinal slip of wheel, %,  
 $v_{Vx}$  – longitudinal velocity of vehicle, m/s,  
 $v_{Wx}$  – longitudinal velocity of wheel, m/s.

The longitudinal wheel velocity is proportional to the angular wheel speed measured by the sensor (Kiencke & Nielsen, 2005):

$$v_{Wx} = r_W \cdot \omega_W, \quad (2.6)$$

where  $r_W$  – radius of tire, m,  
 $\omega_W$  – angular speed of wheel, rad/s.

The longitudinal wheel velocity in ABS mode is determined by integration of the signal transmitted from the vehicle acceleration sensor (Kiencke & Nielsen, 2005):

$$v_{Vx} = \int a_{Vx} dt, \quad (2.7)$$

where  $a_{Vx}$  – longitudinal acceleration of vehicle, m/s<sup>2</sup>.

The tire–road friction coefficient is determined as a ratio between tire vertical and longitudinal forces (Kiencke & Nielsen, 2005), (I):

$$\mu(\lambda) = \frac{F_x}{F_z} = \frac{m_V \cdot a_{Vx}}{m_V \cdot g} = \frac{a_{Vx}}{g}, \quad (2.8)$$

where  $\mu(\lambda)$  – tire road friction coefficient,  
 $F_x$  – longitudinal force of tire, N,

$F_z$  – vertical force of tire, N,  
 $m_V$  – mass of vehicle, kg,  
 $g$  – gravitational acceleration,  $m/s^2$ .

This blended ABS control method uses vehicle body deceleration rate to comprehend which kind of road is under the tires. In this regard,  $\mu$  is connected to  $a_{vx}$ , and, as the variable has vague characteristic, the road recognition is performed by the fuzzy logic, which is described in the following subsection.

### 2.1.2 Fuzzy logic controller

The FLC is composed of four main elements: fuzzification, inference mechanism, rule base, and defuzzification. In fuzzification interface, the crisp inputs are transformed into fuzzy sets, each of which includes a MF and a membership degree of an input. Referring to the pre-defined rule base (i.e. a set of *modus ponens* form rules) and using an inference engine, the input and output fuzzy sets are mapped. Rule base is a tabular representation of input–output relation. It contains expert’s linguistic knowledge about how to control the plant. The finite number of MFs guarantees the finite number of fuzzy rules. Finally, defuzzification procedure transforms consequent linguistic outputs back into numerical value (Passino & Yurkovich, 1998). Sugeno’s type inference mechanism based on matrix operation is used for blended ABS control method (II).

#### 2.1.2.1 Fuzzification

The first FLCs’ input, wheel slip, has seven MFs symmetrically dispersed and overlapping between each other over the whole UOD (Figure 5). The input contains a set of linguistic variables {"slip equals to 0" ( $S_0$ ); "slip equals to 3" ( $S_3$ ); "slip equals to 6" ( $S_6$ ); "slip equals to 9" ( $S_9$ ); "slip equals to 12" ( $S_{12}$ ); "slip equals to 15" ( $S_{15}$ ); "slip equals to 18" ( $S_{18}$ )}. Its UOD is bounded inside of [0 18] limit, which provides the range of values the  $\lambda$  can assume. The second input is  $\mu^*$ . It has five symmetrically dispersed and overlapping MFs. Its set of MF values is {"Zero"; "Icy"; "Wet"; "Damp"; "Dry"}. The UOD is bounded inside [0 10]. All MFs have triangular form (X).

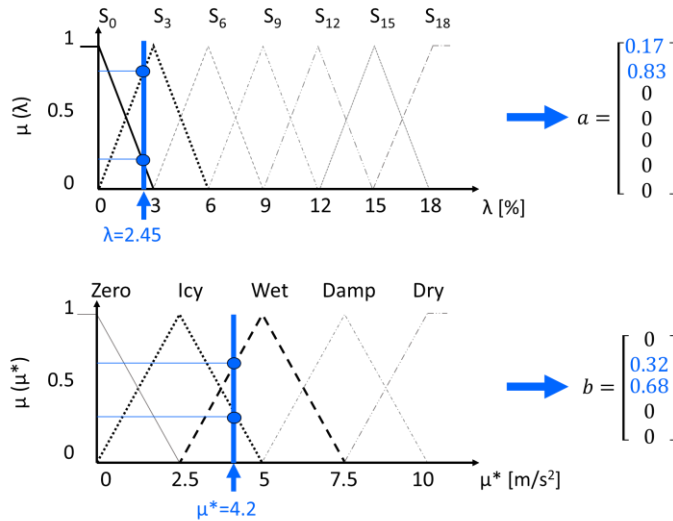


Figure 5. Fuzzy logic controller’s membership functions and fuzzification interface for randomly chosen  $\lambda$  and  $\mu^*$ :  $\mu(\lambda/\mu^*)$  – membership degree of an input.

Symmetrical MFs' dispersion is due to equal sensitivity of the inputs. Triangular shapes of MFs are characterized by fast response and simplicity. The UODs are selected based on the inputs' workspace (Passino & Yurkovich, 1998).

In Figure 5, a fuzzification operation for the designed control method is introduced. The numerical inputs are fuzzified with fuzzy singleton functions (blue). Fuzzification results in formation of two arrays,  $a$  and  $b$  (VII). Each position of the array corresponds to an appropriate MF's linguistic value, and it contains a rate of its degree of membership (value between 0 and 1) for a given input. When the input singleton does not intersect a MF, its array position value is equal to zero. Thereafter, a dyadic product of two arrays is calculated resulting in matrix  $C$  (II):

$$C \equiv a \otimes b \equiv ab^T. \quad (2.9)$$

### 2.1.2.2 Rule base and inference mechanism

The output of the RB FLC is the requested torque  $T_{RB}^{req\_in}$ . In total, it has eleven possible values starting from 0 to 200 with equal step of 20 between variables. Its rule base is presented in Table 1 for front and rear wheels. The requested FB pressure  $p_b^{req\_in}$  (proportional to  $T_{FB}^{req\_in}$ ) is limited to 150 bar in this application. Therefore, its consequent values from 0 to 150 form sixteen output options with a fixed step of 10 between each other. Input–output mapping of the FB FLC for front and rear wheels is introduced in Table 2. Each FLC has 35 rules (X).

Table 1. Fuzzy logic controller rule base for regenerative braking for front / rear wheels.

$T_{RB}^{req\_in}$ [Nm]		$\mu^*$ [m/s <sup>2</sup> ]				
		Zero	Icy	Wet	Damp	Dry
$\lambda$ [%]	$S_0$	60	80	160	200 / 120	200 / 140
	$S_3$	40	60	140	200 / 100	200 / 120
	$S_6$	20	40	120	200 / 60	200 / 100
	$S_9$	0	20	100	180 / 40	200 / 80
	$S_{12}$	0	0	60	160 / 20	200 / 40
	$S_{15}$	0	0	20	140 / 0	180 / 20
	$S_{18}$	0	0	0	120 / 0	160 / 0

Table 2. Fuzzy logic controller rule base for friction braking for front / rear wheels.

$p_b^{req\_in}$ [bar]		$\mu^*$ [m/s <sup>2</sup> ]				
		Zero	Icy	Wet	Damp	Dry
$\lambda$ [%]	$S_0$	20	30	60	90 / 70	150 / 90
	$S_3$	10	20	50	80 / 50	130 / 80
	$S_6$	0	10	30	70 / 30	110 / 70
	$S_9$	0	0	10	50 / 10	90 / 50
	$S_{12}$	0	0	0	30 / 0	60 / 30
	$S_{15}$	0	0	0	10 / 0	30 / 10
	$S_{18}$	0	0	0	0 / 0	0 / 0

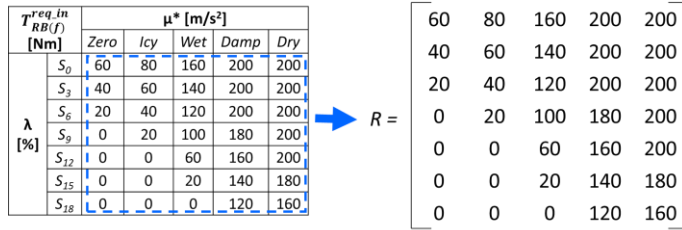


Figure 6. Front wheel RB FLC rule base (Table 1) transformation into matrix  $R$ .

The rule bases are designed to keep wheel slip as close as possible to its optimal rate on a given road surface. Linguistic quantification for one of the rear wheels in RB mode (Table 1) may be realised as follows: **If** wheel “slip equals to 6” **And** road surface is “Dry” **Then** request from the SRM  $T_{RB}^{req.in}$  equals to “100” Nm (X).

In Figure 6, rule base expression as matrix  $R$  is depicted. Matrix  $R$  has the same size as matrix  $C$  (e.g.  $7 \times 5$ ), which depends on the number of MFs of every input. The same transformation is true for other rule bases. Finally, fuzzy inference is done via Hadamard<sup>10</sup> product of two matrices of the same dimension,  $C$  and  $R$  (II):

$$D = C \circ R. \tag{2.10}$$

### 2.1.2.3 Defuzzification

The last element of the FLC is defuzzification interface. Here, the resultative numerical (crisp) value is generated. For this, two derived matrices,  $D$  and  $C$  are utilized to calculate the single output. A weighted average of the matrix elements is calculated: the sum of the elements in matrix  $D$  is divided to the sum of the elements in matrix  $C$ . The output  $u$  is calculated as follows (II):

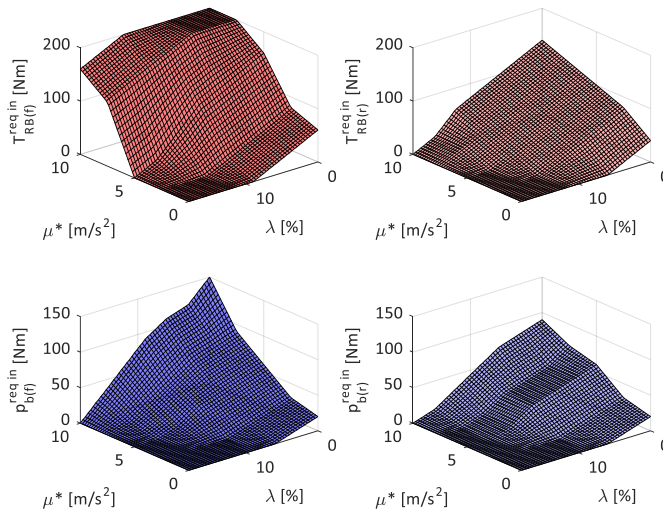


Figure 7. FLC 3D surfaces for RB and FB front (subscript ‘f’) and rear (subscript ‘r’) wheels.

<sup>10</sup> Jacques Salomon Hadamard (1865 – 1963) – French mathematician.

$$u = \frac{\sum_{i=1; j=1}^{M; N} d_{ij}}{\sum_{i=1; j=1}^{M; N} c_{ij}}, \quad (2.11)$$

where  $i = 1, 2, \dots, M$  and  $j = 1, 2, \dots, N$ ,  
 $d_{ij}$  – element of  $i^{th}$  row and  $j^{th}$  column of matrix  $D$ ,  
 $c_{ij}$  – element of  $i^{th}$  row and  $j^{th}$  column of matrix  $C$ ,  
 $u$  – output of an FLC.

Finally, in Figure 7, the nonlinear 3D control surfaces for every FLC are generated (X). The surfaces represent the outputs of the FLCs against the controller inputs (Passino & Yurkovich, 1998). The FLCs output shows requested braking torques,  $T_{RB}^{req.in}$  and  $T_{FB}^{req.in}$ , that follow inside the Torque blending block (Figure 4).

### 2.1.3 Torque blending strategy

Torque blending strategy is designed to maximize the usage of the SRMs during the braking process without overcharging (i.e. without damaging) the battery of the EV (IX). Therefore, it guarantees a highest energy recuperation capability on a given road surface (VII). Torque blending strategy is completed with binary logic. The strategy's flowchart is presented in Figure 8 (IX).

First, the algorithm checks the velocity of the vehicle. When vehicle longitudinal speed  $v_{Vx}$  is slower than fixed minimum threshold  $v_{Vx}^{min}$  (e.g. 15 – 8 km/h), the ABS control is deactivated, because the distance travelled with very low speed with locked wheels is not critical (IX).

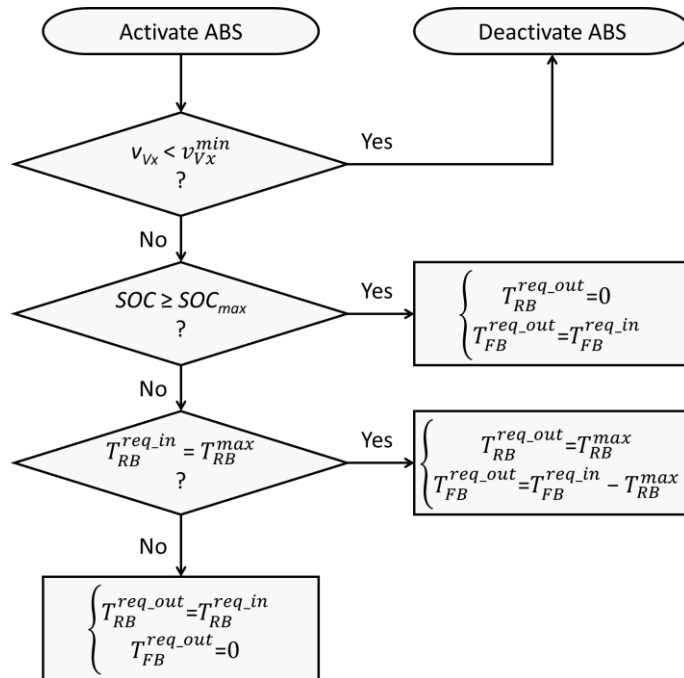


Figure 8. Torque blending strategy flowchart for a single wheel.

Second, when the SOC reaches maximum allowed threshold  $SOC_{max}$  (e.g. 90%), braking switches to pure FB mode, where the torque for the SRM is equal to zero (IX):

$$\begin{cases} T_{RB}^{req\_out} = 0 \\ T_{FB}^{req\_out} = T_{FB}^{req\_in} \end{cases} \quad (2.12)$$

Third, the blended ABS considers the SRM's peak performance. Specifically, when peak torque  $T_{RB}^{max}$  of the SRM is requested by the FLC, the block supplies the peak torque request to the SRM and calculates additional torque for the FB actuator to ensure optimal  $\lambda$  deceleration as (IX):

$$\begin{cases} T_{RB}^{req\_out} = T_{RB}^{max} \\ T_{FB}^{req\_out} = T_{FB}^{req\_in} - T_{RB}^{max} \end{cases} \quad (2.13)$$

Finally, when none of the previous conditions are true, the EV decelerates only with SRMs as the ABS actuators (IX):

$$\begin{cases} T_{RB}^{req\_out} = T_{RB}^{req\_in} \\ T_{FB}^{req\_out} = 0 \end{cases} \quad (2.14)$$

## 2.2 Experimental verification

The blended ABS control method was tested in sets of experiments. First, the control method was applied to an SUV model with conventional FB system (I). Thereafter, the control method has been combined with torque blending strategy and simulated for the fully electric SUV with four on-board motors powertrain (VII). Finally, its functionality was verified against the HIL platform available at Technische Universität Ilmenau<sup>11</sup> (IX), (X). The outcomes of the latter are presented in this Chapter.

### 2.2.1 Vehicle modelling and parameterization

Vehicle under investigation is an electric SUV with four independent SRM drives connected through half-shaft transmission on each wheel as a propulsion system (Appendix 2, Figure A2.1). A schematic drawing of four on-board motors powertrain architecture is introduced in Appendix 2 (Figure A2.2). Vehicle and powertrain configurations are listed in Appendix 2 (Table A2.1) (VII), (X).

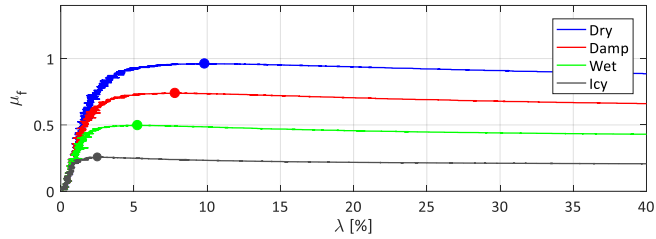
An experimentally validated SUV is modelled as 14 degree of freedom vehicle in IPG CarMaker<sup>12</sup> 6.0. The model is integrated with MATLAB/Simulink<sup>13</sup> R2015a (64 bit) simulation environment. Visual representation of the simulation allows users for deep understanding of the vehicle behaviour (X).

The SRM's torque-rotational speed characteristics are obtained experimentally. The plots are delivered in Appendix 2 (Figure A2.3). Taking into account transmission gear ratio (i.e. 1:10.56) and motor's peak torque (i.e. 200 Nm), the maximum achievable torque on the wheel is 2100 Nm. The SRM's dynamic performance is described by the second-order transfer function (VII).

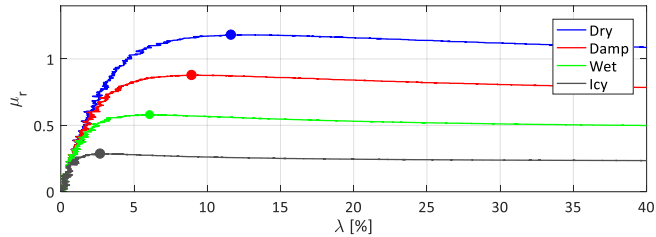
<sup>11</sup> Ilmenau, Germany.

<sup>12</sup> CarMaker is a registered trademark of the IPG Automotive GmbH (Germany, Karlsruhe).

<sup>13</sup> MATLAB/Simulink is a registered trademark of the MathWorks, Inc. (Natick, MA, USA).



(a)



(b)

Figure 9. Tire–road friction–slip curves for a modelled with Pacejka’s “Magic Formula 6.1” (Pacejka, 2012) tire on various road surfaces: (a) front wheels; (b) rear wheels.

Table 3. Optimal wheels’ slip rates and vehicle’s body deceleration values for common road surfaces.

	Icy	Wet	Damp	Dry
Front wheel $\lambda$ [%]	2.51	5.25	7.81	9.83
Rear wheel $\lambda$ [%]	2.71	6.09	8.95	11.64
Peak $a_{vx}$ [ $m/s^2$ ]	2.66	5.12	7.66	10.03

### 2.2.2 Tire model

The tires are modelled with Pacejka’s “Magic Formula 6.1” (Pacejka, 2012). In Figure 9, the slip–friction curves for front and rear wheels on common road surfaces (i.e. dry, damp, wet, and icy) are shown. Table 3 contains the optimal wheel slip values together with vehicle body peak deceleration rates for a given tire and vehicle (X).

The peaks of the curves are emphasized with dots, where the wheel slip is optimal for a given road surface. The region from zero slip to its optimal value is called stable. In the stable region due to positive force–slip gradient, the vehicle presumes steerability. The remaining curve region is called unstable, where the vehicle lateral control is no longer possible (Rajamani, 2012).

### 2.2.3 Hardware–in–the–loop test bed

In Figure 10, the EHB is presented. The system is based on the slip control boost technology developed by the ZF TRW Automotive<sup>14</sup>. The test rig contains EHB and its control unit. The test rig’s task is to reproduce real pressure dynamics of the brake circuit. It consists of the brake calipers mounted on two brake disks fixed with respect to the structure frame. The test bed is equipped with sensors for brake line pressure

<sup>14</sup> Koblenz, Germany.

measurement in four brake calipers in a range from 0 to 20 MPa with cut-off frequency of 1 kHz (X).

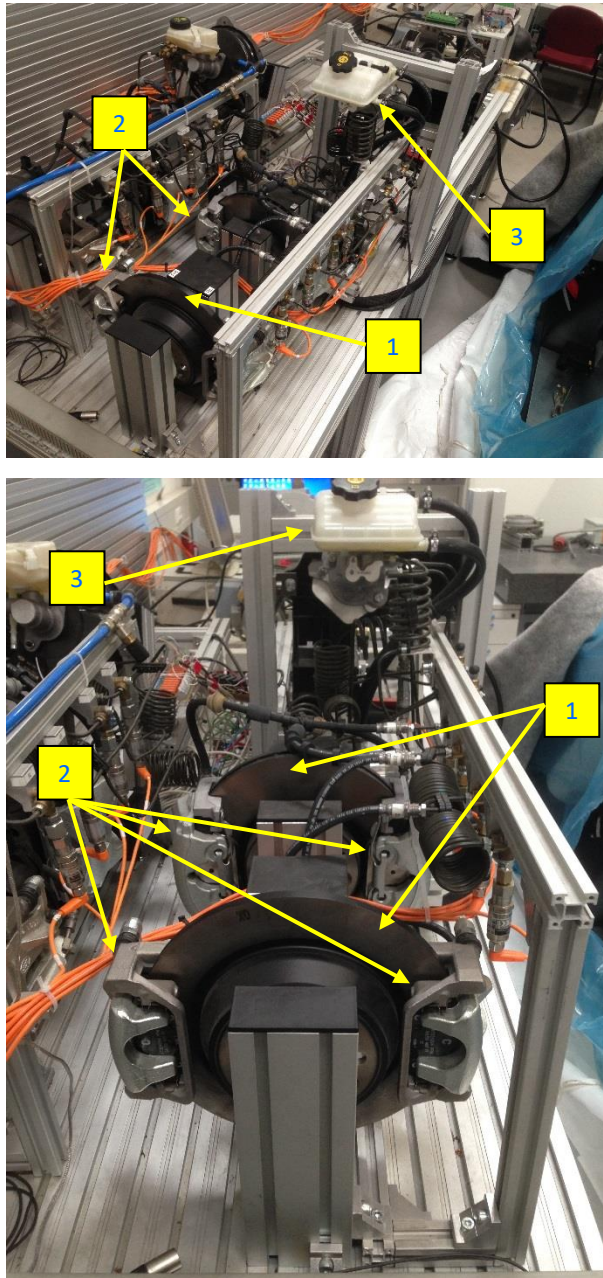


Figure 10. EHB hardware-in-the-loop test bed at Technische Universität Ilmenau (Germany): 1 – brake disk; 2 – brake caliper; 3 – master cylinder with reservoir.

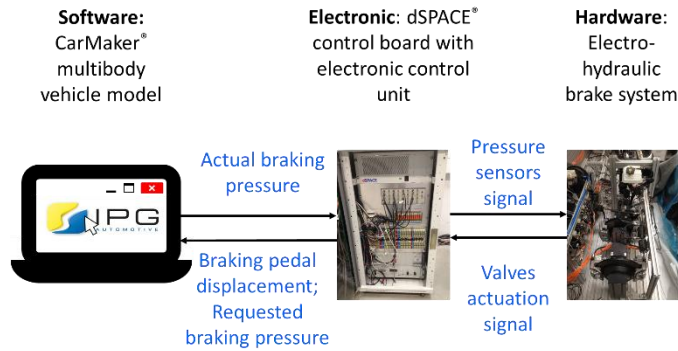


Figure 11. Hardware-in-the-loop hardware and software communication.

The ABS test rig is connected to the host personal computer via dSPACE<sup>15</sup> electronic platform (Figure 11). The latter unit serves as an intermediate connection between EHB system and vehicle model. Its task is to convert signals from digital and analogue and back. The personal computer runs multibody electric SUV model (X).

#### 2.2.4 Experimental results

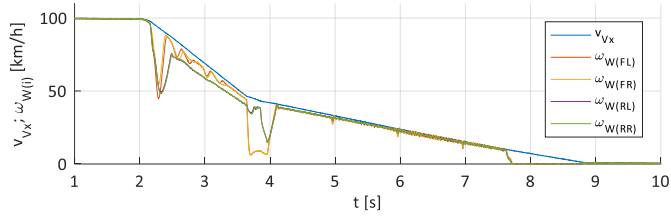
The simulation results of the FLC-based ABS control method on various road surfaces and under complex braking manoeuvres, like curved split- $\mu$ , straight split- $\mu$ , braking on changing road surfaces, etc., are elaborately discussed in I. The comparison between no control braking and braking with intelligent FLC ABS is also presented. Supreme functionality of the control method proves its robustness to changing environmental conditions and advanced safety performance of the ABS, namely stability maintenance and braking distance reduction.

In VII, the ABS control method is simulated for both FB and RB actuators. The results of braking with decoupled regenerative, pure friction, and locked wheels braking performance on different road surfaces are provided and compared between each other. The proposed control method is not only capable of decelerating EV with decoupled braking system faster than with conventional EHB system, but also of recuperating up to 10.27 % (save up to 17.74 kJ) of energy spent on braking.

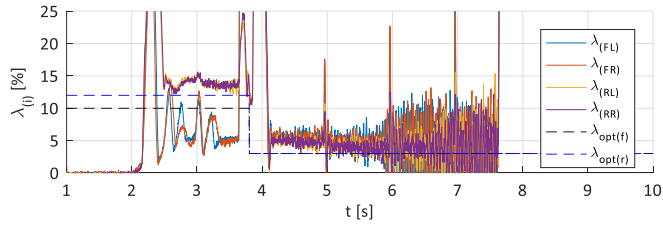
Torque blending strategy functionality is studied in IX. The HIL simulation on high- $\mu$  surface is conducted with battery SOC and vehicle speed taken into consideration. The blended ABS control method showed high efficiency and robustness against varying road conditions and changing system's states. During the experiment, the SOC of the battery achieves its maximum threshold. As a result, the torque blending switched from RB to a pure FB mode. The SUV continues deceleration with optimal slip without SRMs' intervention and performance degradation.

The blended ABS control method functionality on real EHB system is performed in IX and X. The HIL simulation is conducted for decoupled braking system and compared to pure FB system. The results on low- $\mu$  and transient road surface (i.e. from high- $\mu$  to low- $\mu$ ) are presented. The latter is scoped in Figure 12, where the vehicle starts deceleration on high- $\mu$  surface and proceeds to low- $\mu$  one.

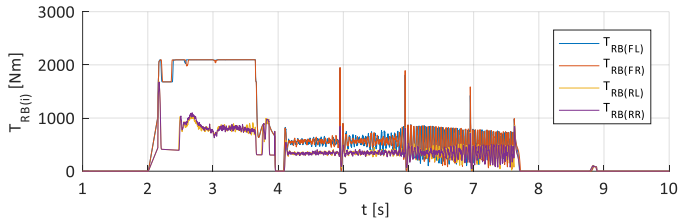
<sup>15</sup> dSPACE (digital signal processing and control engineering) is a registered trademark of the dSPACE GmbH (Paderborn, Germany).



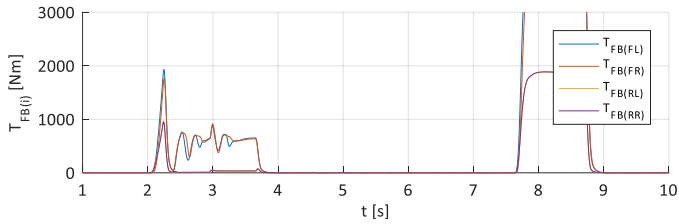
(a)



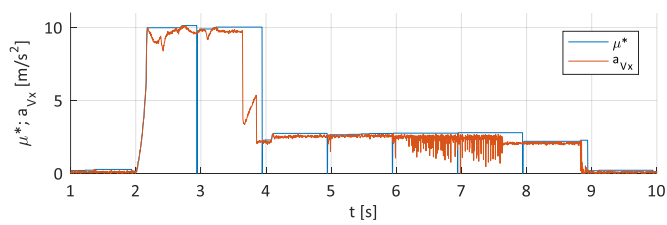
(b)



(c)



(d)



(e)

Figure 12. Hardware-in-the-loop simulation results of blended antilock braking system control method from braking on varying road surface (from high- $\mu$  to low- $\mu$ ): (a) vehicle and wheels speed; (b) wheels longitudinal slips; (c) RB torques; (d) FB torques; (e) road detection with vehicle body deceleration. Subscript “i” is for each wheel: [front left (FL), front right (FR), rear left (RL), rear right (RR), f – front, r – rear].

In Figure 12. (a), wheel speeds and vehicle longitudinal velocity diagrams are plotted. The wheels' speeds tend to follow the vehicle body velocity, while the controller does not allow the wheels' lockage. The vehicle decelerates with higher wheel slip values at the beginning of the manoeuvres (Figure 12. (b)). Whilst the slip of the rear wheels is close to its optimal value, for the front wheels the value is much lower. This phenomenon is because the peak braking torque for the front wheels exceeds the SRMs limits (Figure 12. (c)). Consequently, the controller activates the FB to supply the braking torque gap (Figure 12. (d)). However, the FB dynamics are not as fast as RB's one, what leads to the control accuracy losses (X).

The road estimator successfully detects transient road conditions (Figure 12. (e)). At the beginning, the peak deceleration is around  $10 \text{ m/s}^2$ , which refers to high- $\mu$  surface (Table 3). After 4 seconds, the vehicle drives on a low- $\mu$  road, the control method resets  $\mu^*$  and measures peak  $a_{vx}$  again. As the road surface has changed, a new value of  $\mu^*$  is recognized. Thereafter, the controller reduces the braking torques (Figure 12. (c)) to maintain the wheel slip rates close to their optimal values for a low- $\mu$  road surface (Table 3). The FB torque is no longer requested (Figure 12. (d)), because the SRM's torque is enough to decelerate the SUV with optimal wheel slips (Figure 12. (b)) (X).

## 2.3 Summary

In this Chapter the blended ABS control method is proposed. The method uses vehicle body deceleration to recognise road surface under the tires. Intelligent FLC simultaneously considers detected road and longitudinal wheel slip to determine an appropriate braking torque for RB and FB separately to hold optimal wheel slip during the whole braking manoeuvre for a given tire-road friction coefficient. Hence, the method reaches maximum braking potential on various road surfaces. The FLC designed for each actuator and every wheel separately (I), (VII).

Torque blending strategy accounts battery's SOC, vehicle speed, and requested RB and FB braking torques. The strategy focuses on usage of the electric motors as brakes on their maximum potential. The conventional EHB system is added only, when braking torque generated by the SRM is not enough to keep wheel slip on its optimal value. Therefore, blended ABS control method not only diminishes braking distance with maintained steerability, but also regenerates peak energy during braking. Thus, it allows for enhancing the EV's driving range (IX), (X).

A set of experiments on HIL test bed was conducted with various road conditions. The case with transient road surface (i.e. braking from high- $\mu$  to low- $\mu$ ) is presented and discussed. Thanks to intelligent FLC accompanied with road detection and torque blending strategy, the control method adapts to stochastic environmental conditions. Consequently, the maximum deceleration force is reached with concurrently peak recuperation energy for a given electric SUV (X).

### 3 Method for driver distraction detection and evaluation

Present Chapter is dedicated to the DD detection and evaluation method. It is organized in three subchapters: Method description, Experimental verification, and Summary. In the first one, the method for driver distraction detection and evaluation is described. The second subchapter is dedicated to DIL experimental study, which was conducted for multiple STs. Finally, the Chapter is briefly outlined in Summary.

#### 3.1 Method description

A block scheme of the method for detection and evaluation of DD induced by secondary activity while operating a vehicle is introduced in Figure 13. The method includes three blocks. The first one is a model of normal driving performance of an individual participant, which is unique for every single driver (IV). Next, the distracted driving performance is compared to the predicted one in the Error Calculation block. As a result, the performance-based errors caused by the ST are calculated. Finally, the model for total DD evaluation merges the data from the previous step into a single variable (II).

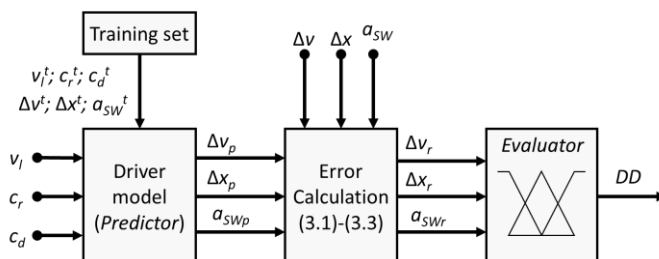


Figure 13. Drive distraction detection and evaluation method block scheme. The symbols' descriptions are listed in Symbols. Superscript "t" refers to "training set" collected during the distraction-free driving.

The main idea of the method is to observe the difference between person's driving without distraction and driving under the influence of distractive ST. To explain the principle of the DD evaluation Figure 14 is added. It depicts one of the driver performance-based measures, lane keeping ability  $\Delta x$ .

The transparent vehicle symbolizes driver's usual angle cutting in turning manoeuvre. The vehicle's centreline trajectory is drawn with light blue dotted line. Assume that when the driver is distracted, the vehicle's centreline trajectory follows the blue solid line (Figure 14, filled vehicle). By comparing the normal driving performance with the one under DD, the difference can be noticed (Figure 14, red surface). This difference is a resultative lane keeping ability for each individual driver (V).

In the same way the second driver performance-based measure, speed limit holding ability  $\Delta v$ , is tracked. A schematic explanation is presented in Figure 15. Again, the dotted light blue line symbolizes participant's usual speed keeping ability on a specific road segment, which in this instance is 90 km/h. On the contrary, when driving under distraction, the speed of the vehicle was held around 78 km/h (Figure 15, blue solid line). Thus, the deviation between normal and distracted speed limit maintenances is another performance-based measure for DD detection and evaluation method (Figure 15, red surface). Finally, the third measure is the difference between normal (i.e. predicted) steering wheel acceleration and steering wheel acceleration while completing the ST (V).

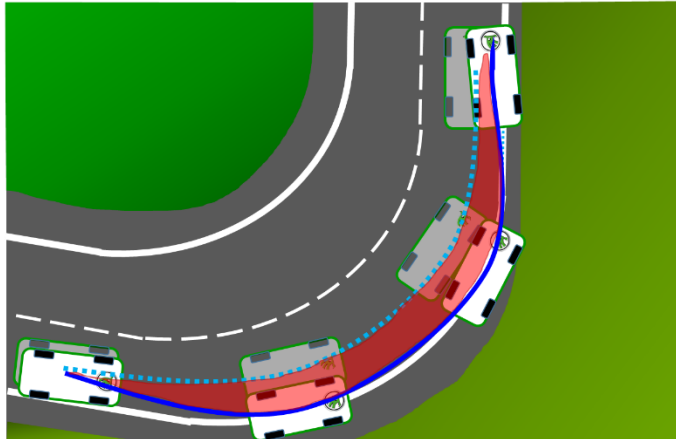


Figure 14. Driver performance–based measure, lane keeping ability: light blue dotted line –  $\Delta x_p$ ; blue solid line –  $\Delta x$ ; red surface –  $\Delta x_r$ .



Figure 15. Driver performance–based measure, speed limit keeping ability: light blue dotted line –  $\Delta v_p$ ; blue solid line –  $\Delta v$ ; red surface –  $\Delta v_r$ .

### 3.1.1 Driver model

The first step of the DD detection and evaluation method is to predict with a reasonable degree of accuracy driver's normal performance on a specific road segment. The segment is described with an information about the road, namely speed limit  $v_l$ , road curvature (radius)  $c_r$ , and road curve direction  $c_d$ . The latter is a Boolean type with the crisp values: -1 meaning that the road curve goes to the left, 0 – it is straight, 1 – it turns to the right. As the Driver model tends to forecast driver performance, it is also called the Predictor (V).

The Driver model uses the pre–processed Training set collected for each individual driver during a DD–free run in DIL experiment. During the experiment, the participants are requested to drive as accurate as possible obeying all the traffic rules, in particular by remaining inside of the driving lane and by holding all the speed limits. Hence, they are completely dedicated to show their best performance from the safety point of view (VI).

The model receives an information about the road segment and outputs driver's performance, what are the lane and speed limit keeping abilities and the force applied to the steering wheel. Therefore, the Predictor forecasts driver's lateral and longitudinal behaviour on a given road segment (IV).

To complete the task of mapping the pre-collected and newly received data, a CI algorithm, i.e. ML, is applied. To generate continues output, regression algorithms that are widely used in practice are exploited (Alpaydin, 2004). Among them are Gaussian process regression model, ANN, layer recurrent ANN, neuro-fuzzy system, and  $k$ -NN. The detailed information about models design and parameters selection as well as their prediction accuracies comparison are introduced in (IV), (VI), (VIII).

In short, the  $k$ -NN outperformed in prediction accuracy other known nonlinear regression algorithms (VIII). The  $k$ -NN comparing to other CI methods used for prediction (e.g. neuro-fuzzy system, ANN, etc.) achieves minimum possible training error on any regression dataset (Goodfellow, Bengio, & Courville, 2016). The principle of the algorithm's operation for DD detection and evaluation method is described in (VI).

### 3.1.2 Error calculation

The second block is Error calculation. During this stage, the predicted driver performance-based measures generated by the Predictor,  $\Delta x_p$ ,  $\Delta v_p$ ,  $a_{SWp}$ , are compared to the driving under the influence of ST,  $\Delta x$ ,  $\Delta v$ ,  $a_{SW}$ . The outcomes of this block are the resultative performance,  $\Delta x_r$ ,  $\Delta v_r$ ,  $a_{SWr}$ , calculated using the following rules (III):

$$\Delta v_r = \begin{cases} \Delta v - \Delta v_p, & \text{if } \Delta v > 0; \Delta v_p > 0; |\Delta v| > |\Delta v_p| \\ \Delta v - \Delta v_p, & \text{if } \Delta v < 0; \Delta v_p < 0; |\Delta v| > |\Delta v_p| \\ \Delta v + \Delta v_p, & \text{if } \Delta v > 0; \Delta v_p < 0; |\Delta v| > |\Delta v_p|, \\ \Delta v + \Delta v_p, & \text{if } \Delta v < 0; \Delta v_p > 0; |\Delta v| > |\Delta v_p| \\ 0, & \text{if } |\Delta v| \leq |\Delta v_p| \end{cases} \quad (3.1)$$

where  $\Delta v_r$  – resultative vehicle speed deviation, km/h,  
 $\Delta v$  – real vehicle speed deviation, km/h,  
 $\Delta v_p$  – predicted vehicle speed deviation, km/h.

$$\Delta x_r = \begin{cases} \Delta x - \Delta x_p, & \text{if } \Delta x > 0; \Delta x_p > 0; |\Delta x| > |\Delta x_p| \\ \Delta x - \Delta x_p, & \text{if } \Delta x < 0; \Delta x_p < 0; |\Delta x| > |\Delta x_p| \\ \Delta x + \Delta x_p, & \text{if } \Delta x > 0; \Delta x_p < 0; |\Delta x| > |\Delta x_p|, \\ \Delta x + \Delta x_p, & \text{if } \Delta x < 0; \Delta x_p > 0; |\Delta x| > |\Delta x_p| \\ 0, & \text{if } |\Delta x| \leq |\Delta x_p| \end{cases} \quad (3.2)$$

where  $\Delta x_r$  – resultative lane keeping offset, m,  
 $\Delta x$  – real lane keeping offset, m,  
 $\Delta x_p$  – predicted lane keeping offset, m.

$$a_{SWr} = \begin{cases} a_{SW} - a_{SWp}, & \text{if } a_{SW} > 0; a_{SWp} > 0; |a_{SW}| > |a_{SWp}| \\ a_{SW} - a_{SWp}, & \text{if } a_{SW} < 0; a_{SWp} < 0; |a_{SW}| > |a_{SWp}| \\ a_{SW} + a_{SWp}, & \text{if } a_{SW} > 0; a_{SWp} < 0; |a_{SW}| > |a_{SWp}|, \\ a_{SW} + a_{SWp}, & \text{if } a_{SW} < 0; a_{SWp} > 0; |a_{SW}| > |a_{SWp}| \\ 0, & \text{if } |a_{SW}| \leq |a_{SWp}| \end{cases} \quad (3.3)$$

where  $a_{SWr}$  – resultative steering wheel acceleration,  $^{\circ}/s^2$ ,  
 $a_{SW}$  – real steering wheel acceleration,  $^{\circ}/s^2$ ,  
 $a_{SWp}$  – predicted steering wheel acceleration,  $^{\circ}/s^2$ .

More precisely, the block assigns zero to any variable, when the performance measure under DD is smaller or equal to its predicted one. It means that the driver passed the road segment in the same way as she/he does in normal driving and, thus, was not distracted. Contrariwise, if the value under DD is greater than the predicted one, the difference between two values is calculated. Hence, when the performance becomes worse due to DD, the block detects unusual vehicle dynamic performance and measures, how much does the ST influence vehicle dynamic performance from the safety point of view (III).

For a given road segment, positive values of  $\Delta x_r$ ,  $\Delta v_r$ ,  $a_{SWr}$  mean driving to the right from its normal trajectory, excess its normal speed, and turning the steering wheel to the right, respectively. Contrariwise, negative values of  $\Delta x_r$ ,  $\Delta v_r$ ,  $a_{SWr}$  mean driving to the left from its normal trajectory, slowdown its normal speed, and turning the steering wheel to the left, accordingly (V).

### 3.1.3 Driver distraction evaluation

To evaluate DD, another CI-based (i.e. fuzzy logic) solution is promoted. In this method, the main purpose of the FLC is to fuse the resultative performance-based measures into a uniform output, which symbolizes a level of driver distraction in percentage  $DD$ . The algorithm serves here as an artificial decision-making system.

The fuzzy Evaluator is realised using the same approach as described in (II), hence, Sugeno's type inference engine is applied. However, now the FLC has three inputs and a single output (Figure 13), making it, just like in case with the blended ABS controller (2.1.2), a MISO system.

#### 3.1.3.1 Fuzzification

The Evaluator input MF's are depicted in Figure 16. The first input,  $\Delta v_r$ , has five symmetrically dispersed and overlapping each other triangular shape MFs (Figure 16.(a)). It has a set of linguistic variables for speed deviation from segment speed limit: {"negatively high deviation" ( $neg\_high$ ); "negatively low deviation" ( $neg\_low$ ); "no deviation" ( $zero$ ); "positively low deviation" ( $pos\_low$ ); "positively high deviation" ( $pos\_high$ )}. The UOD is restricted inside  $[-12\ 12]$  (V).

The second input, resultative lane keeping offset  $\Delta x_r$ , MFs are illustrated in Figure 16.(b). As the first input, it has five triangular shape symmetrically dissipated and overlapping between each other over the whole UOD MFs. The UOD is constrained between  $[-1.5\ 1.5]$ . Its linguistic variables are {"negatively far offset" ( $neg\_far$ ); "negatively close offset" ( $neg\_close$ ); "no offset" ( $zero$ ); "positively close offset" ( $pos\_close$ ); "positively far offset" ( $pos\_far$ )} (V).

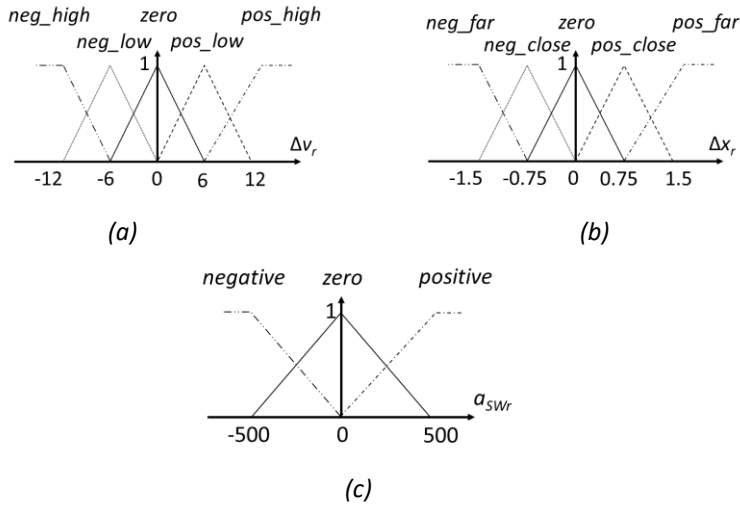


Figure 16. DD detection and evaluation method's input MFs: (a) resultative speed keeping ability; (b) resultative lane keeping offset; (c) resultative steering wheel acceleration.

Table 4. Fuzzy logic Evaluator rule base.

$a_{swr} [^{\circ}/s^2] = \text{negative}$						
DD [%]		$\Delta x_r$ [m]				
		neg_far	neg_close	zero	pos_close	pos_far
$\Delta v_r$ [km/h]	neg_high	100	85.8	42.9	85.8	100
	neg_low	100	57.2	14.3	57.2	100
	zero	57.2	28.6	0	28.6	57.2
	pos_low	85.8	42.9	14.3	42.9	85.8
	pos_high	100	85.8	42.9	85.8	100
$a_{swr} [^{\circ}/s^2] = \text{zero}$						
DD [%]		$\Delta x_r$ [m]				
		neg_far	neg_close	zero	pos_close	pos_far
$\Delta v_r$ [km/h]	neg_high	100	71.5	42.9	71.5	100
	neg_low	85.8	14.3	0	14.3	85.8
	zero	42.9	0	0	0	42.9
	pos_low	71.5	14.3	0	14.3	71.5
	pos_high	85.8	57.2	28.6	57.2	85.8
$a_{swr} [^{\circ}/s^2] = \text{positive}$						
DD [%]		$\Delta x_r$ [m]				
		neg_far	neg_close	zero	pos_close	pos_far
$\Delta v_r$ [km/h]	neg_high	100	85.8	42.9	85.8	100
	neg_low	100	57.2	14.3	57.2	100
	zero	57.2	28.6	0	28.6	57.2
	pos_low	85.8	42.9	14.3	42.9	85.8
	pos_high	100	85.8	42.9	85.8	100

The last input is a resultative steering wheel acceleration  $a_{swr}$ , which is also composed of triangular symmetrically disseminated and overlapping between each other MFs (Figure 16.(c)). It has three MFs, with a set of linguistic variables: {"negative acceleration (i.e. to the left)" (*negative*); "zero acceleration" (*zero*); "positive acceleration (i.e. to the right)" (*positive*)}. The UOD is settled in [-500 500] (V).

Fuzzification is completed in accordance with equation (2.9). Nonetheless, in this method, there are three input variables. Thus, matrix  $C$  takes size of  $5 \times 5 \times 3$ , which is proportional to the number of MFs for each input of the Evaluator (VIII).

### 3.1.3.2 Rule base and inference mechanism

The output of the Evaluator is a level of DD expressed in percentage  $DD$ . Therefore, the UOD is bounded between [0 100]. It has eight possible values with equal step of 14.3 between each other {0; 14.3; 28.6; 42.9; 57.2; 71.5; 85.8; 100}, what gives also equal responsiveness of the output MFs (II).

The input–output mapping is completed via 75 *modus ponens* form linguistic rules. The rule base is introduced in Table 4. An example of the input–output relation is as follows: **If** steering wheel acceleration is "*positive*", **And** vehicle speed deviation is "*neg\_low*", **And** lane keeping offset is "*pos\_close*", **Then** DD is "57.2" % (VIII).

On the same principle as in Figure 6, the rule base forms matrix  $R$  of  $5 \times 5 \times 3$  in size, where for every layer of 3D matrix a rule base exists. Again, Hadamard product of two matrices  $C$  and  $R$  of the same size results in matrix  $D$  applying equation (2.10) (II). Each element of  $D$  contains information about certainty of every output MF activation for a given input.

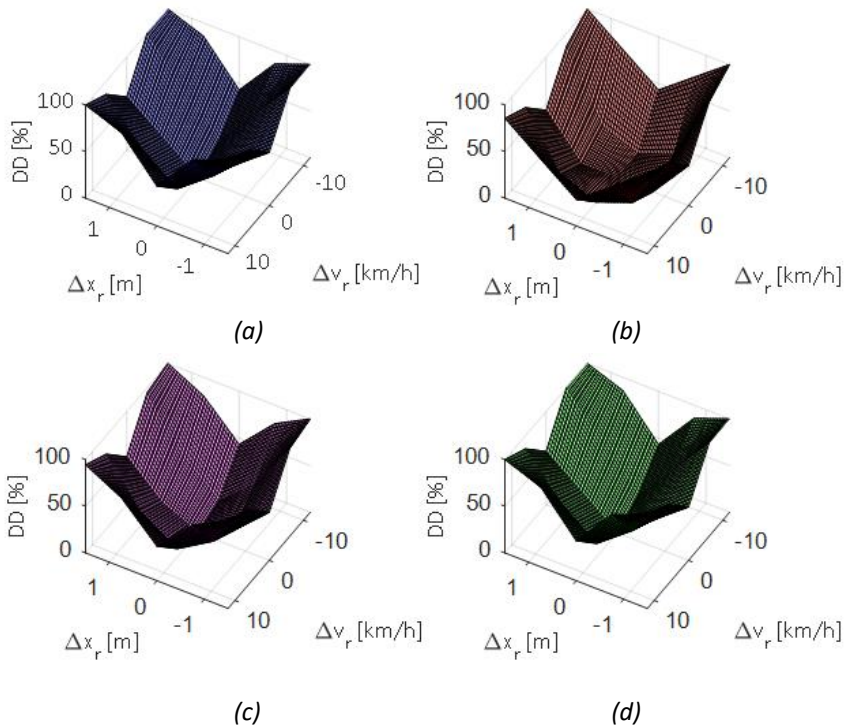


Figure 17. Fuzzy logic Evaluator 3D surfaces for several constant steering wheel acceleration values: (a) -500; (b) 0; (c) 300; (d) 500.

### 3.1.3.3 Defuzzification

The final stage of the fuzzy Evaluator is conversion of the calculated matrices  $D$  and  $C$  back into a single crisp number. The centre of gravity is used, where the sum of elements in  $C$  is divided by the sum of elements in  $D$ , applying equation (2.11). The result of the designed Evaluator is observable in Figure 17, where nonlinear 3D surfaces are introduced for several constant  $a_{swr}$  values (III).

## 3.2 Experimental verification

The DD detection and evaluation method is verified in DIL experiments in two stages. First, the DIL experiment with a single ST exploiting the simple driver simulator was conducted. The DIL experiment was organized in cooperation with IPG Automotive GmbH<sup>16</sup>. Text messaging on a cellular phone while driving served as a ST. The participants were instructed to have natural chat conversation with an experimenter. Furthermore, the DD was evaluated only with two performance-based measures: lane keeping ability and speed limit maintenance. The methodology described in this subchapter was also true for the single ST experiment (II), (VI). Thereafter, the method functionality was studied in DIL with multiple IVIS-induced STs on advanced driver simulator (III), (V), (VIII). The list of the tasks is located in Appendix 3 (Table A3.1). These studies were conducted in cooperation with ŠKODA Auto a.s.<sup>17</sup>, and the results are presented in this subchapter. The  $k$ -NN is used in DD detection and evaluation method experimental verification as the Driver model, because it appeared to be the most accurate Predictor among the tested algorithms (VIII).

### 3.2.1 Participants

Thirty drivers without serious physical or mental health disorders contributed to this study. They were regular participants of the DIL DD experiments, and, thus, were well acquainted with the simulator. The participants owned valid driving licenses and daily used personal vehicles for transportation. Five contributors were women, the rest – men. The participation in the DIL experiment was rewarded (V), (VIII).

### 3.2.2 Apparatus

The DIL experiment was performed using the advanced vehicle simulator (Figure 18) available at ŠKODA Auto laboratory in Mladá Boleslav, Czech Republic. It is a fixed-base vehicle mock-up with the screen in front of the wall, where the virtual world is projected. A two-lane rural highway road with different curvatures and speed limits (i.e. 30, 50, 90 km/h) was modelled in the virtual world. The lane width was 3.5 m. The lane can be roughly divided into two parts: the one that has a lower speed limitation (i.e. 30 and 50 km/h) with lots of curvatures, and the one that has a higher speed limit, 90 km/h, but almost straight road (i.e. big road radius). The road shape is identical to the one existing in the Czech Republic. Its total distance is 10626 m, what takes about 10 mins of driving a full lap, if all the traffic signs are respected. There were no other dynamic objects (e.g. other vehicles, pedestrians, etc.) introduced in the virtual world (II). The road shape together with speed limits is presented in Appendix 3, in Figure A3.1.

---

<sup>16</sup> Karlsruhe, Germany.

<sup>17</sup> Mladá Boleslav, Czech Republic.



(a)



(b)

Figure 18. Multiple secondary tasks experiment test facilities: (a) advanced vehicle simulator; (b) a participant operating the simulator while performing a secondary task.

A participant is settled down inside the simulator. As the test rig has an automatic transmission, the driver operates it by acting only on steering wheel and throttle and braking pedals. The simulator cockpit is identical to the one used in ground vehicles. Its head-up instrumental panel displays vehicle velocity. All the STs are executed via the IVIS display, which is placed, like in most of the European countries, on the driver's right. The data are collected with 10 Hz frequency (III).

The vehicle and the virtual world scene are modelled with an open source library for C++<sup>18</sup> programming language, Open Dynamics Engine v 5.0 (Smith, 2006). This model includes vehicle body, suspension system, and four wheels completed with Pacejka's "Magic Formula" (Pacejka, 2012). The vehicle is parametrized according to Škoda Yeti SK316 with 1.4 liters twin charged stratified injection 77 kW engine specifications (VIII).

The steering wheel acceleration was obtained from a signal transmitted from the steering wheel sensor mounted on the shaft end of the steering axle. Lane keeping ability

---

<sup>18</sup> An object-oriented extension of C programming language.

and vehicle velocity abnormalities were calculated from  $x$ ,  $y$ , and  $z$  coordinates received from the global positioning system of the virtual world (V). More information with visual illustration on the data extraction is provided in (VI).

### 3.2.3 Procedure

Before the DIL experiment, the participants received unlimited time to get acquainted with the simulator. In addition, before the beginning of the DIL test, the drivers were well instructed to the exploited IVIS and all the STs (Table A3.1) execution (III).

The DIL experiment had two steps. First, the participants were asked to pass two laps in the virtual world fully dedicated to safe vehicle operation. They were requested to drive in the middle on their lane and to hold speed limit as good as possible. No DD appeared during this step. The collected data were utilized for the Driver model (Figure 13) for each individual participant.

For the second step, the participants were requested to continue driving following all the traffic rules as accurate as feasible, though, this time they were requested to submit a ST in parallel to vehicle control. The drivers had no time restriction for the STs execution. What is more, each task was called with a reasonable time delay. Therefore, the participants drove roughly equal time under DD and free from secondary activity (III).

The experimenter sent the vocal order to execute a random ST from the list (Table A3.1). Each ST was executed several times during the experiment. When ST is accomplished, the driver sent a feedback via windshield washer switch behind the steering wheel. If the task is correctly completed, the driver heard a vocal signal that informed about the correctness of the submitted task. When the task is wrong and the participant did not hear the vocal confirmation, she/he had to perform the ST again (VIII).

### 3.2.4 Experimental results

The results of DD detection and evaluation for a random DIL experiment participant are introduced. During the experiment each driver drove more than two laps under distraction. Nevertheless, for better observability the results from only one lap (i.e. 10 minutes of experimentation) are presented. The DD detection and evaluation is realized offline after the data collection phase (3.2.3).

#### 3.2.4.1 Driver model

In Figure 19, the prediction results (blue curve) versus the training set (black curve) are presented. The bright green curve represents the information about the road segment, namely speed limit (Figure 19.(a)) and curvature (Figure 19.(b)). The small radius designates a sharp turn, while the big radius – almost straight road.

The speed deviation on a 50 km/h speed limit road segment (Figure 19.(a), from 630 to 890 s) is relatively low, in average 3 km/h below the limit (i.e. 47 km/h). The  $k$ -NN well copes with this data, and accurately predicts this speed maintenance ability. On the other hand, when the participant drove on high speed limit segment (Figure 19.(a), from 900 to 1200 s), in average the vehicle speed was up to 5 km/h lower. This approximation is also true for the Predictor.

Lane keeping ability is depicted in Figure 19.(b). The model precisely predicts driver's performance on a low speed limit segment (Figure 19.(b), from 630 to 890 s). This segment is characterized with numerous different road curvatures (bright green line). On the straight road segment (Figure 19.(b), from 900 to 1200 s) the lane keeping ability is averaged to almost constant variable, 0.1 m (blue line), what means that the

driver stayed in the middle of the lane almost for the whole segment. However, it was not true in practice (black curve).

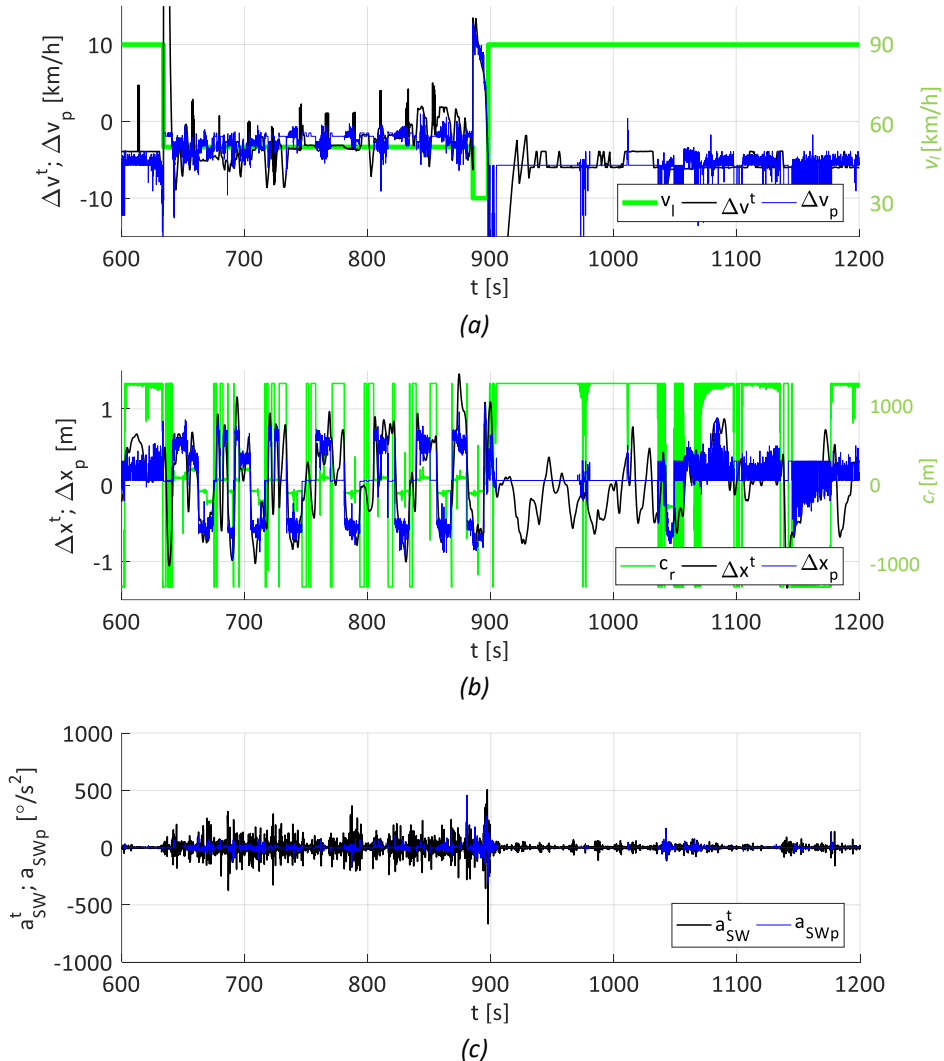


Figure 19. Driver performance prediction in comparison to training set: (a) vehicle speed deviation; (b) lane keeping offset; (c) steering wheel acceleration.

In case of steering wheel acceleration (Figure 19.(c)), high acceleration rates were predicted and indeed were executed on curvy road segment (Figure 19.(c), from 630 to 890 s). On the contrary, low acceleration rates were recognized by the Predictor on straight road segment with high speed limit (Figure 19.(c), from 900 to 1200 s). This is logical, because the one does not need to act actively on steering wheel on a straight road.

In short, the prediction is not accurate enough for some performance-based variables on some specific road segments, what can negatively affect the DD detection and evaluation method functionality. The accuracy losses can be explained with highly

nonlinear data of human behaviour and complexity of the driver modelling challenges. Nevertheless, for this application the driver modelling is accepted as satisfactory, due to relatively low mean square error for each variable (VI).

In Figure 20, the predicted performance versus the driving under the influence of DD is introduced. The grey background on each figure depicts the period of ST execution. The black-colour number on the grey background on top of each figure is the number of the ST (Table A3.1). The blue curve is again the variable forecasted by the Driver model, and red curve is distracted driving.

For instance, the driver significantly dropped the speed of the vehicle, while completing the task number 9 (media item selection) (Figure 20.(a)). The prediction assigns around 3 km/h speed deviation on this segment, yet, the speed was decreased by more than 20 km/h when submitting the ST. For the same ST, the driver failed to keep the lane (Figure 20.(b)) as she/he stayed relatively far to the left from the middle lane instead of predicted 0.5 m to the right of the road lane centre. Needless to say, the acceleration of the steering wheel was very high to both the left and the right directions (Figure 20.(c)), what is unusual for the given driver. It symbolizes that the driver had to act on a steering wheel very intensively to pass the curvy segment. In addition, the task took the driver considerable time to complete.

Another example is noticed in case of the tasks 14 and 15 (both are operation in IVIS navigation). Both STs lead the driver to diminish the speed (Figure 20.(a)): the velocity was dropped to 75 km/h on a 90 km/h speed limit segment. The Predictor instead outputs not more than 5 km/h, what is normal for this participant.

Moreover, while operating the in-vehicle navigation system, the driver conducted a swing manoeuvre completing task 14 and went too far from the middle lane to the left submitting the task number 15 (Figure 20.(b)). These manoeuvres were especially dangerous for holding the stability of the vehicle, even if the road was almost straight. What is more, the tasks were performed on high speed limit road (90 km/h), what makes the mentioned mistakes more dangerous for the driver and other traffic participants.

For steering wheel acceleration (Figure 20.(c)), the ST number 14 and 15 were noticeably demanding. Again, considering almost straight road of the segment, the prediction suggests that the minimum force must be applied on a steering wheel by the driver. Though, the participant had to energetically act on the steering wheel.

On one hand, some tasks lead to comparative impact on driver's control over the vehicle. For this driver, the tasks number 6, 7, 8, 9, 14, and 15 were very influential. They caused speed decrease, what normally would irritate other traffic members. Simultaneously, the DD was the reason for departing the driving lane and unnecessarily active control of the steering wheel. The first one is a potential danger of collision, while the second one – of vehicle stability degradation.

Contrariwise, there are STs, which execution while driving does not affect driver's behaviour. For example, tasks 3, 4, 10, and 11 did not cause the driver either to increase/decrease vehicle velocity, or to drive the car off the driving lane, or to drastically act on the steering wheel (Figure 20). Consequently, by comparing the predicted driver performance to the performance under the influence of the ST, the abnormal driving behaviour can be easily recognized. Taking into consideration that this behaviour is accompanied with distractive ST accomplishment, it can be concluded that the method is effectively capable of DD detection.

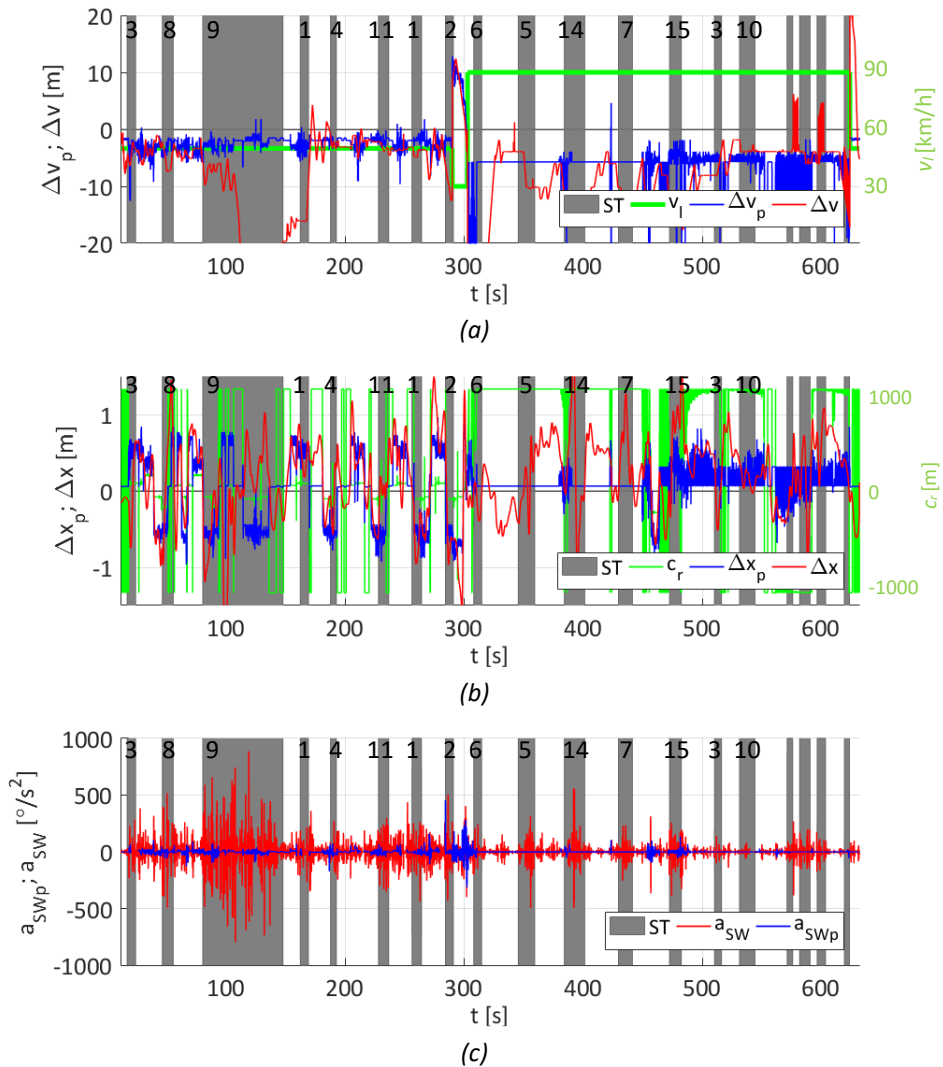


Figure 20. Driving with ST accomplishment versus driver performance prediction: (a) vehicle speed deviation; (b) lane keeping offset; (c) steering wheel acceleration.

### 3.2.4.2 Resultative performance

The resultative driving performance,  $\Delta v_r$ ,  $\Delta x_r$ ,  $a_{swr}$ , diagrams are presented in Figure 21. The red curve depicts driver's performance while completing the STs. The purple lines are the resultative performances, which are the products of equations (3.1) – (3.3). The plots show the difference between predicted and real values. Fundamentally, the purple curve is a difference between red and blue plots from Figure 20 for each performance-based variable.

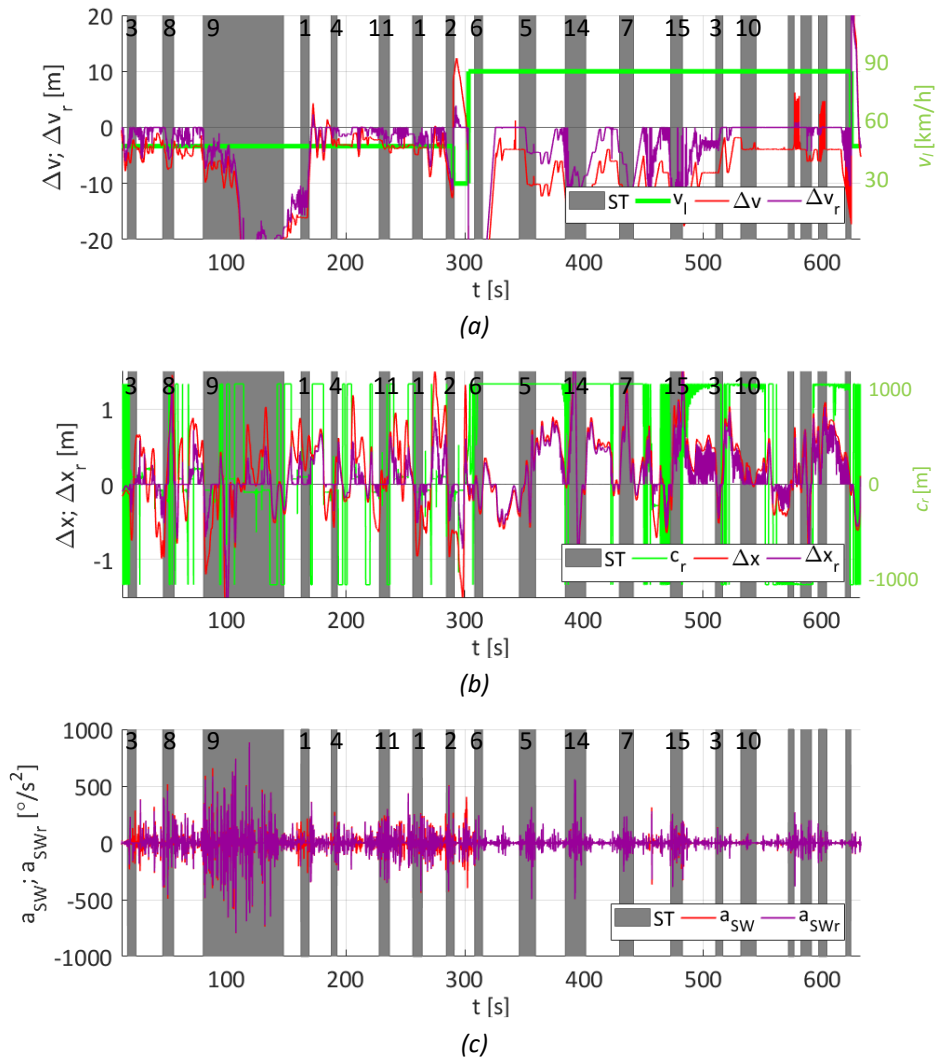


Figure 21. Resultative driver performance-based measures versus driving with secondary task accomplishment: (a) vehicle speed deviation; (b) lane keeping offset; (c) steering wheel acceleration.

### 3.2.4.3 Driver distraction evaluation

The final stage of the method is DD evaluation with fuzzy logic. The results of performance-based data fusion by the FLC are shown in Figure 22. The black area shows the level of DD expressed in percentage.

In 3.2.4.2, it has been concluded that STs 6, 7, 8, 9, 14, and 15 were very demanding, what caused considerable variation in driver's vehicle operation. This variation had sensible impact on safe vehicle driving. As a result, the fuzzy-logic-based Evaluator measures exclusively high level of *DD* for these STs, while for the other tasks and also for normal driving with ST (white background) the level of *DD* is very low, less than 20%.

Driver distraction remains high even after ST fulfilment. As it has been noticed by the experimenter, it happens, because the drivers, after completing the ST, realize their

performance errors and try to correct them as fast as feasible. This leads to additional mistakes in vehicle control. Therefore, DD is dangerous not only during the IVIS operation, but also after the secondary activity execution.

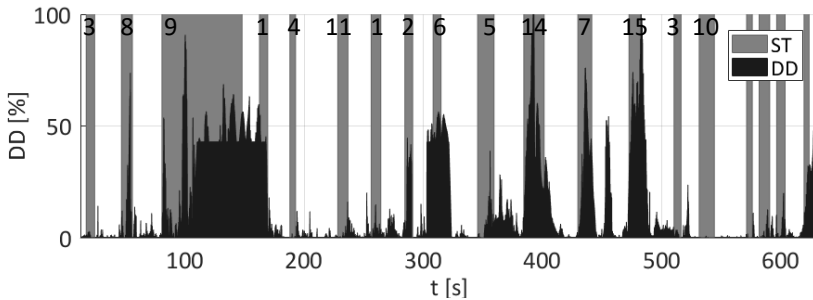


Figure 22. Driver distraction evaluation.

### 3.3 Summary

The DD detection and evaluation method based on CI algorithms combination is described in this Chapter. The method contains three blocks: a unique for each individual Driver model, a subsystem for driver performance errors measurement, and total DD calculation with fuzzy logic. The method tends to predict human performance on a given road segment using previously collected data. This performance is then compared to driving under DD. At last, the result of the data comparison passes through fuzzy-logic-based Evaluator to turn into the conclusive level of DD measured in percentage (VI).

A sub-block of the method, Driver model (Figure 13), is completed with ML algorithm. It acquires an information about the road (i.e. curvature, direction, and speed limit) and generates vehicle dynamic performance on a given road segment. Several nonlinear regression methods were examined on accuracy of driver performance prediction (VIII). The most precise model was achieved using  $k$ -NN, which is recommended for creating a unique driver performance model for each person for DD and autonomous driving research (IV).

The method is verified in a set of DIL experiments with real people. First, a single ST's (i.e. text messaging on a cellular phone) impact on DD was studied on a simple car simulator (II), (VI). The final experiment was conducted on an advanced driver simulator with an identical to ground vehicles cockpit. Multiple STs from IVIS were studied on their influence on DD. The methodology is divided to two phases. During the first one the data from DD-free driving is collected for driver performance modelling. The second stage involves ST accomplishment in parallel to driving a vehicle (III), (V), (VIII).

The results showed that the method is efficient in abnormal driving recognition simultaneously considering multiple performance-based measures. From the recognized unusual behaviour, the method is capable of not only detecting DD, but also of precisely measuring its level. Hence, it allows for studying the secondary activity impact on safe vehicle control and for comparative analysis of different STs' influences on DD. The method is exploited as a benchmark for safe and intuitive IVIS design with minimum DD in passenger vehicles (VI).

## 4 Conclusions and future works

### 4.1 Conclusions

In addition to transportation, vehicle technology (i.e. marine, air, and ground vehicles) must ensure safety of occupants, goods, and environment, which has higher priority than time or cost. Vehicle safety systems address a large variety of safety matters such as providing optimal stability control, collision avoidance, enhanced vehicle handling, etc. One of the oldest vehicle safety systems, ABS, aims at decelerating a vehicle as fast as possible along with simultaneous maintaining steerability and driving stability during an emergency braking manoeuvre. Furthermore, in addition to vehicle longitudinal and lateral control, traffic perception, route planning, etc., drivers often perform secondary activities, like interaction with IVIS. Due to exceeding multitasking, ST-induced DD contributes to a significantly large number of traffic accidents with fatal outcomes. Therefore, DD elimination is a vital challenge for human, vehicle, and environmental safety.

To meet rapidly expanding safety requests, the FLC-based blended ABS control method accompanied with simple, yet effective road surface recognition is herein presented. With respect to other related works analysed in subchapter 1.2.2, the MISO structured FLC recognizes road surface and holds optimal wheel slip simultaneously for each wheel of electric SUV separately. Hence, the CI method works as a vehicle–environment interaction and as a controller at the same time and can potentially be adopted to any other ground vehicle. The offered control method avoids complex mathematical modelling, state estimation, and feedback control loop. What is more, it secures an efficient interaction between ill-defined environment and vehicle for such a complex and nonlinear plant, like ABS.

The road identification is accomplished through vehicle body deceleration rate and inferred by the FLC, which serves as a knowledge-based artificial decision-making system. By tracking current wheel slip, the same FLC determines optimal braking torque for both FB and RB actuators to ensure maximum efficient deceleration on a various road surfaces. The systems are blended to achieve high safety performance during emergency braking. Priority is given to the RB with electric motors to maximize energy recuperation on a given road surface. Only when the torque generated from electric motors is not enough to reach the optimal slip, the control method requests additional braking force from the conventional FB. Moreover, the blending strategy considers the SOC of a battery to make sure that it will not lead to overcharge during energy recuperation. Therefore, the new blended mechanism allows for recovering as much energy as possible from braking manoeuvres, decelerating vehicle as fast as feasible, and mitigating the use of conventional braking, hence, reducing the energy dissipation.

The blended ABS control method is verified in HIL test with experimentally validated electric SUV equipped with four on-board electric motors. The HIL platform features a personal computer connected to the EHB test rig capable of reproducing real pressure dynamics of the brake circuit and simulating a variety of tire–road adhesions conditions and brake blending scenarios. The experiment is conducted on transient road surface. The results promise vehicle's stopping distance decrease in comparison to deceleration with only conventional EHB or no ABS activation. In addition, torque blending strategy allows for up to 10% of energy recovery and simultaneous vehicle battery safety

consideration. The results also demonstrate method's robustness against dynamically changing environment and ABS's supreme safety feature functionality.

From the other side, the state-of-the-art solutions analysed in 1.3.2 propose accurate DD detection in human interacting with ST. The common disadvantage of the conventional approaches is binary classification allowing for output only two variables: distracted/non-distracted. This simple classification is not sufficient for precise HMI technology comparative analysis and consequent ground vehicle cockpit design prioritizing occupants and vehicle safety on fullest. Therefore, a new method is herein introduced capable not only to detect DD, but also to measure and evaluate its impact on vehicle dynamic performance by solving a nonlinear regression problem. This method is essential for passenger vehicle cockpit and HMI technology design.

The method combines CI algorithms. It includes several steps: a model of normal driving for each individual person built with ML techniques; a subsystem for performance-based errors calculation; and an intelligent module for data fusion and total level of DD evaluation. The ML defines a usual driver performance on a specific road segment. To recognize DD, a normal driving is compared to a distracted human behaviour. The final step is fulfilled with FLC, whose main task is to evaluate and measure the level of DD in percentage referring to vehicle dynamic performance errors.

A novel driver model is introduced in a framework of the DD detection and evaluation methodology. It accepts an information about the road environment, namely road segment speed limitation, direction, and curvature, and outputs each individual driver's road lane keeping and speed maintenance abilities and steering wheel force. Hence, a model forecasts, how accurate each driver performs on various road segments from safety point of view. Several most superb and practically applicable ML algorithms for nonlinear regression are compared on a precision of driver performance prediction. The  $k$ -NN outperformed such other studied algorithms as ANN, fuzzy-neural system, layer-recurrent ANN, and Gaussian process regression models.

The designed method is verified on a fixed-base vehicle simulator identical to ground vehicles. Virtual world is shown on the wall in front of the test rig. Thirty drivers contributed to the DIL experimental study. Several IVIS operations were exploited as STs. The DIL results demonstrate that the method is capable to detect abnormal and hazardous driving and to measure a level of DD for specifically driver-IVIS interactions. The results delivered precise measurement of DD level, allowing for examining each ST separately and comparing them between each other on a degree of safety.

In sum, the experimental results have shown that CI-based control systems have a huge potential in improving existing safety systems in ground vehicles. With human-driver-environment interaction, vehicle, driver, and environmental sustainability are significantly improved. This has been achieved thanks to novel intelligent control algorithms, namely CI, what is not possible for traditional controllers due to lack of robustness to dynamically changing environment and human factors.

## 4.2 Future works

As it is mentioned in Chapter 1 (Figure 1), ground vehicle safety systems are not limited with only ABS and DD detection systems. There are lots of other systems exist, moreover, new safety systems will likely appear in the nearest future as the transportation systems are constantly being developed. In the future, the extension of CI-based safety systems is planned, firstly, on theoretical level, and after – in practical application.

Traction control system and electronic stability control will be interacted with human and environment, because in those systems the latter plays an essential role in case of efficiency and functionality. Electronic stability program, for example, will take into consideration road curvature and applied steering wheel angle by the driver to ensure stability of the vehicle on a changing road surfaces. Traction control system will, for instance, consider vehicle tilt angle, etc. For collision avoidance system, vehicle must interact not only with the environment, but also with other humans (e.g. pedestrians, other drivers, cyclists).

Passive safety systems have also room for improvement, what can be fulfilled with CI. For instance, ML will be used in vehicle body design, which will be optimal under various deformation cases. Airbags, for example, thanks to interaction with the environment and other drivers will be inflating before the actual collision, avoiding traumatic impact on occupants, what can be again completed by CI algorithms.

As for the blended ABS control method, it will be tested on a real SUV with four on-board motors powertrain. Concerning DD detection and evaluation method, its slightly simplified version will be used for practical evaluation of the HMI concepts before installation in ground vehicle. Another possible system's extension is a DD alert system, which can be installed in a ground vehicle as an advanced safety system. Ultimately, the DD detection and evaluation method also misses statistical analysis of every possible ST.

## List of Figures

Figure 1. Road safety concept and influencing variables (adapted from (Post, Motor–vehicle safety, 2014)).	16
Figure 2. Road safety concept and influencing variables of the studied safety systems.	17
Figure 3. A simplified schematic drawing of a braked wheel for a single–wheel model.	24
Figure 4. Block scheme of the blended antilock braking system control method for a single wheel: RB FLC – regenerative braking fuzzy logic controller; FB FLC – friction braking fuzzy logic controller. The symbols’ description is introduced in Symbols.	26
Figure 5. Fuzzy logic controller’s membership functions and fuzzification interface for randomly chosen $\lambda$ and $\mu^*$ : $\mu(\lambda / \mu^*)$ – membership degree of an input.	28
Figure 6. Front wheel RB FLC rule base (Table 1) transformation into matrix R.	30
Figure 7. FLC 3D surfaces for RB and FB front (subscript ‘f’) and rear (subscript ‘r’) wheels.	30
Figure 8. Torque blending strategy flowchart for a single wheel.	31
Figure 9. Tire–road friction–slip curves for a modelled with Pacejka’s “Magic Formula 6.1” (Pacejka, 2012) tire on various road surfaces: (a) front wheels; (b) rear wheels.	33
Figure 10. EHB hardware–in–the–loop test bed at Technische Universität Ilmenau (Germany): 1 – brake disk; 2 – brake caliper; 3 – master cylinder with reservoir.	34
Figure 11. Hardware–in–the–loop hardware and software communication.	35
Figure 12. Hardware–in–the–loop simulation results of blended antilock braking system control method from braking on varying road surface (from high- $\mu$ to low- $\mu$ ): (a) vehicle and wheels speed; (b) wheels longitudinal slips; (c) RB torques; (d) FB torques; (e) road detection with vehicle body deceleration. Subscript “i” is for each wheel: [front left (FL), front right (FR), rear left (RL), rear right (RR), f – front, r – rear].	36
Figure 13. Drive distraction detection and evaluation method block scheme. The symbols’ descriptions are listed in Symbols. Superscript “t” refers to “training set” collected during the distraction–free driving.	38
Figure 14. Driver performance–based measure, lane keeping ability: light blue dotted line – $\Delta x_p$ ; blue solid line – $\Delta x$ ; red surface – $\Delta x_r$ .	39
Figure 15. Driver performance–based measure, speed limit keeping ability: light blue dotted line – $\Delta v_p$ ; blue solid line – $\Delta v$ ; red surface – $\Delta v_r$ .	39
Figure 16. DD detection and evaluation method’s input MFs: (a) resultative speed keeping ability; (b) resultative lane keeping offset; (c) resultative steering wheel acceleration.	42
Figure 17. Fuzzy logic Evaluator 3D surfaces for several constant steering wheel acceleration values: (a) -500; (b) 0; (c) 300; (d) 500.	43
Figure 18. Multiple secondary tasks experiment test facilities: (a) advanced vehicle simulator; (b) a participant operating the simulator while performing a secondary task.	45
Figure 19. Driver performance prediction in comparison to training set: (a) vehicle speed deviation; (b) lane keeping offset; (c) steering wheel acceleration.	47
Figure 20. Driving with ST accomplishment versus driver performance prediction: (a) vehicle speed deviation; (b) lane keeping offset; (c) steering wheel acceleration.	49
Figure 21. Resultative driver performance–based measures versus driving with secondary task accomplishment: (a) vehicle speed deviation; (b) lane keeping offset; (c) steering wheel acceleration.	50
Figure 22. Driver distraction evaluation.	51

## List of Tables

Table 1. Fuzzy logic controller rule base for regenerative braking for front / rear wheels.	29
Table 2. Fuzzy logic controller rule base for friction braking for front / rear wheels. ....	29
Table 3. Optimal wheels' slip rates and vehicle's body deceleration values for common road surfaces.....	33
Table 4. Fuzzy logic Evaluator rule base.....	42

## References

- Alizadeh, V., & Dehzangi, O. (2016). The Impact of Secondary Tasks on Drivers During Naturalistic Driving: Analysis of EEG Dynamics. *Proceedings of the 2016 IEEE 19th International Conference on Intelligent Transportation Systems (ITSC)* (pp. 2493–2499). Rio de Janeiro: IEEE.
- Alpaydin, E. (2004). *Introduction to Machine Learning*. Cambridge, MA, USA: MIT Press.
- Aly, A. A. (2010). Intelligent Fuzzy Control for Antilock Brake System with Road–Surfaces Identifier. *Proceedings of the 2010 IEEE International Conference on Mechatronics and Automation* (pp. 699–705). Xi'an: IEEE.
- Arun, S., Sundaraj, K., & Murugappan, M. (2012). Driver Inattention Detection Methods: A review. *Proceedings of the 2012 IEEE Conference on Sustainable Utilization and Development in Engineering and Technology (STUDENT)* (pp. 1–6). Kuala Lumpur: IEEE.
- Ashenbrenner, K. M., Biehl, B., & Wurm, G. W. (1987). Einfluss Der Risikokompensation auf die Wirkung von Verkehrssicherheitsmassnahmen am Beispiel ABS. *Unfall- und Sicherheitsforschung Strassenverkehr*(63), 65–70.
- Azman, A., Ibrahim, S. Z., Meng, Q., & Edirisinghe, E. A. (2014). Physiological Measurement Used in Real Time Experiment to Detect Driver Cognitive Distraction. *Proceedings of the 2014 International Conference on Electronics, Information and Communications (ICEIC)* (pp. 1–5). Kota Kinabalu: IEEE.
- Babaeian, M., Bhardwaj, N., Esquivel, B., & Mozumdar, M. (2016). Real Time Driver Drowsiness Detection Using a Logistic–Regression–Based Machine Learning Algorithm. *Proceedings of the 2016 IEEE Green Energy and Systems Conference (IGSEC)* (pp. 1–6). Long Beach: IEEE.
- Başlamışlı, S. Ç., Köse, İ. E., & Anlaş, G. (2007). Robust control of anti–lock brake system. *Vehicle System Dynamics, International Journal of Vehicle Mechanics and Mobility*, 45(3), 217–232. doi:10.1080/00423110600882498
- Billah, T., Rahman, S. M., Ahmad, M. O., & Swamy, M. (2018). Recognizing Distractions for Assistive Driving by Tracking Body Parts. *IEEE Transactions on Circuits and Systems for Video Technology (Early Access)*, 1–15.
- Cabrera, J. A., Ortiz, A., Castillo, J. J., & Simon, A. (2005). A Fuzzy Logic Control for Antilock Braking System Integrated in the IMMa Tire Test Bench. *IEEE Transactions on Vehicular Technology*, 54(6), 1937–1949.
- Castillo, J. J., Cabrera, J. A., & Guer, A. J. (2016). A Novel Electrohydraulic Brake System with Tire–Road Friction Estimation and Continuous Brake Pressure Control. *IEEE Transactions on Industrial Electronics*, 63(3), 1863–1875.
- Castillo, O. (2012). *Type–2 Fuzzy Logic in Intelligent Control Applications*. Berlin, Germany: Springer–Verlag Berlin Heidelberg.
- Chen, H., Yang, J., Du, Z., & Wang, W. (2010). Adhesion Control Method Based on Fuzzy Logic Control for Four–Wheel–Driven Electric Vehicle. *SAE International Journal of Passenger Cars – Mechanical Systems*, 3(1), 217–225.
- Choi, I.–H., Hong, S. K., & Kim, Y.–G. (2016). Real–Time Categorization of Driver's Gaze Zone Using the Deep Learning Techniques. *Proceedings of the 2016 International Conference on Big Data and Smart Computing (BigComp)* (pp. 143–148). Hong Kong: IEEE.
- Cikaneck, S. R. (1994, October 25). *USA Patent No. 5 358 317*.

- Communication from the Commission to the European Parliament, the Council, the European Economic and Social Committee and the Committee of the Regions. (2018, May 17). *Europe on the Move. Sustainable Mobility for Europe: safe, connected, and clean*. Retrieved from [https://ec.europa.eu/https://ec.europa.eu/transport/sites/transport/files/3rd-mobility-pack/com20180293-communication\\_en.pdf](https://ec.europa.eu/https://ec.europa.eu/transport/sites/transport/files/3rd-mobility-pack/com20180293-communication_en.pdf)
- Craye, C., Rashwan, A., Kamel, M. S., & Karray, F. (2016). A Multi-Modal Driver Fatigue and Distraction Assessment System. *International Journal of Intelligent Transportation Systems Research*, 14(3), 173–194.
- Ehsani, M., Gao, Y., Gay, S. E., & Emadi, A. (2005). *Modern Electric, Hybrid Electric, and Fuel Cell Vehicles: Fundamentals, theory, and design*. Boca Raton, Florida, USA: CRC Press LLC.
- El-Garhy, A. M., El-Sheikh, G. A., & El-Saify, M. H. (2013). Fuzzy Life-Extending Control of Anti-Lock Braking System. *Ain Shams Engineering Journal*, 734–751.
- Ersal, T., Fuller, H. J., Tsimhoni, O., Stein, J. L., & Fathy, H. K. (2010). Model-Based Analysis and Classification of Driver Distraction Under Secondary Tasks. *IEEE Transactions on Intelligent Transportation Systems*, 11(3), 692–701.
- European Union. (2017). *Road Safety Newsletter*. Brussels: Directorate-General for Mobility and Transport. Retrieved from [https://ec.europa.eu/transport/road\\_safety/sites/roadsafety/files/nl27\\_en.pdf](https://ec.europa.eu/transport/road_safety/sites/roadsafety/files/nl27_en.pdf)
- Goodfellow, I., Bengio, Y., & Courville, A. (2016). *Deep Learning*. Cambridge, MA, USA: MIT Press.
- Guo, J., Jian, X., & Lin, G. (2014). Performance Evaluation of an Anti-Lock Braking System for Electric Vehicles with a Fuzzy Sliding Mode Controller. *Energies*, 7(10), 6459–6476.
- Hart, S. G., & Staveland, L. E. (1988). Development of NASA-TLX (Task Load Index): Results of empirical and theoretical research. *Advances in Psychology*, 52, 139–183.
- Horberry, T., Anderson, J., Regan, M. A., Triggs, T. J., & Brown, J. (2006). Driver Distraction: The effects of concurrent in-vehicle tasks, road environment complexity and age on driving performance. *Accident Analysis and Prevention*, 38, 185–191.
- Huynh, X.-P., Park, S.-M., & Kim, Y.-G. (2017). Detection of Driver Drowsiness Using 3D Deep Neural Network and Semi-Supervised Gradient Boosting Machine. In C. Chen, J. Lu, & K. Ma, *Computer Vision – ACCV 2016 Workshops. ACCV 2016. Lecture Notes in Computer Science* (pp. 134–145). Springer.
- Im, S., Lee, C., Yang, S., Kim, J., & You, B. (2014). Driver Distraction Detection by In-Vehicle Signal Processing. *Proceedings of the 2014 IEEE Symposium on Computational Intelligence in Vehicles and Transportation Systems (CIVTS)* (pp. 64–68). Orlando: IEEE.
- Iranmanesh, S. M., Mahjoub, H. N., Kazemi, H., & Fallah, Y. P. (2018). An Adaptive Forward Collision Warning Framework Design Based on Driver Distraction. *IEEE Transactions on Intelligent Transportation Systems*, 19(12), 3925–3934.
- Ivanov, V. (2015). A Review of Fuzzy Methods in Automotive Engineering Applications. *European Transport Research Review*, 7(29), 19–29.
- Ivanov, V. G., Algin, V. B., & Shyrokau, B. N. (2006). Intelligent Control for ABS Application with Identification of Road and Environmental Properties. *International Journal of Vehicle Autonomous Systems*, 4(1), 44–67.

- Ivanov, V., & Shyrokau, B. (2010). Fuzzy Architecture of Safety–Relevant Vehicle Systems. *Proceedings of the 4th International Workshop on Reliable Engineering Computing (REC 2010)*, (pp. 57–75). Singapore.
- Jacquet, A., Chamaillard, Y., Basset, M., Gissinger, G., Frank, D., & Garcia, J. P. (2008). Anti-Lock Braking System Using Predictive Control and On-Line Tire/Road Characteristics Estimation. *IFAC Proceedings Volumes*, 41(2), 2099–2104.
- Jalali, K., Uchida, T., McPhee, J., & Lambert, S. (2012). Development of a Fuzzy Slip Control System for Electric Vehicles with In–wheel Motors. *SAE International Journal of Alternative Powertrains*, 1(1), 46–64.
- Jang, J.–S. R., Sun, C.–T., & Mizutani, E. (1997). *Neuro–Fuzzy and Soft Computing: A computational approach to learning and machine intelligence*. NJ, USA: Prentice–Hall, Inc.
- Jiao, Y., Peng, Y., Lu, B.–L., Chen, X., Chen, S., & Wang, C. (2014). Recognizing Slow Eye Movement for Driver Fatigue Detection with Machine Learning Approach. *Proceedings of the 2014 International Joint Conference on Neural Networks (IJCNN)* (pp. 4035–4041). Beijing: IEEE.
- Jiménez, P., Bergasa, L. M., Nuevo, J., Hernández, N., & Daza, I. G. (2012). Gaze Fixation System for the Evaluation of Driver Distraction Induced by IVIS. *IEEE Transactions on Intelligent Transportation Systems*, 13(3), 1167–1178.
- Jo, J., Lee, S. J., Jung, H. G., Park, K. R., & Kim, J. (2011). Vision–Based Method for Detecting Driver Drowsiness and Distraction in Driver Monitoring System. *Optical Engineering*, 50(12), 1–24.
- Khatun, P., Bingham, C. M., Schofield, N., & Mellor, P. H. (2003). Application of Fuzzy Control Algorithms for Electric Vehicle Antilock Braking/Traction Control Systems. *IEEE Transactions on Vehicular Technology*, 52(5), 1356–1364.
- Kiencke, U., & Nielsen, L. (2005). *Automotive Control Systems: For engine, driveline, and vehicle* (2nd ed.). Berlin: Springer–Verlag Berlin Heidelberg.
- Kim, D.–H., Kim, J.–M., Hwang, S.–H., & Kim, H.–S. (2007). Optimal Brake Torque Distribution for a Four–Wheeldrive Hybrid Electric Vehicle Stability Enhancement. *Proceedings of the Institution of Mechanical Engineers, Part D: Journal of Automobile Engineering*, 221(1), 1357–1366.
- Kim, M. H., & Son, J. (2011). On–Road Assessment of In–Vehicle Driving Workload for Older Drivers: Design guidelines for intelligent vehicles. *International Journal of Automotive Technology*, 12(2), 265–272.
- Koch–Dücker, H.–J., & Papert, U. (2014). Antilock braking system (ABS). In K. Reif, *Brakes, Brake Control and Driver Assistance Systems: Function, regulation and components* (pp. 74–93). Wiesbaden: Springer Vieweg.
- Lex, F., Langhans, P., Lee, J., & Reimer, B. (2016). Driver Gaze Region Estimation without Use of Eye Movement. *IEEE Intelligent Systems*, 31(3), 49–56.
- Li, H.–Z., Li, L., He, L., Kang, M.–X., Song, J., Yu, L.–Y., & Wu, C. (2012). PID Plus Fuzzy Logic Method for Torque Control in Traction Control System. *International Journal of Automotive Technology*, 13(3), 441–450.
- Li, Z., Bao, S., Kolmanovsky, I. V., & Yin, X. (2018). Visual–Manual Distraction Detection Using Driving Performance Indicators with Naturalistic Driving Data. *IEEE Transactions on Intelligent Transportation Systems*, 19(8), 2528–2535.
- Liang, Y., Lee, J. D., & Reyes, M. L. (2007). Nonintrusive Detection of Driver Cognitive Distraction in Real Time Using Bayesian Networks. *Transportation Research Record: Journal of the transportation research board*, 2018(1), 1–8.

- Liang, Y., Reyes, M. L., & Lee, J. D. (2007). Real-Time Detection of Driver Cognitive Distraction Using Support Vector Machines. *IEEE Transactions on Intelligent Transportation Systems*, 8(2), 340–350.
- Liao, Y., Li, S. E., Wang, W., Wang, Y., Li, G., & Cheng, B. (2016). Detection of Driver Cognitive Distraction: A comparison study of stop-controlled intersection and speed-limited highway. *IEEE Transactions on Intelligent Transportation Systems*, 17(6), 1628–1637.
- Lin, C.-M., & Hsu, C.-F. (2003). Self-Learning Fuzzy Sliding-Mode Control for Antilock Braking Systems. *IEEE Transactions on Control Systems Technology*, 11(2), 273–278.
- Lin, C.-M., & Li, H.-Y. (2013). Intelligent Hybrid Control System Design for Antilock Braking Systems Using Self-Organizing Function-Link Fuzzy Cerebellar Model Articulation Controller. *IEEE Transactions on Fuzzy Systems*, 21(6), 1044–1055.
- Liu, T., Yang, Y., Huang, G.-B., Yeo, Y. K., & Lin, Z. (2016). Driver Distraction Detection Using Semi-Supervised Machine Learning. *IEEE Transactions on Intelligent Transportation Systems*, 17(4), 1108–1120.
- Martínez, V., del Campo, I., Echanobe, J., & Basterretxea, K. (2015). Driving Behavior Signals and Machine Learning: A personalized driver assistance system. *Proceedings of the 2015 IEEE 18th International Conference on Intelligent Transportation Systems* (pp. 2933–2940). Las Palmas: IEEE.
- Matsuo, H., & Khiat, A. (2012). Prediction of Drowsy Driving by Monitoring Driver's Behavior. *Proceedings of the 21st International Conference on Pattern Recognition (ICPR2012)* (pp. 3390–3393). Tsukuba: IEEE.
- Mauer, G. F. (1995). A Fuzzy Logic Controller for an ABS Braking System. *IEEE Transactions on Fuzzy Systems*, 3(4), 381–388.
- Mirzaei, A., Moallem, M., Dehkordi, B. M., & Fahimi, B. (2006). Design of an Optimal Fuzzy Controller for Antilock Braking Systems. *IEEE Transactions on Vehicular Technology*, 55(6), 1725–1730.
- Miyajima, C., & Takeda, K. (2016). Driver-Behavior Modeling Using On-Road Driving Data: A new application for behavior signal processing. *IEEE Signal Processing Magazine*, 33(6), 14–21.
- Mühlbacher-Karrer, S., Mosa, A. H., Faller, L.-M., Ali, M., Hamid, R., Zangl, H., & Kyamakya, K. (2017). A Driver State Detection System – Combining a Capacitive Hand Detection Sensors with Physiological Sensors. *IEEE Transactions on Instrumentation and Measurement*, 66(4), 624–363.
- National Traffic Law Center. (2017). *Investigation and Prosecution of Distracted Driving Case*. Washington, DC: National Highway Traffic Safety Administration.
- Negnevitsky, M. (2005). *Artificial Intelligence: A guide to intelligent systems* (2nd ed.). Harlow, UK: Addison-Wesley.
- Pacejka, H. (2012). *Tyre and Vehicle Dynamics* (3rd ed.). Oxford, UK: Butterworth-Heinemann.
- Papantoniou, P., Papadimitriou, E., & Yannis, G. (2017). Review of Driving Performance Parameters Critical for Distracted Driving Research. *Transportation Research Procedia*, 25, 1798–1805.
- Passino, K., & Yurkovich, S. (1998). *Fuzzy Control*. Menlo Park, California, USA: Addison-Wesley Longman, Inc.

- Paul, D., Velenis, E., Cao, D., & Dobo, T. (2017). Optimal  $\mu$ -Estimation Based Regenerative Braking Strategy for an AWD HEV. *IEEE Transactions on Transportation Electrification*, 3(1), 249–258.
- Peng, X., Jia, M., He, L., Yu, X., & Lv, Y. (2018). Fuzzy Sliding Mode Control Based on Longitudinal Force Estimation for Electro-Mechanical Braking Systems Using BLDC Motor. *CES Transactions on Electrical Machines and Systems*, 2(1), 142–151.
- Perić, S. L., Antić, D. S., Milovanović, M. B., Mitić, D. B., Milojković, M. T., & Nikolić, S. S. (2016). Quasi-Sliding Mode Control With Orthogonal Endocrine Neural Network-Based Estimator Applied in Anti-Lock Braking System. *IEEE/ASME Transactions on Mechatronics*, 21(2), 754–764.
- Post, W. (2014). Car braking systems. In K. Reif, *Brakes, Brake Control and Driver Assistance Systems: Function, regulation and components* (pp. 28–39). Wiesbaden, Germany: Springer Vieweg.
- Post, W. (2014). Motor-vehicle safety. In K. Reif, *Brakes, Brake Control and Driver Assistance Systems: Function, regulation and components* (pp. 2–11). Wiesbaden, Germany: Springer Vieweg.
- Pusca, R., Ait-Amirat, Y., Berthon, A., & Kauffmann, J.-M. (2004). Fuzzy-Logic-Based Control Applied to a Hybrid Electric Vehicle with Four Separate Wheel Drives. *IEE Proceedings – Control Theory and Applications*, 151(1), 73–81.
- Rajamani, R. (2012). *Vehicle Dynamics and Control* (2nd ed.). New York, NY, USA: Springer.
- Rajesh, R., Srinath, R., Sasikumar, R., & Subin, B. (2016). Modeling Safety Risk Perception due to Mobile Phone Distraction Among Four Wheeler Drivers. *IATSS Research*, 41, 30–37.
- Regan, M. A., Young, K. L., & Lee, J. D. (2009). Introduction. In M. A. Regan, J. D. Lee, & K. L. Young, *Driver Distraction: Theory, effects, and mitigation* (pp. 3–7). Boca Raton, FL, USA: Taylor & Francis Group, LLC.
- Regan, M. A., Young, K. L., Lee, J. D., & Gordon, C. P. (2009). Sources of driver distraction. In M. A. Regan, K. L. Young, & J. D. Lee, *Driver Distraction: Theory, effects, and mitigation* (pp. 249–279). Boca Raton, FL, USA: Taylor & Francis Group, LLC.
- Regolin, E., Incremona, G. P., & Ferrara, A. (2017). Longitudinal Vehicle Dynamics Control via Sliding Modes Generation. In A. Ferrara, *Sliding Mode Control of Vehicle Dynamics* (pp. 33–76). IET Digital Library.
- Schwarz, C., Brown, T., Lee, J., Gaspar, J., & Kang, J. (2016). The Detection of Visual Distraction Using Vehicle and Driver-Based Sensors. *Proceedings of the SAE 2016 World Congress and Exhibition*. SAE.
- Sharkawy, A. B. (2010). Genetic Fuzzy Self-Tuning PID Controllers for Antilock Braking Systems. *Engineering Applications of Artificial Intelligence*, 23(7), 1041–1052.
- Sigari, M.-H., Fathy, M., & Soryani, M. (2013). A Driver Face Monitoring System for Fatigue and Distraction Detection. *International Journal of Vehicular Technology*, 1–11.
- Smith, R. (2006, February 23). *Open Dynamics Engine v0.5: User guide*. Retrieved from <http://ode.org>: <http://ode.org/ode-latest-userguide.html>
- Taherisadr, M., Asnani, P., Galster, S., & Dehzangi, O. (2018). ECG-Based Driver Inattention Identification During Naturalistic Driving Using Mel-Frequency Cepstrum 2-D Transform and Convolutional Neural Networks. *Smart Health*, 9(10), 50–61.

- Takahashi, H., & Ishikawa, Y. (1989, June 27). *USA Patent No. 4 842 342*.
- Tanelli, M., Astolfi, A., & Savaresi, S. M. (2006). Robust Nonlinear Proportional-Integral Control for Active Braking Control Systems. *Proceedings of the 45th IEEE Conference on Decision and Control*. San Diego: USA. doi:10.1109/CDC.2006.377194
- Tango, F., & Botta, M. (2013). Real-Time Detection System of Driver Distraction Using Machine Learning. *IEEE Transactions on Intelligent Transportation Systems*, *14*(2), 894–905.
- The International Traffic Safety Data and Analysis Group. (2018). *Road Safety Annual Report 2018*. ITF/OEDC.
- Vora, S., Rangesh, A., & Trivedi, M. M. (2018). Driver Gaze Zone Estimation Using Convolutional Neural Network: A general framework and ablative analysis. *IEEE Transactions on Intelligent Vehicles*, *3*(3), 254–265.
- Wang, S., Zhang, Y., Wu, C., Darvas, F., & Chaovalitwongse, W. A. (2014). Online Prediction of Driver Distraction Based on Brain Activity Patterns. *IEEE Transactions on Intelligent Transportation Systems*, *16*(1), 135–150.
- Westin, M., Dougherty, R., Depcik, C., Hausmann, A., & Sprouse III, C. (2013). Development of an Adaptive Human–Machine–Interface to Minimize Driver Distraction and Workload. *Proceedings of the ASME 2013 International Mechanical Engineering Congress and Exposition* (pp. 1–13). San Diego: ASME.
- Wöllmer, M., Blaschke, C., Schindl, T., Schuller, B., Färber, B., Mayer, S., & Trefflich, B. (2011). Online Driver Distraction Detection Using Long Short-Term Memory. *IEEE Transactions on Intelligent Transportation Systems*, *12*(2), 574–582.
- World Health Organization. (2018). *Global Status Report on Road Safety 2018*. Geneva: World Health Organization.
- Xu, G., Xu, K., Zheng, C., Zhang, X., & Zahid, T. (2016). Fully Electrified Regenerative Braking Control for Deep Energy Recovery and Maintaining Safety of Electric Vehicles. *IEEE Transactions on Vehicular Technology*, *65*(3), 1186–1198.
- Yang, J., Chang, T. N., & Hou, E. (2010). Driver Distraction Detection for Vehicular Monitoring. *Proceedings of the IECON 2010 – 36th Annual Conference on IEEE Industrial Electronics Society* (pp. 108–113). Glendale: IEEE.
- Young, K. L., Regan, M. A., & Lee, J. D. (2009). Measuring the effects of driver distraction: direct driving performance methods and measures. In M. A. Regan, K. L. Young, & J. D. Lee, *Driver Distraction: Theory, effects, and mitigation* (pp. 85–105). Boca Raton, FL, USA: Taylor & Francis Group, LLC.
- Zabler, E. (2014). Sensors for brake control. In K. Reif, *Brakes, Brake Control and Driver Assistance Systems: Function, regulation and components* (pp. 142–153). Wiesbaden, Germany: Springer Vieweg.

## Acknowledgements

First of all, the author would like to express his sincere gratitude to his family and friends for their kind support, inspiration, motivation, and infinite love. This work would not be possible without their contribution.

Secondly, the author would like acknowledge his supervisors from Tallinn University of Technology (Estonia), senior lecturer Valery Vodovozov and Professor Eduard Petlenkov, and from Škoda Auto a.s. (Czech Republic), Dr Pavel Nedoma and Mr. Zdeněk Franc, for their motivation, help, supervision, and cooperation. The author would also like to acknowledge the contributions of both host organization Tallinn University of Technology and Škoda Auto a.s. administrative and teaching personal, where the author has been studying and working during his Ph.D. program. Additionally, special thanks to Professor Antonella Ferrara for pre-review of the draft dissertation, and to both opponents, PD Dr.–Ing. habil. Valentin Ivanov and Professor Alessandro Corrêa Victorino, for priceless comments on thesis improvement. Special thanks to the publications co-authors and reviewers.

The author would like to thank several funding organizations for financial support of the research conducted during the Ph.D. program: the European Union's Horizon 2020 research and innovation program under grant agreement No. 675999, MOE Scholarship Research Program of the German Federal Environmental Foundation (Deutsche Bundesstiftung Umwelt, DBU), and Estonian Ministry of Education and Research.

The author extends his appreciation to Secondments organisation for having him and supporting with the laboratory equipment. They are Technische Universität Ilmenau (Germany), IPG Automotive GmbH (Germany), and Virtual Vehicle Research Center (Austria).

Finally, the author shares his gratitude to the co-workers and friends from ITEAM<sup>19</sup> project, Tallinn University of Technology, Škoda Auto a.s., and many other organizations with whom the author had pleasure to cooperate.

---

<sup>19</sup> <https://iteam-project.net/>

## **Abstract**

### **Research and Development of Computational–Intelligence–Based Safety Systems for Ground Vehicles**

Traffic accidents have a terrible impact on societal, environmental, and economical norms all over the world. Unfortunately, the number of deplorable road accidents does not decrease annually even with constant advancements in transportation and road security. To raise the safety systems of ground vehicles to a new advanced level, vehicle–environment–driver interaction is of high importance. To some extent, due to problem uncertainty and complexity, multiple restrictions are caused by lack of intelligent control methods, what requires multidisciplinary solutions not attainable by classical controllers. Nonetheless, novel computational intelligence algorithms (i.e. artificial neural networks, fuzzy system, etc.) open a great opportunity for managing and creating synergy between complex stochastic plants and human factor. These algorithms provide capability to approximate qualitative aspect of human reasoning and decision–making process in human-machine-environment systems.

Hence, the motivation of this research is to significantly improve such essential and comprehensive ground vehicle safety modules, as antilock braking system and driver distraction detection and evaluation system, applying the computational intelligence approaches. On one hand, the antilock braking system complexity is caused by many nonlinearities, such as the hydraulic brake circuit dynamics and the tire–road adhesion coefficient characteristic, which considerably depends on road states (i.e. weather conditions and quality of the surface, temperature, etc.), as well as on vehicle conditions. On the other hand, driver distraction hardship is resonated with human factor, which is unpredictable and very comprehensive to deal with.

The developed antilock braking system control method accompanied with advanced torque blending strategy competently identifies the road surface and supplies optimal braking torque to each wheel for braking force maximization on varying driving conditions. Besides, the method utilizes electric actuators on their full potential to guarantee supreme energy recuperation under dynamically changing environment. It leads to vehicle steerability preservation, braking distance decrease, and maximum energy recuperation on highly changing road surfaces, what in its turn consolidates vehicle, occupants, and environmental safety at once. Accordingly, the new driver distraction detection and evaluation method based on the driver–vehicle interaction model provides minimization of secondary task impact on safe vehicle operation and traffic accidents, as well as human life protection. The machine–learning–based personalized detection method is unique for each independent driver, what only increases evaluation accuracy.

The results of hardware–in–the–loop experimentation with real electro–hydraulic brakes and electric sport utility vehicle model showed that the blended antilock braking system control method successfully recognizes road surface even under dynamically changing weather conditions, and supplies appropriate braking torque to guarantee maximum braking force on a given road surface. Moreover, the control method concentrates on regenerative braking on its full potential and turns on the conventional braking actuator only when maximum braking force is not achieved by the electric one.

The results of driver–in–the–loop experiment on advanced driver simulator and thirty participants demonstrated that the driver distraction detection and evaluation method not only detects driver distraction induced by abnormal driver’s behaviour, but also

precisely measures and predicts its impact on safe vehicle operation. The method's personalization allows for exclusive interaction between driver and vehicle. Hence, it promises comparative analyses of different human-machine interaction technologies in ground vehicles.

Comparing to other existing solutions the proposed blended antilock braking system is managed by a universal fuzzy logic unit, which serves as a road surface identifier and a controller simultaneously. Consequently, this research goes well beyond traditional mathematical modelling, state estimation, and set-point-oriented control in favour of enhanced system safety. Furthermore, the developed driver distraction detection and evaluation method, with respect to other related works, avoids simple solutions, where the output obtains only Boolean variables (i.e. distracted/non-distracted). It results in continuous level of driver distraction estimation, what allows for precise measurement of driver distraction influence on the secure vehicle control, and, consequent human-machine interface technology comparative analysis for safe vehicle cockpit design. The method combines machine learning as driver model and fuzzy logic as an intelligent evaluation.

In short, the dissertation results have shown that the computational intelligence methods permit a relevant improvement of stochastic ground vehicle safety at changing environmental and human factors, like antilock braking system and driver distraction detection and evaluation. Therefore, with the reinforced ground vehicle safety systems road security, environmental sustainability, and human life protection are noticeably improved.

## Lühikokkuvõte

### Tehisintellekti meetoditel põhinevate ohutussüsteemide uurimine ja arendamine maapealsete sõidukite jaoks

Liiklusõnnetused kohutavalt mõjutavad kogu maailma ühiskondlikke, keskkondlikke ja majanduslikke norme. Kahjuks ei vähene liiklusõnnetuste arv isegi transpordi- ja liiklusohutuse pideva edenemisega. Selleks, et tuua maapealsete sõidukite ohutussüsteemid uuele tasemele on sõiduki-keskkonna-juhi koostoime hädavajalik. Mingil määral, probleemi määramatuse ja keerukuse tõttu on ohutussüsteemide paranemine piiratud tarkade juhtimismeetodite puudumisega, mis nõuab teadmistel põhinevaid interdistsiplinaarseid lahendusi, ja mida klassikalised regulaatorid ei võimalda. Siiski, avavad uued tehisintellekti meetoditel põhinevad algoritmid (s. o. tehisnärvivõrgud, hägusloogikasüsteemid, jne.) suurepäraselt võimalust juhtida ning luua interaktsiooni keeruliste stohhastiliste protsesside vahel, nagu inimene-masin-keskkond süsteemid, mida iseloomustab täpse informatsiooni puudumine ja inimfaktor. Need algoritmid modelleerivad inimeste mõtlemise ja otsustuste tegemise protsessi kvalitatiivse aspekti.

Selle uurimistöo eesmärgiks on märkimisväärselt parandada maapealsete sõidukite olulised kuid väga keerulised ohutussüsteemid, nagu ABS-pidurid (blokeerumisvastane pidurisüsteem) ja sõidukijuhi tähelepanu häirituse tabamise ning hindamise meetod. Eesmärgi saavutamiseks sõiduki-keskkonna-juhi koostoime meetodid on täiendatud arukate algoritmidega. Ühelt poolt, põhjustavad ABS-pidurite keerukust mitmed dünaamilised mittelineaarsused ja rehvi-tee haardeteguri omadused, mis oluliselt sõltuvad tee (s. o. ilmastikutingimused ja teepinna kvaliteet, temperatuur, jne.) ja sõiduki seisukorrast (s. o. mass, rehvid, jne.). Teiselt poolt, häirib sõidukijuhi tähelepanu ettearvamatu inimfaktor.

Elektriautodele on välja töötanud ABS-piduri juhtimismeetod, millega kaasneb efektiivne rekuperatiivpidurduse ja mehaanilise piduri koostöö strateegia, ja mis tuvastab teepinna ja loob erinevatel teepindadel igale rattale optimaalse pidurdusjõu. Pealegi, kasutab juhtimismeetod pidurdamisel täielikku potentsiaaliga elektri ajameid. See garanteerib sõiduki juhitavuse tagamise, pidurdusteekonna vähenemise ja maksimaalse energia regenererimise pidevalt muutavas keskkonnas. Samuti tagab see sõiduki-, autojuhi- ja keskkonnaturvalisuse. Uus sõidukijuhi tähelepanu häirituse tabamise ja hindamise meetod määrab inimese-masina koostoime abil muude tingimuste mõju sõiduki ohutu juhtimisele, mis vähendab liiklusõnnetuste arvu ja avaldab positiivset mõju inimese kaitsele. Masinõpe algoritmil põhinev personaliseeritud sõidukijuhi tähelepanu häirituse tuvastamise mudel on igale juhile ainulaadne, mis ainult suurendab hindamise täpsust.

Hardware-in-the-loop simulatsiooni tulemused, kus elektro-hüdraulilise pidurisüsteemi katseseade on kombineeritud elektri-sportmaasturi matemaatilise mudeliga, näitasid, et ABS-piduri juhtimismeetod edukalt tuvastab teepinna dünaamiliselt muutavas keskkonnas ja annab sobiva pidurdusjõudu, et suurendada pidurdusvõimet antud teepinna peal. Peale selle, keskendub juhtimismeetod täielikku potentsiaaliga rekuperatiivpidurduse peale ja lülitab mehaanilise piduri sisse ainult siis, kui rekuperatiivpidurdusel genereeritud moment ei ole maksimaalse pidurdusjõudu saavutamiseks piisav.

Kolmekümne osalejatega sõidusimulaatoril läbi viidud driver-in-the-loop katsed näitasid, et pakutud ohutussüsteem edukalt tuvastab nii sõidukijuhi tähelepanu häirituse,

kui ka täpselt hindab selle mõju sõiduki ohutule juhtimisele. Meetodi personaliseerimine võimaldab unikaalse juhi–sõiduki vahelist koostoimet ja erinevate inimene–masinate liidesetehnoloogiate võrdleva analüüsi läbi viimist maapealsete sõidukite jaoks.

Võrreldes varem kasutusel olnud ABS–pidurite juhtimismeetoditega, kus olid samuti kasutatud arukad algoritmid, pakutud ABS–piduri juhtimismeetod juhib protsessi uude hägusloogika–kontrolleriga, mis toimib nii teepinna tuvastajana kui ka kontrollerina. Tulemusena, juhtimismeetod väldib keerulist matemaatilist mudelit, olekutaastajat ja seadesuurusele–orienteeritud juhtimist, kuid aga ohutussüsteemi funktsionaalsust kahjustamata. Peale selle, väldib arendatud sõidukijuhi tähelepanu häirituse tuvastamise ja hindamise meetod võrreldes varem välja töötatud meetoditega klassifitseerimist, kus väljund omab ainult binaarse väärtuse (s. o. häiritud / mittehäiritud). Selle tulemusena on sõidukijuhi tähelepanu häirituse pidevajanaline tuvastamine ja hindamine, mis mõõdab sõidukijuhi tähelepanu häirituse mõju auto juhtimisele. Järelikult, meetod võimaldab erinevate inimese–masinate liidesetehnoloogiate võrdleva analüüsi ja ohutu sõiduki kabiini projekteerimist. Meetod põhineb masinõpe ja hägusloogika algoritmide kombinatsioonil.

Kokkuvõtteks, kõik doktoritöös püstitatud eesmärgid on edukalt saavutatud. Katsetulemused näitasid, et tehisintellekti meetoditel põhinevad algoritmid võimaldavad oluliselt parendada maapealsete stohhastiliste sõidukite ohutussüsteeme, mis on seotud pidevalt muutuva keskkonna– ja / või inimfaktoriga, nagu näiteks ABS–piduri juhtimine ning sõidukijuhi tähelepanu häirituse tuvastamine ja hindamine. Selliste ohutussüsteemide funktsionaalsuse paranemiseks on inimese–masina–keskkonna koostöö vältimatu. Seetõttu, on paranenud uute ohutussüsteemidega sõidukite liiklusohutus, sealhulgas ka keskkonna ja inimelu turvalisus.



# Appendix 1

## Publication I

**Aksjonov, A.**, Augsburg, K., & Vodovozov, V. (2016). Design and Simulation of the Robust ABS and ESP Fuzzy Logic Controller on the Complex Braking Maneuvers. *Applied Sciences*, 6(12), 1–18. doi: 10.3390/app6120382



Article

# Design and Simulation of the Robust ABS and ESP Fuzzy Logic Controller on the Complex Braking Maneuvers

Andrei Aksjonov <sup>1,2,\*</sup>, Klaus Augsburg <sup>2</sup> and Valery Vodovozov <sup>1</sup>

<sup>1</sup> Faculty of Power Engineering, Tallinn University of Technology, Tallinn 12616, Estonia; valery.vodovozov@ttu.ee

<sup>2</sup> Department of Mechanical Engineering, Technische Universität Ilmenau, Ilmenau 98693, Germany; klaus.augsburg@tu-ilmenau.de

\* Correspondence: andrei.aksjonov@ttu.ee; Tel.: +49-157-8899-8333

Academic Editor: Arun Somani

Received: 5 September 2016; Accepted: 17 November 2016; Published: 25 November 2016

**Abstract:** Automotive driving safety systems such as an anti-lock braking system (ABS) and an electronic stability program (ESP) assist drivers in controlling the vehicle to avoid road accidents. In this paper, ABS and the ESP, based on the fuzzy logic theory, are integrated for vehicle stability control in complex braking maneuvers. The proposed control algorithm is implemented for a sport utility vehicle (SUV) and investigated for braking on different surfaces. The results obtained for the vehicle software simulator confirm the robustness of the developed control strategy for a variety of road profiles and surfaces.

**Keywords:** energy-efficient computing; fuzzy control; high-performance computer systems; road vehicles; vehicle safety

---

## 1. Introduction

The rapidly growing demand for passenger and commercial vehicles increases the number of road accidents around the world. In addition to their negative influence on road safety, accidents also have an indirect harmful impact on the environment and cause threats to human health and life. In cases when the human factor plays an important role, modern electronics and control systems may support the driver's reaction and skills to improve the stability and performance of the vehicle and avoid accidents. Two of the most important on-board safety systems are ABS and ESP. Both systems have become mandatory for all passenger vehicles and most commercial vehicles. The ABS and ESP safety features in vehicle dynamics control have been known for a long time. However, the existing control algorithms are rarely investigated from the viewpoint of robust operation in different road conditions. Many of the results discussed in the published studies are describing simple maneuvers, such as straight-line braking with a uniform road surface. Few investigations are known for emergency braking on complex road profiles, such as a curved road with split- $\mu$  or a curved road with varying tire-road friction coefficients.

Within the framework of the presented study, fuzzy theory has been selected for the controller implementation. The fuzzy logic controllers (FLC) are known as efficient tools in solving complex tasks such as ABS and ESP control. A combination of ABS and ESP can solve the robustness problem of the braking performance. To confirm it, the FLC-based braking will be discussed for the different complex maneuvers such as a combination of road profiles and split- $\mu$  road surfaces.

The first ABS applications arose several decades ago [1] and still use rule-based methods as the dominant control approach. In the modern ABS systems installed in commercial vehicles, the

braking pressure is increased or reduced based on the wheel speed and the slip switching threshold comparison [1]. The slip is set to a constant value, for instance 20% as it is optimal for the most common surface—dry asphalt. The braking surface is not recognized and the threshold value is equal for every road condition. This approach leads to energy losses because each road adhesive characteristic requires its optimal wheel slip value. This is why many researchers have focused on intelligent control algorithms for braking processes, trying to estimate an optimal one for every road condition slip threshold.

However, the analysis of the bibliography presented in [2] shows that nowadays the FLC is also being intensively used in ABS and ESP design. One of the first ABS control mechanisms based on the fuzzy algorithm was patented in 1989 by the Nissan Motor Co., Ltd., (Yokohama, Japan) [3]. Furthermore, many other solutions based on the FLC were proposed. Thanks to its simplicity and robustness, FLC proved to be equally applicable to on-road [4] and off-road vehicles [5].

In [6], a model reference adaptive control (MRAC) was introduced to tune the FLC in order to be able to control all kinds of nonlinear systems. Furthermore, the MRAC was used in a braking system in [7] as an ABS intelligent control. The simulation results were shown for a variety of road conditions (from icy to wet). The proposed solution requires a reference slip value, which is set to 20% for any kind of road surface. A similar assumption for the constant value of the optimal wheel slip is also proposed for ABS, as described in [8]. Another example is the model-based Takagi–Sugeno (T–S) FLC designed for a single-car model [9]. The controller copes well in optimal braking wheel slip maintenance, which the model considers a reference constant. Many different fuzzy proportional-integral-derivative (PID) approaches were also investigated [10–12]. Yet the results are limited because the situation considered in most cases is braking on a straight road with an optimal slip of 20%.

Adaptive and self-tuning intelligent FLC solutions have also been introduced in various studies [13,14]. In [15] a genetic neural FLC is designed, where the algorithm requires the reference wheel slip profile. The approach with the estimation of road parameters is used in [16], where various roads can be identified to keep the optimal slip by the controller. This controller demonstrated good performance but its operation was illustrated for simple straight braking maneuvers.

Many studies have presented the validation of fuzzy-based ABS algorithms through tests on a hardware-in-the-loop (HIL) experimental setup or ABS test bench connected to the real-time vehicle software simulator. For example, in [17] the authors introduced the fuzzy ABS with the road friction estimation algorithm. Consequently, the experiments were conducted for the variable road conditions proving the FLC robustness. In [18] the ABS algorithm holds the optimal wheel slip for different roads and is validated for quarter-car HIL systems.

For complex braking maneuvers on split- $\mu$  surfaces and curved roads the activation of the ESP system can be required. In this field, fuzzy logic methods are also finding wide application. For example, patents have been issued to FLC control algorithm, where yaw rate and steering wheel angle signals were considered the control inputs to maintain vehicle stability during braking [19]. Nevertheless, the described controller is still P or PD FLC, which requires the reference input.

In addition, many known examples are validated for specific maneuvers only. In particular, the PID FLC for yaw motion control [20,21] was investigated on double line maneuvers. The FLC neural network [22] shows the experimentation results conducted for split- $\mu$  straight road maneuvers. The T–S FLC [23] and fuzzy robust H $\infty$  [24] methods were tested on line change maneuvers. The authors in [25] have integrated yaw moment and active front steering controllers based on the FLC. The results are demonstrated by the single line change maneuvers.

It should be noted that the use of simple maneuvers for the controller validation cannot demonstrate the FLC robustness. In reality, the driver deals with different road scenarios. Therefore, the controller applicability has to be studied on more complex and different braking maneuvers such as emergency braking on curved split- $\mu$  or variable road surfaces to assure controller robustness. Moreover, the reference slip direct control does not guarantee safety assistance on the split- $\mu$  surfaces as the steerability is not preserved. This issue must also be addressed.

As suggested in many previous studies, controllers as well as the currently installed systems in the vehicles set the slip value at 20% for any kind of roads. On the one hand, such an approach can be enough to maintain the steering ability. On the other hand, it leads to a decline in braking performance. For example, on average the optimal slip for icy roads is between 7% and 10%. Thus  $\lambda = 20\%$  would cause a more than 50% loss of braking performance and the vehicle operation would become unstable, i.e., a diminution in steerability. Therefore, by holding the optimal wheel slip value and avoiding the controller restriction with reference variable, as it is proposed in the current paper, the effectiveness and energy efficiency of the braking process is maintained [1] (pp. 74–94).

This paper contributes to the advancement of ABS and brake-based ESP systems using FLC. In particular, the article describes the research results connected with the following topics:

- ESP and ABS control combination, both designed using fuzzy theory.
- Use of a 10 degrees-of-freedom (10 DOF) four-wheel vehicle model in the controller.
- Demonstration of the control robustness on different road surfaces and profiles.

The paper is organized as follows. The next section is dedicated to vehicle dynamics and model parameterization. Section 3 explains the FLC design. The Section 4 is devoted to the experimental facilities. Next, the simulation outcomes are provided. Conclusions are summarized in Section 6.

## 2. Vehicle Dynamics

### 2.1. Vehicle Model

The single-wheel model of the vehicle is shown in Figure 1a. The single-track (bicycle) model is introduced in Figure 1b. Table 1 introduces nomenclature for all variables used in these and other models mentioned in the paper.

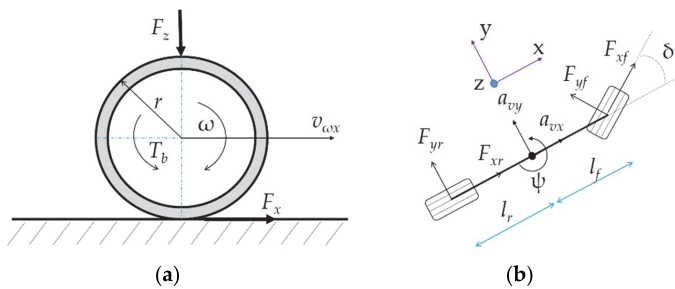


Figure 1. Vehicle model schematic drawing: (a) single-wheel model; (b) single-track model.

Single wheel dynamics can be expressed by the following equations:

$$I_{wi} \cdot \dot{\omega}_i = T_{ti} - r_i \cdot F_{xi} - T_{bi} \tag{1}$$

$$F_{xi} = m \cdot \dot{v}_{xi} \tag{2}$$

$$F_{zi} = m \cdot g. \tag{3}$$

Brake torque depends on the applied brake pressure:

$$T_{bi} = r_i \cdot k_b \cdot p_{bi}, \tag{4}$$

where  $k_b$  is the braking coefficient, which depends on the brake disc friction area, mechanical efficiency of the brake components, and the braking factor is the constant value. In this paper, the ABS controller output variable is the braking pressure for each wheel,  $p_{bi}$ .

The wheel slip at braking is calculated as follows:

$$\lambda_i = \frac{v_v - v_{wx_i}}{v_v} \tag{5}$$

The longitudinal wheel speed be can also simply calculated as:

$$v_{wx_i} = r_i \cdot \omega_i. \tag{6}$$

**Table 1.** Parameters description.

Symbol	Description	Annotation
$\omega$	Wheel angular speed <sup>1</sup>	rad/s
$a_{vx}$	Vehicle longitudinal acceleration <sup>1</sup>	m/s <sup>2</sup>
$a_{vy}$	Vehicle lateral acceleration <sup>1</sup>	m/s <sup>2</sup>
$\psi$	Yaw rate <sup>1</sup>	rad/s
$\delta$	Steering wheel angle <sup>1</sup>	rad
$p_b$	Braking pressure <sup>1</sup>	bar
$r$	Wheel radius	m
$m$	Mass of the vehicle	g
$g$	Gravitational acceleration	m/s <sup>2</sup>
$T_b$	Braking torque	Nm
$T_t$	Traction torque	Nm
$k_b$	Braking coefficient	-
$v_{vx}$	Vehicle longitudinal velocity	m/s
$v_{wx}$	Wheel longitudinal velocity	m/s
$\lambda_i$	Wheel slip	%
$\mu$	Tire-road friction coefficient (general)	-
$\mu_x$	Tire-road friction coefficient based on vehicle longitudinal acceleration	-
$l_f$	Distance from the vehicle Center of Gravity (COG) to the front axles	m
$l_r$	Distance from the vehicle COG to the rear axles	m
$I_z$	Yaw moment of inertia about z-axis	g·m <sup>2</sup>
$F_x$	Longitudinal force	N
$F_y$	Lateral force	N
$F_z$	Vertical force	N
$p_{ABS}$	Pressure generated for ABS braking	bar
$p_{ESPl}$	Pressure generated for the yaw rate regulation for the left side wheels of the vehicle	bar
$p_{ESPr}$	Pressure generated for the yaw rate regulation for the right side wheels of the vehicle	bar
$s$	Distance	m
$-a_{average}$	Average deceleration	m/s <sup>2</sup>
$ABS_{IP}$	ABS operation index of performance	-
$\lambda_{average}$	Average wheel slip value	%
$\omega_{p-t-p}$	ABS adaptability peak-to-peak value	%
$i$	Subscript for each wheel; $i \in [FL, FR, RL, RR]$ <sup>2</sup>	-

<sup>1</sup> Measured by the sensor; <sup>2</sup> (Front Left, Front Right, Rear Left, Rear Right).

In reality the tire radius  $r_i$  is a dynamic variable. In our case we simplify the equation and consider it as a constant value as the change in radius dimension is negligibly small.

The FLC design requires information about the friction-slip curves. Tire-road friction coefficient can be determined as follows:

$$\mu_x(\lambda) = \frac{F_x}{F_z} \tag{7}$$

Using Equations (2) and (3),  $\mu_x$  can be estimated:

$$\mu_x \approx \frac{\dot{v}_x}{g} \tag{8}$$

The 3 DOF single-track model, 0b, is required for the formulation of control inputs in the case of vehicle maneuvers with lateral dynamics. The model is described by the following system of equations:

$$\begin{cases} m \cdot a_{vx} = F_{xf} \cdot \cos\delta + F_{xr} - F_{yf} \cdot \sin\delta + m \cdot \dot{\gamma} \cdot \psi \\ m \cdot a_{vy} = F_{xf} \cdot \sin\delta + F_{yf} \cdot \cos\delta + F_{yr} - m \cdot \dot{x} \cdot \psi \\ \dot{\psi} \cdot I_z = l_f (F_{xf} \cdot \sin\delta + F_{yf} \cdot \cos\delta) - l_r \cdot F_{yr} \end{cases} \tag{9}$$

2.2. Model and Controller Parameterization

Before the simulation, the vehicle model is parameterized according to the sport-utility vehicle. The parameters are taken from the vehicle manufacturer. The total mass is 2170.39 kg. The tires for each wheel are set Continental® (Hanover, Germany) 235/55 R19 and are modeled with Pacejka’s tire magic formula, the coefficients are also provided by the tire manufacturer.

In order to set the initial parameterization of the FLCs, a specific case study was conducted first. The model was simulated under heavy braking conditions on different surfaces to obtain the wheel lock. The ABS and ESP control was not activated. During the case study simulation, the normalized traction/braking forces for every road condition with the locked wheels were evaluated. Therefore, the curves of the normalized traction/braking force of the tire  $\mu$  versus the wheel slip  $\lambda$  for different road surfaces were built (Figure 2).

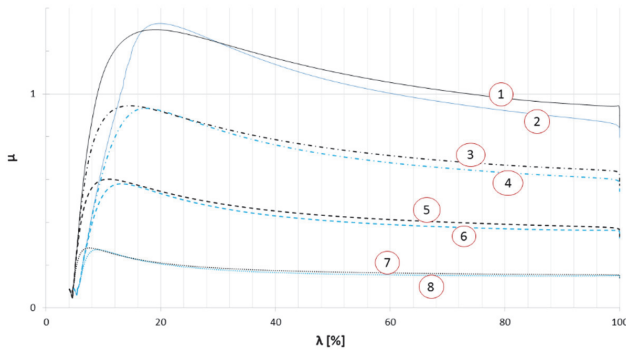


**Figure 2.** The  $\mu$  versus  $\lambda$  curves for the different road surfaces for the studied vehicle model: 1—dry road rear wheels, 2—dry road front wheels, 3—damp road rear wheels, 4—damp road front wheels, 5—wet road rear wheels, 6—wet road front wheels, 7—icy road rear wheels, 8—icy road front wheels.

The stable area is where the curve grows from 0 by  $\lambda$  to its maximum value of  $\mu$ . The second part of the curve is the unstable region, when the steering remains uncontrollable. Efficient ABS performance depends on the road surface. Each surface (dry, damp, wet, icy) has its own optimal slip while braking. The optimal slip refers to the top area of the curve where  $\mu$  obtains its maximum value during braking (Figure 2), thus remaining stable. The optimal slip values for each curve, according to the plots in Figure 2, are presented in Table 2.

**Table 2.** Optimal wheel slip values for several road conditions.

$\lambda$ (%)	Front Wheels	Rear Wheels
Dry road surface	19.85	18.96
Damp road surface	17.53	14.65
Wet road surface	13.21	10.88
Icy road surface	8.95	7.55

The plots are important for the FLC universe of discourse (UOD) design, to set the workspace for the slip input variables in order to guarantee the controller robustness. During the case study the workspace for friction coefficient was also investigated. In addition, the yaw rate UOD was explored in the case study for emergency braking.

### 3. Fuzzy Logic Control Design

When the dynamical behavior of the object is studied, the controller is ready to be designed. One of the advantages of the solution described in this paper is that the controller requires the input variables, for which signals are transmitted in real time by the sensors available in modern vehicles.

The fuzzy logic controller architecture is shown in Figure 3. In this case the plant is a vehicle model. The FLC consists of four design steps. Fuzzification is the process of converting the “crisp” (real number) input into fuzzy sets. A fuzzy set in turn is a pair consisting of an element in UOD and membership degree. The inference mechanism (engine) is used to turn the fuzzy input into a fuzzy output, using the composed rule-base block. Finally, defuzzification converts the fuzzy output into a numerical value.

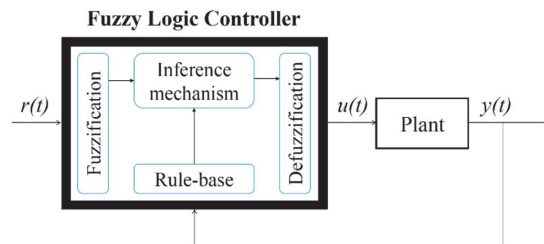


**Figure 3.** Fuzzy logic controller system block diagram:  $r(t)$ —reference input,  $u(t)$ —process inputs,  $y(t)$ —process.

The MATLAB® (Natick, MA, USA) Fuzzy Logic Toolbox™ is used to design the FLC. At the beginning, the inputs and outputs must be stated. Two separate FLCs for ABS and ESP are introduced and combined to obtain robust brake and stability control.

The block diagram scheme for a single wheel is presented in Figure 4. The anti-lock braking system controller involves longitudinal wheel speeds and vehicle acceleration. Using Equations (5) and (6), the slip for each wheel  $\lambda_i$  is calculated and the variable serves as an input. The second input is the tire–road friction coefficient, which corresponds to the vehicle body acceleration and is denoted as  $\mu_x$ , as stated in Equation (8).

The ABS is activated together with the braking pedal displacement. When the vehicle velocity is lower than 8 km/h, the ABS does not function because, after the vehicle speed of 8 km/h, the distance traveled with locked wheels is not critical. The activation requirements are taken from [1] (pp. 74–94).

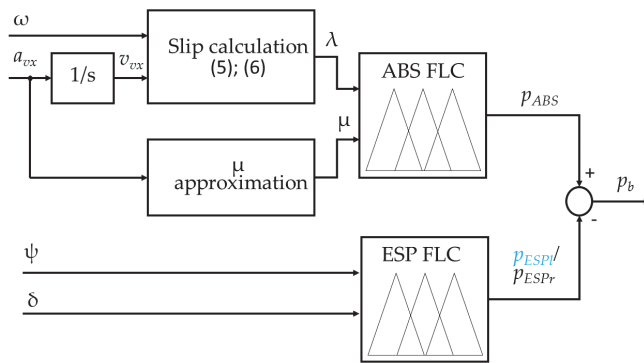


**Figure 4.** Controller block scheme for a single wheel: ABS FLC—anti-lock braking system fuzzy logic controller, ESP FLC—electronic stability program fuzzy logic controller, 1/s—integrational operation.

As soon as the emergency brake (full pedal actuation) is deployed, before the ABS is activated, the controller has enough time to measure the car’s maximum deceleration and use it as a constant variable to understand the road surface. Moreover, the controller resets the  $\mu_x$  variable every second and the maximum value of  $a_{vx}$  is measured again. The fast reset has no effect on driving comfort as the process is very rapid. The reset is necessary for the FLC to understand if the road condition has remained the same, for example, when the road changes from a dry to an icy surface.

The inputs of the ESP are the angular velocity of the vehicle about the vertical axis  $\psi$  and the steering wheel angle  $\delta$  operated by the driver (Figure 4). The ESP is activated together with the braking pedal and deactivates when the vehicle speed is below 8 km/h.

The output of the ABS and the ESP is the braking pressure. The yaw controller has no impact when the yaw moment is not created, thus only ABS is responsible for efficient braking on a straight homogeneous road.

The ESP FLC controls both sides of the vehicle. It either regulates the right or left pair of the vehicle wheels, depending on the body yaw rate direction. According to the curves in Figure 2, the front and rear wheels require different optimal wheel slip values. Therefore, the front and rear wheels will have different membership functions (MFs) for the  $\lambda$  input in ABS. Consequently, each wheel has a different controller. When the yaw FLC understands that the driver is losing vehicle control, it reduces the braking pressure from the side of the car, in which direction the vehicle starts to spin around its center of gravity (COG). Otherwise, only the ABS control is operating.

The next step is to design membership functions for all the inputs and outputs (Figure 5). The linear (triangular) MFs were applied, which are characterized by fast reaction due to the narrow shape as compared to other MFs (exponential, quadratics).

The MFs are symmetrical to provide an equal sensitivity for the whole UOD and obtain the whole overlap of the UOD between the MFs. Each variable UOD must have a closed frontier between  $[min, max]$ . For the input variables, the bounds are obtained during the parameterization described in Section 2.

The slip input MFs for the ABS are introduced in Figure 5. There are nine MFs in total. The UOD for the front wheels lay between  $[0.08, 0.22]$ . This area is accepted according to the operational space obtained in Figure 2 for the front wheels. The only difference between the front and the rear wheels is that the UOD of the slip input for the last ones is accepted in a range  $[0.07, 0.2]$ , which is also based on the rear slip curves in Figure 2 for the rear wheels. In short, UOD for the slip covers all stable areas for relevant roads.

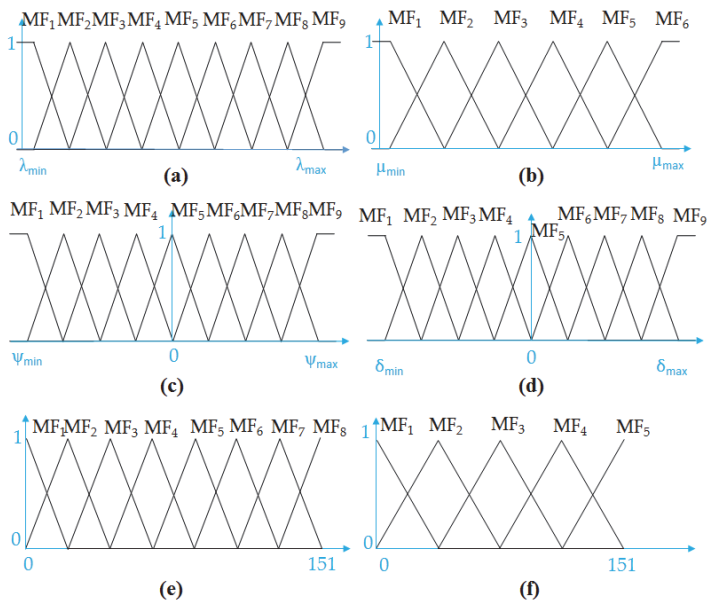


**Figure 5.** Fuzzy logic controller membership functions: (a) ABS  $\lambda$  input; (b) ABS  $\mu_x$  input; (c) ESP  $\psi$  input; (d) ESP  $\delta$  input; (e) ABS  $p_{ABS}$  output; (f) ESP  $p_{ESPl}$  and  $p_{ESP_r}$  outputs.

The  $\mu_x$  MFs are plotted in Figure 5b. The UOD parameterization was obtained during the case study. The  $\mu_x$  operational space is bounded between [10, 40].

The first input of the ESP FLC is the yaw rate. The state consists of nine MFs; UOD is limited in the range between [−4, 4] and introduced in Figure 5c. The reason behind the range for the UOD is next: when the angular velocity exceeds 4 rad/s and the steering wheel angle change is not conducted, vehicle spin appears and the driver is no longer able to act on lateral control.

The second input of the ESP steering wheel angle MFs is shown in Figure 5d. Like the first input, it has nine symmetrically dispelled MFs that are normalized between [−180, 180]. It is assumed that driver reaction in extreme situation must be limited to half of one full steering wheel turn to each side, left or right, which gives in total 360°.

The maximum pressure of the braking system for the studied case is 151 bar. The UOD for the output pressure variables (Figure 5e) is therefore located between [0, 151] and consists of eight MFs. The FLC decides how many bars shall be provided to obtain an optimal slip. Finally, the pressure output for the ESP is obtained in Figure 5f. Likewise, for the ABS the UOD lay between [0, 151]. The ESP has two outputs (Figure 4): brake pressure for the left and the right sides. The decision of which side of the vehicle to control is determined by the rule-base operator.

The modus ponens (If–Then) form has been used in this paper for the rule-base design. The multiple input, single output (MISO) form of the linguistic rules for ABS is (taken from [6]):

$$\text{If } u_1 \text{ is } A^j_1 \text{ and } u_2 \text{ is } A^k_2 \dots \text{ Then } y_q \text{ is } B^p_q, \tag{10}$$

where  $u_1$  and  $u_2$  denote the FLC inputs wheel slip and road condition, respectively;  $y_q$  denotes the brake pressure;  $A^j_1$  and  $A^k_2$  relate to the  $j$ th and  $k$ th linguistic value associated with  $\lambda$  and  $\mu_x$ , respectively; and  $B^p_q$  is the linguistic value of the output braking pressure.

Linguistic values for the ABS are expressed in Table 3. There are 54 rules for the ABS control in total. The rule base for the ESP is observable in Table 4. It has a multi input, multi output (MIMO) structure. In total, 81 rules are required to control the state. The controlled side of the vehicle depends on the yaw moment direction from the center line of the car.

Table 3. Fuzzy linguistic rules for the ABS control.

$\lambda$ $\mu_x$	MF <sub>1</sub>	MF <sub>2</sub>	MF <sub>3</sub>	MF <sub>4</sub>	MF <sub>5</sub>	MF <sub>6</sub>	MF <sub>7</sub>	MF <sub>8</sub>	MF <sub>9</sub>
MF <sub>1</sub>	MF <sub>2</sub>	MF <sub>1</sub>							
MF <sub>2</sub>	MF <sub>4</sub>	MF <sub>3</sub>	MF <sub>2</sub>	MF <sub>1</sub>					
MF <sub>3</sub>	MF <sub>6</sub>	MF <sub>5</sub>	MF <sub>4</sub>	MF <sub>3</sub>	MF <sub>2</sub>	MF <sub>1</sub>	MF <sub>1</sub>	MF <sub>1</sub>	MF <sub>1</sub>
MF <sub>4</sub>	MF <sub>8</sub>	MF <sub>7</sub>	MF <sub>6</sub>	MF <sub>5</sub>	MF <sub>4</sub>	MF <sub>3</sub>	MF <sub>2</sub>	MF <sub>1</sub>	MF <sub>1</sub>
MF <sub>5</sub>	MF <sub>8</sub>	MF <sub>8</sub>	MF <sub>8</sub>	MF <sub>7</sub>	MF <sub>6</sub>	MF <sub>5</sub>	MF <sub>3</sub>	MF <sub>1</sub>	MF <sub>1</sub>
MF <sub>6</sub>	MF <sub>8</sub>	MF <sub>7</sub>	MF <sub>5</sub>	MF <sub>3</sub>	MF <sub>1</sub>				

Table 4. Fuzzy linguistic rules for the ESP regulation: blue—left side of the vehicle, black—right side of the vehicle.

$\psi$ $\delta$	MF <sub>1</sub>	MF <sub>2</sub>	MF <sub>3</sub>	MF <sub>4</sub>	MF <sub>5</sub>	MF <sub>6</sub>	MF <sub>7</sub>	MF <sub>8</sub>	MF <sub>9</sub>
MF <sub>1</sub>	MF <sub>1</sub>	MF <sub>2</sub>	MF <sub>2</sub>	MF <sub>3</sub>	MF <sub>3</sub>	MF <sub>4</sub>	MF <sub>4</sub>	MF <sub>5</sub>	MF <sub>5</sub>
MF <sub>2</sub>	MF <sub>2</sub>	MF <sub>1</sub>	MF <sub>2</sub>	MF <sub>2</sub>	MF <sub>3</sub>	MF <sub>3</sub>	MF <sub>4</sub>	MF <sub>4</sub>	MF <sub>5</sub>
MF <sub>3</sub>	MF <sub>2</sub>	MF <sub>2</sub>	MF <sub>1</sub>	MF <sub>2</sub>	MF <sub>2</sub>	MF <sub>3</sub>	MF <sub>3</sub>	MF <sub>4</sub>	MF <sub>4</sub>
MF <sub>4</sub>	MF <sub>3</sub>	MF <sub>2</sub>	MF <sub>2</sub>	MF <sub>1</sub>	MF <sub>2</sub>	MF <sub>2</sub>	MF <sub>3</sub>	MF <sub>3</sub>	MF <sub>4</sub>
MF <sub>5</sub>	MF <sub>3</sub>	MF <sub>3</sub>	MF <sub>2</sub>	MF <sub>2</sub>	MF <sub>1</sub>	MF <sub>2</sub>	MF <sub>2</sub>	MF <sub>3</sub>	MF <sub>3</sub>
MF <sub>6</sub>	MF <sub>4</sub>	MF <sub>3</sub>	MF <sub>3</sub>	MF <sub>2</sub>	MF <sub>2</sub>	MF <sub>1</sub>	MF <sub>2</sub>	MF <sub>2</sub>	MF <sub>3</sub>
MF <sub>7</sub>	MF <sub>4</sub>	MF <sub>4</sub>	MF <sub>3</sub>	MF <sub>3</sub>	MF <sub>2</sub>	MF <sub>2</sub>	MF <sub>1</sub>	MF <sub>2</sub>	MF <sub>2</sub>
MF <sub>8</sub>	MF <sub>5</sub>	MF <sub>4</sub>	MF <sub>4</sub>	MF <sub>3</sub>	MF <sub>3</sub>	MF <sub>2</sub>	MF <sub>2</sub>	MF <sub>1</sub>	MF <sub>2</sub>
MF <sub>9</sub>	MF <sub>5</sub>	MF <sub>5</sub>	MF <sub>4</sub>	MF <sub>4</sub>	MF <sub>3</sub>	MF <sub>3</sub>	MF <sub>2</sub>	MF <sub>2</sub>	MF <sub>1</sub>

For further fuzzy inference, Mamdani’s method is applied in this paper. The last step in every FLC design is the defuzzification procedure. Relying on experience and due to the good computational complexity, the ABS is defuzzified by the centroid and the ESP by the smallest-of-maxima methods.

When all the design steps are finished, the rule base FLC can be expressed in a three-dimensional surface form. The ABS FLC for the front wheels is presented in Figure 6, whereas the ESP FLC for the left side of the vehicle surface is shown in Figure 7.

The ABS algorithm controls the slip by acting on the braking pressure of each wheel. The ESP stabilizes the yaw rate by influencing the braking pressure with subtraction from the pressure generated for the ABS control. Table 5 summarizes the FLC design in this work.

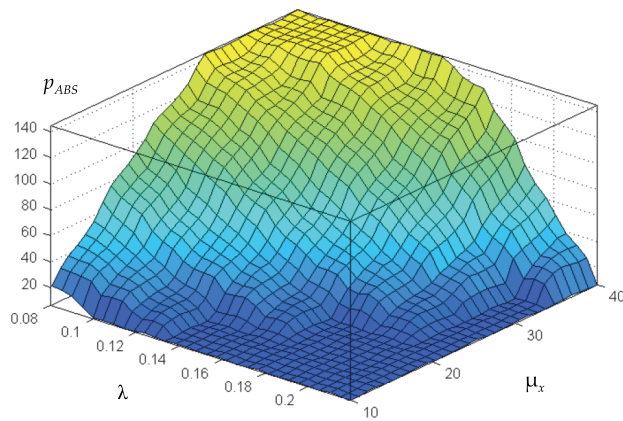


Figure 6. ABS FLC rule surface for the front wheels.

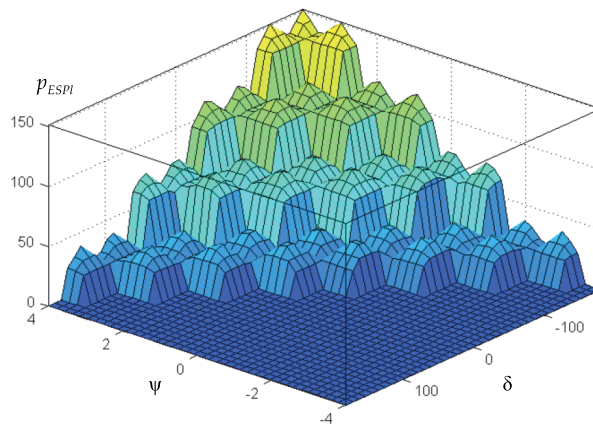


Figure 7. ESP FLC rule surface for the left side of the vehicle.

Table 5. Fuzzy logic controller design conclusion.

Parameter	ABS FLC	ESP FLC
Structure	MISO	MIMO
Crisp input	Slip $\lambda$ (9 MFs), Road condition $\mu_x$ (6 MFs)	Yaw rate $\psi$ (9 MFs), Steering wheel angle $\delta$ (9 MFs)
Crisp output	Braking pressure $p_{ABS}$ (8 MFs)	Braking pressure left side $p_{ESPl}$ (5 MFs), Braking pressure right side $p_{ESP_r}$ (5 MFs)
Fuzzy conjunction	AND = $\min(\lambda, \mu_x)$	AND = $\min(\psi, \delta)$
MFs	Linear Symmetric	Linear Symmetric
Inference method	Mamdani's	Mamdani's
Rule-base	54 Modes Ponens	81 Modes Ponens
Implication operation	$\min(p_{ABS})$	$\min(p_{ESPl}) \vee \min(p_{ESP_r})$
Aggregation method	$\max(p_{ABS})$	$\max(p_{ESPl}) \vee \max(p_{ESP_r})$
Defuzzification	Geometric center	Smallest-of-maxima

#### 4. Simulation Conditions

The control algorithm is designed in Automotive Simulation Models™ (ASM) provided by the dSPACE® GmbH Software 2014-B (64-bit, Paderborn, Germany) and interacted with the MATLAB®/Simulink® R2013b (64 Bit, Natick, MA, USA). The ASM allows the multibody vehicle simulation procedures. The car model has 10 DOF. An overall software interface is presented in Figure 8.

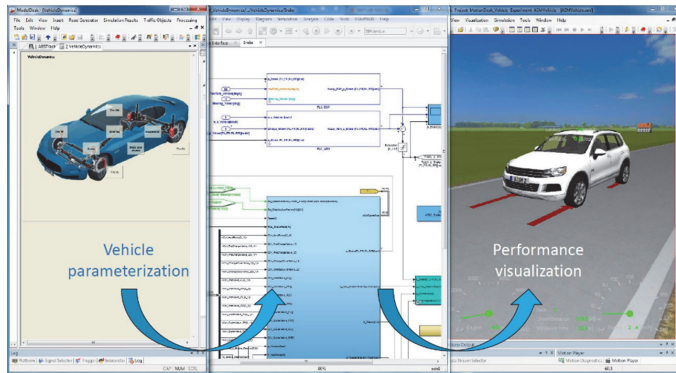


Figure 8. Simulation software interface by the dSPACE® GmbH.

During the simulation, the braking processes were conducted on a straight road as well as in combination with cornering maneuvers. Different complex maneuvers, such as straight or cornering braking on a split- $\mu$  road surface and straight or cornering with change of the tire–road friction coefficients, were simulated. The results are introduced as a comparison of the vehicle motion with and without the activated controllers. Road variations such as dry, wet, and icy surfaces as well as their combinations were designed and simulated to prove the ABS controller robustness and its ability to hold the optimal wheel slip in different road conditions.

The reaction of the ABS controller on the wheel slip characterizes the system adaptability. The factor can be expressed in percentage and calculated by the following equation:

$$\omega_{p-t-p} = \frac{\omega_{\max} - \omega_{\min}}{\omega_{\max}} \cdot 100. \quad (11)$$

Furthermore, the effect of the ABS controller performance can be described with the index of performance  $ABS_{IP}$ . The variable is a ratio between the vehicle deceleration with and without the controller and is found as follows:

$$ABS_{IP} = \frac{-a_{ABS}}{-a_{skid}}. \quad (12)$$

First, the simulation is dedicated to split- $\mu$  roads. When half of the road has a significantly higher friction coefficient as compared to the other half, a high yaw moment occurs. The driver is not able to compensate properly for the yaw dynamics, and the vehicle can spin around the COG. The corresponding simulation in this study is performed for cornering and straight braking maneuvers.

For the straight road, half wet–half dry and half icy–half wet surfaces were chosen. For the curved road, half dry–half icy and half wet–half dry surface profiles were designed.

Next, the model was simulated on a curved road line for different tire–road friction characteristics. The road friction conditions vary during the braking process from icy and dry to wet. Afterwards, the same road conditions were applied to the straight road profile. In this experimentation part the controller robustness is studied.

## 5. Results

### 5.1. Study on Controller Functionality

The first part of the simulation experiments is addressed to the vehicle safety investigation on the split- $\mu$  surface profiles. The maneuvers are simulated on straight and curved roads. For the straight braking, the vehicle was accelerated to 100 km/h and after that the emergency braking was conducted. For curved road braking the vehicle was accelerated to 65 km/h while the transport is cornering left.

Braking on a curved road with a split- $\mu$  surface is the most extreme situation for vehicle safety, because the yaw rate is created by the driver while cornering. The left side of the road is dry and the right side is icy in the present instance. The vehicle body and the wheel speed curves are shown in Figure 9.

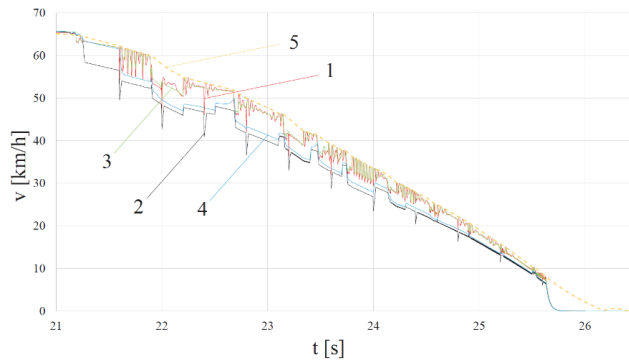


**Figure 9.** Braking on a curved split- $\mu$  road with a half dry–half icy surface; velocity profile curves: 1—FL wheel velocity, 2—FR wheel velocity, 3—RL wheel velocity, 4—RR wheel velocity, 5—vehicle velocity.

Before the ABS is activated, the ESP is already reducing the braking pressure from the left side of the vehicle (the dry surface). The slip values of the left side wheels are therefore lower compared to the right side (Figure 10). Although the left side of the road is dry, the left wheels have less than 10% of the wheel slip values, because the ESP reduces the braking pressure from the left half of the vehicle. The driver, thus, is able to control the car path to follow the road.

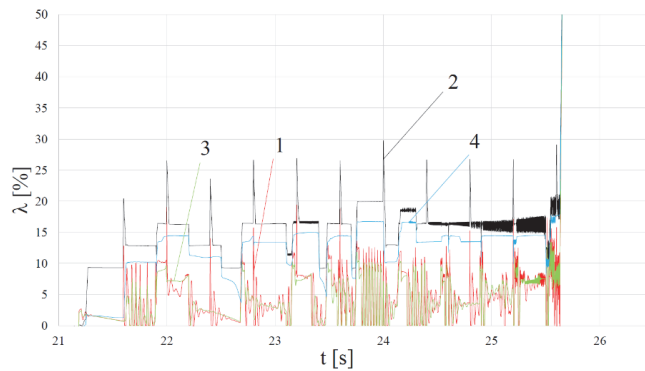


**Figure 10.** Braking on a curved split- $\mu$  road with a half dry–half icy surface; slip profile curves: 1—FL wheel slip, 2—FR wheel slip, 3—RL wheel slip, 4—RR wheel slip.

The dry surface has a higher friction coefficient than the icy road. In this case, the yaw rate is extremely high due to the left cornering. The yaw rate grows after the start of the braking process (Figure 11). However, the ESP reacts very fast and the braking pressure is minimized rapidly. Therefore, the yaw rate remains almost zero during the whole braking distance on the cornering maneuvers. Hence, the driver is able to maintain lateral stability during emergency braking.

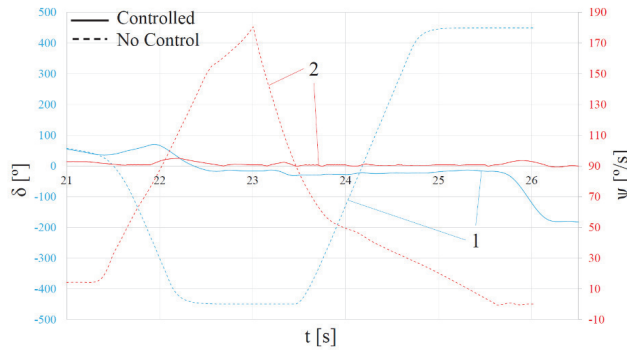


**Figure 11.** Braking on a curved split- $\mu$  road with a half dry–half icy surface profile angle curves: 1—steering wheel angle  $\delta$ , 2—yaw rate  $\psi$ .

When the controller is switched off (Figure 11, dashed lines), the vehicle spins left. The driver turns the steering wheel to the right until the maximum allowed angle. Nevertheless, the high yaw rate in the opposite direction makes the car spin.

The simulation results with other split- $\mu$  road maneuvers are introduced in Table 6, the plots are represented in Figures S1–S9. The ESP safety assistance performance is also compared to the same condition simulations with the turned-off controller. The maximum yaw rate  $\psi_{max}$  does not exceed  $26^\circ/s$ . When the controller is turned off the yaw rate is very high, which makes the car spin around its COG even if the driver tries to keep the vehicle following the road. The braking distance  $s$  and the average body deceleration  $-a_{average}$  for no control simulation are not introduced in the table, because in every case, when the controller is turned off, the car spins.

**Table 6.** Controller functionality results.

Type	Criterion	Braking Performance		ABS Control Performance		ESP Control Performance	
	$s$ (m)	$-a_{average}$ (m/s <sup>2</sup> )	$\lambda_{average}$ (%)	$\omega_{p-t-p}$ (%)	$\delta_{max}$ (°) Controlled/ No Control	$\psi_{max}$ (°/s) Controlled/ No Control	
Straight split- $\mu$ wet/dry	47.16	−4.25	FL	18.41	46.91	175.00/449.96	−16.86/−268.52
			FR	13.97	46.10		
			RL	14.20	45.37		
			RR	14.20	45.61		
Straight split- $\mu$ icy/wet	102.51	−3.31	FL	12.74	32.51	60.16/450	−7.08/−313.73
			FR	7.34	27.63		
			RL	10.62	24.85		
			RR	5.10	18.15		
Cornering split- $\mu$ dry/icy	44.74	−3.14	FL	4.71	28.26	−182.46/−450	25.49/−180.71
			FR	15.96	35.04		
			RL	4.40	23.24		
			RR	13.05	28.58		
Cornering split- $\mu$ wet/dry	20.19	−5.23	FL	19.29	49.36	363.52/450	−15.42/−78.78
			FR	14.32	46.95		
			RL	17.30	48.16		
			RR	13.77	46.49		

In short, the comparison simulation, where the controller was turned on and turned off, shows the importance of the proposed solution in terms of vehicle safety. Different complex maneuvers were studied. The driver is able to remain on the road, following the path. When the controller is turned off, steering is impossible and, the vehicle starts to spin around the COG, causing unfortunate car accidents.

5.2. Study on Controller Robustness

The next simulation study is devoted to an investigation of the controller robustness on curved and straight road profiles. The road surfaces are even. However, they are different for the whole braking distance. Again, in cornering maneuvers the vehicle is accelerated to 65 km/h in a straight line—to 100 km/h. Afterwards, emergency braking is performed.

The vehicle body and the vehicle wheels velocity plots for the varying road conditions on a straight road maneuvers are introduced in Figure 12. The vehicle starts braking on a dry road with transition to a wet surface. The car finishes braking on icy asphalt. The vehicle changes the deceleration according to the tire–road adhesive characteristics. The algorithm is able to recognize the road surface and, according to the obtained information supply, appropriate pressure to maintain efficient braking is applied.

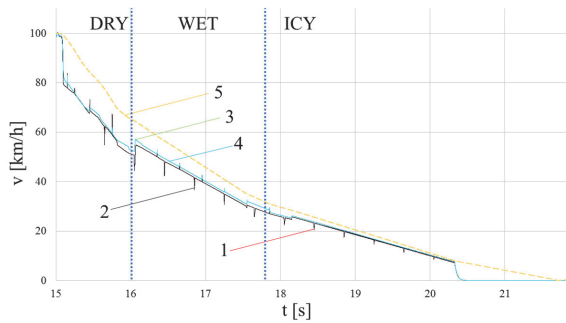


Figure 12. Braking on a straight road with dry–wet–icy surfaces profile speed curves: 1—FL wheel velocity, 2—FR wheel velocity, 3—RL wheel velocity, 4—RR wheel velocity, 5—vehicle velocity.

The slip curves for the each wheel are shown in Figure 13. No wheel lock has been obtained. The controller holds the optimal slip for each wheel on every road surface. The wheel pressure distribution aims to obtain an optimal wheel slip.

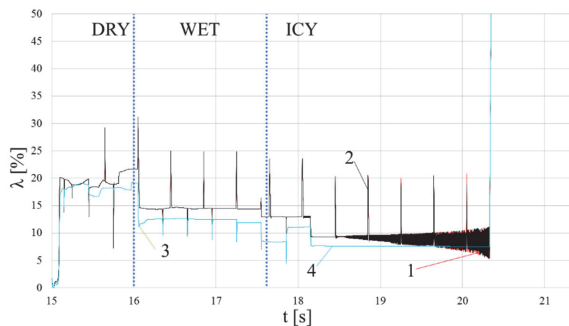


Figure 13. Braking on a straight road with dry–wet–icy surfaces profile slip curves: 1—FL wheel slip, 2—FR wheel slip, 3—RL wheel slip, 4—RR wheel slip.

Other braking results for the maneuvers with even road profiles studied in this paper are introduced in Figures S10–S17. To conclude the wheel slip control robustness and compare it to the theoretical energy efficient values from Figure 2, Table 7 is introduced. The simulation wheel slip results are taken as the average numbers. It can be concluded that the controller is able to maintain the optimal slip to maintain energy-efficient braking.

**Table 7.** Controller robustness results.

Type	Criterion	Braking Performance			ABS Control Performance		ESP Control Performance		
		s (m) Controlled/ No Control	$-a_{average}$ (m/s <sup>2</sup> ) Controlled/ No Control	ABS <sub>IP</sub>	$\lambda_{average}$ (%)	$\omega_{p-t-p}$ (%)	$\delta_{max}$ (°) Controlled/ No Control	$\psi_{max}$ (°/s) Controlled/ No Control	
Cornering even wet to dry		21.59/30.88	−6.75/−3.48	1.94	FL	11.45–16.62	34.76	103.55/450	10.82/−27.89
					FR	14.27–17.79	37.88		
					RL	9.94–16.94	32.93		
					RR	11.61–17.90	35.44		
Cornering even dry to icy to wet		31.28/31.33	−3.69/−2.99	1.23	FL	19.14–3.68–9.918	50.25	160.05/450	10.61/−20.72
					FR	19.93–9.30–11.07	50.96		
					RL	17.34–2.94–8.93	48.04		
					RR	17.85–1.37–11.16	48.86		
Straight even icy to dry to wet		88.49/140.04	−4.29/−2.36	1.82	FL	10.01–18.99–14.16	28.64	0/0	0/0
					FR	18.49–18.99–14.13	28.64		
					RL	7.73–17.13–12.33	19.58		
					RR	7.73–17.13–12.33	19.59		
Straight even dry to wet to icy		62.51/140.04	−3.85/−1.97	1.95	FL	19.71–14.24–9.30	55.66	0/0	0/0
					FR	19.71–14.24–9.30	55.66		
					RL	18.05–11.56–7.68	48.52		
					RR	18.05–11.56–7.68	48.53		

In cornering maneuvers, as the vehicle is turning left, the wheel slip values for the left side of the vehicle are smaller compared to the right side. The difference is caused by the ESP assistance. In addition, even when the road surface is even, the yaw rate appears when the vehicle starts to brake. However, the driver reacts by controlling the steering wheel and the car remains on the road. Therefore, the robustness of the proposed controller is investigated through several examples of different complex maneuvers.

The braking and ESP performance results on the same roads without controllers are also introduced in Table 7. It is clear that the braking distances without the controllers are longer for every considered case. Due to the wheels' blockage, the average deceleration results ( $-a_{average}$ ) are lower.

When the controllers are turned off, the driver rotates the steering wheel as far as possible to remain on the road while conducting the cornering maneuvers. The car, however, drives off the road without controller assistance. When the controllers are turned on, contrarily, it is enough for the driver to slightly control the vehicle steering wheel to remain on the road.

All in all, the ABS FLC is able to recognize the tire–road adhesive coefficient and supply the appropriate braking pressure to maintain energy-efficient deceleration. The simulation results of the controller on the straight and cornering profiles prove the controller's robustness.

## 6. Discussion and Conclusions

This paper describes the FLC algorithm for vehicle safety assistance control. The ABS and the ESP integration introduced in this work provides energy-efficient and robust responses to different road surfaces and curved braking performance. In order to design a robust FLC, the tire–road adhesive coefficients versus tire slip curves for dry, damp, wet, and icy roads were plotted first (Figure 2). The studied vehicle model was parameterized according to the SUV parameters. The proposed solution is suitable for the studied SUV model.

A combination of ABS and ESP controllers both based on FLC theory is introduced. Each wheel has an independent controller. The simulation results conducted on different complex maneuvers

involving curved road profiles and split- $\mu$  road surfaces as well as varying road friction coefficients prove the controller robustness. The algorithm assists the driver with steering. Thus, a driver with average reaction times is able to follow the road during emergency heavy braking.

The simulation results introduced in Section 5 prove the FLC robustness to varying road surfaces and split- $\mu$  profiles. Moreover, optimal slip braking on even road profiles is maintained, providing energy-efficient braking. Comparing the research results to other intelligent computation control algorithms introduced in Section 1, the current study offers several novel proposals for the vehicle dynamics and safety control fields.

First, the proposed controller does not require a reference error and change of error input variables as in [10–12,15]. Instead, the controller covers the whole braking process stable area. The human experience containing rule-base block provides a suitable pressure to hold an optimal for every studied road surface slip value. Therefore, the dependence on the constant reference value, which is unpredictable in reality, is avoided.

Second, in most of the previously proposed cases, as for instance in [10–12,16], braking on a straight even surface excludes the lateral dynamics influence on the controller, and, thus, on the vehicle safety performance. The simulation results in Section 5 show that the lateral dynamics during cornering maneuvers and on split- $\mu$  road profiles braking must be taken into consideration as they are essential in car spin and roll-over avoidance. Otherwise, the ABS and ESP safety assistance cannot be ensured.

Third, the simple quarter-car model studied in [9,18] is not enough to prove the controller productivity and robustness. In reality, the four-wheel vehicle model represents a more complex control task. Consequently, the vehicle model examined in this paper has an advantage over other similar works.

Finally, regarding the ESP performance, most researchers [20,21,23–25] limit their results with a simple line change maneuver. There were no publications found testing the ABS and ESP designed with FLC on a cornering split- $\mu$  road profile, as has been done in the current work.

In short, the results obtained from the current research are as follows:

- The ESP and ABS FLC control integration to obtain energy-efficient braking performance.
- The controls safety and robustness in different kinds of complex maneuvers is studied.
- Use of a complex 10 DOF vehicle model in the controller simulation.

The main drawback of the presented work, however, is its restriction by the numerical simulation. In the PC software simulation, the real vehicle dynamics and physical behavior are missing. A computer simulation does not completely solve the problem.

Future research covers the experimentation on the HIL brakes test bench. Moreover, the controller will be designed and applied on a four in-wheel-motor drive passenger electric vehicle providing the torque-base brake solution to study recuperative braking.

**Supplementary Materials:** The following are available online at [www.mdpi.com/2076-3417/6/12/382/s1](http://www.mdpi.com/2076-3417/6/12/382/s1), Figure S1: Straight split- $\mu$  road with a half wet-half dry surface profile velocity curves, Figure S2: Straight split- $\mu$  road with a half wet-half dry surface profile wheel slip curves, Figure S3: Straight split- $\mu$  road with a half wet-half dry surface profile angle curves, Figure S4: Straight split- $\mu$  road with a half icy-half wet surface profile velocity curves, Figure S5: Straight split- $\mu$  road with a half icy-half wet surface profile wheel slip curves, Figure S6: Straight split- $\mu$  road with a half icy-half wet surface profile angle curves, Figure S7: Curved split- $\mu$  road with a half wet-half dry surface profile velocity curves, Figure S8: Curved split- $\mu$  road with a half wet-half dry surface profile wheel slip curves, Figure S9: Curved split- $\mu$  road with a half wet-half dry surface profile angle curves, Figure S10: Curved even road with wet-dry surface profile velocity curves, Figure S11: Curved even road with wet-dry surface profile wheel slip curves, Figure S12: Curved even road with wet-dry surface profile angle curves, Figure S13: Curved even road with dry-icy-wet surface profile velocity curves, Figure S14: Curved even road with dry-icy-wet surface profile wheel slip curves, Figure S15: Curved even road with dry-icy-wet surface profile angle curves, Figure S16: Straight even road with icy-dry-wet surface profile velocity curves, Figure S17: Straight even road with icy-dry-wet surface profile wheel slip curves.

**Acknowledgments:** This research work was supported by the Deutschen Bundesstiftung Umwelt (DBU) exchange scholarship program and the European Union's Horizon 2020 research and innovation programme under the

Marie Skłodowska-Curie grant agreement No 645736. We acknowledge support for the Article Processing Charge from the German Research Foundation and the Open Access Publication Fund of the Technische Universität Ilmenau.

**Author Contributions:** Andrei Aksjonov conceived designed and performed the experiments. Klaus Augsburg and Valery Vodovozov analyzed the data; all the authors prepared the manuscript.

**Conflicts of Interest:** The authors declare no conflict of interest.

## References

1. Post, W.; Koch-Dücker, H.-J.; Papert, U. Car braking systems. Antilock braking system. In *Brakes, Brake Control and Driver Assistance Systems: Function, Regulation and Components*; Reif, K., Ed.; Springer: Friedrichshafen, Germany, 2014; pp. 28–40, 74–94.
2. Ivanov, V. A review of fuzzy methods in automotive engineering applications. *Eur. Transp. Res. Rev.* **2015**, *7*, 1–10. [[CrossRef](#)]
3. Takahashi, H.; Ishikawa, Y. Antiskid Brake Control System Based on Fuzzy Inference. U.S. Patent 4,842,344, 27 June 1989.
4. Mauer, G.F. A fuzzy logic controller for an ABS braking system. *IEEE Trans. Fuzzy Syst.* **1998**, *3*, 381–388. [[CrossRef](#)]
5. Klaus, K.; Hasemann, M. An embedded fuzzy anti-slippage system for heavy duty off road vehicles. *Inf. Sci.* **1995**, *4*, 1–27. [[CrossRef](#)]
6. Passino, K.M.; Yurkovich, S. *Fuzzy Control*; Addison Wesley Longman, Inc.: Menlo Park, California, CA, USA, 1998; pp. 317–413.
7. Layne, J.R.; Passino, K.M.; Yurkovich, S. Fuzzy learning control for antiskid braking systems. *IEEE Trans. Control Syst. Technol.* **1993**, *2*, 122–129. [[CrossRef](#)]
8. Dai, C.L.; Xu, L.J. The Simulation Research of Automobile ABS System Based on Fuzzy Theory. In Proceedings of the 2015 International Conference on Intelligent Transportation, Big Data and Smart City (ICITBS), Halong Bay, Vietnam, 19–20 December 2015; pp. 922–926.
9. Du, H.; Li, W.; Zhang, Y. Tracking Control of Wheel Slip Ratio with Velocity Estimation for Vehicle Anti-Lock Braking System. In Proceedings of the 2015 27th Chinese Control and Decision Conference (CCDC), Qingdao, China, 23–25 May 2015; pp. 1900–1905.
10. Raesian, N.; Khajepour, N.; Yaghoobi, M. A New Approach in Anti-lock Braking System (ABS) Based on Adaptive Neuro-Fuzzy Self-tuning PID Controller. In Proceedings of the 2011 2nd International Conference on Control, Instrumentation and Automation (ICCIA), Shiraz, Iran, 27–29 December 2011; pp. 530–535.
11. Kejun, J.; Chengye, L. Application Study of Fuzzy PID Control with S-function on Automotive ABS. In Proceedings of the 2010 International Conference on Future Information Technology and Management Engineering (FITME), Changzhou, China, 9–10 October 2010; pp. 467–470.
12. Jidu, H.; Yongjun, Z.; Gang, W. Research on Vehicle Anti-braking System Control Algorithm Based on Fuzzy Immune Adaptive PID Control. In Proceedings of the 2012 Third International Conference on Digital Manufacturing and Automation (ICDMA), Guilin, China, 31 July–2 August 2012; pp. 723–726.
13. Lin, C.-M.; Li, H.-Y. Intelligent hybrid control system design for antilock braking systems using self-organizing function-link fuzzy cerebellar model articulation controller. *IEEE Trans. Fuzzy Syst.* **2013**, *21*, 1044–1055. [[CrossRef](#)]
14. Mirzaei, A.; Moallem, M.; Dehkordi, B.M.; Fahimi, B. Design of an optimal fuzzy controller for antilock braking system. *IEEE Trans. Vehicul. Technol.* **2006**, *55*, 1725–1730. [[CrossRef](#)]
15. Yonggon, L.; Zak, S.H. Designing a genetic neural fuzzy antilock-brake-system controller. *IEEE Trans. Evol. Comp.* **2002**, *6*, 198–211. [[CrossRef](#)]
16. Wang, W.-Y.; Li, L.H.; Chen, M.-C.; Su, S.-F.; Hsu, S.-B. Dynamic slip-ratio estimation and control of antilock braking systems using an observer-based direct adaptive fuzzy-neural controller. *IEEE Trans. Ind. Electron.* **2009**, *56*, 746–756.
17. Cabrera, J.A.; Ortiz, A.; Castello, J.J.; Simon, A. A fuzzy logic control for antilock braking system integrated in the IMM<sub>a</sub> tyre test bench. *IEEE Trans. Veh. Technol.* **2005**, *54*, 1937–1949. [[CrossRef](#)]
18. Khatun, P.; Bingham, C.M.; Schofield, N.; Mellor, P.H. Application of fuzzy control algorithms for electric vehicle antilock braking-traction control systems. *IEEE Trans. Veh. Technol.* **2003**, *52*, 1356–1364. [[CrossRef](#)]

19. Cao, C.-T.; Becker, R.; Belzner, U.; Moeller, T.-W.; Lieberoth-Leden, B. System for Controlling Brake Pressure Based on Fuzzy Logic Using Steering Angle and Yaw Speed. U.S. Patent 5,634,698, 3 June 1997.
20. Zhou, H.; Chen, H.; Ren, B.; Zhao, H. Yaw Stability Control for In-wheel-motored Electric Vehicle with a Fuzzy PID Method. In Proceedings of the 27th Chinese Control and Decision Conference (2015 CCDC), Qingdao, China, 23–25 May 2015; pp. 1876–1881.
21. Wei, Z.; Guizhen, Y.; Jian, W.; Tianshu, S.; Xiangyang, X. Self-tuning Fuzzy PID Applied to Direct Yaw Moment Control for Vehicle Stability. In Proceedings of the 9th International Conference on Electronic Measurement & Instruments, 2009, (ICEMI '09), Beijing, China, 16–19 August 2009; pp. 2-257–2-261.
22. Tahami, F.; Kazemi, R.; Farhanghi, S. A novel driver assist stability system for all-wheel-drive electric vehicle. *IEEE Trans. Vehicul. Technol.* **2003**, *52*, 683–692. [[CrossRef](#)]
23. Geng, C.; Mostefai, L.; Denai, M.; Hori, Y. Direct yaw-moment control of an in-wheel-motored electric vehicle based on body slip angle fuzzy observer. *IEEE Trans. Ind. Electron.* **2009**, *56*, 1411–1419. [[CrossRef](#)]
24. Oudghiri, M.; Chadli, M.; Hajjaji, A.E. Vehicle Yaw Control Using a Robust  $H_{\infty}$  Observer-based Fuzzy Controller Design. In Proceedings of the 2007 46th IEEE Conference on Decision and Control, New Orleans, LA, USA, 12–14 December 2007; pp. 3895–3900.
25. Wu, Y.; Song, D.; Hou, Z.; Yuan, X. A Fuzzy Control Method to Improve Vehicle Yaw Stability Based on Integrated Yaw Moment Control and Active Front Steering. In Proceedings of the 2007 International Conference on Mechatronics and Automation, Harbin, China, 5–8 August 2007; pp. 1508–1512.



© 2016 by the authors; licensee MDPI, Basel, Switzerland. This article is an open access article distributed under the terms and conditions of the Creative Commons Attribution (CC-BY) license (<http://creativecommons.org/licenses/by/4.0/>).

# Supplementary Materials: Design and Simulation of the Robust ABS and ESP Fuzzy Logic Controller on the Complex Braking Maneuvers

Andrei Aksjonov, Klaus Augsburg and Valery Vodovozov

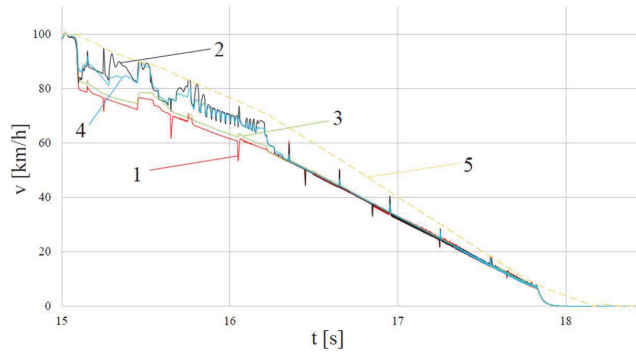


**Figure S1.** Straight split- $\mu$  road with a half wet-half dry surface profile velocity curves: 1—FL wheel velocity, 2—FR wheel velocity, 3—RL wheel velocity, 4—RR wheel velocity, 5—vehicle velocity.

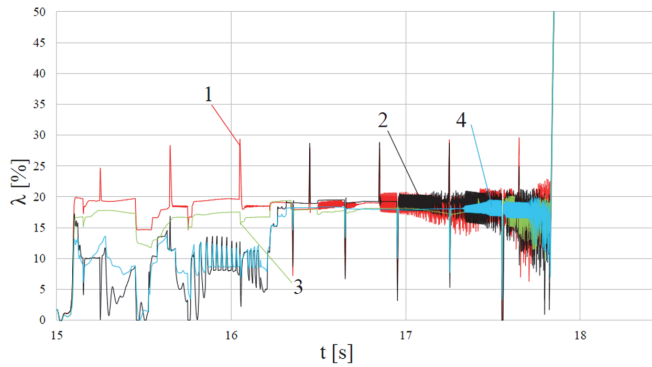


**Figure S2.** Straight split- $\mu$  road with a half wet-half dry surface profile wheel slip curves: 1—front left, 2—front right, 3—rear left, 4—rear right.

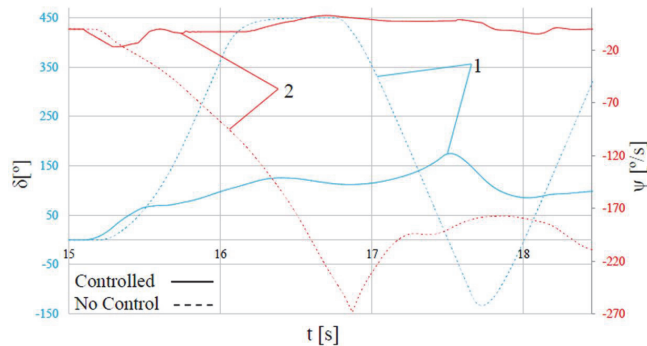


**Figure S3.** Straight split- $\mu$  road with a half wet-half dry surface profile angle curves: 1—steering wheel angle  $\delta$ , 2—yaw rate  $\psi$ .

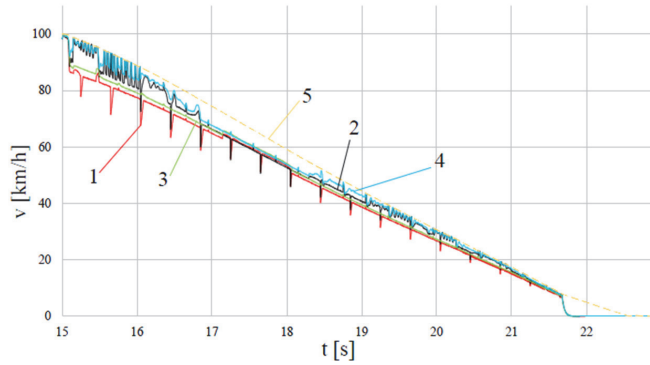


**Figure S4.** Straight split- $\mu$  road with a half icy-half wet surface profile velocity curves: 1—front left wheel, 2—front right wheel, 3—rear left wheel, 4—rear right wheel, 5—vehicle.

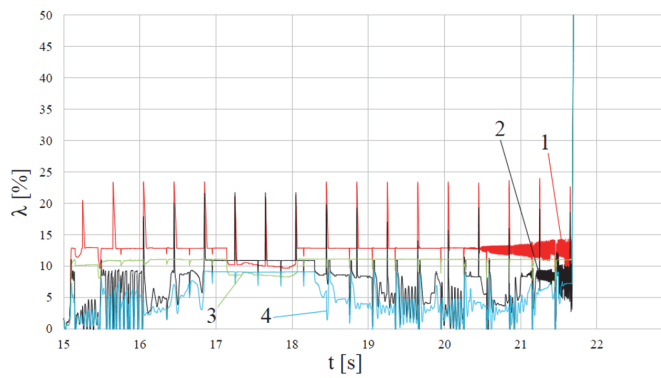


**Figure S5.** Straight split- $\mu$  road with a half icy-half wet surface profile wheel slip curves: 1—front left, 2—front right, 3—rear left, 4—rear right.

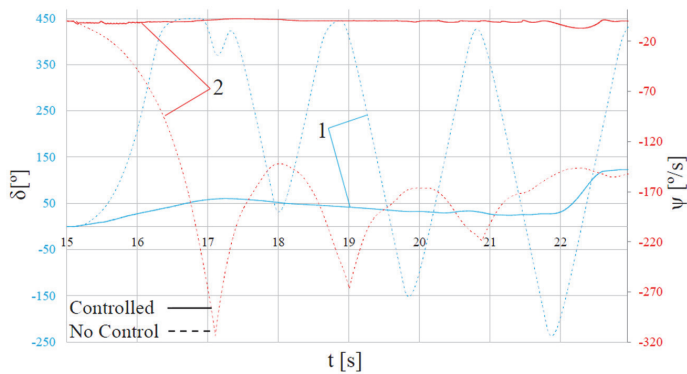


**Figure S6.** Straight split- $\mu$  road with a half icy-half wet surface profile angle curves: 1—steering wheel angle  $\delta$ , 2—yaw rate  $\psi$ .

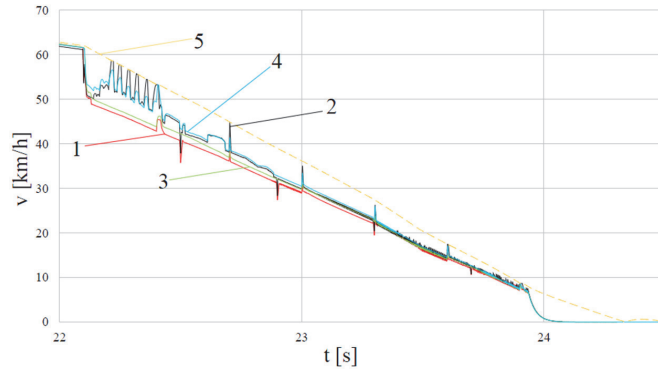


**Figure S7.** Curved split- $\mu$  road with a half wet-half dry surface profile velocity curves: 1—front left wheel, 2—front right wheel, 3—rear left wheel, 4—rear right wheel, 5—vehicle.

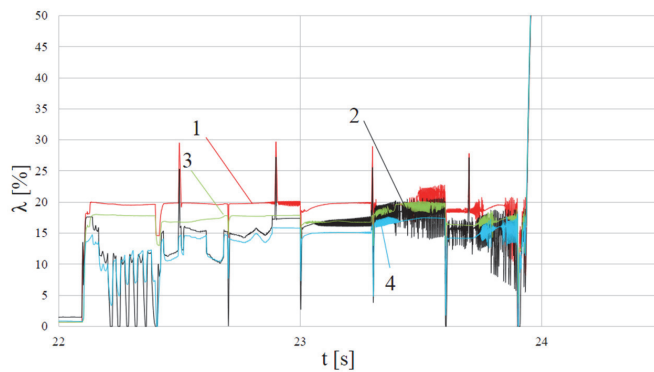


**Figure S8.** Curved split- $\mu$  road with a half wet-half dry surface profile wheel slip curves: 1—front left, 2—front right, 3—rear left, 4—rear right.

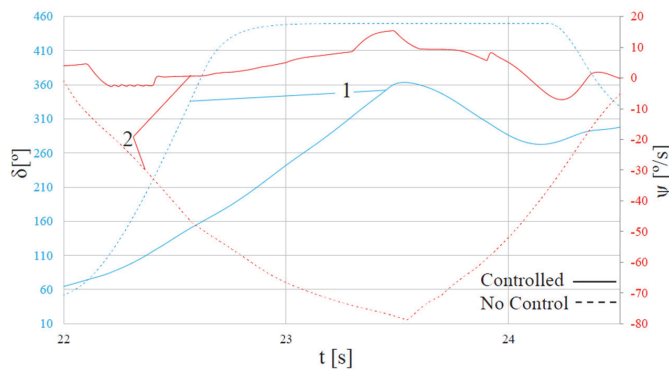


**Figure S9.** Curved split- $\mu$  road with a half wet-half dry surface profile angle curves: 1—steering wheel angle  $\delta$ , 2—yaw rate  $\psi$ .

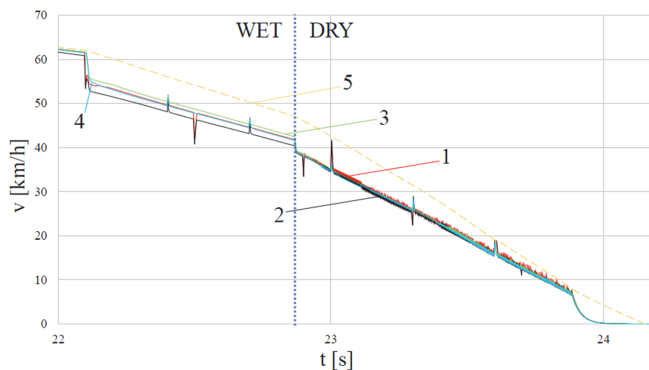


Figure S10. Curved even road with wet-dry surface profile velocity curves: 1—front left wheel, 2—front right wheel, 3—rear left wheel, 4—rear right wheel, 5—vehicle.

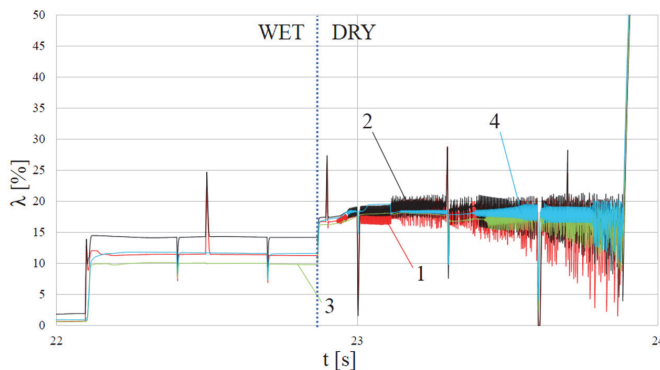


Figure S11. Curved even road with wet-dry surface profile wheel slip curves: 1—front left, 2—front right, 3—rear left, 4—rear right.

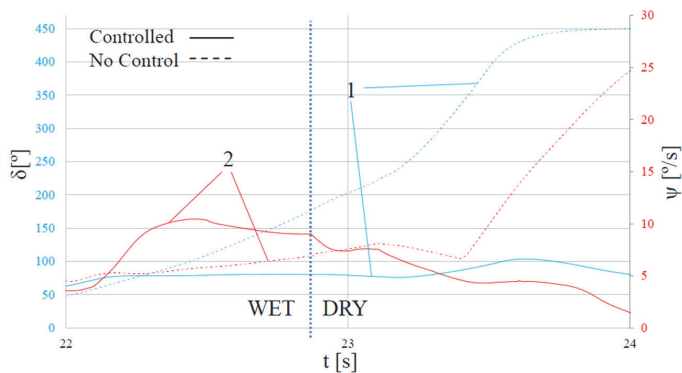
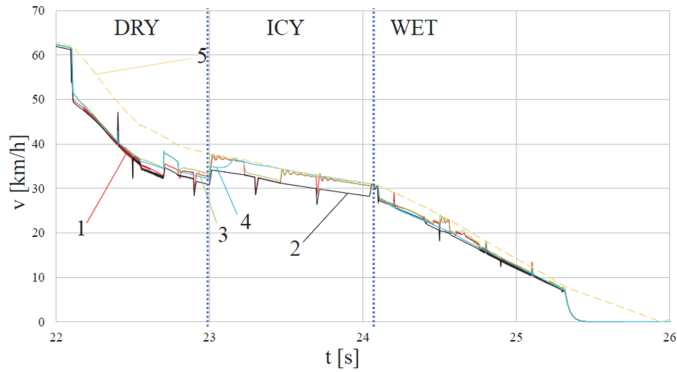
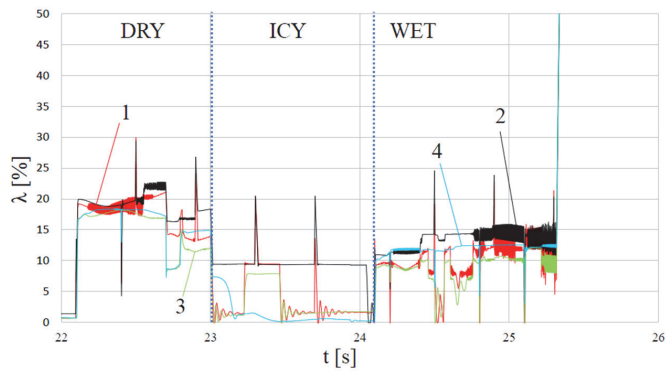


Figure S12. Curved even road with wet-dry surface profile angle curves: 1—steering wheel angle  $\delta$ , 2—yaw rate  $\psi$ .



**Figure S13.** Curved even road with dry-icy-wet surface profile velocity curves: 1—front left wheel, 2—front right wheel, 3—rear left wheel, 4—rear right wheel, 5—vehicle.



**Figure S14.** Curved even road with dry-icy-wet surface profile wheel slip curves: 1—front left, 2—front right, 3—rear left, 4—rear right.

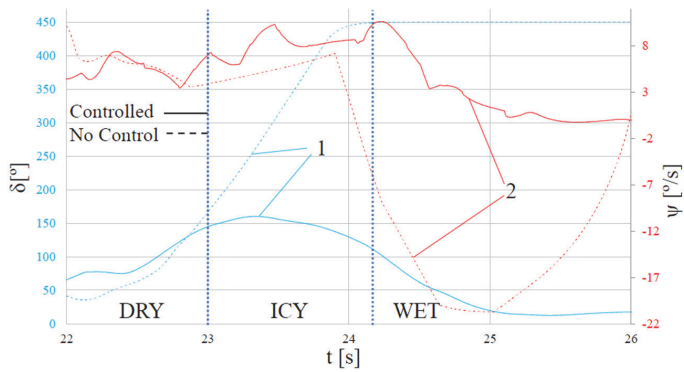


**Figure S15.** Curved even road with dry-icy-wet surface profile angle curves: 1—steering wheel angle  $\delta$ , 2—yaw rate  $\psi$ .

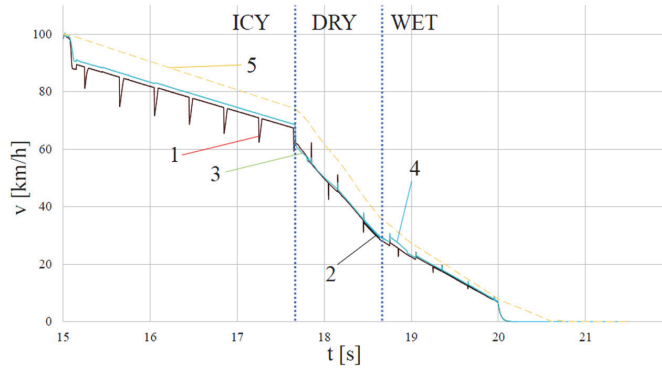


**Figure S16.** Straight even road with icy-dry-wet surface profile velocity curves: 1—front left wheel, 2—front right wheel, 3—rear left wheel, 4—rear right wheel, 5—vehicle.

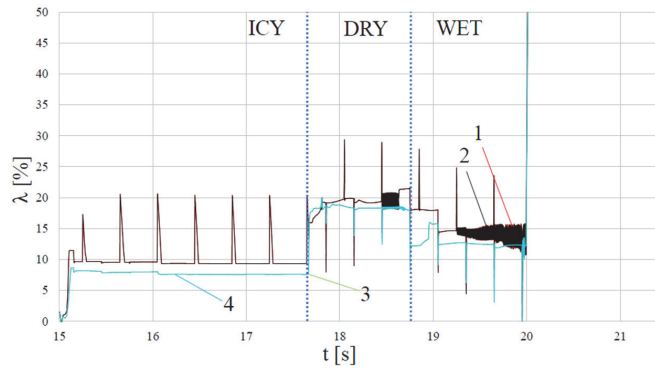


**Figure S17.** Straight even road with icy-dry-wet surface profile wheel slip curves: 1—front left, 2—front right, 3—rear left, 4—rear right.

#### **Publication II**

**Aksjonov, A.**, Nedoma, P., Vodovozov, V., Petlenkov, E., & Herrmann M. (2017). A Method of Driver Distraction Evaluation Using Fuzzy Logic. Phone usage as a driver's secondary activity: Case study. *Proceedings of the 26th IEEE International Conference on Information, Communication and Automation Technologies (ICAT2017)* (pp. 23–28). Sarajevo: IEEE. doi: 10.1109/ICAT.2017.8171599



# A Method of Driver Distraction Evaluation Using Fuzzy Logic

Phone usage as a driver's secondary activity: Case study

Andrei Aksjonov<sup>1</sup>, Pavel Nedoma<sup>2</sup>

ŠKODA Auto a.s.  
Mladá Boleslav, Czech Republic  
<sup>1</sup>andrei.aksjonov@skoda-auto.cz,  
<sup>2</sup>pavel.nedoma@skoda-auto.cz

Valery Vodovozov<sup>1</sup>, Eduard Petlenkov<sup>2</sup>

<sup>1</sup>Department of Electrical Power Engineering and Mechatronics,  
<sup>2</sup>Department of Computer Systems  
Tallinn University of Technology  
Tallinn, Estonia  
<sup>1</sup>valery.vodovozov@ttu.ee,  
<sup>2</sup>eduard.petlenkov@ttu.ee

Martin Herrmann  
IPG Automotive GmbH  
Karlsruhe, Germany  
martin.herrmann@ipg-automotive.com

**Abstract**—A novel method for evaluating driver distraction and situation awareness while performing a secondary task using a fuzzy set theory is proposed in this paper. A fuzzy inference engine realization process based on simple matrix operations is described in detail. The drivers' performance is evaluated referring to the vehicle behavior, in particular, the abilities to keep the vehicle in the center of the lane and to observe the speed limit. The evaluation technique was tested on a vehicle mock-up driving simulator. Text messaging on a cell phone is studied as a secondary distractive activity. Driver-in-the-loop experimental results as well as the conclusions regarding different age, gender, and driving experience groups are discussed.

**Keywords**—fuzzy logic; performance evaluation; vehicle safety; real-time systems

## I. INTRODUCTION

Nowadays, people spend more time than ever behind a steering wheel. However, not all drivers can remain constantly focused on their primary tasks – performing maneuvers, reading traffic signs, monitoring traffic, overcoming weather – while driving. Frequently, they perform different kinds of secondary tasks that are not related to safe driving and, on the contrary, may be extremely dangerous due to drivers' increasing workload [1, 2, 3].

The tasks that may potentially affect driving are divided into two main groups: interaction with in-vehicle features, such as vehicle information and entertainment systems, and items brought into the vehicle, such as portable devices [1]. Nevertheless, there are no certain measures which could evaluate the influence of the secondary tasks on drivers' situation awareness and level of vigilance and therefore conclude what secondary activity leads to a potential traffic accident, to what degree it can be dangerous, and how to eliminate its effect.

In the current decade, portable electronic devices, such as cell phones or smartphones, became an essential part of everyday life. However, phones are often used in cases when

they may lead to a dramatic aftermath and even cause serious accidents with fatal consequences [4].

Only in the USA, fatalities of drivers involved in vehicle crashes increased by 7.2% in 2015 over 2014 [5]. Among different causes of traffic accidents, driver distraction is considered one of the most common, especially among young drivers (58% in the period 2007–2013) [6]. Notably dangerous is the usage of portable electronic devices, such as e-readers, cell phones, tablets, or MP3 players while driving [7]. Although the AAA Foundation for Traffic Safety reports that 81.1% of surveyed drivers are aware that “text messaging or emailing while driving are a very serious threat to their personal safety”, still 11.2% of drivers regularly read text messages while driving. What is more, 8.2% of them admit to typing or sending texts [7].

The development of a robust method for driver distraction evaluation while performing a secondary task is of interest for both road safety foundations and vehicle manufacturers. It could help the first group in establishing traffic safety policies, and the second one in improving human-machine interface systems that would be intuitive and logical, thus producing minimum drivers' disturbance. A driver distraction and human-machine interface evaluation technique also offer the possibility to test and evaluate such advanced driver assistance systems as collision avoidance, lane departure warning, and others.

Various approaches were offered for an evaluation of driver distraction and situation awareness. Drivers' eye tracking or head movement are among the oldest techniques [8]. The effect of hands-free cell phone conversations was examined in [9] using eye-tracking data. Different age groups of drivers (novice drivers, young adults, and older adults) were studied on their ability to recognize risks [10]. Separate groups of novice drivers were tested on risk awareness in [11]. Eye movement was involved in evaluation in the above studies. Eye tracking was also used in driver distraction evaluation while having a conversation with a passenger [12].

Another widely used group of evaluation methods is based on vehicle dynamic performance. Using driving simulators, drivers' steering ability, speed limit maintenance, brake and gas pedal actuation as well as reaction time can be accepted as a measure for the driver distraction estimation. In [4, 13], the level of driver distraction was evaluated via steering wheel performance and lane-keeping ability. In the first work, the effects of handheld and hands-free phone conversations while driving were studied. In the second one, the steerability was tested using clear, large, and high luminance visual scenes.

Driving behavior characterization was developed by combining fuzzy and probabilistic models [14]. The driving performance was tested in real time. A gap between vehicles and vehicle velocity were used as evaluation measures.

Another methodology uses the ability of experimentation subjected for maintenance the spatial location knowledge while performing dynamic real-time tasks, such as driving, air traffic control, flying, and others. For example, a recall of vehicle location and focus on the location of potentially hazardous cars were used in [3] as a measures for the level of situation awareness.

Finally, some researchers went further and combined several measures to evaluate driver distraction while interacting with in-vehicle secondary tasks. Researchers in [2] used the mean speed and deviation from the posted speed limit to measure driver distraction. Thereafter, a multidimensional subjective workload index, the NASA Task Load Index, of the perceived workload was recorded. In [15], the authors combined eye and head movement data with lane keeping.

Fuzzy theory [16] is not a novel idea in driver behavior and distraction detection. Fuzzy logic (FL) was applied as an online driving style recognition system [17]. The system has a high accuracy in driving style classification. However, the application was tested only via simulation. In [18], a driver activity index was designed using FL.

In [19, 20], driver face monitoring systems were introduced. The fuzzy algorithms were applied to detect driver fatigue and distraction. The first work uses the driver's position in a vehicle. The system in the second paper collects the driver's eye and face symptoms as the fuzzy expert system inputs. Finally, four levels of driver distraction FL classification using EEG signals were offered [21]. Unfortunately, the researchers did not study yet the secondary task influence on the driving quality.

An old evaluation method used in ŠKODA AUTO a.s. Technology Centre (Mladá Boleslav, Czech Republic) has some drawbacks. First, driver distraction is only recorded when the participant drives outside the road boundaries. Even driving close to a road marking can be significantly dangerous for both the driver and for other traffic participants, which is not yet considered. Second, vehicle speed maintenance is not considered in the old method. However, it has been observed that many drivers significantly decelerate (even down to a full stop) while performing a secondary task. To study the level of driver distraction while performing a secondary activity more accurately, the development of a new advanced driver

situation awareness and distraction evaluation technique is required. Following the driver's expectations, the most suitable in view of driving safety human-machine interface is to be suggested for installation in a real passenger vehicle.

In the first step of the research, it is proposed to extend the driver performance evaluation by two measures: lane keeping and optimal vehicle velocity maintenance ability. The authors believe that these two measures are among the most important ones for safe vehicle operation, which, in turn, is a driver's primary task. Considering that it is quite difficult to use two independent variables for a comparative evaluation, FL is applied in this study to transform the vehicle dynamic behavior into a single output, namely, the level of driver distraction. FL is known to be a perfect approach for empirical modeling of human behavior reasoning because it allows considering several vague inputs simultaneously [16, 22].

Furthermore, the Sugeno-type fuzzy inference system is realized here with simple matrix operations. This approach makes a fuzzy algorithm easy to program using such languages as C, C++, MATLAB<sup>®</sup> script, and many others.

The next section describes the fuzzy inference system as well as the evaluation method in detail. The driver distraction test is conducted on a driving simulator test rig. As cell phone usage while driving is one of the most dangerous tasks [7], it is studied as a secondary activity. The participants of the driver-in-the-loop experiment were divided into three groups based on their gender, age, and driving experience. Section III is dedicated to the experimental facilities and procedure. The experiment results are introduced and discussed in Section IV. Finally, the research outcomes are concluded in Section V.

## II. FUZZY LOGIC DRIVER DISTRACTION EVALUATOR

A general FL inference system diagram is introduced in Fig. 1. It may have a multiple number of inputs and outputs. The input numerical signals are called "crisp". They are translated into the fuzzy sets through a fuzzification process. A fuzzy set, in turn, is a pair consisting of an element in the universe of discourse (UOD) and a degree of certainty of a membership function (MF). The rule-base block stores a linguistic knowledge, which is used to convert the fuzzy input sets into the fuzzy output sets by the inference engine. The fuzzy set outputs are then turned back to the real numbers using a defuzzification procedure.

### A. Inference mechanism

In the fuzzy inference engine presented here, the fuzzification process turns the crisp input into a column vector every element of which equals to a degree of certainty a relevant MF  $\mu^{\text{MF}}$ , which can be any quantity between 0 and 1.

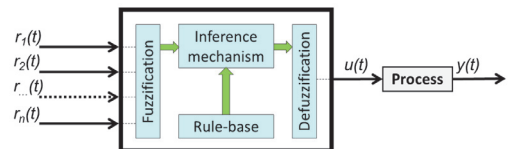


Fig. 1. Fuzzy logic inference diagram:  $r_1(t)$  – first input;  $r_2(t)$  – second input;  $r_n(t)$  –  $n^{\text{th}}$  input;  $u(t)$  – fuzzy logic output/process input;  $y(t)$  – process output.

For a “2 inputs – 1 output” system, for instance, the first input turns into an  $n \times 1$  column vector  $a$ , where  $n$  is a number of MFs for the first input. The second input turns into an  $m \times 1$  column vector  $b$ , where  $m$  is a number of MFs for the second input. Next, a dyadic product of two vectors,  $a$  and  $b$ , generates an  $m \times n$  matrix  $C$ :

$$C = b \otimes a = ba^T = \begin{bmatrix} b_1 \\ b_2 \\ \vdots \\ b_m \end{bmatrix} [a_1 \ a_2 \ \dots \ a_n] = \begin{bmatrix} b_1 \cdot a_1 & b_1 \cdot a_2 & \dots & b_1 \cdot a_n \\ b_2 \cdot a_1 & b_2 \cdot a_2 & \dots & b_2 \cdot a_n \\ \vdots & \vdots & \ddots & \vdots \\ b_m \cdot a_1 & b_m \cdot a_2 & \dots & b_m \cdot a_n \end{bmatrix} = \begin{bmatrix} c_{11} & c_{12} & \dots & c_{1n} \\ c_{21} & c_{22} & \dots & c_{2n} \\ \vdots & \vdots & \ddots & \vdots \\ c_{m1} & c_{m2} & \dots & c_{mn} \end{bmatrix} \quad (1)$$

The fuzzification procedure example for a “2 inputs – 1 output” system with the linear MFs is introduced in Fig. 2. The first input is turned into a  $3 \times 1$  while the second input is turned into a  $5 \times 1$  column vector. The size of each vector depends on the number of MFs chosen for each input variable. After applying (1), the  $5 \times 3$  matrix  $C$  is obtained (Fig. 2) every element of which is a real number between 0 and 1.

A fuzzy logic rule-base consists of the modus-ponens-form linguistic rule “If-Then”, and is often introduced as a table. In our approach, a rule-base table is represented as an  $m \times n$  matrix  $R$ . This transformation from the modus-ponens rules table to a matrix is shown in Fig. 3. It is important to note that the matrix elements are the constant values. Thus, this fuzzy inference method makes the system similar to the zero-order Sugeno inference system.

Next, matrix  $D$  is obtained as a Hadamard product for the same dimension matrices  $C$  and  $R$ :

$$D = C \circ R = \begin{bmatrix} b_1 \cdot a_1 \cdot r_{11} & b_1 \cdot a_2 \cdot r_{12} & \dots & b_1 \cdot a_n \cdot r_{1n} \\ b_2 \cdot a_1 \cdot r_{21} & b_2 \cdot a_2 \cdot r_{22} & \dots & b_2 \cdot a_n \cdot r_{2n} \\ \vdots & \vdots & \ddots & \vdots \\ b_m \cdot a_1 \cdot r_{m1} & b_m \cdot a_2 \cdot r_{m2} & \dots & b_m \cdot a_n \cdot r_{mn} \end{bmatrix} = \begin{bmatrix} d_{11} & d_{12} & \dots & d_{1n} \\ d_{21} & d_{22} & \dots & d_{2n} \\ \vdots & \vdots & \ddots & \vdots \\ d_{m1} & d_{m2} & \dots & d_{mn} \end{bmatrix} \quad (2)$$

The defuzzification process is the last step in every fuzzy inference system. During the defuzzification procedure, the fuzzy sets are converted back to the crisp output. In our case, the constructed matrices are transformed to a single numerical value by finding a weighted average of the matrix elements. The FL inference technique output  $u$  is obtained by dividing the sum of the elements in matrix  $D$  by the sum of the elements in matrix  $C$ :

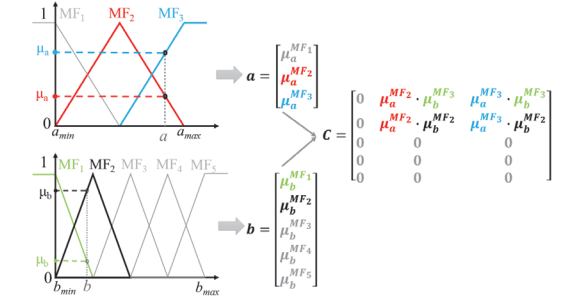


Fig. 2. Fuzzification process visual explanation.

$$u = \frac{\sum_{i=1}^m \sum_{j=1}^n d_{ij}}{\sum_{i=1}^m \sum_{j=1}^n c_{ij}}; \quad i = 1, 2, \dots, n; \quad j = 1, 2, \dots, m \quad (3)$$

where  $d_{ij}$  is an element of the  $i^{\text{th}}$  row and  $j^{\text{th}}$  column of  $D$  and  $c_{ij}$  is an element of the  $i^{\text{th}}$  row and  $j^{\text{th}}$  column of  $C$ .

### B. Fuzzy logic driver distraction evaluator

The FL driver distraction evaluator has a “2 inputs – 1 output” structure. The offset  $dx$  between the road centerline and the position of the car on the road serves as a first input. Second input is the difference  $dv$  between the speed limit on a road segment and the real vehicle speed. Thus, the vehicle dynamic performance is tracked for driver distraction evaluation.

Symmetrically dispersed MFs of the triangular (linear) shape are designed for both inputs. The linear narrow shape of MFs ensures fast response and they are simple for programming. The MFs overlap with each other over the whole UOD. Symmetrical dispersion guarantees equal sensitivity of the inputs.

The FL input and output variables must have a closed frontier  $[min, max]$  of the UOD. For  $dx$ , a UOD restriction was narrowed to  $[0, 1.5]$ . A UOD of the speed difference input  $dv$  lies in the range  $[0, 12]$ . Both inputs have three MFs.

The output variable represents the driving distraction in percentages. Thus, the output UOD is bounded within  $[0, 100]$ .

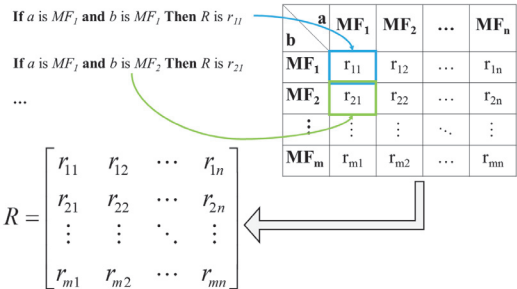


Fig. 3. Transformation of a fuzzy logic rule-base into an  $m \times n$  matrix.

TABLE II. FUZZY LOGIC EVALUATION RULE-BASE

Driver Distraction		dx		
		close	far	out
dv	good	no	negligible	low
	bad	no	medium	high
	awful	very_low	very_high	inacceptable

Singletons represent the consequent MFs as the set of values with an equal step between each set:  $\{no = 0, negligible = 14.3, very\_low = 28.6, low = 42.9, medium = 57.2, high = 71.5, very\_high = 85.8, inacceptable = 100\}$ .

The FL evaluation was realized via the modus-ponens-form rule “If-Then”. The inference system has two inputs and one output. The linguistic knowledge is stored in a  $3 \times 3$  matrix, the elements of which are the values of the output sets. Table I shows the linguistic relation between the variables. The MFs are named suitably for human understanding. An example of the linguistic input-output mapping is as follows:

**IF** the vehicle middle point is “far” off the road centerline **AND** driver’s speed limit observation is “bad”, **THEN** Driver Distraction is “medium”.

The three-dimensional surface of the designed FL inference mechanism is displayed in Fig. 4. The FL driver distraction evaluator design summary is introduced in Table II.

### III. METHODOLOGY

#### A. Subjects

The participants of the driver distraction experiment were employees of IPG Automotive GmbH (Karlsruhe, Germany). All participants (13 male and 5 female) took part in the experiment voluntarily. Their age ranged between 24 and 39 (mean 30.11). The participants’ driving experience ranged between 1 and 21 years (mean 11.33).

Before the experiment, the drivers were questioned regarding their use of electronic devices, such as tablets, smartphones, laptops, or e-readers while driving. Two participants stated that they never use them while driving; two drivers admitted to the occasional use of a device. The rest of

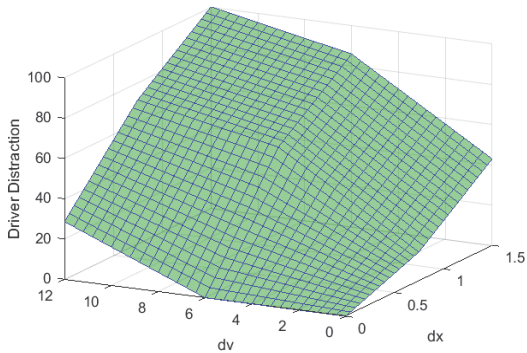


Fig. 4. Driver distraction fuzzy evaluator three-dimensional surface.

TABLE I. FUZZY LOGIC EVALUATOR OUTLOOK

Parameter	Fuzzy logic evaluator
Structure	Multi-input, single-output
Crisp input	$dx = [0, 1.5]$ (3 MFs) $dv = [0, 12]$ (3 MFs)
Crisp output	Driver Distraction = $[0, 100]$ (8 Singletons)
Input membership functions	Linear symmetric
Inference mechanism	Matrix (Sugeno’s)
Rule-base	9 modus ponens
Defuzzification	Geometric center

the participants reported that they rarely use electronic devices. All the participants pointed out that they are aware of the danger of using devices while driving.

#### B. Apparatus

The vehicle mock-up driving simulator equipment System Experience Platform (SEP) is shown in Fig. 5. The test rig has a steering wheel and two pedals: acceleration and brake. The SEP has two liquid-crystal displays and it can be extended to up to three displays. The virtual world is shown on a display which is placed in front of the driver. The SEP has an adjustable driver’s seat.

The virtual vehicle model has a manual transmission. The driver can monitor the vehicle’s speed on the head-up display. The performance data are collected with 50Hz frequency (0.02 s sample period). The SEP supports real-time integration with MATLAB®/Simulink® (Natick, MA, USA) and CarMaker by IPG Automotive (Karlsruhe, Germany).

#### C. Procedure

The participants drove a two-way, two-lane highway road of a total length of 10,626 m. The lane width was 3.5 m. The road had three segments with different speed limits (30, 50 and 90 km/h) and curvatures. The road shape was displayed on one of the SEP screens. The drivers could also track their position on the road. There were neither other vehicles nor



Fig. 5. The static System Experience Platform driving simulator.

pedestrians nor animals modeled in the virtual world.

Before the experiment, the drivers received unlimited time to familiarize themselves with the test rig. Each driver passed at least one full road lap. Thus, the participants were familiar with the road in advance.

During the experiment, the drivers were asked to drive in the right lane, keeping the car in the middle of the lane, and to observe all traffic signs. While the participants were driving in the virtual world, one of the experiment organizers sent text messages to the cell phone prepared for the participants. The drivers were requested to answer the text messages and to continue driving following all traffic rules.

The drivers were instructed to have a natural chat conversation. The experimenter asked the participants simple questions. For instance, “How are you?”, “What are your plans for the weekend?” and similar. The secondary task period was captured starting when the drivers took the phone in their hands and ending when they put the phone aside. The experimenter allowed a reasonable time between the distractive messages. Therefore, each participant drove roughly the equal amount of time both when distracted and when free of the secondary task.

#### IV. RESULTS AND DISCUSSIONS

In this section, the outcomes of the driver-in-the-loop experiment are discussed. The results of driver distraction evaluation based on the FL for a random driver are shown in Fig. 6. The periods with a green background represent the time of interaction between the driver and the cell phone. The blue curves indicate the driver distraction level in percent. For all the participants, the evaluation results are quite similar: a high percentage during texting and a low evaluation during free driving.

Although all the participants were familiar with the road curvature, they were performing significantly better (low percentage of distraction) during normal driving compared to the times when they were texting. For instance, one random driver whose drive is presented in Fig. 6, in a period from 350 to 410 seconds, was performing badly for a quite lengthy

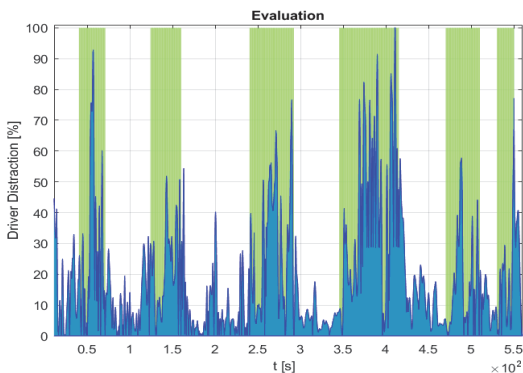


Fig. 6. Driver distraction versus time plot: green background symbolizes the secondary task accomplishment period. Evaluation example for one of the experiment participants.

period, around one minute. In real life, this could potentially lead to severe injury or even fatal accidents. In short, the proposed evaluation technique recognizes when and how strongly (in percent) the driver is distracted.

To calculate the driver distraction performance, first, the area of the driver distraction curve was found (Fig. 6, blue) using a trapezoidal rule. Second, the area value was divided by the total time the driver was distracted with the cell phone texting chat (Fig. 6, green background).

Therefore, all the driver’s evaluations were summarized and distributed between three main groups that were formed according to the participants’ gender, age, and driving experience. The average performance for different group members was calculated. Fig. 7 introduces the results of driver distraction in each group.

Two subgroups according to the participants’ responses were formed for a gender group: female and male. Referring to the experiment results, the male drivers performed a secondary activity better than their female colleagues did.

Two groups were distributed into subgroups regarding the mean age and driving experience of the participants. In the age group, the drivers were divided into younger than 30 years old and the ones of 30 years or older. The last group formed the drivers with less than 11 years of driving experience and the drivers who had at least 11 years of experience.

Among young experiment participants and those older than 30 years, the performance difference was not significant. Younger drivers showed slightly better performance. In contrast, in the experienced group, participants that were more skilled performed noticeably better than the beginners did.

#### CONCLUSION

This paper presents an evaluation method based on a fuzzy set theory focusing on a driver distraction while performing a secondary task. An inference mechanism easily realizable in programming languages and based on matrix operations is described. A driver-in-the-loop experiment on driving while performing a secondary task is conducted. Text messaging on the cell phone was examined as a secondary task.

The designed FL inference system evaluates driver distraction considering several aspects concurrently: lane keeping and the ability to observe the speed limit. The

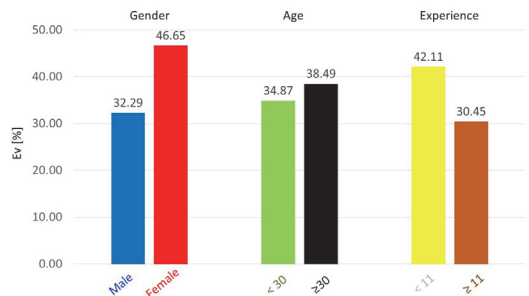


Fig. 7. Driver distraction comparison results for the three groups: gender, age and driving experience.

experiment's results show that the proposed method allows to recognize and to calculate the level of driver distraction in percentage based on safe vehicle dynamic performance. The presented method allows for driver distraction experiments to be conducted more accurately compared to the old one used in the laboratory as it involves more input measures.

Further research might be directed towards the advancement of the evaluation methodology. In particular, other parameters of vehicle dynamics are expected as new algorithm inputs. In addition, the mechanism improvement via the combination of different evaluation approaches is planned.

#### ACKNOWLEDGMENTS

The authors would like to thank IPG Automotive GmbH (Karlsruhe, Germany) for providing the test rig. We extend our special thanks to the volunteers from IPG Automotive GmbH for participating in the driver-in-the-loop experiment.

#### REFERENCES

- [1] M. Westin, R. Dougherty, C. Depcik, A. Hausmann and C. Sprouse III, "Development of an adaptive-human-machine-interface to minimize driver distraction and workload," ASME 2013 International Mechanical Engineering Congress & Exposition (IMECE2013), San Diego, California, USA, 2013, pp. 1-13.
- [2] T. Horberry, J. Anderson, M. A. Regan, T. J. Triggs and J. Brown, "Driver distraction: the effect of concurrent in-vehicle tasks, road environment complexity and age on driving performance," *Acc. Anal. and Prev.*, vol. 38, pp. 185-191, January 2006.
- [3] L. J. Gugerty, "Situation awareness during driving explicit and implicit knowledge in dynamic spatial memory," *J. of Exper. Psych.: Appl.*, vol. 3, pp. 42-66, March 1997.
- [4] K. A. Brookhuis, G. de Vries and D. de Waard, "The effect of mobile telephoning on driving performance," *Accid. Anal. & Prev.*, vol. 23, pp. 309-316, August 1991.
- [5] National Center for Statistics and Analysis. 2015 Motor Vehicle Crashes: Overview. Report no. DOT HS 812 318. Washington, DC: National Highway Traffic Safety Administration, 2016
- [6] AAA Foundation for Traffic Safety. Using Naturalistic Driving Data to Assess the Prevalence on Environmental Factors and Driver Behaviors in Teen Driver Crashes. Washington, DC: AAA Foundation for Traffic Safety, 2015. Available: <https://www.aaafoundation.org/sites/default/files/2015TeenCrashCausati onReport.pdf>
- [7] AAA Foundation for Traffic Safety. 2016 Traffic Safety Culture Index. Washington, DC: AAA Foundation for Traffic Safety, 2017. Available: [https://www.aaafoundation.org/sites/default/files/2016TrafficSafetyCult ureIndexReportandCover\\_0.pdf](https://www.aaafoundation.org/sites/default/files/2016TrafficSafetyCult ureIndexReportandCover_0.pdf)
- [8] R. R. Mouton and T. H. Rockwell, "Strategy of visual search by novice and experienced drivers," *Hum. Fac.*, vol. 14, pp. 325-335, August 1972.
- [9] D. L. Strayer, F. A. Drews and W. A. Johnston, "Cell phone-induced failure of visual attention during simulated driving," *J. of Exper. Psych.: App.*, vol. 9, pp. 23-32, March 2003.
- [10] A. K. Pradhan, K. R. Hammel, R. DeRamus, A. Pollatsek, D. A. Noyce and D. L. Fisher, "Using eye movement to evaluate effects of driver age on risk perception in a driving simulator," *Hum. Fac.*, vol. 47, pp. 840-852, January 2005.
- [11] A. Pollatsek, V. Narayana, A. Pradhan and D. L. Fisher, "Using eye movement to evaluate a PC-based risk awareness and perception training program on a driving simulator," *Hum. Fac.*, vol. 48, pp. 447-464, May 2005.
- [12] G. Tillman, D. Strayer, A. Eidsels and A. Heathcote, "Modeling cognitive load effects of conversation between a passenger and driver", *Atten. Perc. & Psycho.*, pp. 1-9, May 2017.
- [13] J. O. Brooks, R. A. Tyrrell and T. A. Franks, "The effect of severe visual challenges on steering performance in visually healthy young drivers," *Optom. & Vis. Sci.*, vol. 82, pp. 689-697, August 2005.
- [14] D. Filev, J. Lu, F. Tseng and K. Prakah-Asante, "Real-time driver characterization during car following using stochastic evolving models," 2011 IEEE International Conference on Systems, Man, and Cybernetics (SMC), Anchorage, AK, USA, 2011, pp. 1031-1036.
- [15] W. J. Horrey, C. D. Wickens and K. P. Consalus, "Modeling drivers visual attention allocation while interacting with in-vehicle technologies," *J. of Exper. Psych.: Appl.*, vol. 12, pp. 67-78, June 2006.
- [16] K. M. Passino and S. Yurkovich, *Fuzzy Control*, California: USA, Addison Wesley, 1998, pp.10-101.
- [17] D. Dörr, D. Grabengieser and F. Gauterin, "Online driving style recognition using fuzzy logic," 2014 IEEE 17th International Conference on Intelligent Transportation Systems (ITSC), Quindao, China, 2014, pp. 1-6.
- [18] A. Shaout and R. Tonshal, "Real time driver activity index detection using fuzzy logic," *Int. J. Of Adv. Res. In Electri. Electro. & Instrum. Eng. India*, vol. 3, pp. 1-8, September 2014.
- [19] D. K. Saini and J. H. Youisif, "Reduction in accidental death: determining driver behavior using fuzzy theory," 5th Annual International Commerce Conference, Delhi, India, 2016, pp. 1-7.
- [20] M.-H. Sigari, M. Fathy and M. Soryani, "A driver face monitoring system for fatigue and distraction detection," *Int. J. Of Veh. Tech. London*, vol. 2013, pp. 1-11, November 2012.
- [21] M. K. Wali and M. Murugappan, "Subtractive fuzzy classifier based driver distraction levels classification using EEG," *J. of Phys. Ther. Sci.*, vol. 25, pp. 1055-1058, September 2013.
- [22] A. Aksjonov, K. Augsburg, and V. Vodovozov, (2016). "Design and simulation of the robust ABS and ESP fuzzy logic controller on the complex braking maneuvers," *Appl. Sci.*, vol. 6, pp. 382-390, November 2016.

**Andrei Aksjonov** received his B.Sc. and M.Sc. in electrical engineering and electrical drives and power electronics with automation specialization from Tallinn University of Technology in 2013 and 2015, respectively. He is currently a Marie Skłodowska-Curie research fellow. His research topic is the development of driver distraction detection and human-machine interface evaluation methods for multi-actuated ground vehicles. His research interests include HMI, fuzzy systems, machine learning, vehicle safety, ADAS.

**Pavel Nedoma** received his M.Sc. and Ph.D. from Czech Technical University in Prague in 1985 and 2007, respectively. Since 1985, he has been working at the ŠKODA AUTO Development Department as a Development Engineer. He is responsible on development experimental tools for simulation, supervision, analysis, processing and visualization HMI interaction between driver and other on-board systems, HMI measurements in car ride simulators and comparative measurements performed in real vehicles.

**Valery Vodovozov** received his Candidate of Science degree and Associate Professor and Senior Researcher academic titles in Electrical Engineering from St. Petersburg Electrotechnical University, Russia. He is a professor of Tallinn University of Technology, Estonia, a member of IEEE, International Institute of Informatics and Systemics (IIS), and Global Research Alliance of Texas Institute of Science (TxIS GRA). His research interests include power electronics and electrical drives areas.

**Eduard Petlenkov** received his B.Sc., M.Sc. and Ph.D. degrees in computer and systems engineering from Tallinn University of Technology. He is an Associate Professor in the Department of Computer Systems at Tallinn University of Technology. His main research interests lie in the domain of nonlinear control, system analysis and computational intelligence.

**Martin Herrmann** received his B.Sc. and M.Sc. in automotive engineering from Ilmenau University of Technology in 2012 and 2014. He is currently Business Development Manager at IPG Automotive focusing on methods for testing ADAS and automated driving functions in virtual environments. This includes especially road, traffic and sensor modeling.

**Publication III**

**Aksjonov, A.**, Nedoma, P., Vodovozov, V., & Petlenkov, E. (2018). Driver Distraction Detection and Evaluation with Artificial Neural Network and Fuzzy Logic. In-vehicle information system as a driver's secondary activity: Case study. *Proceedings of the 15th IEEE International Workshop on Advanced Motion Control (AMC2018)* (pp. 523–528). Tokyo: IEEE. doi: 10.1109/AMC.2019.8371148



# Driver Distraction Detection and Evaluation with Artificial Neural Network and Fuzzy Logic

In-vehicle information system as a driver's secondary activity: Case study

Andrei Aksjonov, Pavel Nedoma

Concept Development  
ŠKODA AUTO a.s.

Mladá Boleslav, Czech Republic

{ andrei.aksjonov; pavel.nedoma }@skoda-auto.cz

Valery Vodovozov, Eduard Petlenkov

Department of Electrical Power Engineering and  
Mechatronics

Tallinn University of Technology

Tallinn, Estonia

{ valery.vodovozov; eduard.petlenkov }@ttu.ee

**Abstract**—A robust methodology for detecting and evaluating driver distraction induced by in-vehicle information system using artificial neural network and fuzzy logic is introduced in this paper. An artificial neural network is used to predict driver's performance on a specific road segment. The predicted performance-based measures are compared to the driving with secondary task accomplishment. Fuzzy logic is applied to fuse the variables into a single output, which constitutes a level of driver distraction in percentage. The technique was tested on a vehicle simulator by ten drivers that exploited in-vehicle information system as a secondary activity. The driver-in-the-loop experiment outcomes are discussed.

**Keywords**—artificial neural networks; fuzzy logic; vehicle safety; machine learning; prediction methods

## I. INTRODUCTION

Driver distraction (DD) causes serious environmental problem every year. Not to mention injuries, DD contributes to more than 5000 traffic fatalities yearly in the USA alone. Unfortunately, this trend does not tend to decline [1].

DD is defined as "anything that delays the recognition of information necessary to safety maintain the lateral and longitudinal control of the vehicle (driver's primary task) due to some event, activity, object or person, within or outside the vehicle that compels or tends to induce the driver's shifting attention away from the fundamental driving task by compromising the driver's auditory, biomechanical, cognitive or visual faculties or combinations thereof". The activities not related to primary tasks driver perform while driving are defined as secondary activities [2, 3, 4, 5].

There are two types of secondary tasks: interaction with in-vehicle information system (IVIS) (e.g. controlling comfort and entertainment), and interaction with the items brought to a vehicle (e.g. portable electronic devices, passengers, pets) [2]. DD minimization caused by IVIS is under vehicle manufacturers' responsibility. In particular, the vehicle cockpit and human-machine interface (HMI) must be safe for operation, intuitive, well organized, and, what is most important, not distract a driver from her/his primary task.

Development of a robust DD detection and assessment methodology while interacting with IVIS allows testing different HMI technologies and cockpit designs before they are accepted in series vehicle. DD evaluation is also applied in advanced driver assistance systems impact on driver's situation awareness. Today, there are still no accurate evaluation technologies for DD induced by IVIS [2, 6, 7].

Previously, many different attributes were proposed for DD detection. Among them, psychological [8], behavioral [9], subjective [10], performance-based or their combinations [11] are known. For DD detection, machine learning (e.g. support vector machine, graph-regularized extreme learning machine,  $k$ -nearest neighbor) deserved special attention among other algorithms [12].

Artificial neural network (ANN) is one of the most popular machine learning approaches [13] due to its robustness, ability to learn by example, and efficiency in intelligent systems. The ANNs are used in various disciplines: physics, statistics, psychology, cognitive science, neuroscience, and linguistics, not to mention computer science, electrical engineering, and adaptive control [14]. Many researchers on DD detection and assessment applied ANN to solve their problems.

In [15], a three-dimensional convolutional neural network (CNN) and gradient boosting algorithms combination were proposed for drowsiness classification. Gaze zone categorization was designed using CNN in [16]. A probabilistic restricted Coulomb energy ANN was implemented for drowsy driving prediction in [17]. In these works, the researchers preferred behavioral attributes. Unfortunately, behavioral and psychological attributes always require supplementary devices (e.g. cameras and neuro-scan systems) that increase system cost and complexity [18].

Another famous approach of DD detection - performance-based - does not require additional devices. These methods depend on vehicle dynamic performance, which is tracked by the sensors available in modern vehicles (e.g. vehicle velocity and steering wheel angle). In [19], the scholars proposed DD detection using in-vehicle signals without planned distraction. The machine learning schemes, ANN, and Gaussian mixture

models were combined to solve the problem. In [20], a real-time DD detection classifier using vehicle dynamic data was introduced. Different machine learning algorithms, including static and dynamic ANNs, adaptive neuro-fuzzy inference system, and support vector machine, were compared. The last one outperformed all the other classifiers.

For accurate DD detection, different attributes can be combined. For example, behavioral (i.e. head movement) and performance-based data were integrated for the online DD detection with long- and short-term memory recurrent ANN in [21]. In [22], an adaptive neuro-fuzzy inference system for DD prediction was developed. This approach showed better performance comparing to the ANN and radial basic function prediction algorithms.

Another computational intelligence method, fuzzy logic (FL), is also widely used in automotive engineering, from vehicle dynamics control [23] to DD evaluation [24]. A thorough review on fuzzy methods in automotive engineering applications can be found in [25].

Although the results of the related works were very positive in DD detection, they all use the 2-class classification: distracted or not distracted. This classification is not suitable for measuring the DD level and consequent IVIS HMI technology comparative evaluation. Hence, in this paper a solution of the regression problem is proposed for DD detection with performance-based attributes bearing in mind that ANNs are actively used for nonlinear regression [14].

An ANN is designed as a driver performance predictor in a name of lane keeping ability and speed limit maintenance. First, the ANN is trained with data collected during the DD-free driving. Next, the predicted variables are compared to the same variables collected during driver's run with completing secondary task in parallel to driving. The comparison is used for DD detection. As FL is efficient in data fusion [26, 27], it is applied to merge vehicle dynamics into a single variable. This variable depicts a level of DD in percentage caused by a secondary activity.

Next Section is dedicated to the methodology based on ANN and FL combination description. The driver-in-the-loop experiment was conducted on an advanced driving simulator provided by ŠKODA AUTO (Mladá Boleslav, Czech Republic). The experiment procedure, subjects, and apparatus are described in Section III. The DD detection and evaluation methodology outcomes are stressed in Section IV. Finally, the research conclusion is provided in Section V.

## II. DRIVER DISTRACTION DETECTION METHOD

The block scheme of the DD detection and evaluation method is presented in Fig. 1. The symbols' description and annotation are introduced in Table I. The method involves three steps. First, the ANN predicts a vehicle dynamic performance on a specific road segment taking as the inputs an information about the road segment: speed limit  $V_l$  and curvature (radius)  $r$ . The outputs of the ANN describe predicted driver performance on a specific road segment: ability to hold a speed limit  $\Delta v_p$  and to stay in the middle of the road lane  $\Delta x_p$ . The training data for the ANN are collected

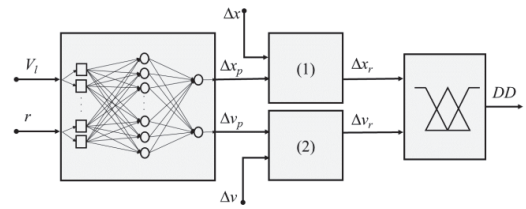


Fig. 1. DD detection and evaluation method block scheme.

during the first phase of the experiment, when the driver demonstrates her/his normal vehicle operation, without secondary activity.

Second, the predicted variables are compared to a real driving performance  $\Delta x$  and  $\Delta v$  with IVIS interaction. The comparison outcomes are the resultative variables  $\Delta x_r$  and  $\Delta v_r$ , calculated using the following rules:

$$\Delta x_r = \begin{cases} \Delta x - \Delta x_p, & \text{if } \Delta x > 0; \Delta x_p > 0; |\Delta x| > |\Delta x_p| \\ \Delta x - \Delta x_p, & \text{if } \Delta x < 0; \Delta x_p < 0; |\Delta x| > |\Delta x_p| \\ \Delta x + \Delta x_p, & \text{if } \Delta x > 0; \Delta x_p < 0; |\Delta x| > |\Delta x_p| \\ \Delta x + \Delta x_p, & \text{if } \Delta x < 0; \Delta x_p > 0; |\Delta x| > |\Delta x_p| \\ 0, & \text{if } |\Delta x| \leq |\Delta x_p| \end{cases} \quad (1)$$

$$\Delta v_r = \begin{cases} \Delta v - \Delta v_p, & \text{if } \Delta v > 0; \Delta v_p > 0; |\Delta v| > |\Delta v_p| \\ \Delta v - \Delta v_p, & \text{if } \Delta v < 0; \Delta v_p < 0; |\Delta v| > |\Delta v_p| \\ \Delta v + \Delta v_p, & \text{if } \Delta v > 0; \Delta v_p < 0; |\Delta v| > |\Delta v_p| \\ \Delta v + \Delta v_p, & \text{if } \Delta v < 0; \Delta v_p > 0; |\Delta v| > |\Delta v_p| \\ 0, & \text{if } |\Delta v| \leq |\Delta v_p| \end{cases} \quad (2)$$

Negative  $\Delta x$  means that the vehicle drives closer to the road dividing line. Contrariwise, positive  $\Delta x$  means that the vehicle drives towards off road from the middle of the lane. Negative  $\Delta v$  shows that the vehicle velocity is lower than the speed limit on a road segment whereas positive  $\Delta v$  signifies speeding. Finally, FL completes data fusion and outputs a level of DD in percentage  $DD$ .

The evaluation method is programmed in MATLAB® (Natick, MA, USA) environment. The Neural Network Toolbox™ was exploited for the design of the ANN driver performance predictor. One of the most popular methods due to its optimal computation complexity - backpropagation [13] -

TABLE I. PARAMETERS DESCRIPTION

Symbol	Description	Unit
$r$	Road radius	m
$V_l$	Speed limit	km/h
$\Delta x$	Real lane keeping offset	m
$\Delta v$	Real vehicle speed deviation	km/h
$\Delta x_p$	Predicted lane keeping offset	m
$\Delta v_p$	Predicted vehicle speed deviation	km/h
$\Delta x_r$	Resultative lane keeping offset	m
$\Delta v_r$	Resultative vehicle speed deviation	km/h
$DD$	Driver distraction in percentage	%

TABLE II. RULE-BASE OF THE FL EVALUATOR

DD [%]		$\Delta x_r$ [m]				
		very close	close	zero	far	very far
$\Delta v_r$ [km/h]	very_low	100	71.5	42.9	71.5	100
	low	85.8	14.3	0	14.3	85.8
	zero	42.9	0	0	0	42.9
	high	71.5	14.3	0	14.3	71.5
	very_high	85.8	57.2	28.6	57.2	85.5

was used for computing gradients in the ANN. The algorithm detailed description for training a multilayer perceptron for regression is reported in [14].

The Levenberg-Marquardt method is the most suitable for training an ANN with nonlinear regression (function fitting) purposes. In practice, ANNs incorporate three and sometimes four layers, including one or two hidden layers with 10 to 1000 neurons in each. More hidden layers do not guarantee better ANN performance likewise the greater number of neurons does. On the contrary, each additional layer increases the computational burden exponentially [14, 15].

Two hidden layers were used for ANN in this study. The network performance was tested on different number of neurons in each layer. However, we did not notice the ANN significant enhancement with more than 100 neurons. Due to its simplicity and superior performance [13], the tangent-sigmoid activation function was applied in the hidden layers. As a rule, for the outputs the linear transfer functions are used in regression [13]. In short, a feedforward ANN with two hidden layers of 100 neurons each, with a tangent-sigmoid transfer function in the hidden layer, and a linear transfer function in the output layer was designed using the Levenberg-Marquardt training method.

In this research, an FL Sugeno’s type inference mechanism based on simple matrix operations suitable for C, C++, MATLAB® script, and other programming languages was used [24]. The FL DD evaluator has a “2 inputs - 1 output” structure. The inputs are  $\Delta x_r$  and  $\Delta v_r$ . The DD output represents a level of DD in percentage (Fig. 1).

Five symmetrically dispersed and overlapped over the whole universe of discourse (UOD) triangular membership functions (MFs) capable for fast response and easy for

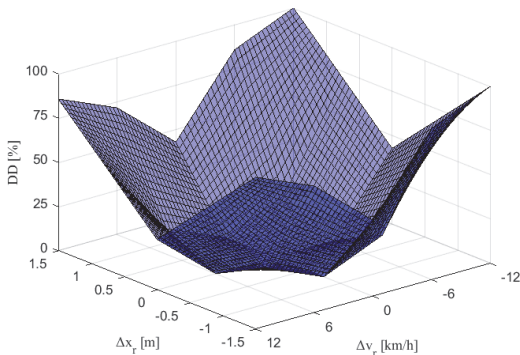


Fig. 2. The DD FL evaluator nonlinear control surface.

programming were designed for both inputs. Inputs’ equal sensitivity is guaranteed by the symmetric MFs dispersion. The  $\Delta x_r$  UOD was bounded between [-1.5, 1.5] whereas the  $\Delta v_r$  UOD was narrowed in [-12, 12].

The output UOD is bounded within [0, 100]. The output MFs represent eight singletons with equal step 14.3 between each other: {0, 14.3, 28.6, 42.9, 57.2, 71.5, 85.8, 100}. The step is calculated by dividing the highest value of UOD boundary by an amount of MFs starting from the second singleton, because the first one is equal to zero. Consequently, the fixed step between the output MFs guarantees their equal sensitivity inside of the UOD.

Modus-ponens-form rules “If-Then” are applied to connect the inputs with the output. The input-output linguistic relation is presented in Table II. The control surface for the designed FL evaluator is shown in Fig. 2. An example of the linguistic input-output mapping is performed as follows:

**IF** the vehicle center is “far” from the road dividing line **AND** driver’s speed is “low” comparing to the road speed limit, **THEN** driver distraction is “14.3%”.

### III. METHODOLOGY

#### A. Subjects

Ten driver-in-the-loop experiment participants were members of the Interdisciplinary Training Network in Multi-Actuated Ground Vehicles (ITEAM) project. In this study, only male drivers participated. Their age ranged between 27 and 31 years old. Every participant owned a valid driver license. All drivers took part in the experiment voluntarily.

The experiment participation was not paid. However, for their contribution the participants were awarded with a guided tour to ŠKODA AUTO museum and vehicle production plant (Mladá Boleslav, Czech Republic) free of charge.

#### B. Apparatus

The experiment was conducted on available in ŠKODA AUTO HMI laboratory (Mladá Boleslav, Czech Republic) facilities that consist of a fixed-base vehicle mockup and a wall screen in front of the driver, where the virtual world is projected (Fig. 3). A driver settled down inside the vehicle simulator, which has an automatic gearbox, steering wheel, adjustable driver’s seat, acceleration and brake pedals. The



Fig. 3. Driver-in-the-loop experiment facility.

TABLE III. IN-VEHICLE SECONDARY TASKS

#	In-vehicle secondary task	
1.	Volume	Volume regulation
2.	Context selection	Radio
3.		Media
4.		Telephone
5.		Navigation
6.	Radio	Radio station selection from a primary list
7.		Radio station selection from an overall list
8.	Media	Media source selection (e.g. CD, SD-card)
9.		Media item selection
10.		Song shuffle
11.	Telephone	Call a number from a favorite contact list
12.		Call a number from an overall contact list
13.	Navigation	Input location
14.		Input of a next target
15.		Zoom operation

vehicle cockpit is identical to the one used in commercial vehicles. The simulator's head-up instrument panel displays current vehicle velocity. All the secondary tasks are conducted via the HMI display placed, like in most of the European countries, on the driver's right.

Vehicle dynamics and virtual world are modelled using an open source library for simulating rigid body dynamics Open Dynamics Engine™ v 0.5 in C++ programming language [28]. The vehicle model consists of the vehicle body, suspension system, four wheels, and the tire model completed with Pacejka's Magic Formula [29]. The vehicle is parametrized according to Škoda Yeti SK316 with 1.4 liters twincharged stratified injection 77 kW engine specifications. The drivers could understand when they drive off the road on a grass by the screen vibration. However, they could not feel crossing the road dividing line.

Three coordinates (i.e.  $x$ ,  $y$ ,  $z$ ) are saved in the virtual world for each wheel with 0.1 seconds sample period. These data are exploited for lane keeping offset and for vehicle speed deviation calculations. The drivers control the vehicle via the steering wheel and the brake and acceleration pedals.

### C. Procedure

The driver-in-the-loop experiment participants were asked to drive the two-way lap of a total length of 10626 meters with a 3.5 meters width lane. The road has two main segments: the curvy road with a speed limit of 50 km/h and the almost straight road with slight curvature of 90 km/h. When all the speed limits are respected, one lap takes approximately 10 minutes for driving. There were no other traffic participants modelled, neither pedestrians nor other vehicles.

To familiarize with the simulator, the drivers were allowed to drive it unlimited time, before the start of the driver-in-the-loop experiment. Thus, they were aware of the test rig and the road shape preliminary. What is more, the participants were instructed to the studied HMI display. They could try all the secondary tasks in advance.

The experiment for each participant was divided into two parts. First, the drivers were asked to pass two laps showing their best performance in lane keeping ability and following all the traffic regulations (i.e. speed limits). They were not fulfilling a secondary activity during the first part of the experiment. The data collected during the free from the secondary task driving were used for the ANN training. During the second part, the drivers were asked to continue driving obeying the traffic rules and staying in the middle of the lane as good as feasible. However, this time they drove the same road performing a secondary activity in parallel. The participants

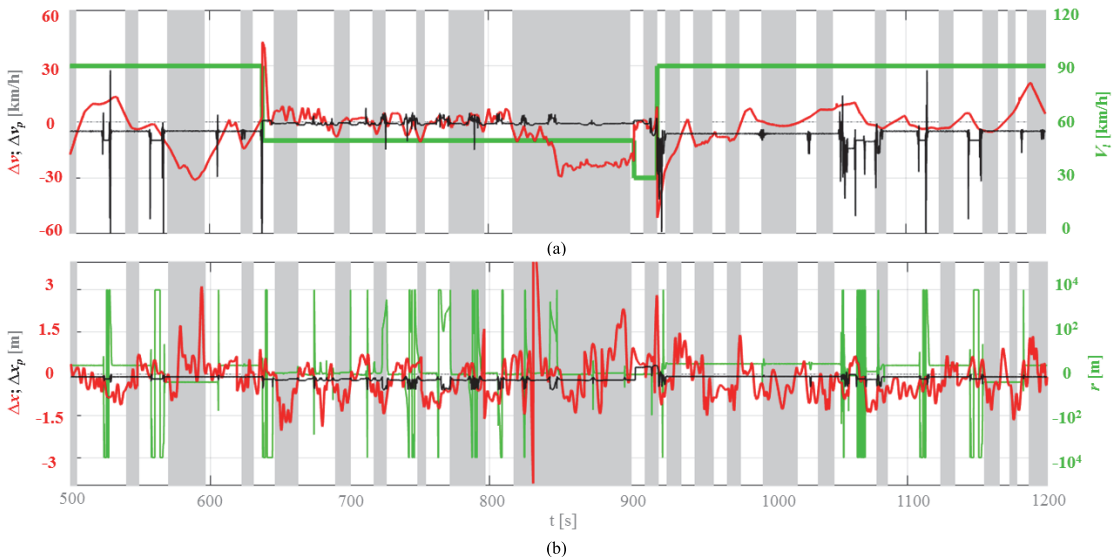


Fig. 4. Driver performance prediction versus real driver performance example for one of the experiment participants: gray background — the secondary task accomplishment period; red line — real driver performance; black line — predicted performance; green line — road information; (a) speed difference  $\Delta v$  and road speed limit  $V_l$ ; (b) center lane keeping offset  $\Delta x$  and road radius  $r$ .

were allowed to take a break between the experiment parts.

The in-vehicle secondary tasks are introduced in Table III. The experiment organizer sent the vocal command to the driver for a secondary activity request. When the secondary task is accomplished, the driver sent a feedback to the experimenter via a switch around the steering wheel. If the task is correct, the driver heard a vocal signal informing that the submitted task is correct. If the completed task is wrong and the driver did not hear the sound signal, she/he had to perform the secondary activity again. The participant had a reasonable time between each secondary task request. No time restriction for a secondary task realization was applied.

#### IV. RESULTS

The driver-in-the-loop experiment outcomes are presented in this section. A random driver performance prediction, DD detection and evaluation with FL is studied here in details. For the rest of the participants the results are very similar: low DD during normal driving and high level of DD while performing a secondary activity.

In Fig. 4, the driver performance prediction for  $\Delta v_p$  and  $\Delta x_p$  versus real performance  $\Delta v$  and  $\Delta x$  with secondary activity is introduced. During the experiment, the driver passed more than two full laps. However, in this paper the results only from the last lap are presented.

Within normal driving, the driver tended to keep the speed slightly lower its road segment limit (Fig 4a; black curve). In average, the speed deviation did not exceed 5 km/h. When the secondary task is performed (Fig. 4a; red curve), the speed limit maintenance ability has higher oscillation. For example, in the period from 820 s to 900 s the driver slowed the speed by more than 25 km/h, while during the DD-free run the participant was able to keep  $\Delta v$  almost at zero.

The lane keeping ability along with road radiuses are introduced in Fig. 4b. In average, the participant was holding

the middle line with 0.2 m error. On the contrary, when the driver was performing a secondary activity, his driving performance was significantly burdened. The lane keeping ability lower than -1 m or higher than 1 m means that the vehicle was driving out of the road bounds. When the participant performed secondary tasks, in most of the cases the vehicle went outside the road limits.

As it is noticed in Fig. 4, the interaction with the IVIS influences the vehicle dynamic performance. The impact depends on a task complexity. The proposed DD detection method easily recognizes the difference between normal DD-free driving and driving while performing the secondary task. Thereafter, the FL evaluates the level of DD.

In Fig. 5, DD evaluation is presented. It is seen that DD is noticeably higher when the driver interacts with HMI by executing the secondary activity. For some tasks (Table III), the DD is low, for example, in case of the task number 1 - volume regulation. On the contrary, some tasks caused very high DD. For instance, with the task number 13 - searching for a new location in a navigation system, the driver performed badly for a quite long period (Fig. 5, inset). It can also be observed from Fig. 4 for the period between 820 s and 900 s. During this secondary task accomplishment, the driver dropped the speed and went off the road several times (Fig. 4). The method easily detects these mistakes in vehicle dynamic performance and provides an appropriate evaluation (Fig. 5).

#### V. CONCLUSION

A DD detection and evaluation method based on ANN and FL combination is presented in this paper. An ANN is applied to solve a regression problem in driver performance prediction on a specific road segment. The prediction is based on normal driving without performing a secondary activity. Next, the predicted performance-based variables are compared to the same vehicle dynamics data collected during the driver run with secondary activity accomplishment. The performance

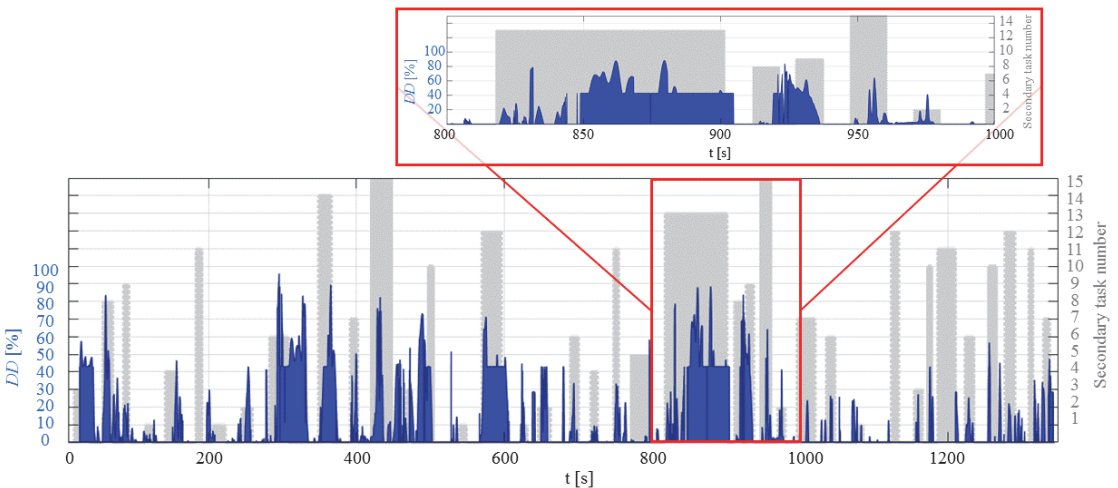


Fig. 5. Driver distraction evaluation results: gray background — the secondary task accomplishment period; blue curve — DD. The secondary task number refers to Table III.

degradation is accepted as a DD detection. Finally, the data pass through FL evaluator, which outputs a level of DD.

The method is verified in driver-in-the-loop experiment on an advanced driver decoy simulator with ten participants. The results show that the methodology is always capable to detect DD when an experiment participant interacts with IVIS. The evaluation by FL allows an accurate comparison of different in-vehicle secondary tasks. In particular, it shows what secondary tasks lead to higher level of DD comparing to another ones. The proposed methodology provides a practical tool for HMI technologies comparative analysis.

In the future, more driver-in-the-loop participants will be studied on IVIS-induced DD detection and evaluation with the proposed methodology. Moreover, other machine learning algorithms (e.g. *k*-nearest neighbor, adaptive neuro-fuzzy inference system, and long short-term memory) efficient in nonlinear regression [14] will be applied and compared to an ANN. Different attributes combination and more performance-based variables will be used for the method improvement.

#### ACKNOWLEDGMENT

This project has received funding from the European Union's Horizon 2020 research and innovation program under grant agreement No. 675999. The authors extend their gratitude to the volunteers from ITEAM (<https://iteam-project.net>) project for participating in the driver-in-the-loop experiment.

#### REFERENCES

- [1] AAA Foundation for Traffic Safety. 2016 Traffic Safety Culture Index. Washington, DC: AAA Foundation for Traffic Safety, 2017. [Online] Available: [https://www.aaafoundation.org/sites/default/files/2016TrafficSafetyCultureIndexReportandCover\\_0.pdf](https://www.aaafoundation.org/sites/default/files/2016TrafficSafetyCultureIndexReportandCover_0.pdf)
- [2] M. Westin, R. Dougherty, C. Depcik, A. Hausmann, and C. Sprouse III, "Development of an adaptive-human-machine-interface to minimize driver distraction and workload", in Proc. in the ASME 2013 Int. Mechan. Engin. Cong. and Expos., San Diego, California, USA, 2013, pp. 1-13.
- [3] J. L. Hansen, C. Busso, Y. Zheng, and A. Sathyanarayana, "Driver modeling for detection and assessment of driver distraction: Examples from the UTDrive test bed," IEEE Sig. Proc. Mag., vol. 34, no. 4, pp. 130-142, Jan. 2017.
- [4] S. Arun, K. Sundaraj, and M. Murugappan, "Driver inattention detection method: A review," in 2012 IEEE Cong. On Sust. Utiliz. And Develop. in Engin. and Technol. (STUDENT), Kuala Lumpur, Malaysia, 2013, pp. 1-6.
- [5] Q. Wu, "An overview of driver distance measure methods," in IEEE 10th Intern. Conf. on Comp.-Aided Ind. Design & Concept. Design, 2009 (CAID & CD 2009), Wenzhou, China, 2009, pp. 2391-2394.
- [6] C. A. Pickering, K. J. Bunnham, and M. J. Richardson, "A review of automotive human machine interface technologies and techniques to reduce driver distraction," in 2<sup>nd</sup> IET Int. Conf. on Syst. Safety 2007, London, UK, 2007, pp. 223-228.
- [7] A. Amditis, L. Andreone, K. Pagle, G. Markkula, E. Deregis, M. R. Rue, F. Bellotti, A. Engelsberg, R. Brouwer, B. Peters, and A. De Gloria, "Towards the automotive HMI of the future overview of the AIDE-integrated project results," IEEE Trans. on Intel. Transp. Syst., vol. 11, no. 3, pp. 567-578, Sept. 2010.
- [8] S. Wang, Y. Zhang, C. Wu, F. Darvas, and W. A. Chaovalitwongse, "Online prediction of driver distraction based on brain activity patterns," IEEE Trans. on Intel. Transp. Syst., vol. 16, no. 1, pp. 136-150, Feb. 2015.
- [9] C. Ahlstrom and K. Kirscher, "Review of real-time visual driver distraction detection algorithms," in Proc. of the 7<sup>th</sup> intern. Conf. on Methods and Techniq. in Behavi. Research, Eindhoven, The Netherlands, 2010, pp. 310-313.
- [10] T. Horberry, J. Anderson, M. A. Regan, T. J. Triggs, and J. Brown, "Driver distraction: The effect of concurrent in-vehicle tasks, road environment complexity and age on driving performance," Acc. Anal. and Prev., vol. 38, pp. 185-191, January 2006.
- [11] M. Miyaji, H. Kawanaka, and K. Oguri, "Study on effect of adding pupil diameter as recognition features for driver's cognitive distraction detection," in 2010 7<sup>th</sup> Intern. Symp. On Communi. Syst., Netw. And Digit. Signal Proc. (CSNDSP 2010), Newcastle upon Tyne, UK, 2010, pp. 1-6.
- [12] Y. Jiao, Y. Peng, B.-L. Lu, X. Chen, S. Chen, and C. Wang, "Recognizing slow eye movement for driver fatigue detection with machine learning approach," in 2014 Intern. Joint Conf. on Neural Netw. (IJCNN), Beijing, China, 2014, pp. 4035-4041.
- [13] M. Negnevitsky, Artificial Intelligence: A Guide to Intelligent System. 2nd ed. Harlow, England: Adison-Wesley, 2005, pp. 165-217.
- [14] E. Alpaydin, Introduction to Machine Learning. Cambridge, Massachusetts: USA: The MIT Press, 2004, pp. 229-373.
- [15] X.-P. Huynh, S.-M. Park, and Y.-G. Kim, "Detection of driver drowsiness using 3D deep neural network and semi-supervised gradient boosting machines," in Asian Conf. on Comp. Vision (ACCV) Lecture Notes in Computer Science, vol. 10118. Springer, 2016, pp. 134-145.
- [16] I.-H. Choi, S. K. Hong, and Y.-G. Kim, "Real-time categorization of driver's gaze zone using the deep learning techniques," in 2016 Intern. Conf. on Big Data and Smart Comp. (BigComp), Hong Kong, China, 2016, pp. 143-148.
- [17] H. Matsuo and A. Khat, "Prediction of drowsy driving by monitoring driver's behavior," in 21<sup>st</sup> Inter. Conf. on Pattern Recogn. (ICPR 2012), Tsukuba, Japan, 2012, pp. 3390-3393.
- [18] C. Ahlstrom, K. Kircher, and A. Kircher, "A gaze-based driver distraction warning system and its effect on visual behavior," IEEE Trans. on Intel. Transp. Syst., vol. 14, no. 2, pp. 965-973, June 2013.
- [19] S. Im, C. Lee, S. Yang, J. Kim, and B. You, "Driver distraction detection by in-vehicle signal processing," in 2014 IEEE Symp. On Comput. Intel in Vehic. and Transp. Syst. (CIVTS), Orlando, FL, USA, 2015, pp. 1-5.
- [20] F. Tango and M. Botte, "Real-time detection system of driver distraction using machine learning," IEEE Trans. on Intel. Transp. Syst., vol. 14, no. 2, pp. 894-905, June 2013.
- [21] M. Wollmer, C. Blaschke, T. Schmidl, B. Schuller, B. Farber, S. Mayer, and B. Treflich, "Online driver distraction detection using long short-term memory," IEEE Trans. on Intel. Transp. Syst., vol. 12, no. 2, pp. 574-582, June 2011.
- [22] F. Tango, C. Calefato, L. Minin, and L. Canovi, "Moving attention from the road: A new methodology for the driver distraction evaluation using machine learning approach," in 2009 2<sup>nd</sup> Conf. on Human. Syst. Interact., Catania, Italy, 2009, pp. 596-599.
- [23] A. Aksjonov, K. Augsburg, and V. Vodovozov, "Design and simulation of the robust ABS and ESP fuzzy logic controller on the complex braking maneuvers," Appl. Sci., vol. 6, pp. 382-390, Nov. 2016.
- [24] A. Aksjonov, P. Nedoma, V. Vodovozov, E. Petlenkov, and M. Herrmann, "A method of driver distraction evaluation using fuzzy logic," in 2017 XXVI Intern. Conf. on Inform., Commun. and Autom. Techn. (ICAT), Sarajevo, Bosnia & Herzegovina, pp 23-28.
- [25] V. Ivanov, "A review of fuzzy methods in automotive engineering applications", Europ. Transp. Res. Rev., vol. 7, no. 3, pp. 1 - 10, Aug. 2015.
- [26] C. Craye, A. Rashwan, M. S. Kamel, and F. Karray, "A multi-modal driver fatigue and distraction assessment system," Intern. Jour. of Intel. Transp. Syst. Research, vol. 14, no. 3, pp. 173-179, Sep. 2016.
- [27] K. M. Passino and S. Yurkovich, Fuzzy Control. California: USA: Addison Wesley, 1998.
- [28] R. Smith, Open Dynamics Engine v0.5: User Guide, 2006. [Online] Available: <http://ode.org/ode-latest-userguide.html>
- [29] H. B. Pacejka, Tyre and Vehicle Dynamics: Second Edition, Oxford: Great Britain: Butterworth-Heinemann, 2006.

**Publication IV**

**Aksjonov, A.**, Nedoma, P., Vodovozov, V., Petlenkov, E., & Herrmann, M. (2018). A Novel Driver Performance Model Based on Machine Learning. *Proceedings of the 15th IFAC Symposium on Control in Transportation Systems (CTS 2018)* (pp. 267–272). Savona: IFAC. doi: 10.1016/j.ifacol.2018.07.044



## A Novel Driver Performance Model Based on Machine Learning

Andrei Aksjonov\*, Pavel Nedoma\*, Valery Vodovozov\*\*,  
Eduard Petlenkov\*\*, Martin Herrmann\*\*\*,

\*ŠKODA Auto a.s., Mladá Boleslav, Czech Republic  
(Tel: +420-734-249-830; e-mail: {andrei.aksjonov, pavel.nedoma} @skoda-auto.cz)

\*\*Tallinn University of Technology, Tallinn, Estonia  
(e-mail: {valery.vodovozov, eduard.petlenkov} @ttu.ee)

\*\*\*IPG Automotive GmbH, Karlsruhe, Germany  
(e-mail: martin.herrmann@ipg-automotive.com)

---

**Abstract:** Models of road vehicle driver behaviour are widely used in several disciplines, like driver distraction and autonomous driving. In this paper, a novel driver performance model, which is unique for every driver, is introduced. The driver is modelled with machine learning algorithms, namely artificial neural network and adaptive neuro-fuzzy inference system. Every model is trained and validated with the data collected during the real-time driver-in-the-loop experiment on a vehicle simulator for each driver separately. In total, 18 participants contributed to the experiment. Although the prediction accuracy of the models depends on the algorithm specifications, the artificial neural network was slightly more accurate in driver performance prediction comparing to the adaptive neuro-fuzzy inference system. The driver models may be used in detection of driver distraction induced by in-vehicle information system.

**Keywords:** Neural networks; Neural fuzzy modelling and control; Machine learning for environmental applications; Vehicle dynamic systems; Human factors in vehicular system; Learning and adaptation in autonomous vehicles; Safety.

---

### 1. INTRODUCTION

In 2016, 25500 people died and 135000 were seriously injured in traffic accidents in Europe alone (European Commission, 2017). Thanks to the traffic policies (e.g. obligatory seat belt usage) and in-vehicle active and passive safety features, such as anti-lock braking system, electronic stability program, lane departure warning, and many others, road fatality rates have dramatically decreased within past 10 years (European Commission, 2016). Nevertheless, the traffic safety is still a very serious environmental challenge we are involved in today.

Every year, almost half of the lost lives in road accidents are due to improper driver behaviour. The most dangerous driver mistakes are speeding, driving under the alcohol or forbidden drugs influence, and driver distraction. Traffic safety foundations (e.g. the European Commission Directorate General for Mobility & Transport and the AAA Foundation for Traffic Safety) along with vehicle manufacturers are constantly working on new ideas dedicated to road safety improvement. The first ones mainly focus on transport policies establishment and road environment improvement. The seconds concentrate on advanced driver assistance systems development to reduce driver workload and to avoid driver's inattention, and induced by in-vehicle information system driver distraction diminishment.

Driver modelling is successfully used in development of autonomous driving systems. For instance, lane change (Vallon et al., 2017), trajectory forecasting (Doshi and

Trivedi, 2011), and human-like steering or lane keeping control model (Hubschneider et al., 2017; Kolekar et al., 2017; Saleh et al., 2011) were introduced previously. In addition, Pasquier et al. (2001) developed an automated driver prototype model, which emulates human driving expertise with self-organising fuzzy rule-base system.

Another widely used discipline, where driver modelling is useful, is driver distraction with secondary activity. Driver distraction is defined as "anything that delays the recognition of information necessary to safely maintain the lateral and longitudinal control of the vehicle (driver's primary task) due to some event, activity, object or person, within or outside the vehicle that compels or tends to induce the driver's shifting attention away from the fundamental driving task by compromising the driver's auditory, biomechanical, cognitive or visual faculties or combinations thereof" (Hansen et al., 2017). Driver's secondary tasks are defined as all the activities different from primary tasks the drivers perform while driving.

Brookhuis et al. (1991) made a comparison between normal driving and driving with cell phone interaction. These scholars studied heartrate indices and some of vehicle performance measures. Wang et al. (2015) presented a driver distraction start and end period prediction based on brain activity measured by electroencephalographic signals. The signals were monitored online with an adaptive-threshold-based prediction framework. Choudhary and Velaga (2017) collected driver performance data under a non-distracted driving. Thereafter, non-distracted driver performance was

compared to the driving with mobile phone use applying an analysis of variance test. Simple comparison is not enough for accurate driver distraction study. Therefore, driver modelling is necessary to conduct the research on different distraction case studies.

Hermannstädter and Yang (2013) applied a driver model adopted from literature to real-road driving of a distracted experiment in order to assess the driver state. The distraction experiment data comprised real road driving with distraction, as well as reference driving. The driver model features an anticipatory and a compensatory tracking component, a processing time delay, and a neuromuscular subsystem with a torque control loop. Yang et al. (2010) developed a two-class classifier based on driver behavior for driver distraction using the nonlinear extended two-wheel vehicle dynamic model. However, in both references, the models are derived mathematically and have many approximations comparing to the real driving performance.

Ersal et al. (2010) proposed a model-based approach to analyse different effects of secondary tasks on individual driver. For this, the authors introduced a radial-basis model-network-based modelling framework for normal (not distracted) driving behaviour characterization. Next, the method was combined with support vector machines for normal or distracted driving classification. The driver model was expressed mathematically and was fitted with normal driving data. Unfortunately, the model was used for all drivers and, therefore, was not applicable for individual driver distraction studies.

Kirscher and Ahlstrom (2010) attempted to predict visual distraction with driver performance model. Based on the results, each experiment participant was classified as either distracted or attentive. Five-class drowsy driving classifier was introduced in (Matsuo and Khiat, 2012). The authors monitored driver's behaviour (i.e. head sway, eye closure rate, and frequency of subsidiary behaviour).

This work is dedicated to driver model development, which is capable to predict each individual driver normal driving on a specific road segment with a reasonable degree of accuracy. Thus, machine learning techniques, like classification, proposed by other researchers (Kirscher and Ahlstrom, 2010; Matsuo and Khiat, 2012; Ersal et al., (2010)) are not suitable for accurate driver modelling, because driver performance is a highly nonlinear activity and cannot be limited with several classes (Alpaydin, 2004). Contrariwise, nonlinear regression methods, where the predicted responses are real numbers, are efficient in accurate prediction from data sample. Hence, machine learning algorithms, namely artificial neural network (ANN) and adaptive neuro-fuzzy inference system (ANFIS), are applied in this paper for driver performance modelling.

Moreover, the model depends on each driver individual performance and unique for every driver. The model does not require complex mathematical representation, like the ones proposed in (Hermannstädter and Yang, 2013; Yang et al., 2010; Ersal et al., 2010).

To verify driver models, driver performance data were collected for each individual participant in driver-in-the-loop experiment using a vehicle simulator. Next, the unique performance models for every driver were built. Finally, new data were obtained on the same testbed to test the prediction accuracy for each participant separately.

The models refer to the road segments, which are defined by road curvature and speed limit. Thus, the models predict driver's manoeuvrability on a specific road section. The predicted variables are road middle line keeping and speed limit maintenance abilities for each individual participant.

In next section, the driver models are designed. Data collection and driver-in-the-loop experiment is described in Section 3. In Section 4, the experimental results of driver performance prediction are introduced and are discussed. Finally, the research is concluded in Section 5.

## 2. DRIVER MODELS

In Fig. 1, a driver model is presented. It receives an information about a road as the inputs, which characterize a road segment: curvature (radius)  $r$  and speed limit  $V_l$ . The information about the road is instantaneous. Two variables describe driver performance. The first one is a difference between a vehicle velocity and a road segment speed limitation (speed error)  $\Delta v$ . The second output is a distance between a road middle line and vehicle geometric centreline (line error)  $\Delta x$ . For simplicity, both variables are accepted as absolute values. Therefore, a driver model forecasts, how well a person drives in the middle of the lane and maintains the speed limit on various road segments.

Drivers are modelled with machine learning algorithms. In this paper, two methods, namely ANN and ANFIS, are applied independently. Both the ANN and the ANFIS are trained and tested with the data set gathered separately for every experiment participant. In this regard, the participants drive a vehicle simulator for three laps, two of which are exploited in algorithms training, and the third one – for prediction precision testing. The results of the algorithms prediction accuracies are compared for both algorithms.

Both the ANN and the ANFIS are the reasoning models based on human brain. They are widely used as nonlinear regression algorithms. In fact, ANFIS is a symbiosis of an ANN and fuzzy logic. For both algorithms training the sample data are required. Here, the same data are exploited for both models' training.

Driver models are designed in MATLAB® R2016b from

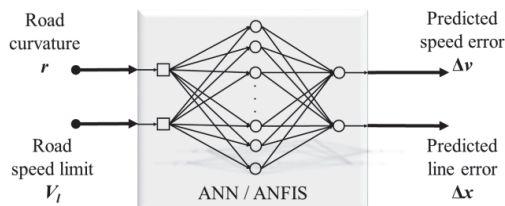


Fig. 1. Driver performance model.

MathWorks, Inc. (Natick, Massachusetts, USA) environment. The Fuzzy Logic Toolbox™ was exploited for ANFIS, and the Neural Network Toolbox™ was applied in ANN modelling. The ANN and the ANFIS practical designing guidance can be found in (Negnevitsky, 2005).

### 2.1 Artificial Neural Network

The feedforward ANN constructed in this work has an input layer, hidden layer with 500 neurons, and output layer. For maximum performance accuracy, it is recommended to use as much neurons in hidden layers as possible, if it does not bring a network overfitting. The number of neurons were selected with trial and error method. In this respect, several ANNs with 100 to 1000 neurons were designed and were compared between each other. Better network performance was not discerned with more than 500 neurons.

Initially, the hyperparameters are set by default in the Toolbox, while the training parameters (i.e. initial weights and threshold levels) are selected randomly. The last ones are uniformly distributed inside a small range, whose limits depend on a number of inputs of a neuron in the network.

Hyperbolic tangent transfer functions are applied to hidden layers, because of their simplicity and good performance. The output neuron transfer functions are linear. The ANN is trained with Levenberg-Marquardt learning algorithm, because it is the most popular, fast, and widely used approach in nonlinear regression. In this algorithm, a backward propagation of errors (back-propagation) method is applied for gradients computation. It employs a dynamic programming strategy to reuse rather than re-compute partial sums associated with the gradients on intermediate nodes, what makes the back-propagation approach one of the fastest and the most efficient methods (Goodfellow et al., 2016).

### 2.2 Adaptive Neuro-Fuzzy Inference System

An ANFIS performance mainly depends on the membership functions (MFs) quantity, and less – on the MFs type. Nevertheless, the MFs' shape is mostly responsible for the output smoothness and reaction time. A number of MFs is

proportional to a number of linguistic rules. Higher number of fuzzy rules allows more precise network tuning.

Like ANN, the ANFIS model is designed with trial and error method. In particular, different MF numbers and shapes were studied. The significantly better model performance was achieved with nine Gaussian shape MFs for each input. The MFs are symmetrically dispersed and overlap between each other over the whole universe of discourse.

In total, 81 rules were generated after training the ANFIS. As ANFIS is an equivalent to a first-order Sugeno fuzzy model, the output MFs are 81 singletons, which were tuned automatically. Defuzzification method is a weighted average. Hybrid training method composed of the least-squares estimator and the gradient descent methods was applied.

## 3. DATA COLLECTION

### 3.1 Participants

Overall, 13 male and 5 female participated in a driver-in-the-loop experiment. The participation in the experiment was voluntary and did not intend a reward. The drivers were workers of the IPG Automotive GmbH (Karlsruhe, Germany). Every one owned a valid driver license and had at least one year of driving experience in Europe.

The youngest driver was 24 years old, and the oldest – 39. Average participators' age was 30.1 years old. The most experienced driver owned a driving license for 21 years, while the average driving experience was 11.3 years.

### 3.2 Apparatus

In Fig. 2, the experiment facilities are shown. The driver simulator System Experience Platform was provided by the IPG Automotive GmbH (Karlsruhe, Germany). The vehicle mockup includes an automatic gearbox, a steering wheel, pedals (i.e. gas and brake), and an adjustable driver's seat. The virtual world is depicted on a liquid-crystal screen in front of the driver, where the vehicle speed, road shape, and vehicle position on the route were displayed.



Fig. 2. Driver-in-the-loop experiment simulator.

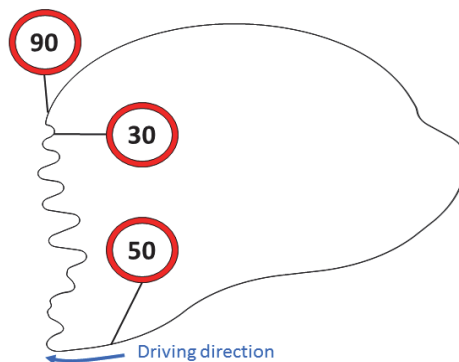


Fig. 3. Road shape and segments speed limitations.

The test-rig runs a vehicle model from IPG CarMaker® (Karlsruhe, Germany). It is capable for real-time integration with MATLAB® (Natick, Massachusetts, USA) environment. Thus, it allows conducting real-time drive-in-the-loop experiments. The data are saved with 50 Hz frequency.

A two-lane rural highway road with different curvatures and speed limits (i.e. 30, 50, and 90 km/h) was modelled in the virtual world. Its distance was 10 626 m/lap. The road shape along with the speed limitations is introduced in Fig. 3. One lap requires about ten minutes of driving, when all the traffic rules are obeyed. There were no other dynamic objects (e.g. pedestrians, other vehicles) introduced in the virtual world. However, many different static objects (e.g. trees, houses, traffic signs) were designed in the simulated world.

### 3.3 Procedure

The experiment participants' mission was to drive the simulator respecting all the traffic rules, reading and following all the traffic signs. In particular, their main task was to drive in the middle of the lane and to maintain the speed limits as precisely as manageable. Not to mention that all the drivers had an opportunity to pass one lap to become acquainted with the test-rig before the test, due to time

restriction each participant drove only three full laps during the experiment.

The data collected during the first two laps were utilized for each individual driver performance modelling. Every driver passes the same road segment in different way. Although the difference is very small, every driver completes the same road segment slightly differently. By this reason, the data gathered from driving at least two identical laps is necessary. The data from the third lap were utilized in the ANN and the ANFIS prediction performance testing.

## 4. RESULTS

The results of the driver performance prediction for a random driver are presented in this section. For different driver-in-the-loop experiment participants the results of the models prediction accuracy are very similar. From three laps driving around 80 000 nodes were collected for each individual driver. These data were divided into a training data (67%) and a testing (33%) for every participant separately. Therefore, the data from approximately two full laps were applied to driver performance model design, whereas the data from the last lap were exploited for models testing. The models were trained and verified off-line, after the driver-in-

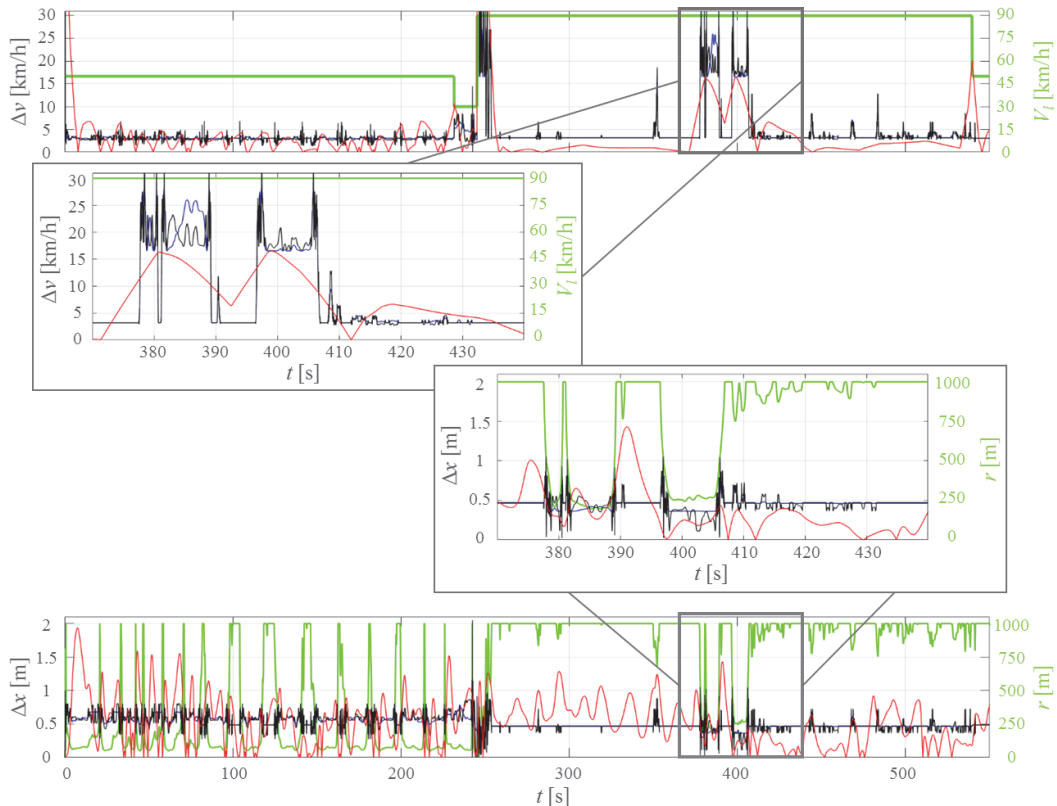


Fig. 4. Results of the driver performance prediction: red line – testing performance; black line – prediction with ANN; blue line – prediction with ANFIS; green line – information about the road segment.

the-loop experiment. The procedures are unique for every participant. Therefore, every performance model is suitable for a single driver only.

In Fig. 4, the prediction results along with models test are presented. The red curve symbolizes the test data gathered from the last lap. The black line is a predicted result by the ANN, while the blue line – by the ANFIS. Both the ANN and the ANFIS have very similar driver modelling results. For most of the experiment period, performance results by the ANN overlap with the performance results by the ANFIS.

In Fig. 4, the green curve represents an information about the road segment, namely road speed limitation and curvature. The prediction models read an instantaneous information about the road shape and speed limitation. The lap can be roughly divided into two parts (Fig. 3). The first part has a lower speed limitation (i.e. 30 and 50 km/h) and frequent curvature. The participant drove this part for the first 250 seconds (Fig. 4). The second part has a higher speed limit of 90 km/h with a high road radius, which the driver passed for the rest of the validation time (Fig. 4).

In Fig. 4, upper scope, the speed limit maintenance ability  $\Delta v$  is introduced. Both the ANN and the ANFIS predict slight oscillation in ability to keep speed limit for the first road part. Roughly, the predicted  $\Delta v$  varies between 2 and 4 km/h. In fact, the driver did not hold the speed limit precisely. The error oscillates between 0 and 6 km/h without noticeable extremums. Thus, the prediction is reasonable enough considering that the road on this segment is very curvy.

On the second road phase with higher speed limit (i.e. 90 km/h), the models show a high error in speed maintenance, when the limits were changed from 30 km/h to 90 km/h. An average driver is not able to instantly accelerate the vehicle or drop the speed to its road speed limit. Consequently, this phenomena is detected by the model.

Moreover, on the speedy segment there are also two curvy phases (Fig. 3). Both the ANN and the ANFIS recognize a significant speed reduction, and the driver dropped the speed on this segment during the last validation lap as well (Fig. 4 inset, upper scope). The rest of the segment the predicted vehicle velocity was almost linear, around 3 km/h faster or slower than its road limit. The driver, however, passed the rest of the road with smaller speed limit maintenance error, what was unusual for her/his algorithms training phase.

In Fig. 4, lower scope, a middle line keeping ability  $\Delta x$  is shown. The first part of the road is characterized with frequent curvature (Fig. 3; Fig. 4, green curve). It is obvious that lane keeping ability is harder. The amplitude is predicted by the machine learning algorithms, where in average the participant drove further than 0.5 m away from the middle of the lane. The red curve on the plot indeed proves the same driver's behaviour on the road segment with frequent vehicle body lateral oscillation. In some moment during the third validation lap, the participant passed the segment with considerably high error.

On the second road part, the ANN and the ANFIS demonstrate almost linear behaviour, where the driver was

**Table 1. Algorithms comparison**

Algorithm	$e_{\Delta v}$	$e_{\Delta x}$	Training time [s]
ANN	2.7243	0.2712	379
ANFIS	2.8294	0.2742	549

able to stay in the middle of the road with slightly less than 0.5 m error to the left or to the right during the training period. Nevertheless, during the validation the vehicle body also oscillates on this segment, but with longer period.

Thus, the networks approximate the driver performance almost linearly. It is worth to point out that on the two curvy segments on the speedy curve the driver was able to keep the road lane with the same error as predicted by the networks (Fig. 4 inset, lower scope). It can be concluded that this driver tends to drop the speed limit on this specific road shape rather than cut the road curve (Fig. 4, insets), this characterizes the specific behaviour of the particular driver.

The ANN and the ANFIS are compared on prediction accuracy. In this regard, an average error between predicted speed limit maintenance and real vehicle speed  $e_{\Delta v}$  and an average error between predicted and real middle line keeping ability  $e_{\Delta x}$  are calculated. The results are presented in Table 1. Although it was not important in our studies, the algorithms training times are delivered in Table 1. In short, the designed ANN driver model conducted more accurate prediction than the ANFIS model. However, in this experiment, the difference in prediction is insignificant.

The prediction by the ANFIS is also somewhat smoother than by the ANN. It can be explained by the ANFIS algorithm itself, because it uses a fuzzy set theory applying the training capabilities for the rule-base optimization. Although, it depends on the fuzzy logic MFs, mostly the algorithm is more smooth and precise in control or decision making systems (Negnevitsky, 2005). In fact, a smooth MFs types (Gaussian shape) were used in this paper.

Networks predict driver performance with almost 3 km/h and 0.3 m error for  $\Delta v$  and  $\Delta x$ , respectively. Considering that  $\Delta v$  ([0 50]) has higher amplitude than  $\Delta x$  ([0 2]), the driver models are accepted as reasonably accurate.

## 5. CONCLUSIONS

In this paper, the driver models with machine learning algorithms are introduced. Two nonlinear regression methods, namely ANN and ANFIS, were independently designed to predict driver's middle lane and speed limit keeping abilities. The models are based on the road segments characterized by curvature and speed limitation.

The ANN and the ANFIS were developed with the sample data, collected on a vehicle simulator during a ride in a virtual world. Eighteen drivers participated in the driver-in-the-loop experiment. Thereafter, each driver passed one additional lap, which was used for algorithms accuracy testing of each individual participant. Although the ANN prediction was more accurate comparing to the ANFIS, the

difference in prediction is negligibly small. Overall, both the ANN and the ANFIS prediction accuracy are satisfactory.

The ANN and the ANFIS models have the significant benefits over proposed previously driver performance models for driver distraction studies, where the classification algorithms incapable for accurate driver distraction investigation were introduced. Proposed in this work driver models allow more accurate driver performance analysis. In the future, these models will be combined with driver distraction evaluation method (Aksjonov et. al., 2017) to develop a practical tool for in-vehicle information system human-machine interaction technologies assessment.

#### ACKNOWLEDGMENT

This research receives funding from the European Community Horizon 2020 Framework Programme under grant agreement No. 675999. The authors would like to extend their appreciation for to the IPG Automotive GmbH (Karlsruhe, Germany) for providing the simulator and for organizing the driver-in-the-loop experiment.

#### REFERENCES

- Aksjonov, A., Nedoma, P., Vodovozov, V., Petlenkov, E., and Herrmann, M. (2017). A method of driver distraction evaluation using fuzzy logic: Phone usage as a driver's secondary activity: Case study. *Proc. of the 2017 XXVI International Conference on Information, Communication and Automation Technologies (ICAT)*, Sarajevo, Bosnia & Herzegovina, October 26-28, 23-28.
- Alpaydin, E. (2004). *Introduction to Machine Learning*. The MIT Press, Cambridge, Massachusetts.
- Brookhuis, K. A., de Vries, G., and de Waard, D. (1991). The effects of mobile telephoning on driving performance. *Accident Analysis & Prevention*, 23 (4), 309-316.
- Choudhary, P. and Velaga, N. R. (2017). Analysis of vehicle-based lateral performance measures during distracted driving due to phone use. *Transportation Research Part F*, 44, 120-133.
- Doshi, A. and Trivedi, M. M. (2011). Tactical driver behavior prediction and intent inference: A review. *Proc. of the 2011 14th International IEEE Conference on Intelligent Transportation Systems*, Washington, USA, October 5-7, 1892-1897.
- Ersal, T., Fuller, H. J. A., Tsimhoni, O., Stein, J. L., and Fathy, H. K. (2010). Model-based Analysis and classification of driver distraction under secondary tasks. *IEEE Transactions on Intelligent Transportation Systems*, 11 (3), 692-701.
- European Commission, Directorate General for Mobility and Transport. (2016). *Road safety evaluation in EU*. Available online: [https://ec.europa.eu/transport/road\\_safety/sites/roadsafety/files/pdf/observatory/historical\\_evol.pdf](https://ec.europa.eu/transport/road_safety/sites/roadsafety/files/pdf/observatory/historical_evol.pdf)
- European Commission, Directorate General for Mobility and Transport. (2017). *Road safety newsletter*, No 27. Available online: [https://ec.europa.eu/transport/road\\_safety/sites/roadsafety/files/nl27\\_en.pdf](https://ec.europa.eu/transport/road_safety/sites/roadsafety/files/nl27_en.pdf)
- Goodfellow, I., Bengio, Y., and Courville, A. (2016). *Deep Learning*, MIT Press, Cambridge, MA, USA.
- Hansen, J. L., Busso, C., Zheng, Y., and Sathyanarayana, A. (2017). Driver modeling for detection and assessment of driver distraction: Examples from the UTDrive test bed. *IEEE Signal Processing Magazine*, 34 (4), 130-142.
- Hermannstädter, P. and Yang, B. (2013). Driver distraction assessment using driver modeling. *Proc. of 2013 IEEE International Conference on Systems, Man, and Cybernetics (SMC)*, Manchester, UK, October 13-16, 3693-3698.
- Hubschneider, C., Bauer, A., Doll, A., Weber, M., Klemm, S., Kuhnt, F., and Zöllner, M. (2017). Integrating end-to-end learned steering into probabilistic autonomous driving. *Proc. of 2017 IEEE International Conference on Intelligent Transportation Systems (ITSC)*, Yokohama, Japan, October 16-19.
- Kirscher, K. and Ahlstrom, C. (2010). Predicting visual distraction using driving performance data. *Annals of Advances in Automotive Medicine*, 54, 333-342.
- Kolekar, S., de Winter, J., and Abbink, D. (2017). A human-like steering model: Sensitive to uncertainty in the environment. *Proc. of 2017 IEEE International Conference on Systems, Man, and Cybernetics (SMC)*, Banff, Canada, October 5-8, 1487-1492.
- Matsuo, H. and Khiat, A. (2012). Prediction of drowsy driving by monitoring driver's behavior. *Proc. of 21st International Conference on Pattern Recognition (ICPR 2012)*, Tsukuba, Japan, November 11-15, 3390-3393.
- Negnevitsky, M. (2005). *Artificial intelligence: A guide to intelligent systems, 2<sup>nd</sup> edition*. Addison-Wesley, Harlow, England.
- Pasquier, M., Quek, C., and Toh, M. (2001). Fuzzylot: A novel self-organizing fuzzy-neural rule-base pilot system for automated vehicles. *Neural Networks*, 14, 1099-1112.
- Saleh, L., Chevrel, P., Mars, F., Lafay, J.-F., and Claveau, F. (2013). Human-like cybernetic driver model for lane keeping. *Proc. of 18th IFAC World Congress*, Milano, Italy, August 28 - September 2, 4368-4373.
- Vallon, C., Ercan, Z., Carvalho, A., and Borelli, F. (2017). A machine learning approach for personalized autonomous lane change initiation and control. *Proc. of 2017 IEEE Intelligent Vehicle Symposium (IV)*, Los Angeles, USA, June 11-14.
- Wang, S., Zhang, Y., Wu, C., Darvas, F., and Chaovalitwongse, W.A. (2015). Online prediction of driver distraction based on brain activity patterns. *IEEE Transactions on Intelligent Transportation Systems*, 16 (1), 136-150.
- Yang, J., Chang, T. N., and Hou, E. (2010). Driver distraction detection for vehicular monitoring. *Proc. of 36th Annual Conference on IEEE Industrial Electronics Society (IECON 2010)*, Glendale, USA, November 7-10.

**Publication V**

**Aksjonov, A.**, Nedoma, P., Vodovozov, V., & Petlenkov, E. (2018). An Enhancement of the Driver Distraction Detection and Evaluation Method Based on Computational Intelligence Algorithms. *Proceedings of the 16th IEEE International Conference on Industrial Informatics (INDIN`2018)* (pp. 201–206). Porto: IEEE. doi: 10.1109/INDIN.2018.8472045



# An Enhancement of the Driver Distraction Detection and Evaluation Method Based on Computational Intelligence Algorithms

Andrei Aksjonov, Pavel Nedoma

Innovation and Research

ŠKODA AUTO a.s.

Mladá Boleslav, Czech Republic

{ andrei.aksjonov; pavel.nedoma }@skoda-auto.cz

Valery Vodovozov, Eduard Petlenkov

Department of Electrical Power Engineering and

Mechatronics

Tallinn University of Technology

Tallinn, Estonia

{ valery.vodovozov; eduard.petlenkov }@ttu.ee

**Abstract**—Driver distraction is a fundamental problem for human safety, because the number of traffic accidents due to distracted driving does not decrease. In this paper, an enhancement of previously proposed driver distraction detection and evaluation methodology is introduced. The method is composed of computational intelligence algorithms: a driver performance prediction algorithm with nearest neighbor regression and an intelligent fuzzy logic evaluation algorithm. Thanks to the improvement, an additional variable for driver performance prediction and an additional performance-based indicator were introduced. To verify the novelty, the series of thirty driver-in-the-loop experiments has been delivered on an industrial vehicle simulator. At this, an interaction with a vehicle on-board computer was exploited as a distractive activity. Finally, the enhanced method is compared to the previously described one.

**Keywords**—*computational intelligence; nearest neighbor methods; fuzzy logic; human computer interaction; vehicle safety*

## I. INTRODUCTION

Driver distraction (DD) is a serious problem for the safety of ground vehicles. Its negative impact is measured not only by paid insurances, but also by humans' and animals' injuries and lives. In 2016, only in the EU almost 20 % of drivers ended abruptly in vehicle crashes caused by DD [1]. In the USA, this number is even higher [2]. Therefore, detection and further minimization of DD induced by an interaction with on-board equipment is a significant challenge for all vehicle manufacturers. A development of a practical tool for evaluation of in-vehicle information systems (IVIS) for minimum DD before their installation in series products is an inevitable task.

DD is defined as "anything that delays the recognition of information necessary to safety maintain the lateral and longitudinal control of the vehicle (driver's primary task) due to some event, activity, object or person, within or outside the vehicle that compels or tends to induce the driver's shifting attention away from the fundamental driving task by compromising the driver's auditory, biomechanical, cognitive or visual faculties or combinations thereof" [2]. The secondary task is an activity not related to primary task that drivers perform while controlling a vehicle.

In the literature, there are no standard procedures to test IVIS on the DD level. Several proposed methods rely on surveys and questionnaires of experiment participants [3], [4]. These DD assessment ideas cannot be accepted as objective valuations since they are based on individual opinions. Consequently, the researchers decided to implement computational intelligence (CI) algorithms for replacement of subjective evaluations by artificial intelligence systems.

To detect DD, scholars have proposed applying support vector machines (SVM) [5], fuzzy logic (FL) [6], and artificial neural networks (ANN) with gradient boosting machines [7]. Some authors trusted such driver's behavior measures as gaze and head movement tracking. Others promoted psychological attributes (e.g. driver electrocardio- and electroencephalographical methods) also applying CI approaches [8], [9]. Despite an accurate DD detection, behavioral and psychological measures always require supplementary equipment, such as cameras and neuroscan systems. Furthermore, some devices (e.g. eye-tracking goggles or neuroscan helmets) are often considered as a distraction source themselves. Also, these appliances increase system cost and complexity [10].

Most advantageous approaches consider vehicle dynamic performance (i.e. longitudinal and lateral control quality). Referring to the DD definition, these factors estimate the drivers' primary tasks that must not be worsened due to interaction with vehicle on-board equipment. In addition, these methods do not require supplementary hardware, and turn out to be more applicable in practice, because the data can be gathered using only the sensors available in passenger vehicles, such as steering wheel angle gauges, vehicle velocity transducers, etc. Using these signals, researchers designed different DD detection algorithms based on artificial and computational intelligence: FL [11], SVM [12], Gaussian mixture model (GMM) [13], and their combinations, such as hidden Markov model with GMM [14], ANN with GMM [15], and ANN with SVM [16].

Despite a vast variety of different DD detection solutions, they all have an essential limitation, namely, Boolean logic classification (i.e. distracted/non-distracted). Thus, the methods

are not feasible as a practical tool for different secondary tasks evaluation and comparative analysis on safe vehicle operation.

A novel DD detection and evaluation method using CI algorithms, which is capable not only to detect DD, but also to precisely measure its impact on safe vehicle control was developed in [17]. The method combines ANN for DD detection and FL for DD evaluation. In this paper, an improvement of this methodology is presented. To differentiate the improved approach from the previously proposed one, the earlier developed method [17] is further called “old”, while the last one is named “new” in this paper.

The new method is enhanced with additional performance-based indicator, namely, the steering wheel acceleration. Moreover, one more input is used in driver modelling, which is a road curve direction (i.e. left, straight or right). These innovations are called to improve an accuracy of the DD measurement. And besides, the new method uses a nearest neighbor regression (NNR) for driver modelling. The FL algorithm is also redesigned, because more variables are used now in DD assessment.

The paper is organized as follows. Next Section describes the new DD detection and assessment method. Section III is dedicated to the driver-in-the-loop experiment portfolio. In Section IV, the case study results are presented and discussed. The conclusion is reported in Section V.

## II. DRIVER DISTRACTION DETECTION AND EVALUATION METHOD

In Fig. 1, the DD detection and evaluation method block scheme is presented. Parameters description is listed in Table I. Superscript “*t*” refers to the “training data” collected during the DD-free driving and used for driver performance prediction. Individual detection and evaluation is conducted for each experiment participant in three main steps described below.

A schematic explanation of the two main performance-based variables is shown in Fig. 2. To measure the lane keeping offset  $\Delta x_r$  (Fig. 2a), it is assumed that a transparent vehicle represents driver’s normal angle cutting. The white car represents cornering under DD. The pink surface between these two turns is considered as a difference between normal and distracted road middle line keeping ability.

Similarly, it is anticipated that the speed limit on current

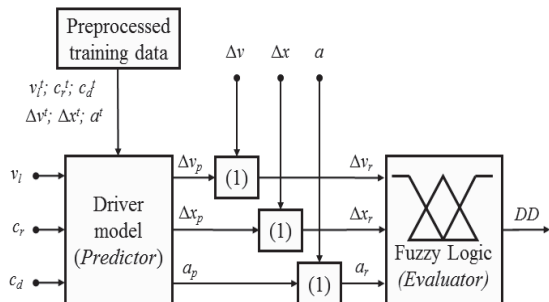


Fig. 1. Driver distraction detection and evaluation block scheme.

TABLE I. PARAMETERS DESCRIPTION

Symbol	Description	Unit
$v_l$	Speed limit	km/h
$c_r$	Road curve radius	m
$c_d$	Road curve direction	Left/Right
$\Delta x$	Real lane keeping offset	m
$\Delta v$	Real vehicle speed deviation	km/h
$a$	Real steering wheel acceleration	$^\circ/s^2$
$\Delta x_p$	Predicted lane keeping offset	m
$\Delta v_p$	Predicted vehicle speed deviation	km/h
$a_p$	Predicted steering wheel acceleration	$^\circ/s^2$
$\Delta x_r$	Resultative lane keeping offset	m
$\Delta v_r$	Resultative vehicle speed deviation	km/h
$a_r$	Resultative steering wheel acceleration	$^\circ/s^2$
$DD$	Driver distraction level	%

road segment is 100 km/h (Fig. 2b). Normally, driver passes this segment with 105 km/h. However, when she/he is distracted, the speed rises to 115 km/h. Thus, the error between normal and distracted speed maintenances  $\Delta v_r$  is calculated as a second performance-based measure. The deviation is also depicted as a pink sector in Fig. 2b. The third variable is simply a difference between normal steering wheel acceleration and a steering wheel acceleration while performing a secondary task.

First, an information about the road segment is inserted inside the Driver model block. As the Driver model tends to forecast driver’s performance, it is called the *Predictor*. The road segment is described by three parameters: segment speed limitation  $v_l$ , road curve radius (curvature)  $c_r$ , and road curve direction  $c_d$ . The last one is a Boolean type with the crisp values: -1 meaning that the road curve goes to the left, 0 — it is straight, and 1 — it turns right.

Based on the received information about the road shape, direction, and speed limit, a predicted driver performance (i.e.  $\Delta v_p$ ,  $\Delta x_p$ , and  $a_p$ ) on this specific road segment appears on the Predictor output. An NNR is applied as a prediction algorithm, which stores a preprocessed training set, uses these data to look up the nearest entry in it, and, finally, returns the associate regression target as offered in [18]. The preprocessed data pass through a dimensional reduction for model simplification and data diminishment, what makes the algorithm more understandable, robust, and computationally cheaper [19].

The main advantage of the NNR learning algorithm comparing to the other CI methods used for prediction (e.g. ANN, fuzzy neural networks, etc.) is its ability to achieve the minimum possible training error on any regression dataset [18]. In principle, the NNR algorithm finds the shortest distance

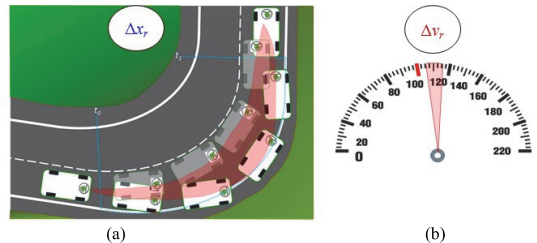


Fig. 2. A schematic explanation of the main performance-based evaluation variables: (a)  $\Delta x_r$ ; (b)  $\Delta v_r$ .

TABLE II. RULE-BASE OF THE FL EVALUATOR

$a_r = \text{negative}$						
DD [%]		$\Delta x_r$				
		neg far	neg close	zero	pos close	pos far
$\Delta y_r$	neg high	100	85.8	42.9	85.8	100
	neg low	100	57.2	14.3	57.2	100
	zero	57.2	28.6	0	28.6	57.2
	pos low	85.8	42.9	14.3	42.9	85.8
	pos high	100	85.8	42.9	85.8	100
$a_r = \text{zero}$						
DD [%]		$\Delta x_r$				
		neg far	neg close	zero	pos close	pos far
$\Delta y_r$	neg high	100	71.5	42.9	71.5	100
	neg low	85.8	14.3	0	14.3	85.8
	zero	42.9	0	0	0	42.9
	pos low	71.5	14.3	0	14.3	71.5
	pos high	85.8	57.2	28.6	57.2	85.5
$a_r = \text{positive}$						
DD [%]		$\Delta x_r$				
		neg far	neg close	zero	pos close	pos far
$\Delta y_r$	neg high	100	85.8	42.9	85.8	100
	neg low	100	57.2	14.3	57.2	100
	zero	57.2	28.6	0	28.6	57.2
	pos low	85.8	42.9	14.3	42.9	85.8
	pos high	100	85.8	42.9	85.8	100

between a sample point with coordinates  $(v_i, c_r, c_d)$  and a set of data points with coordinates  $(v_j, c_r^j, c_d^j)$  applying the Euclidean distance formula. Therefore, the Predictor assigns an output  $(\Delta y_p, \Delta x_p, a_p)$  to a training set point  $(\Delta y^i, \Delta x^i, a^i)$ , which corresponds to an appropriate point with the shortest distance to the sample one.

Next, the driver's performance under interaction with a vehicle on-board computer is compared with the predicted in the previous step one and a resultative performance (i.e.  $\Delta y_r, \Delta x_r, a_r$ ) is calculated. An example of the calculation is presented here for a lane keeping ability  $\Delta x_r$ :

$$\Delta x_r = \begin{cases} \Delta x - \Delta x_p, & \text{if } \Delta x > 0; \Delta x_p > 0; |\Delta x| > |\Delta x_p| \\ \Delta x - \Delta x_p, & \text{if } \Delta x < 0; \Delta x_p < 0; |\Delta x| > |\Delta x_p| \\ \Delta x + \Delta x_p, & \text{if } \Delta x > 0; \Delta x_p < 0; |\Delta x| > |\Delta x_p| \\ \Delta x + \Delta x_p, & \text{if } \Delta x < 0; \Delta x_p > 0; |\Delta x| > |\Delta x_p| \\ 0, & \text{if } |\Delta x| \leq |\Delta x_p| \end{cases} \quad (1)$$

For other variables,  $\Delta y_r$  and  $a_r$ , the same rules are applied. Summarily, when a predicted deviation is smaller comparing to a real one, the difference between two values is calculated and accepted as a resultative output,  $\Delta y_r, \Delta x_r$ , or  $a_r$ . Therefore, when the driver's performance due to DD becomes poorer from the viewpoint of safe vehicle operation, a worsened vehicle dynamic performance is counted. However, if a predicted deviation is greater than or equal to a real one, the output is zero. It means that a driver performs normally to her/his usual driving, the driving is not corrupted by secondary tasks, and, thus, she/he is not distracted.

Negative  $\Delta y_r, \Delta x_r$ , and  $a_r$  mean driving slower its speed limit, driving to the right from the middle of the lane, and turning a steering wheel to the right, respectively. Contrariwise,

TABLE III. IVIS SECONDARY TASKS

#	In-vehicle secondary task	
1.	Volume	Volume regulation
2.		Radio
3.	Context selection	Media
4.		Telephone
5.		Navigation
6.	Radio	Radio station selection from a primary list
7.		Radio station selection from an overall list
8.	Media	Media source selection (e.g. CD, SD-card)
9.		Media item selection
10.		Song shuffle
11.	Telephone	Call a number from the Favorite contact list
12.		Call a number from an overall contact list
13.	Navigation	Input location
14.		Input of a next target
15.		Zoom operation

positive  $\Delta y_r, \Delta x_r$ , and  $a_r$  represent speeding, driving towards opposite lane, and steering to the left, accordingly.

Finally, three resultative variables,  $\Delta y_r, \Delta x_r$ , and  $a_r$ , enter the FL Evaluator, which infers the three inputs into a single variable represented as a DD level in percentage. A FL Sugeno's type inference mechanism based on matrix operations is used [20]. In this work, however, the FL Evaluator has three inputs and, thus, the fuzzification procedure constructs a three-dimensional matrix. Each layer of the matrix has its own rule-base.

Two inputs,  $\Delta y_r$  and  $\Delta x_r$ , have five, and  $a_r$  — three symmetrically dispersed and overlapped between each other over the universe of discourse (UOD) membership functions (MFs). The triangular shapes are preferred for MFs, because they are simple for programming and famous for fast response. The UOD of  $\Delta y_r$  is between  $[-12, 12]$ , while  $\Delta x_r$  is bounded in  $[-1.5, 1.5]$ . The last input is restricted inside  $[-1500, 1500]$ .

As the output  $DD$  represents a level of distraction in percentage, its UOD lays inside  $[0, 100]$ . Eight output MFs have singleton forms. They are dissipated on equal distance between each other starting from 0 to 100 with a step 14.3:  $\{0, 14.3, 28.6, 42.9, 57.2, 71.5, 85.8, 100\}$ . It gives an equal responsiveness for each output MF.

The inputs and output are mapped via modus-ponens-form rules "If-And-Then". The linguistic relation is determined in Table II. The inputs-output relation example may be presented as follows: **IF** the steering wheel acceleration is "negative", **AND** vehicle speed deviation is "pos low", **AND** lane keeping offset is "neg close", **THEN** driver distraction is 42.9%.

### III. METHODOLOGY OF EXPERIMENTATION

#### A. Subjects

The DD detection and evaluation driver-in-the-loop experiment was carried out with thirty drivers. Five experiment participants were female, the rest — male. The drivers' gender, age and driving experience influence on the DD level were out of the scope of this study. Every participant owned a valid driver license and was physically and mentally healthy for safe vehicle operation. The participants were rewarded for their contribution.

## B. Apparatus

An advanced driver simulator for DD tests was provided by ŠKODA Auto a.s. (Mladá Boleslav, Czech Republic). It is a fixed-base passenger vehicle mockup, with a same cockpit as used in modern passenger vehicles. As the test rig has an automatic transmission, drivers operated the simulator by acting on a steering wheel and on the throttle and braking pedals. The mockup head-up instrumental panel displays vehicle speed. The participants drove the test bed in a virtual world projected on a wall screen in front of the simulator.

The vehicle together with the virtual world scene was modelled with an open source library for C++ programming language, Open Dynamics Engine™ v 0.5 [21]. The Škoda Yeti with 77 kW engine model configuration was used for vehicle model parameterization. This model includes a vehicle body, a suspension system, and four wheels with Pacejka's Magic Formula tire models [22].

The road used in the virtual world was identical to the one of the road segments in Czech Republic. It is a two-way lap with 3.5 m width lanes in each direction. Its total length is 10 626 m, what takes approximately 10 minutes to complete it, if all the traffic rules are respected. The road has two main parts: 50 km/h speed limit with frequent sharp turns and 90 km/h speed limit with almost straight road shape. The steering wheel acceleration was obtained from a signal provided by a steering-wheel sensor mounted on the shaft end of the steering axle. Lane keeping ability and vehicle velocity abnormality were calculated from  $x$ ,  $y$ , and  $z$  coordinates received from the global positioning system of the virtual world. All the variables were saved with 10 Hz frequency.

## C. Procedure

As the drivers were regular contributors to the experimental studies, they were familiar with the experiment's facilities. Nevertheless, before the experiment they were allowed to test

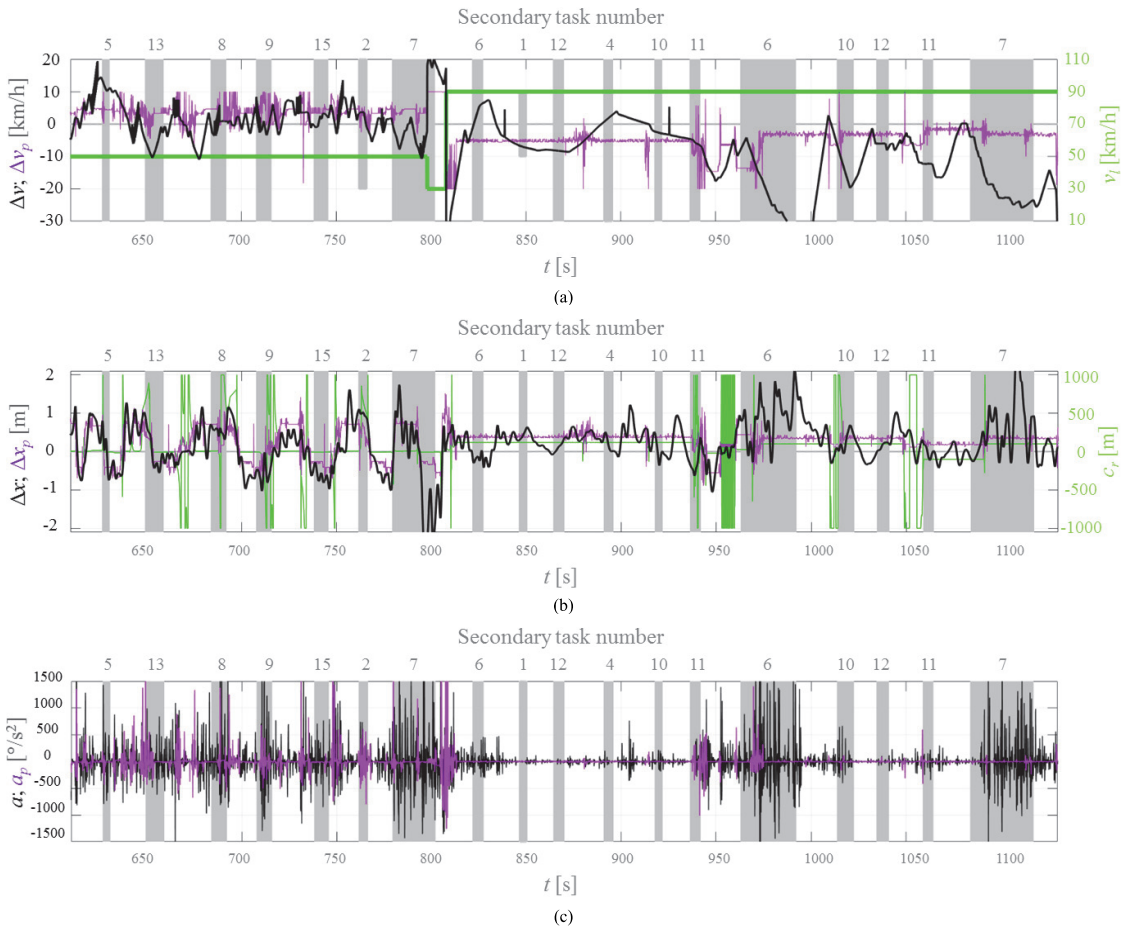


Fig. 3. Driver performance prediction versus real driver performance example for one of the experiment participants: gray background — secondary task accomplishment period; black line — real driver performance; purple line — predicted performance; green line — road information; (a) speed difference  $\Delta v$  and road speed limit  $v_l$ ; (b) center lane keeping offset  $\Delta x$  and curve radius  $c_r$ ; (c) steering wheel acceleration deviation  $a$ .

the simulator as long as they preferred. What is more, the participants were instructed to the exploited IVIS and secondary tasks before the driver-in-the-loop experiment.

The study procedure included two stages. During the first one, the participants were requested to drive two laps obeying all the traffic rules as good as possible. Namely, their only tasks were to stay in the middle of the lane and maintain the speed limit. The collected driver-performance results were utilized as the training data of the Predictor (Fig. 1) for each driver separately. During the second phase, the same traffic regulations fulfillment was again a priority. However, in this stage the drivers were obliged to accomplish the IVIS secondary tasks (Table III) while driving. The tasks were insisted randomly and several times during the phase.

#### IV. RESULTS

In this section, the results of the driver-in-the-loop experiment for a random driver are presented. During experimental DD evaluation, participants were given the opportunity to pass two or more full laps. However, for better observability, only the last lap of the studied driver is analyzed in this section. In Fig. 3, the gray background shows the period of secondary task accomplishment, while the white background is a normal driving between DD tasks. The predicted driver performance,  $\Delta v_p$ ,  $\Delta x_p$ , and  $a_p$ , are shown together with the real one,  $\Delta v$ ,  $\Delta x$ , and  $a$ . The black curve represents driving under distraction, the purple curve — the predicted performance, and the green curve — information about the road segment.

In Fig. 3a, driver's speed maintenance ability is delivered. On a 50 km/h speed limitation segment (Fig. 3a; green line), as predicted by the algorithm, the participant normally held the speed around 5 km/h higher than road's speed limit (Fig. 3a; purple line). However, in driving under the secondary task influence the driver tended to move slower (Fig. 3a; black line). For instance, submitting the tasks 13 and 7 (Table III), the speed deviation was significantly dropped down to -10

km/h. On the contrary, on a faster road segment, 90 km/h, the participant normally kept the speed lower its limit. In average, the vehicle drove 5 km/h slower. Though, some secondary tasks, such as 6, 7, and 10 (Table III), called the speed reduction.

In Fig. 3b, the centerline keeping ability is plotted. Taking into consideration the road lane and vehicle body widths (Section III.B), the vehicle drove out of the road lane bounds with exceeding  $x$  up to 1 or -1 m. However, based on performance prediction (Fig. 3b, purple curve), the driver was always staying inside of the road frontier during the free from the DD run. In fact, on a curvy road segment, when the curve radius  $c_r$  frequently changes (Fig. 3b, green line), the lane keeping ability while interacting with on-board computer (Fig. 3b, black line) was almost the same as it has been predicted. Nevertheless, while fulfilling task 7 (Table III), the driver was not able to keep the car inside of the road bounds and went off the road several times. On the straight road segment with higher speed limit (i.e. 90 km/h), the algorithm predicted smooth lane keeping offset (Fig. 3b, purple line). On this segment, despite the DD induced by secondary activities, the participant held a road line very well (Fig. 3b, black line). Yet, tasks 6 and 7 have forced the driver to cross the road lane dividing lines multiple times.

The steering wheel acceleration on a curvy road segment with 50 km/h speed limit was frequent in case of the DD performance (Fig. 3c, black curve). However, the Predictor forecasted almost the same frequent behavior for the free from the secondary activity driving (Fig. 3c, purple line). At this, as in the previous cases, the task 7 (Table III) motivated the driver to act on the steering wheel more frequently (Fig. 3c, black line). Consequently, it led to high steering wheel acceleration  $a$  oscillation comparing to the predicted one  $a_p$ . On a straight road with 90 km/h speed limit,  $a$  under DD (Fig. 3c, black line) was neither higher nor more frequent than during the normal driving (Fig. 3c, purple curve), except for the tasks 6 and 7

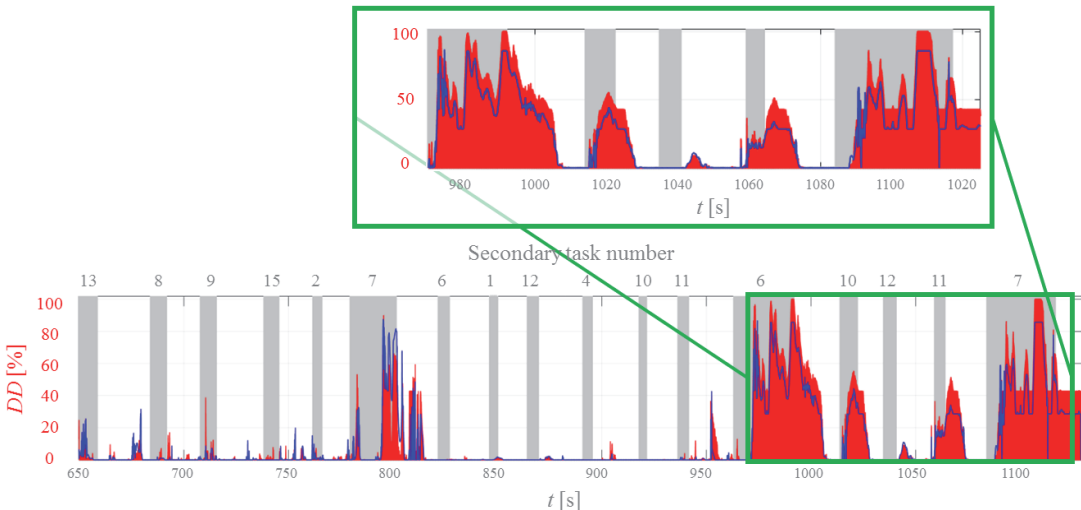


Fig. 4. Driver distraction evaluation results: gray background — the secondary task accomplishment period; red curve — new method; blue curve — old method.

again. A meaningful difference in driving performance can be observed during these tasks execution.

In Fig 4, the *DD* results for old and new methods are reported. The curves were obtained as a result of the fusion of the resultative performances  $\Delta v_r$ ,  $\Delta x_r$ , and  $a_r$  in the FL Evaluator. The blue line symbolizes the *DD* evaluated only with two performance-based variables  $\Delta v_r$  and  $\Delta x_r$ , whereas the red curve constitutes the method enhanced by an additional variable,  $a_r$ . For comparison, both results are shown together.

The new FL Evaluator does not detect higher *DD* level without distraction. Contrariwise, when the experiment participant's performance was vitally burdened (Fig. 3), the FL Evaluator lodges a corresponding evaluation. This is especially noticeable, when driver performed tasks 6, 7, and 10 on a 90 km/h limit straight road segment (Fig. 4; inset). It has been mentioned that these tasks led to greater performance degradation, what was immediately detected by the improved FL Evaluator. Moreover, the evaluation of *DD* is higher than with the old Evaluator, which had only two performance-based indicators. It is worth to note that the tasks 7 and 6 also took more time than others, what multiplies their danger for the safe vehicle operation.

## V. CONCLUSION

An improvement of the *DD* detection and evaluation method based on CI algorithms is suggested in this paper. Similarly, to the old method [17], the new one, first, predicts normal performance for every driver applying NNR algorithm. Second, it compares the predicted performance with the one submitted while accomplishing a secondary task, such as an interaction between the driver and the vehicle on-board computer. Finally, FL completes an evaluation of *DD* using the performance-based indicators. The newly proposed method uses three instead of two road characterization parameters for driver behavior prediction. What is more, the new method applies one additional performance-based variable for *DD* evaluation, namely steering wheel acceleration. The results proved that the new method does not raise *DD*, when the participant is not distracted or drives free from IVIS interaction. Contrariwise, when the driver is distracted, the new method detects greater level of *DD* comparing to the old one.

## ACKNOWLEDGMENT

This project has received funding from the European Union's Horizon 2020 research and innovation program under grant agreement No. 675999. The authors extend their special gratitude to the driver-in-the-loop experiment participants.

## REFERENCES

- [1] European Commission, Directorate General for Mobility and Transport, Road safety newsletter, No 27, 2017. [Online] Available: [https://ec.europa.eu/transport/road\\_safety/sites/roadsafety/files/nl27\\_en.pdf](https://ec.europa.eu/transport/road_safety/sites/roadsafety/files/nl27_en.pdf)
- [2] National Traffic Law Center. Investigation and prosecution of distracted driving cases. Report no. DOT HS 812 407. Washington, DC: National Highway Traffic Safety Administration, 2017.
- [3] M. R. Endsley, "Design and evaluation for situation awareness enhancement," Proc. of the Hum. Fact. and Ergon. Soc. Annual Meeting, vol. 32, no. 2, pp. 97-101, Oct. 1988.
- [4] H. Jander, J. Borgvall, and R. Ramberg, "Towards a methodological framework for HMI readiness evaluation," Proc. of the Hum. Fact. and Ergon. Soc. Annual Meeting, vol. 56, no. 1, pp. 2349-2353, Dec. 2016.
- [5] L. Fridman, P. Langhans, J. Lee, and B. Reimer, "Driver gaze region estimation without use of eye movement," IEEE Intel. Syst., vol. 31, no. 3, pp. 49-56, May 2016.
- [6] M.-H. Sigari, M. Fathy, and M. Soryani, "A driver face monitoring system for fatigue and distraction detection," Intern. Jour. of Vehic. Techn., vol. 2013, pp. 1-11, Jan. 2013.
- [7] X.-P. Huynh, S.-M. Park, and Y.-G. Kim, "Detection of driver drowsiness using 3D deep neural network and semi-supervised gradient boosting machine," in Asian Conf. on Comp. Vision (ACCV), Lecture Notes in Computer Science, vol. 10118, Springer, 2016, pp. 134-145.
- [8] S. Wang, Y. Zhang, C. Wu, F. Darvas, and W. A. Chaovalitwongse, "Online prediction of driver distraction based on brain activity patterns," IEEE Trans. on Intel. Transp. Syst., vol. 16, no. 1, pp. 136-150, Feb. 2015.
- [9] V. Alizadeh and O. Dehzangi, "The impact of secondary tasks on drivers during naturalistic driving: Analysis of EEG dynamics," 19<sup>th</sup> IEEE Intern. Conf. on Intel. Transp. Syst. (ITSC), Rio de Janeiro, Brazil, 2016, pp. 2493-2499.
- [10] C. Ahlstrom, K. Kircher, and A. Kircher, "A gaze-based driver distraction warning system and its effect on visual behavior," IEEE Trans. on Intel. Transp. Syst., vol. 14, no. 2, pp. 965-973, June 2013.
- [11] S. Qiu, R. McGee, and Y. L. Murphey, "Adaptive fuzzy prediction for automotive application usage," 14<sup>th</sup> IEEE Intern. Conf. on Machine Learn. and Applic. Miami, FL, USA, 2015, pp. 19-24.
- [12] T. Ersal, H. J. A. Fuller, O. Tsimhoni, J. L. Stein, and H. K. Fathy, "Model-based analysis and classification of driver distraction under secondary tasks," IEEE Trans. on Intel. Transp. Syst., vol. 11, no. 3, pp. 692-701, Sept. 2010.
- [13] J. Yang, T. N. Chang, and E. Hou, "Driver distraction detection for vehicular monitoring," 36<sup>th</sup> Annual Conf. of IEEE Indust. Electron. Soc. (IECON), Glendale, AZ, USA, 2010, pp. 108-113.
- [14] S. J. Choi, J. H. Kim, D. G. Kwak, P. Angkititirakul, and J. H. L. Hansen, "Analysis and classification of driver behavior using in-vehicle CAN-bus information," IEEE Intern. Conf. on Multim. and Expo (ICME), Barcelona, Spain, 2011, pp. 1-6.
- [15] S. Im, C. Lee, S. Yang, J. Kim, and B. You, "Driver distraction detection by in-vehicle signal processing," IEEE Symp. on Comput. Intel. in Vehic. and Transp. Syst. (CIVTS), Orlando, FL, USA, 2015, pp. 1-5.
- [16] V. Martínez, I. del Campo, J. Echanobe, and K. Basterretxea, "Driving behavior signals and machine learning: A personalized driver assistance system," 18<sup>th</sup> IEEE Intern. Conf. on Intel. Transp. Syst., Las Palmas, Spain, 2015, pp. 2933-1940.
- [17] A. Aksjonov, P. Nedoma, V. Vodovozov, and E. Petlenkov, "Driver distraction detection and evaluation with artificial neural network and fuzzy logic," The 15<sup>th</sup> IEEE Intern. Workshop on Advanced Motion Control (AMC 2018), Tokyo, Japan, 2018, pp. 523-528.
- [18] I. Goodfellow, Y. Bengio, and A. Courville, Deep Learning. Cambridge, Massachusetts: USA: The MIT Press, 2016, pp. 92-154.
- [19] E. Alpaydin, Introduction to Machine Learning. Cambridge, Massachusetts: USA: The MIT Press, 2004, pp. 105-132.
- [20] A. Aksjonov, P. Nedoma, V. Vodovozov, E. Petlenkov, and M. Herrmann, "A method of driver distraction evaluation using fuzzy logic," 26<sup>th</sup> Intern. Conf. on Inform., Commun. and Autom. Techn. (ICAT 2017), Sarajevo, Bosnia & Herzegovina, 2017, pp. 23-28.
- [21] R. Smith, Open Dynamics Engine v0.5: User Guide, 2006. [Online] Available: <http://ode.org/ode-latest-userguide.html>
- [22] H. B. Pacejka, Tyre and Vehicle Dynamics: Second Edition, Oxford: Great Britain: Butterworth-Heinemann, 2006.

**Publication VI**

**Aksjonov, A.**, Nedoma, P., Vodovozov, V., Petlenkov, E., & Herrmann, M. (2018). Detection and Evaluation of Driver Distraction Using Machine Learning and Fuzzy Logic. *IEEE Transactions on Intelligent Transportation Systems, Early Access*. doi: 10.1109/TITS.2018.2857222



# Detection and Evaluation of Driver Distraction Using Machine Learning and Fuzzy Logic

Andrei Aksjonov<sup>1</sup>, Pavel Nedoma, Valery Vodovozov, *Member, IEEE*, Eduard Petlenkov, and Martin Herrmann

**Abstract**—In addition to vehicle control, drivers often perform secondary tasks that impede driving. Reduction of driver distraction is an important challenge for the safety of intelligent transportation systems. In this paper, a methodology for the detection and evaluation of driver distraction while performing secondary tasks is described and an appropriate hardware and a software environment is offered and studied. The system includes a model of normal driving, a subsystem for measuring the errors from the secondary tasks, and a module for total distraction evaluation. A new machine learning algorithm defines driver performance in lane keeping and speed maintenance on a specific road segment. To recognize the errors, a method is proposed, which compares normal driving parameters with ones obtained while conducting a secondary task. To evaluate distraction, an effective fuzzy logic algorithm is used. To verify the proposed approach, a case study with driver-in-the-loop experiments was carried out, in which participants performed the secondary task, namely chatting on a cell phone. The results presented in this research confirm its capability to detect and to precisely measure a level of abnormal driver performance.

**Index Terms**—Euclidean distance, fuzzy logic, fuzzy neural networks, machine learning, prediction method, vehicle safety.

## I. INTRODUCTION

**A** DRIVER is the most important participant of a car control, including steering, throttling, braking, maneuvering, and other operations. These primary tasks must be accomplished safely for all traffic participants and their belongings.

Nevertheless, drivers often dedicate time and attention to other activities, different from the driver's primary ones. All other tasks the drivers perform while driving are defined as secondary tasks. They are divided into interaction with in-vehicle information systems (IVIS) (e.g. monitoring and managing vehicle state, navigating, info- and entertainment, etc.)

Manuscript received October 9, 2017; revised January 31, 2018, April 12, 2018, and June 12, 2018; accepted July 6, 2018. This work was supported by the European Union's Horizon 2020 Research and Innovation Program under Grant 675999. The Associate Editor for this paper was J. M. Alvarez. (*Corresponding author: Andrei Aksjonov.*)

A. Aksjonov and P. Nedoma are with Škoda Auto a.s., 29301 Mladá Boleslav, Czech Republic (e-mail: andrei.aksjonov@skoda-auto.cz; pavel.nedoma@skoda-auto.cz).

V. Vodovozov is with the Department of Electrical Power Engineering and Mechatronics, Tallinn University of Technology, 19086 Tallinn, Estonia (e-mail: valery.vodovozov@ttu.ee).

E. Petlenkov is with the Department of Computer Systems, Tallinn University of Technology, 19086 Tallinn, Estonia (e-mail: eduard.petlenkov@ttu.ee).

M. Herrmann is with IPG Automotive GmbH, 76185 Karlsruhe, Germany (e-mail: martin.herrmann@ipg-automotive.com).

Color versions of one or more of the figures in this paper are available online at <http://ieeexplore.ieee.org>.

Digital Object Identifier 10.1109/TITS.2018.2857222

and interaction with personal (e.g. passengers and pets) or items brought in a vehicle, such as portable electronic devices [1], [2].

Driver distraction (DD) is defined as *an activity performed by a driver that diverts an attention away from the primary activity (vehicle longitudinal and lateral control) potentially leading to safe driving degradation. It appears due to some event, activity, object, or person within or outside the vehicle, which compels or induces the driver's attention away from the primary task* [1]. With an enhancement of IVIS, driving comfort, entertainment, and navigation have dramatically improved. However, at the same time, IVIS attracts additional driver's attention. It increases DD, what often leads to traffic accidents with fatal consequences. Yearly, distracted driving leads to more than 420000 injuries. Furthermore, the number of drivers end abruptly in vehicle crashes due to DD is more than 3100 every year in the USA alone [3].

DD may take several forms: auditory, biomechanical, cognitive, or visual [1], [3]. Auditory distraction means taking ears off the road (e.g. listening to the radio or passengers). Biomechanical one is taking hands off the steering wheel (e.g. eating, texting messages, IVIS adjusting). Cognitive distraction means taking mind off the road (e.g. thinking, talking). Visual distraction is caused by taking eyes off the road (e.g. reading, watching video, road navigating in IVIS). However, most of the secondary tasks take more than one if not all the distraction forms simultaneously [1]–[4], those tasks are among the most dangerous [3]. Texting, for instance, requires manual, visual and cognitive distraction types at once, when the last one is considered as the most essential [3].

Research in driver's decoy caused by the secondary activity, especially by IVIS, arises a great interest of both the vehicle manufacturers and the traffic safety foundations, like the American Automobile Association (AAA) Foundation for Traffic Safety (Washington, DC, USA) and National Highway Traffic Safety Administration (NHTSA) (Washington, DC, USA). It helps to establish traffic safety policies, to contribute to the design, and to improve IVIS, which must be safe, intuitive, reachable, logic, and well organized to decrease driver's workload and disturbance and, consequently, to increase traffic safety.

Therefore, a development of a robust DD detection and evaluation method while performing a secondary task is a significant target in safe intelligent transportation. It gives an opportunity to study and to compare several types of

human-machine interaction (HMI) technologies (e.g. haptic, vocal, gesture) and to use the most appropriate one in IVIS design. DD assessment is also applied in advanced driver assistance systems (ADAS) and in testing and evaluating their impact on driver's level of vigilance and road safety. Today, there are no estimates for evaluating the influence of the secondary tasks on DD that might indicate the secondary activities that lead to potential traffic accidents, assess a degree of their danger, and help mitigate these effects [1].

The goal of the current study is to develop a method of evaluating a secondary task impact to the safe vehicle operation suitable for DD detection, DD level measurement, and comparison of the secondary tasks influence on DD. The method is exploited as a benchmark for safe and clear IVIS design with minimal driver's burden in different HMI technologies (e.g. voice command, hand gesture recognition).

This paper is organized as follows. The next section presents the state of the art of DD detection relevant for current studies. Section III is dedicated to the description of the DD evaluation methodology. The real-time driver-in-the-loop DD experiment is described in Section IV. Section V outlines the experimentally obtained results. The research is concluded in Section VI.

## II. RELATED WORKS AND PROBLEM STATEMENT

In general, there are four attributes suitable for DD measurement and detection: behavioral (e.g. eye and head movement); performance-based (e.g. vehicle lateral and longitudinal control); psychological (e.g. driver electrocardio- and electroencephalographical methods), and subjective (e.g. self-assessment questionnaires and expert evaluations). The first two are the most frequently used ones. Different attributes can be also combined [5]–[7].

On the other side, a variety of algorithms has been offered for the DD detection based on statistical learning theory. The gaze direction and the head orientation are the most popular input attributes [8]. Artificial neural network (NN) and gradient boosting machine combination were proposed in [9]. The glance region prediction algorithm was designed using random forest classifier in [10] and convolutional NN – in [11]. In [12], dynamic Bayesian network (BN) outperformed logic regression (LR), static BN, and support vector machine (SVM) approaches in cognitive DD detection. SVM together with semi-supervised extreme learning machine were combined for the DD detection in [5]. Classification based on Mahalanobis distance calculation was applied for the evaluation of IVIS-induced DD in real-time [13]. Fuzzy expert system combined eye and face regions for the DD level fatigue estimation in [14]. Different machine learning methods, in particular SVM,  $k$ -nearest neighbor ( $k$ -NN), and graph-regularized extreme learning machine were compared in [15]. The complex method designed in [7] connects the principle component analysis, the linear discriminate analysis, and SVM. Finally, in [16], a probabilistic restricted Coulomb energy NN was implemented for drowsy driving prediction.

Multiple psychological attributes were also studied for the DD detection. In [6], the brain activity measured by electroencephalographic signals was involved to predict the

start and the end of a distraction period using an adaptive-threshold-based prediction framework. In [17], the same signal analyses were applied for the DD detection by different machine learning methods: decision tree, random forest,  $k$ -NN, SVM, and Naïve Bayes. The driver drowsiness detection using heart rate electrocardiogram signals with LR and BN was described in [18].

Very popular is the usage or performance-based attributes in the DD detection as an estimate of the vehicle dynamics. As the signals are received here from the sensors available in modern passenger vehicles [19], this approach does not require any additional hardware.

An example of the DD detection usage in ADAS is described in [20]. The scholars presented fuzzy system, which personalizes the fuzzy membership functions based on individual driving habits. The system reflects user's preferences in the cruise control. Vehicle performance-based data were used in the fuzzy system design.

The DD detection with artificial NN and Gaussian mixture model (GMM) using performance-based attributes was introduced in [21] and [22]. The double-class DD classifier based on GMM was described in [23]. Vehicle dynamics and driving performance results were engaged in the DD detection by an extreme learning machine algorithm in [24] and SVM – in [2]. Kumagai and Akamatsu [25] presented the driver behavior prediction with dynamic BN based on preliminary collected data.

Since 1999, on-road data of drivers were collected for their further study in [26]. Statistical signal processing and machine learning techniques, such as GMM, hidden Markov model (HMM), and BN were applied to simulate such aspects of driver's behavior like pedal orientation, car following, and lane change. These data were successfully used for predicting the driver behavior and detecting risky driver frustration.

Many different DD detection algorithms, namely static and dynamic NN, adaptive neuro-fuzzy inference system (ANFIS), and SVM, were compared in [27]. The last one outperformed all other machine learning methods used in the work.

Lastly, different DD detection attributes, like performance-based, psychological, and behavioral, were combined. A gaze angle, a head rotation angle, and an interval between the heart R-wave electrocardiogram signals were used in cognitive DD [28], where the pattern recognition methods based on SVM and adaptive boosting were compared. The last one showed better accuracy. In [29], the control theoretic driver model based on the literary physiological aspect was induced by the driver's behavior predictive model design. This model was compared with a real driver performance.

The driver's eye movement and vehicle performance were integrated as a real-time cognitive DD attribute [4], [30], [31] and the SVM algorithm was applied in these studies. Driving performance and head movement tracking were integrated for the DD detection with random forest model and HMM [32]. In [33], different machine learning methods, SVM, conventional recurrent NN, and long or short-term memory recurrent NN, using the same attributes were compared for continuously driver's state prediction. The last one was more accurate in classification. In [34], DD prediction based on

ANFIS was compared with the artificial NN and radial basic function prediction algorithms. The results proved that ANFIS has more accurate prediction capability. Driver performance along with heart rate and behavioral attribute data were combined for the DD and fatigue detection in [35]. Classification was performed by a multi-modal approach based on HMM, SVM, and BN.

Though the physiological and behavioral attributes represent a trend in DD detection, they always require additional devices, such as cameras and neuroscan systems that multiply system cost and complexity [8]. Moreover, often wearing devices, like eye-tracking goggles or neuroscan helmets, are considered as a distraction source themselves. Then, some scholars consider the behavioral methods as the only capable to detect visual DD. Eye and head movement tracking are not qualified to observe driver's cognitive workload, such as talking to a passenger. It is unknown, how a cognitive distraction depends on eye and head movement required for the primary task performance [4], [27], [30]. This is the reason why the vehicle dynamic performance (center-lane driving and vehicle speed limit maintenance) has been chosen as a driver's primary task in this study.

Despite a variety of machine learning algorithms proposed for the DD detection, all of them use the Boolean binary classification (distracted/not distracted). These solutions are not suitable for different HMI technologies for accurate IVIS comparison. Never approaches have been found for accurate measuring of a DD level, especially in applying the performance-based attributes while interacting with IVIS.

The target of this paper is to propose a method, which not only detects, but also evaluates a DD level of each individual driver considered as an essential task of the safe IVIS design. To this aim, a regression problem of the DD detection is solved aiming to form the output as a precise number [36] using the machine learning approach. Thanks to accurate measurement, the level of the secondary task influences on the driver's performance is evaluated here. Nonlinear regression based on Euclidean distance (ED) calculation is applied for the DD detection. Fuzzy logic (FL) is used for fusion of vehicle performance data to assemble a level of DD from two independent variables. The driver-in-the-loop experiment on DD detection and evaluation was conducted, in which text messaging on a cell phone has been chosen as a secondary distractive activity required several modes of distraction simultaneously [3]. In this way, a difference in vehicle performance at normal driving (fully dedicated to a primary activity) and accomplishing a secondary task while driving was observed aiming to estimate a personal degree of the secondary tasks influence on driving [2].

Vehicle dynamics highly depend on the driver experience [35]. By this reason, a model of driver performance is created, which is assumed as a normal driving for each experiment participant. Next, the driving destructive performance is compared with normal driving in the real-time driver-in-the-loop experiment. To predict driver's normal performance, a regression-based machine learning algorithm is developed for participants' data collecting during a free run. In this paper, a technique that solves a regression problem and predicts

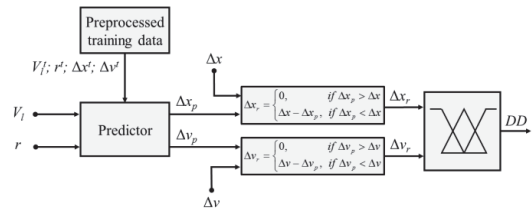


Fig. 1. DD detection and evaluation block scheme. Parameters description is presented in Table I.

TABLE I  
PARAMETERS DESCRIPTION

Symbol	Description	Unit
$r$	Road radius (curvature)	m
$V_i$	Speed limit	km/h
$\Delta x$	Real lane keeping offset	m
$\Delta v$	Real vehicle speed deviation	km/h
$\Delta x_p$	Predicted lane keeping offset	m
$\Delta v_p$	Predicted vehicle speed deviation	km/h
$\Delta x_r$	Resultative lane keeping offset	m
$\Delta v_r$	Resultative vehicle speed deviation	km/h
$DD$	Driver distraction level	%

driver performance on a specific road segment is defined as a predictor. What is more, as an ANFIS has very accurate prediction capability [27], the prediction approach based on ED formula is compared to an identical ANFIS predictor.

Next, the driving performance data are merged into a uniform variable, which represents a percentage level of DD caused by the secondary task. To this aim, the FL method is used. Among the most popular signal fusion techniques – FL, BN, and machine learning – FL is known as a perfect approach for empirical modeling of human behavior reasoning, because it simultaneously concerns several vague inputs, and for the vigilance information fusion [35]–[37].

### III. DESCRIPTION OF THE METHOD

A scheme of the DD detection and evaluation is shown in Fig. 1. The symbols' description and annotation are introduced in Table I. The superscript "t" determines "training data".

The method involves three steps. First, referring to a road segment specification (road curvature  $r$  and speed limit  $V_i$ ), it predicts driver's ability to keep the centerline  $\Delta x_p$  and to maintain the speed limit  $\Delta v_p$ . The predictor is trained preliminary without secondary activity for every driver, and training data are collected. Second, the predicted driver performance is compared with a performance with the secondary task  $\Delta x$  and  $\Delta v$ . As a result, their differences  $\Delta x_r$  and  $\Delta v_r$  are calculated. Finally, the FL evaluator using linguistic rules normalizes two independent variables into a uniform variable  $DD$ , which designates the DD level in percentage.

#### A. Prediction of Driver Performance Based on Euclidean Distance Calculation

To create a prediction model for an individual driver, he/she must drive a road segment without a distraction.

$V_l^t$ [km/h]	$r^t$ [m]	$\Delta x^t$ [m]	$\Delta v^t$ [km/h]	$V_l^t$ [km/h]	$r^t$ [m]	$\Delta x^t$ [m]	$\Delta v^t$ [km/h]
...	...	...	...	...	...	...	...
30	79.73	0.4593	3.5496	30	80	0.25939	3.53968
30	79.05	0.4818	3.5889	30	79	0.28267	3.58507
30	78.49	0.4978	3.6282	...	...	...	...
30	78.03	0.5080	3.6673	30	78	0.29787	3.62820
...	...	...	...	...	...	...	...
30	77.66	0.5132	3.7065	30	78	0.30808	3.66738
...	...	...	...	...	...	...	...
...	...	...	...	30	79	0.31220	3.70650
...	...	...	...	30	78	0.33638	3.66736
...	...	...	...	...	...	...	...
50	625.38	0.5109	3.7455	...	...	...	...
50	625.18	0.5047	3.7845	50	625	0.51992	3.74556
50	625.18	0.5047	3.7845	50	625	0.50477	3.78457
50	625.04	0.4960	3.8235	50	625	0.49602	3.82352
50	624.96	0.4851	3.8624	50	625	0.48515	3.86242
50	624.92	0.4725	3.9012	50	625	0.47252	3.90127
...	...	...	...	...	...	...	...
90	357.17	0.1515	0.9805	90	357	0.15156	0.98058
90	309.62	0.1833	1.0082	90	310	0.18333	1.00827
...	...	...	...	...	...	...	...

Fig. 2. Training data dimensional reduction.

During this run, the driver is asked to demonstrate an accurate performance: to obey the speed limits and to keep the middle lane of the road as perfectly as possible. The predictors' training data include four variables: speed limit  $V_l^t$ ; radius of the road  $r^t$ ; lane keeping offset  $\Delta x^t$ ; vehicle speed deviation from a speed limit  $\Delta v^t$ . The first two variables are related to the road information whereas two others – to driver performance. Thus, a map of driver performance is created on each specific road segment, described by the road curvature (radius)  $r$  and speed limit  $V_l$ .

Further, the obtained data are passed through preprocessing (dimensional reduction), during which this training information is diminished or simplified to reduce memory, computation, and inference complexity. Besides, the model simplification makes the method more robust, understandable, and easy to plot and analyze. There exist some preprocessing algorithms, such as the subset selection, the principle components analysis, the factor analysis, etc. [23], [36]. An approach used in this study is described below.

First, the training data are stored in a table. Second, the radiuses of the road segments are rounded to the whole numbers. Third, the unique pairs of a road curvature and a speed limit are found. Finally, a mean offset between the road centerline and a position of the car on the road, and a mean difference between the speed limit on a road segment and a real vehicle speed for each unique pair of road information are calculated. This preprocessing allows shrinking significantly the size of the data sample. For instance, the data collected during the 20-minute driving consisted of about 50 000 nodes. After preprocessing, these data shrank to 10% of total points. Described preprocess steps separated with blue arrows are shown in Fig. 2.

Consequently, the data table is obtained where every possible pair of input variables (road information) corresponds to a pair of output variables (driver performance). The outputs symbolize an average lane keeping and speed limit maintenance ability for a specific road segment. Input/output mapping is fulfilled with ED calculation.

During the experiment with the secondary activity, the information about the road segment is inserted into a prediction block containing preprocessed training data (Fig. 1). The predictor inputs are the real-time speed limit  $V_l$  and road radius  $r$ . The input road information is aligned with unique

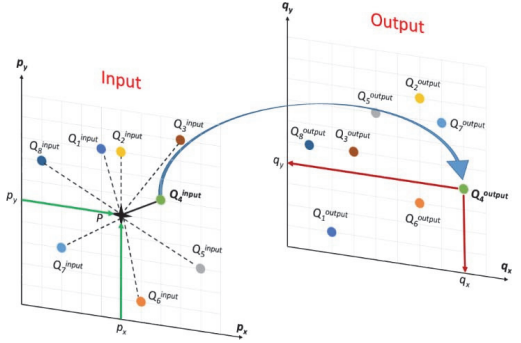


Fig. 3. Visual explanation of predicted value search based on Euclidean distance calculation.

pairs of the road set from the data table. The ED function  $d(P, Q)$  is used to search a closest pair of the prediction model input sets:

$$d(P, Q) = \sqrt{\sum_{i=1}^k (q_i - p_i)^2}, \quad (1)$$

where  $k$  is a spatial dimension.

The predicted searching procedure with ED calculation is simplistically illustrated in Fig. 3. Assume that  $P$  is a point with coordinates  $(p_x = r, p_y = V_l)$ . Points  $Q_n^input$  have coordinates  $(q_{xn}^{input} = r_n^t, q_{yn}^{input} = V_{ln}^t)$  from the training data table, where  $n$  is a row number in the table. All the distances are calculated between a single input point  $P$  and each point  $Q_n^input$  from the table with simplified training data. A set of point coordinates  $Q_n^input$  with the shortest distance between  $P$  and  $Q_4^input$  in Fig. 3 is accepted as possible driver performance on a road segment and returns the predicted output values  $(q_{xn}^{output} = \Delta x_{pn}, q_{yn}^{output} = \Delta v_{pn})$  that correspond to their row in the table.

A predictor input and output pair matching is depicted in Fig. 4. The input and output values are presented in separate Cartesian coordinate systems. Each coordinate in the first system has a unique pair of the coordinates in the parallel two-dimensional one. By finding the nearest set of trained input, the possible output is predicted and stored in the parallel coordinate system. Accordingly, possible driver performance is estimated, in a name of lane keeping and speed maintenance, on each road segment given by its speed limit and curvature.

Next, as it is also seen in Fig. 1, driver predicted performances  $\Delta x_p$  and  $\Delta v_p$  are compared with the real ones  $\Delta x$  and  $\Delta v$  using the following rules:

$$\Delta x_r = \begin{cases} 0, & \text{if } \Delta x_p > \Delta x \\ \Delta x - \Delta x_p, & \text{if } \Delta x_p < \Delta x, \end{cases} \quad (2)$$

$$\Delta v_r = \begin{cases} 0, & \text{if } \Delta v_p > \Delta v \\ \Delta v - \Delta v_p, & \text{if } \Delta v_p < \Delta v. \end{cases} \quad (3)$$

More precisely, if a predicted value is higher than a real value, the algorithm sends zero as a system output. It means that driving is normal for the current driver. When a predictive

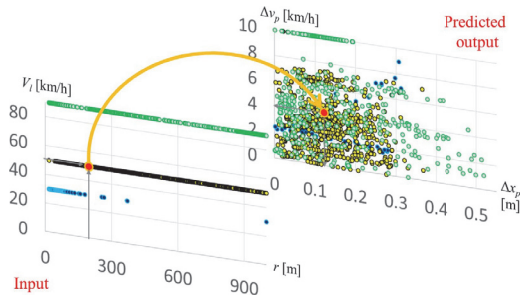


Fig. 4. Visual explanation of driver performance prediction using Euclidean distance formula.

value is smaller than a real value, the difference between two values is calculated and assigned as a system output. Hence, a hypothesis is posed that when the driver performance becomes worse due to distraction, the algorithm detects unusual vehicle dynamic performance. Finally, the obtained lane keeping offset  $\Delta x_r$  and speed difference  $\Delta v_r$  serve as the inputs to the FL reasoning to evaluate a level of distraction.

#### B. Driver Performance Prediction With an Adaptive Neuro-Fuzzy Inference System

To study the degree of accuracy of the prediction method described in the previous subsection, an ANFIS prediction model has been designed for a driver. Therefore, the ED and ANFIS predictors are compared during driver-in-the loop experimentation.

ANFIS is a feedforward five-layer network with supervised learning capability. It is functionally equivalent to a first-order Sugeno's fuzzy model. To support both the batch (off-line) and the pattern (on-line) learning, ANFIS combines least-squares estimator and the gradient descent method as training algorithms. During the single training epoch, ANFIS applies both the forward and the backward passes [38]. Significant improvement in ANFIS performance accuracy can be achieved with a greater number of membership functions (MFs) for the prediction model rather than an increasing number of training epochs [36]. In our case, trained ANFIS is integrated with the real-time experiment identically to the ED predictor. The same training data without preprocessing as in the ED predictor are utilized in ANFIS training. MATLAB<sup>®</sup> Fuzzy logic Toolbox<sup>™</sup> from MathWorks, Inc. (Natick, Massachusetts, USA) is used to design an ANFIS predictor for each experiment participant.

The difference in accuracy at applying 5, 50 or even 100 epochs is not sensitive [38]. The minimum possible for current training data set sum of squared errors was obtained with five MFs for every input variable. Hence, the network generates 25 rules, what took only three epochs. As suggested in [38]: 70% of sample data were used for training, 15% – for testing and the rest – for validation.

When the secondary task experiment is performed, the ANFIS model receives the same information about the road as the ED predictor. The outputs of ANFIS represent the driver

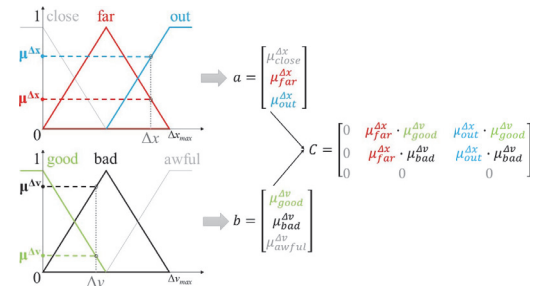


Fig. 5. Fuzzification procedure.

performance predictions  $\Delta x_p$  and  $\Delta v_p$ . Thus, two equivalent predictors are trained with the same data to compare.

#### C. DD Evaluator With FL

FL system design includes four stages: fuzzification, inference engine, rule-base, and defuzzification. It may have many inputs and outputs represented the real numbers. The first stage in fuzzy reasoning is a fuzzification, where each real number on the input is transformed into a fuzzy set, that is a pair consisting of an element in universe of discourse (UOD) and a degree of certainty of MF. The rule-base stores linguistic rules and is exploited to match fuzzy input with fuzzy output sets via an inference mechanism. Finally, a defuzzification procedure transforms fuzzy output sets back to real numbers [37].

In [39], a fuzzy inference process based on simple matrix operations is introduced. In the current study, the same approach is used for FL evaluator design. It has two inputs: an offset of the car position on the road  $\Delta x_r$  from the road centerline and a difference between the speed limit on a road segment and a real vehicle speed  $\Delta v_r$ . The inputs are generated during the driver prediction and real-time performance comparison described previously.

Both inputs  $\Delta x_r$  and  $\Delta v_r$  have symmetrically dispersed triangular MFs, what guarantee fast response and equal sensitivity of the input variables [37]. MFs are overlapped over the whole UOD. The  $\Delta x_r$  is restricted to [0 1.5]. The UOD of the  $\Delta v_r$  is narrowed in [0 12].

The inputs are transformed into appropriate column vectors  $a$  and  $b$ , those elements are equal to a degree of certainty of a relevant MF. MFs that are not crossed by the input variable are equal to 0. Every input has three MFs. Therefore, the fuzzified column vectors have the size of  $3 \times 1$ . The dyadic product of obtained vectors generates a  $3 \times 3$  matrix  $C = ba^T$ . Each element of the generated matrix  $C$  is a real number between zero and one. The fuzzification process together with the designed MFs is shown in Fig. 5.

The FL rule-base stores the linguistic rules relation between the input and output MFs. The linguistic knowledge is expressed in modes-pens-form rules "If-Then". As the system has two inputs and one output, nine rules are designed in total for the FL evaluator. The rule-base is presented in Table II, where the MFs are named suitably for human understanding. The distance from a vehicle and road centerline

TABLE II  
RULE-BASE OF THE FL EVALUATOR

$DD$		$\Delta x_r$		
		close	far	out
$\Delta v_r$	good	<i>no</i>	<i>negligible</i>	<i>low</i>
	bad	<i>no</i>	<i>medium</i>	<i>high</i>
	awful	<i>very_low</i>	<i>very_high</i>	<i>inacceptable</i>

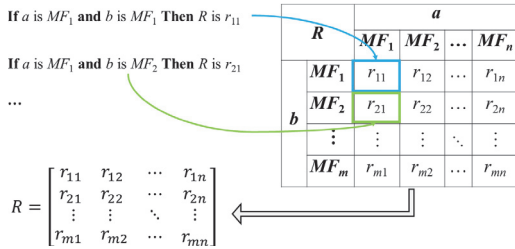


Fig. 6. Transformation of a FL rule-base into an  $m \times n$  matrix.

$\Delta x_r$  consists of 3 levels: “close” (to the centerline), “far” (from the centerline) or “out” (of the road bounds). The ability of the speed limit maintenance  $\Delta v_r$  is defined as “good”, “bad” or “awful”. An example of the linguistic rule meaning is as follows (Table II): **IF** the vehicle middle point is “far” from the road centerline **AND** driver’s speed limit maintenance is “awful”, **THEN** driver distraction is “very\_high”.

Next, this linguistic knowledge is represented as a  $3 \times 3$  matrix  $R$ , the elements of which are the values of the output singleton MFs: {*no* = 0, *negligible* = 14.3, *low* = 28.6, *very\_low* = 42.9, *medium* = 57.2, *high* = 71.5, *very\_high* = 85.8, *inacceptable* = 100}. The FL output presents DD in percentage, where each MF has equal step between each other in the UOD from 0 to 100. In Fig. 6, the transformation from the FL linguistic knowledge into an  $m \times n$  matrix  $R$  is shown. In our case, both  $m$  and  $n$  are equal to three.

After that, equally sized matrices  $C$  and  $R$  are multiplied with Hadamard product approach resulting in matrix  $D = C \circ R$ . Each element of  $D$  contains information about the certainty of each output MF activation for a specific input.

The last stage of the FL inference system is the conversion of fuzzy matrices back to a numerical value. This is done via one of the most popular defuzzification methods, center of gravity. To transform the matrices into a number, a weighted average of the matrix elements is found as the sum of the elements in matrix  $D$  divided by the sum of the elements in matrix  $C$ . The three-dimensional surface of the designed FL DD evaluator is observed in Fig. 7. The FL design specification is summarized in Table III.

#### IV. CASE STUDY

##### A. Participants

The participants of the driver distraction experiment were employees from IPG Automotive GmbH (Karlsruhe, Germany). All the participants (13 males and 5 females) took

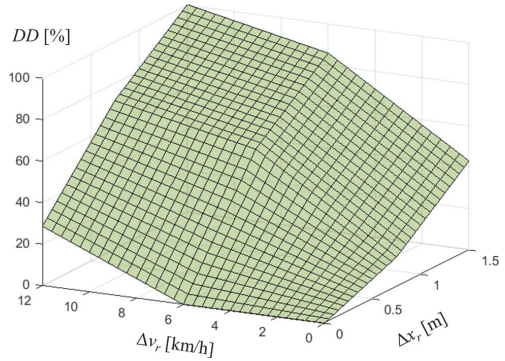


Fig. 7. Three-dimensional surface of the DD fuzzy evaluator.

TABLE III  
FL SPECIFICATION

Parameter	Fuzzy logic evaluator
Structure	Multi-input, single-output
Crisp inputs	$\Delta x_r = [0 \ 1.5]$ (3 MFs) $\Delta v_r = [0 \ 12]$ (3 MFs)
Crisp output	$DD = [0 \ 100]$ (8 MFs)
Input membership functions	Triangular symmetric
Output membership functions	Singleton symmetric
Inference mechanism	Matrix (Sugeno’s)
Rule-base	9 modes ponens
Defuzzification	Geometric center

part in the experiment voluntarily. Their age ranged between 24 and 39 (mean 30.11) years. The participants’ driving experience ranged between 1 and 21 years (mean 11.33).

Before the experiment, the drivers were questioned regarding the electronic devices, such as tablets, smartphones, laptops, e-readers usage while driving. Two participants admitted that they never use them while driving; two drivers noted that they use a device sometimes. Remaining drivers reported that they rarely use electronic devices. All the participants pointed out that they are aware about a danger of using devices while driving. After the experiment, the drivers also described their impression of distractive driving.

##### B. Apparatus

The vehicle mockup driving simulator equipment System Experience Platform (SEP) is demonstrated in Fig. 8. The fixed-base test rig has a steering wheel and two pedals: acceleration and brake. SEP has an adjustable driver sit and two liquid-crystal displays. The virtual world is performed on a display placed in front of the driver. The virtual vehicle model has an automatic transmission. The vehicle speed is observable for the driver from the head-up display. The performance data are collected at a frequency of 50 Hz. The SEP supports MATLAB®/Simulink® (Natick, Massachusetts, USA) and IPG CarMaker® (Karlsruhe, Germany) real-time integration.



Fig. 8. SEP driving simulator.

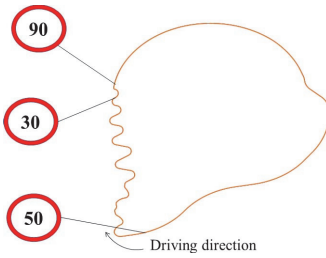


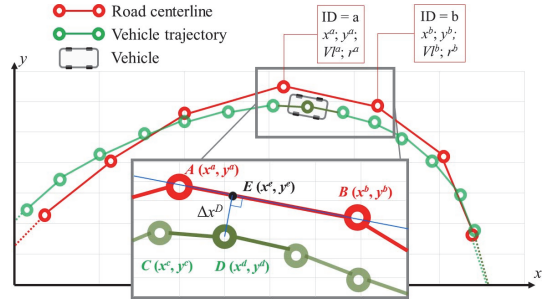
Fig. 9. Road shape with speed limits.

### C. Procedure

The participants drove a two-way, two-line highway road of the total length of 10626 m and the line width of 3.5 m. The road had three segments with different speed limits (30, 50, and 90 km/h) and curvatures. The road shape along with the segments speed limits is plotted in Fig. 9. There were neither other vehicles or pedestrians nor animals modeled in the virtual world. Before the experiment, the drivers received unlimited time to familiarize themselves with the test rig and with the road. Moreover, during the experiment, the road shape and the vehicle location on the road were also displayed in the corner of one of the SEP's screens.

The first part of the experiment was dedicated to the data collection for ANFIS and ED predictors. Each participant passed two laps without a secondary task. They were asked to drive along the right side of the road and to respect all the traffic signs. The drivers were also informed, what data are used in driving prediction. After passing two laps, the participants continued driving one more lap, during which one of the experiment organizers sent text messages to the cellular phone prepared for the participants. The drivers were requested to answer the text messages and to continue driving respecting all the traffic rules. There was no time restriction for secondary task execution. The data collected in the third lap were used in the DD recognition.

The drivers were instructed to have a chat conversation naturally. The experimenter asked the participants simple questions, for instance “How are you?”, “What are your plans


 Fig. 10. Visual explanation of data extraction for point  $D$ .

for the weekend?” and similar. The secondary task period was captured since a driver took the phone in a hand and ending when the driver released the phone from the hands. The experimenter gave a reasonable time between the distractive messages. Therefore, each participant drove roughly equal time being distracted and being free from the secondary task.

### D. Data Extraction

The road consists of the nodes with fixed locations in Cartesian coordinate system, which are connected between each other with straight lines. Each node contains data {unique identification number (ID);  $x$  coordinate;  $y$  coordinate; speed limit  $V_I$ ; road radius  $r$ }. During the experiment, the SEP saves the location of the vehicle geometric center in the virtual world with a fixed frequency.

In Fig. 10, an example of calculating  $\Delta x$  is illustrated. The red line symbolizes a road segment of the road curve (Fig. 9), while the green one - vehicle geometric center locations. In the point  $D$  of the vehicle trajectory with the coordinates  $(x^d, y^d)$ , two nearest nodes  $A$  and  $B$  are searched from the road curve applying the ED function (1). Next, the shortest distance from the point  $D$  to the straight line between two nodes  $A$  and  $B$  is assigned as  $\Delta x^D$ . In Fig. 10, this shortest distance is the line  $DE$ .

The maximum speed in the point  $D$  is calculated using the coordinates of this point and the previous one  $C$ :

$$v^D = \frac{\sqrt{(x^d - x^c)^2 + (y^d - y^c)^2}}{\Delta t}, \quad (4)$$

where  $\Delta t$  is the time constant between data measurement for SEP. Finally, the speed deviation  $\Delta v^D$  for the point  $D$  is found as a difference between  $v^D$  and the speed limit  $V_I^a$  of the closest node  $A$ .

The road radius and speed limit for the point  $D$  are assigned from the closest of two nearest nodes of the road trajectory. In Fig. 10, the point  $D$  (green) passes the road segment characterized by the node  $A$  (red). Consequently, after data extraction, the point  $D$  includes attributes  $\{\Delta x^D; \Delta v^D; V_I^D; r^D\}$ .

## V. RESULTS

In this section, the driver-in-the-loop experiment results are presented. Two driver performance predictors,

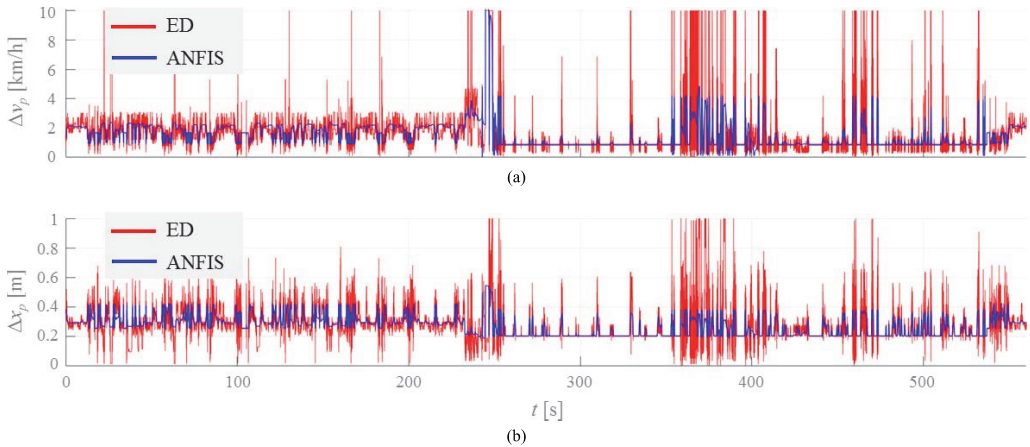


Fig. 11. Driver performance prediction algorithms comparison: the red curve represents performance prediction by the ED; the blue curve displays performance prediction by the ANFIS: (a)  $\Delta v_p$ ; (b)  $\Delta x_p$ .

TABLE IV  
ANFIS AND ED PREDICTION ACCURACY COMPARISON

Predictor	$\Delta v_{RMSE}$ [km/h]	$\Delta x_{RMSE}$ [m]	$t_{train}$ [s]
ANFIS	2.1345	0.1506	148.072
ED	1.9992	0.1405	96.150

ED and ANFIS, are compared. In this paper, the performance results of only one driver are introduced and are studied in detail. A random driver was selected from the group of driver-in-the-loop experiment participants. For all other drivers, the results are very similar.

#### A. A Comparison Between ED and ANFIS Predictors

In Fig. 11, a comparison between ED calculation and ANFIS predictors is reported. The red curve symbolizes performance prediction by the ED, whereas the blue curve – prediction by the ANFIS. Predicted results obtained from the ED and the ANFIS are similar for both  $\Delta v_p$  (Fig. 11 a) and  $\Delta x_p$  (Fig. 11 b).

The main difference between the prediction algorithms is that the ANFIS comparing to the ED has a smooth output. Nevertheless, the average prediction accuracy is almost the same for both algorithms. It can be explained by the ANFIS hybrid training algorithm, where both antecedent and consequent parameters are optimized in the backward and forward passes, respectively [38]. The ED predictor, however, has higher oscillation. The algorithm uses only the preprocessed data with a single simplification. It provides slightly more accurate prediction and, though, frequent fluctuation. Nevertheless, the output response remains identical to the ANFIS.

In Table IV, the root mean squared errors, which are responsible for algorithm prediction accuracy, for every predicted variable,  $\Delta v_{RMSE}$  and  $\Delta x_{RMSE}$ , are reported. In addition, the algorithms' training time  $t_{train}$  is calculated. The ED shows

more accurate prediction capabilities and faster training term comparing to the identical ANFIS predictor. For the rest of the Section only the ED predictor results are studied.

#### B. DD Detection

Fig. 12 demonstrates driving performance of one of the experiment participants conducting a secondary task. The gray background symbolizes a period of the secondary distractive activity (i.e. the cellular telephone is in the driver's hand). Red lines on every plot mark the predicted performance, namely speed limit maintenance (Fig. 12 a) and lane keeping ability (Fig. 12 b). Black line is driver's real performance. Green curves represent an appropriate information about the road segment (Fig. 9): speed limit (Fig. 12 a) and curvature (Fig. 12 b). The small road radius designates a sharp turn, while the big radius – almost straight road.

It is observed that the driver failed in holding optimal speed limits (Fig. 12 a) while performing the secondary activity. The method predicted that the driver would not surpass the difference between actual and optimal for the road speeds in 3 km/h on most of the road segments. Nevertheless, the participant being distracted decreased or increased the vehicle velocity by more than 5 km/h relatively the road speed limit.

For the studied driver, the speed limit maintenance on the 50 km/h speed limit segment was harder than on a high speed limit (i.e. 90 km/h) one (Fig. 12 a). The road is significantly curvy on the low speed road part, whereas the high speed limit segment is almost straight (Fig. 9; Fig. 12 b). This is also predicted by the ED (Fig. 12 a).

The driver faced difficulties keeping the vehicle in the middle of the lane while performing the secondary task (Fig. 12 b). In some moments, the driver went more than 4 m far from the centerline. The width of the modeled in the virtual world vehicle is 1.5 m. The width of a single lane is 3.5 m. It means that when  $\Delta x$  is higher than 1 m, the participants drive outside the lane bounds. Although, the ED predicts

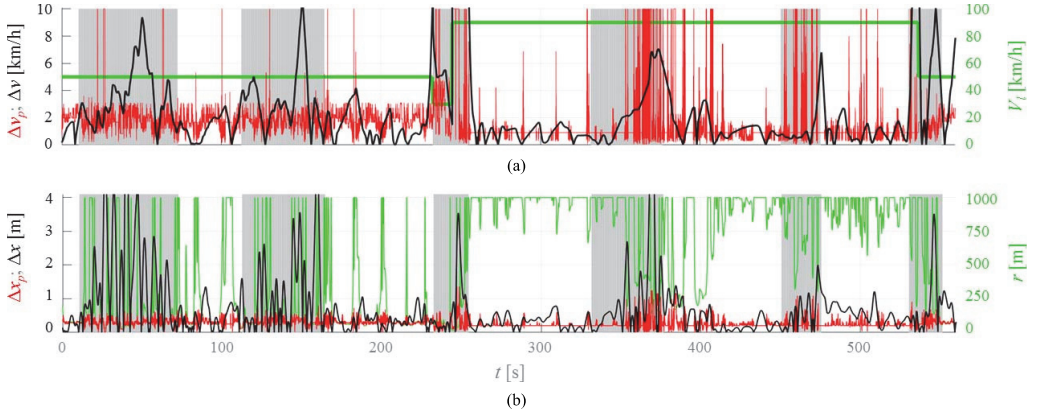


Fig. 12. Driver performance prediction versus real driver performance example: Gray background – the secondary task accomplishment period; black curve – real driver performance; red curve – predicted driver performance by the ED calculation; green curve – information about the road segment: (a)  $\Delta v_p$ ,  $\Delta v$ , and  $v_r$ ; (b)  $\Delta x_p$ ,  $\Delta x$ , and  $r$ .

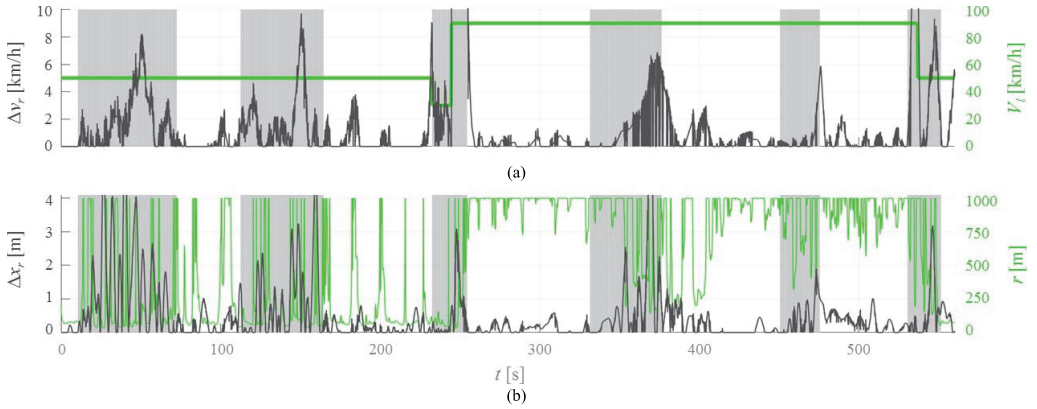


Fig. 13. Resultative driver performance with ED predictor: gray background – the secondary task accomplishment period; dark gray curve – driver resultative performance (Eq. (2), (3)); green curve – information about the road segment: (a)  $\Delta v_r$  and  $V_r$ ; (b)  $\Delta x_r$  and  $r$ .

that the driver's  $\Delta x$  does not exceed 0.5 m while normal performance, the  $\Delta x$  was higher than 1 m when the driver interacted with the mobile phone. Hence, the driver always drove off the road while chatting on a cell phone. Consequently, by applying the methods of the prediction of driver performance, an abnormal driver's behavior may be recognized. As this behavior is caused by the secondary task accomplishment, it can be concluded that the method is suitable for DD detection.

In Fig. 13, the resultative driver performance diagrams are acquainted. The response values were calculated applying (2) and (3) for the ED predictor. The results help estimate the difference between driving with the secondary task and normal driving from the viewpoint of the speed limit maintenance and the lane keeping ability. Both estimates,  $\Delta v_r$  and  $\Delta x_r$ , have similar levels: low at normal driving and significantly high while performing the secondary task.

### C. DD Evaluation

In Fig. 14, a percentage level of DD is shown. The curve represents the result of the FL data fusion. Two variables,  $\Delta v_r$  and  $\Delta x_r$  (Fig. 13), pass through FL evaluator. The prediction method represents normal driving (Fig. 14, white background) for each individual participant, when evaluation of the driving performance does not exceed 20%. On the contrary, when the driver performs secondary task, her/his lane keeping and speed maintenance ability degrade. The algorithm easily detects this phenomenon and FL evaluates driving performance with significantly high percentage (Fig. 14, gray background).

DD remains still high in a few seconds after secondary task accomplishment (Fig. 14) because the drivers, after completing the distractive task, realize the errors and try to return to their lane and increase/decrease the speed as soon as possible. This maneuver causes additional mistakes in vehicle operation. Thus, DD is often dangerous not only during the secondary

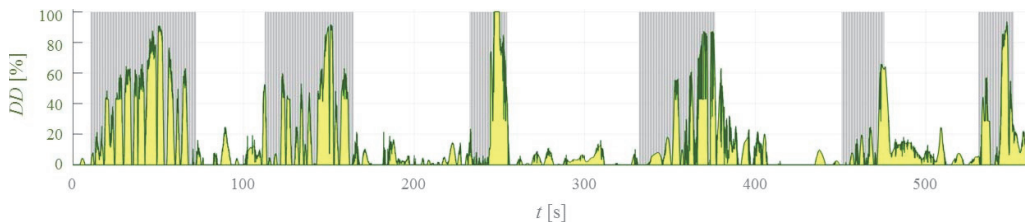


Fig. 14. DD evaluation: gray background – the secondary task accomplishment period; green-yellow curve – DD detected with the ED predictor.

activity execution, but also for few seconds after. Hence, the secondary activity increases the period of distraction.

Using the proposed method and considering 20% of DD as abnormal driving, it can be seen in Fig. 14 that the driver was always distracted while interacting with the mobile phone. The experiment results are also confirmed by the driver-in-the-loop experiment participants' subjective evaluation. All the drivers mentioned that they experienced visual, biomechanical, and cognitive distractions at the same time, what caused their driving performance burden leading to abnormal driving. This phenomenon was assured by the proposed method (Fig. 14).

Furthermore, although the participants were informed about the experiment procedure in details, and they were able to observe their position on a track on one of the SEP screens, it did not help them to avoid distraction induced by the interaction with cell phones (Fig. 14). It also proves the statement from [3]: *"our cognitive ability does not allow us to engage in more than one conscious task simultaneously."* It certifies that when the driver is involved in the secondary activity, safe driving is not guaranteed. Thus, minimization of DD is worthy of significant effort and work.

## VI. CONCLUSION

This paper presents a method for DD detection and evaluation while performing a secondary task. The detection is executed by the machine learning algorithm based on the ED calculation formula. FL fuses the performance-based data to evaluate a level of DD in percentages. The main contribution of this work is solving a regression problem in DD detection and performance-based data fusion into a single variable introduced for the DD assessment. Therefore, the method is capable not only to detect DD, but also to evaluate its influence on safe driving performance.

A machine learning algorithm predicts driver performance in a name of lane keeping and speed maintenance ability on a specific road segment. A road segment is described by speed limit and road curvature. The data used in machine learning are collected during driver's normal performance, when no distraction activity appears. To recognize DD, the proposed method compares distracted while conducting a secondary task driving with normal one, free from distraction, performances.

To verify the proposed DD detection and evaluation method, the driver-in-the-loop experiment on driving decoy performing a secondary task with 18 participants was conducted. Chatting on a cellular telephone is examined as a secondary task.

Data collected during two full laps driving is exploited for predictor design. One more lap is driven with a secondary activity execution. The proposed method enables accurate driver decoy experimentation. The results presented in this paper prove that the proposed method is capable to detect and to measure precisely the percentage level of DD caused by an unusual driver performance. The methodology is adaptable to each individual driver. It allows examination and comparison of the secondary tasks influence on driving quality of various drivers.

The suggested methodology has a certain advantage over other DD detection methods described in Section II. Particularly, as compared to the methods, where the behavioral and psychological attributes are applied [6]–[18], the proposed approach does not require additional devices, such as cameras and neuroscan systems. Those devices increase the system cost [8], what in its turn is a potential resistance for system application in a commercial passenger vehicle. For the same reason, the methods with different attribute combinations (e.g. behavioral, psychological, and subjective) [30]–[35] are not feasible in the real world implementation.

The method introduced here, like in [2] and [20]–[27], uses only performance-based attributes, because the variables can be obtained using the data from the available in modern vehicles sensors [19]. However, the method described here, in comparison with other performance-based approaches and with all the works mentioned in Section II, is able to measure a level of DD. The nonlinear regression technique used for DD detection gives an opportunity for a precise DD measurement. On the contrary, all the previously proposed methods are binary classifiers with Boolean output (distracted/non-distracted). Consequently, the suggested method can be used as a practical tool for different evaluation and comparative analyses of the secondary tasks influence on vehicle safety.

This work, however, has several limitations. Exactly, it misses a statistical analysis with a greater sample size of different driver segments (e.g. distributed between age, gender, driving experience, etc.). This analysis will be conducted in the future works. What is more, in this paper, the case study involved only one secondary task: texting on a cell phone. In the future, a variety of different DD activities will be tested on their influence of the DD level. Like in [33], the IVIS will be exploited as a number of secondary activities. To this regard, the experiments will be conducted on the advanced vehicle mockup with a vehicle cockpit identical to the one

used in commercial vehicles. Finally, the method will be also extended to more driving-performance variables, and different DD recognition attributes will be combined.

#### ACKNOWLEDGMENT

The authors would like to thank IPG Automotive GmbH (Karlsruhe, Germany) for providing the test rig. They extend their special thanks to the volunteers from IPG Automotive GmbH for participating in the driver-in-the-loop experiment.

#### REFERENCES

- [1] M. Westin, R. Dougherty, C. Depcik, A. Hausmann, and C. Sproule, III, "Development of an adaptive human-machine-interface to minimize driver distraction and workload," in *Proc. Int. Mech. Congr. Expo.*, San Diego, CA, USA, 2013, pp. 1–13.
- [2] T. Ersal, H. J. A. Fuller, O. Tsimhoni, J. L. Stein, and H. K. Fathy, "Model-based analysis and classification of driver distraction under secondary tasks," *IEEE Trans. Intell. Transp. Syst.*, vol. 11, no. 3, pp. 692–701, Sep. 2010.
- [3] National Traffic Law Center, "Investigation and prosecution of distracted driving cases." Nat. Highway Traffic Safety Admin., Washington, DC, USA, Tech. Rep. DOT HS 812 407, 2017.
- [4] Y. Liang, J. D. Lee, and M. L. Reyes, "Nonintrusive detection of driver cognitive distraction in real time using Bayesian networks," *Transp. Res. Rec., J. Transp. Res. Board*, vol. 2018, no. 1, pp. 1–8, Dec. 2017, doi: [10.3141/2018-01](https://doi.org/10.3141/2018-01).
- [5] T. Liu, Y. Yang, G.-B. Huang, Y. K. Yeo, and Z. Lin, "Driver distraction detection using semi-supervised machine learning," *IEEE Trans. Intell. Transp. Syst.*, vol. 17, no. 4, pp. 1108–1120, Apr. 2016.
- [6] S. Wang, Y. Zhang, C. Wu, F. Darvas, and W. A. Chaovalitwongse, "Online prediction of driver distraction based on brain activity patterns," *IEEE Trans. Intell. Transp. Syst.*, vol. 16, no. 1, pp. 136–150, Feb. 2015.
- [7] J. Jo, S. J. Lee, J. Kim, H. Gi Jung, and K. R. Park, "Vision-based method for detecting driver drowsiness and distraction in driver monitoring system," *Opt. Eng.*, vol. 50, no. 12, pp. 1–24, 2011.
- [8] C. Ahlstrom, K. Kircher, and A. Kircher, "A gaze-based driver distraction warning system and its effect on visual behavior," *IEEE Trans. Intell. Transp. Syst.*, vol. 14, no. 2, pp. 965–973, Jun. 2013.
- [9] X.-P. Huynh, S.-M. Park, and Y.-G. Kim, "Detection of driver drowsiness using 3D deep neural network and semi-supervised gradient boosting machine," in *Proc. Asian Conf. Comput. Vis.*, in Lecture Notes in Computer Science, Taipei, Taiwan, vol. 10118. Springer, 2016, pp. 134–145.
- [10] L. Fridman, P. Langhans, J. Lee, and B. Reimer, "Driver gaze region estimation without use of eye movement," *IEEE Intell. Syst.*, vol. 31, no. 3, pp. 49–56, May/Jun. 2016.
- [11] I.-H. Choi, S. K. Hong, and Y.-G. Kim, "Real-time categorization of driver's gaze zone using the deep learning techniques," in *Proc. Int. Conf. Big Data Smart Comput. (BigComp)*, Hong Kong, Jan. 2016, pp. 143–148.
- [12] A. Azman, S. Z. Ibrahim, Q. Meng, and E. A. Edirisinghe, "Physiological measurement used in real time experiment to detect driver cognitive distraction," in *Proc. Int. Conf. Electron., Inf. Commun. (ICEIC)*, Kota Kinabalu, Malaysia, Jan. 2014, pp. 1–5.
- [13] P. Jiménez, L. M. Bergasa, J. Nuevo, N. Hernández, and I. G. Daza, "Gaze fixation system for the evaluation of driver distractions induced by IVIS," *IEEE Trans. Intell. Transp. Syst.*, vol. 13, no. 3, pp. 1167–1178, Sep. 2012.
- [14] M.-H. Sigari, M. Fathy, and M. Soryani, "A driver face monitoring system for fatigue and distraction detection," *Int. J. Veh. Technol.*, vol. 2013, Jan. 2013, Art. no. 263983, doi: [10.1155/2013/263983](https://doi.org/10.1155/2013/263983).
- [15] Y. Jiao, Y. Peng, B.-L. Lu, X. Chen, S. Chen, and C. Wang, "Recognizing slow eye movement for driver fatigue detection with machine learning approach," in *Proc. Int. Joint Conf. Neural Netw. (IJCNN)*, Beijing, China, Jul. 2014, pp. 4035–4041.
- [16] H. Matsuo and A. Khait, "Prediction of drowsy driving by monitoring driver's behavior," in *Proc. 21st Int. Conf. Pattern Recognit. (ICPR)*, Tsukuba, Japan, Nov. 2012, pp. 3390–3393.
- [17] V. Alizadeh and O. Dehzangi, "The impact of secondary tasks on drivers during naturalistic driving: Analysis of EEG dynamics," in *Proc. IEEE 19th Int. Conf. Intell. Transp. Syst. (ITSC)*, Rio de Janeiro, Brazil, Nov. 2016, pp. 2493–2499.
- [18] M. Babaeian, N. Bhardwaj, B. Esquivel, and M. Mozumdar, "Real time driver drowsiness detection using a logistic-regression-based machine learning algorithm," in *Proc. IEEE Green Energy Syst. Conf. (IGSEC)*, Long Beach, CA, USA, Nov. 2016, pp. 1–6.
- [19] E. Zabler, "Sensors for brake control," in *Brakes, Brake Control and Driver Assistance Systems: Function, Regulation and Components*, K. Reif, Ed. Wiesbaden, Germany: Springer-Verlag, 2014, pp. 142–153.
- [20] S. Qiu, R. McGee, and Y. L. Murphey, "Adaptive fuzzy prediction for automotive applications usage," in *Proc. IEEE 14th Int. Conf. Mach. Learn. Appl. (ICMLA)*, Miami, FL, USA, Dec. 2015, pp. 19–24.
- [21] S. Choi, J. Kim, D. Kwak, P. Angkititrukul, and J. H. L. Hansen, "Analysis and classification of driver behavior using in-vehicle CAN-bus information," in *Proc. Int. Conf. Multimedia Expo (ICME)*, Barcelona, Spain, 2011, pp. 1–6.
- [22] S. Im, C. Lee, S. Yang, J. Kim, and B. You, "Driver distraction detection by in-vehicle signal processing," in *Proc. IEEE Symp. Comput. Intell. Vehicles Transp. Syst. (CIVTS)*, Orlando, FL, USA, Dec. 2015, pp. 64–68.
- [23] J. Yang, T. N. Chang, and E. Hou, "Driver distraction detection for vehicular monitoring," in *Proc. 36th Annu. Conf. IEEE Ind. Electron. Soc. (IECON)*, Glendale, AZ, USA, Nov. 2010, pp. 108–113.
- [24] V. Martínez, I. Del Campo, J. Echanobe, and K. Basterretxea, "Driving behavior signals and machine learning: A personalized driver assistance system," in *Proc. IEEE 18th Int. Conf. Intell. Transp. Syst.*, Las Palmas, Spain, Sep. 2015, pp. 2933–2940.
- [25] T. Kumagai and M. Akamatsu, "Prediction of human driving behavior using dynamic Bayesian network," *IEICE Trans. Inf. Syst.*, vol. E89-D, no. 2, pp. 857–860, 2006.
- [26] C. Miyajima and K. Takeda, "Driver-behavior modeling using on-road driving data: A new application for behavior signal processing," *IEEE Signal Process. Mag.*, vol. 33, no. 6, pp. 14–21, Nov. 2016.
- [27] F. Tango and M. Botta, "Real-time detection system of driver distraction using machine learning," *IEEE Trans. Intell. Transp. Syst.*, vol. 14, no. 2, pp. 894–905, Jun. 2013.
- [28] M. Miyaji, H. Kawanaka, and K. Oguri, "Effect of pattern recognition features on detection for driver's cognitive distraction," in *Proc. 13th Int. IEEE Conf. Intell. Transp. Syst.*, Sep. 2010, pp. 605–610.
- [29] P. Hermannstädter and B. Yang, "Driver distraction assessment using driver modeling," in *Proc. IEEE Int. Conf. Syst., Man, Cybern.*, Manchester, UK, Oct. 2013, pp. 3693–3698.
- [30] Y. Liao, S. E. Li, W. Wang, Y. Wang, G. Li, and B. Cheng, "Detection of driver cognitive distraction: A comparison study of stop-controlled intersection and speed-limited highway," *IEEE Trans. Intell. Transp. Syst.*, vol. 17, no. 6, pp. 1628–1637, Jun. 2016.
- [31] Y. Liang, M. L. Reyes, and J. D. Lee, "Real-time detection of driver cognitive distraction using support vector machines," *IEEE Trans. Intell. Transp. Syst.*, vol. 8, no. 2, pp. 340–350, Jun. 2007.
- [32] C. Schwarz, T. Brown, J. Lee, J. Gaspar, and J. Kang, "The detection of visual distraction using vehicle and driver-based sensors," SAE Tech. Paper 2016-01-0114, Apr. 2016, doi: [10.4271/2016-01-0114](https://doi.org/10.4271/2016-01-0114).
- [33] M. Wöllmer *et al.*, "Online driver distraction detection using long short-term memory," *IEEE Trans. Intell. Transp. Syst.*, vol. 12, no. 2, pp. 574–582, Jun. 2011.
- [34] F. Tango, C. Calefato, L. Minin, and L. Canovi, "Moving attention from the road: A new methodology for the driver distraction evaluation using machine learning approaches," in *Proc. 2nd Conf. Hum. Syst. Interact.*, Catania, Italy, May 2009, pp. 596–599.
- [35] C. Craye, A. Rashwan, M. S. Kamel, and F. Karray, "A multi-modal driver fatigue and distraction assessment system," *Int. J. Intell. Transp. Syst. Res.*, vol. 14, no. 3, pp. 173–179, 2016.
- [36] E. Alpaydin, *Introduction to Machine Learning*. Cambridge, MA: USA: MIT Press, 2004, pp. 105–132.
- [37] K. M. Passino and S. Yurkovich, *Fuzzy Control*. Menlo Park, CA, USA: Addison-Wesley, 1998.
- [38] M. Negnevitsky, *Artificial Intelligence*, 2nd ed. Harlow, UK: Addison-Wesley, 2005, pp. 259–300.
- [39] A. Aksjonov, P. Nedoma, V. Vodovozov, E. Petlenkov, and M. Herrmann, "A method of driver distraction evaluation using fuzzy logic: Phone usage as a driver's secondary activity: Case study," in *Proc. Int. Conf. Inf. Commun. Automat. Technol.*, Sarajevo, Bosnia-Herzegovina, Oct. 2017, pp. 1–6.



**Andrei Aksjonov** received the B.Sc. and M.Sc. degrees in electrical engineering and electrical drives and power electronics with automation specialization from the Tallinn University of Technology, in 2013 and 2015, respectively. He is currently a Marie Skłodowska-Curie Research Fellow hosted by Škoda Auto a.s. His research topics are the development of driver distraction detection and human-machine interface evaluation methods for multi-actuated ground vehicles. His research interests include HMI, fuzzy systems, machine learning, vehicle safety, and ADAS.



**Eduard Petlenkov** received the B.Sc., M.Sc., and Ph.D. degrees in computer and systems engineering from the Tallinn University of Technology. He is currently a Professor with the Department of Computer Systems, Tallinn University of Technology. His main research interests lie in the domain of nonlinear control, system analysis, and computational intelligence.



**Pavel Nedoma** received the M.Sc. and Ph.D. degrees from Czech Technical University, Prague, in 1985 and 2007, respectively. Since 1985, he has been a Development Engineer with the Škoda Auto Concept Development Department. He is responsible for the development experimental tools for simulation, supervision, analysis, processing, and visualization HMI interaction between driver and other on-board systems, HMI measurements in car ride simulators, and comparative measurements performed in real vehicles.



**Valery Vodovozov** (M'18) received the Candidate of Science degree from Saint Petersburg Electrotechnical University, Russia. He was an Associate Professor and a Senior Researcher in electrical engineering with Saint Petersburg Electrotechnical University. He is currently a Professor with the Tallinn University of Technology, Estonia. His research interests include power electronics and electrical drives areas. He is a member of the International Institute of Informatics and Systemics and the Global Research Alliance of Texas Institute of Science.



**Martin Herrmann** received the B.Sc. and M.Sc. degrees in automotive engineering from the Ilmenau University of Technology, in 2012 and 2014, respectively. He is currently the Business Development Manager at IPG Automotive focusing on methods for testing ADAS and automated driving functions in virtual environments. This includes especially road, traffic, and sensor modeling.

**Publication VII**

**Aksjonov, A.**, Vodovozov, V., Augsburg, K., & Petlenkov, E. (2018). Design of Regenerative Anti-Lock Braking System Controller for 4 In-Wheel-Motor Drive Electric Vehicle with Road Surface Estimation. *International Journal of Automotive Technology*, 19(4), 727–742. doi: 10.1007/s12239-018-0070-8



## DESIGN OF REGENERATIVE ANTI-LOCK BRAKING SYSTEM CONTROLLER FOR 4 IN-WHEEL-MOTOR DRIVE ELECTRIC VEHICLE WITH ROAD SURFACE ESTIMATION

Andrei Aksjonov<sup>1)</sup>, Valery Vodovozov<sup>2)\*</sup>, Klaus Augsburg<sup>3)</sup> and Eduard Petlenkov<sup>4)</sup>

<sup>1)</sup>SKODA AUTO a.s., Tr. Vaclava Klementa 869, Mlada Boleslav 29301, Czech Republic

<sup>2)</sup>Department of Electrical Power Engineering and Mechatronics, School of Engineering, Tallinn University of Technology, Tallinn 19086, Estonia

<sup>3)</sup>Automotive Engineering Group, Department of Mechanical Engineering, Technische Universität Ilmenau, Ilmenau 98693, Germany

<sup>4)</sup>Department of Computer Systems, School of Information Technologies, Tallinn University of Technology, Tallinn 19086, Estonia

(Received 12 June 2017; Revised 19 September 2017; Accepted 24 January 2018)

**ABSTRACT**—This paper presents a regenerative anti-lock braking system control method with road detection capability. The aim of the proposed methodology is to improve electric vehicle safety and energy economy during braking maneuvers. Vehicle body longitudinal deceleration is used to estimate a road surface. Based on the estimation results, the controller generates an appropriate braking torque to keep an optimal for various road surfaces wheel slip and to regenerate for a given motor the maximum possible amount of energy during vehicle deceleration. A fuzzy logic controller is applied to fulfill the task. The control method is tested on a four in-wheel-motor drive sport utility electric vehicle model. The model is constructed and parametrized according to the specifications provided by the vehicle manufacturer. The simulation results conducted on different road surfaces, including dry, wet and icy, are introduced.

**KEY WORDS** : Fuzzy control, Anti-lock braking system, Electric vehicles, Vehicle dynamics, Vehicle safety

### NOMENCLATURE

$\omega$  : wheel angular speed, rad/s  
 $a_{ax}$  : vehicle longitudinal acceleration, m/s<sup>2</sup>  
 $p_b$  : braking pressure, bar  
 $r$  : wheel radius, m  
 $m$  : mass of the quarter vehicle, g  
 $g$  : gravitational acceleration, m/s<sup>2</sup>  
 $T_d$  : driving torque, Nm  
 $T_t$  : tire torque, Nm  
 $T_b$  : total braking torque, Nm  
 $T_{RB}$  : regenerative brake torque, Nm  
 $T_{FB}$  : friction brake torque, Nm  
 $I_w$  : inertia about the wheel rotational axis, gm<sup>2</sup>  
 $k_b$  : braking coefficient  
 $T_j$  : phase torque of motor, Nm  
 $I_j$  : phase current of motor, A  
 $\theta$  : rotor aligned position of motor, °  
 $L$  : phase bulk inductance of motor, H  
 $N$  : number of phases of motor  
 $v_{vx}$  : vehicle longitudinal velocity, m/s  
 $v_{wx}$  : wheel longitudinal velocity, m/s

$\lambda$  : wheel slip, %  
 $\mu$  : tire-road friction coefficient  
 $\mu^*$  : estimated road surface  
 $F_x$  : longitudinal force, N  
 $F_z$  : vertical force, N  
 $E_c$  : net energy consumption, kJ  
 $P_d$  : power spent on driving, W  
 $P_b$  : power recovered via regenerative braking area, W  
 $\eta_m$  : electric motor efficiency, %  
 $s$  : distance, m  
 $a_{average}$  : average deceleration, m/s<sup>2</sup>  
 $ABS_{IP}$  : ABS operation index of performance  
 $\lambda_{average}$  : average wheel slip, %  
 $\lambda_e$  : actual and optimal wheel slip difference absolute value, %  
 $P_{reg}$  : regenerated power comparing to the total power required for deceleration, %

### SUBSCRIPTS

$i$  : subscript for each wheel;  $i \in$  [front left (FL), front right (FR), rear left (RL), rear right (RR)]  
 $j$  : switched reluctance motor phase number

\*Corresponding author: e-mail: valery.vodovozov@ttu.ee

## ABBREVIATIONS

4WD	: 4 in-Wheel-motor Drive
ABS	: Antilock Braking System
ASM	: Automotive Simulation Models™
DOF	: Degree of Freedom
ESP	: Electronic Stability Program
EV	: Electric Vehicle
FLC	: Fuzzy Logic Controller
ICE	: Internal Combustion Engine
MF	: Membership Function
MISO	: Multiple Input, Single Output
PID	: Proportional-Integral-Derivative
SRM	: Switched Reluctance Motor
SUV	: Sport Utility Vehicle
UOD	: Universe of Discourse

## 1. INTRODUCTION

Modern life cannot be imagined without personal vehicles. As the cities grow bigger and business spread wider, people daily pass long distances to their work places or to meet with their business partners in other cities or even other countries. On-ground vehicles have become indispensable machines helping people in overcoming distances and saving time on transportation.

The world population increases every year and a demand for personal vehicles grows in parallel. Within only few past decades the number of internal combustion engine (ICE) cars has dramatically enlarged on the roads. It brings in this connection the biggest disadvantage of a developed industry: the risk of accidents and consequent human fatalities. Thus, a vehicle safety and driving assistance systems' improvement and development is needful. Moreover, the problems related to energy management, oil crisis, greenhouse gases, pollution and environment protection have brought a necessity to create a new type of environmental friendly transport. One of the promising alternatives are the electric vehicles (EV), where an ICE is replaced with an electric motor propulsion system (Bansal, 2005). EVs are not only less polluting, efficient and cheap to operate, but also very quiet (Dhameja, 2002).

The EV batteries' long recharging time, poor durability, weight, cost and short lifetime are causing the largest resistance to the EV mobility infrastructure development (Dhameja, 2002). The biggest drawback of the commercial EVs is their short range due to a small charge capacity.

One of the subtypes of an EV has four in-wheel-motor drives (4WD) powertrain. The technology was already available in 1900, when the great inventor and engineer Ferdinand Porsche introduced a vehicle with wheel hub motors built into steered front wheels. Unfortunately, the mass production failed due to the invention technical complexity.

With the technologies available today, the 4WD

powertrain EVs once again deserve an attention, because they turn out to be perfect candidates for future mobility. Each of the individual 4WD motors' angular velocity and torque can be directly measured. Furthermore, the electric actuator works faster than a conventional hydraulic system used nowadays in ICE vehicles. It opens an opportunity to design a very rapid, efficient and accurate algorithm to control vehicle dynamics via 4WD powertrain (Xiong and Yu, 2011).

The well-known safety systems are an antilock braking system (ABS) and an electronic stability program (ESP). The ABS avoids wheel lock and maintains vehicle steerability (Koch-Dücker and Papert, 2014). The ESP assists in vehicle stability control (Ehret, 2014). The ABS available in commercial vehicles requires a wheel slip threshold that guarantees energy efficient deceleration only on a dry asphalt surface (Koch-Dücker and Papert, 2014). Consequently, it leads to power losses on lower adhesive coefficient surfaces, because the wheel slip requirements are lower on a slippery surface than on a dry road (Doumiati *et al.*, 2013).

In EV, the negative torque from braking inertia rotates the motor in opposite to traction direction. The motor works as a generator and charges an energy storage device by converting kinetic energy created by the vehicle mass into an electric power, instead of wasting it as a heat on the brake pads or into the atmosphere (El-Garhy *et al.*, 2013; Miller, 2005). This process is known as regenerative braking or energy recuperation (Dhameja, 2002). Kinetic energy recycled from braking maneuvers increases the EV driving distance. Thus, an ABS for EVs has a benefit for safety and efficiency improvement via regenerative braking and a challenge for more complex braking control methods design.

This work's aim is to combine the torque blending technique together with a control of robust to different road surfaces ABS. The generators use maximum power as the actuators for the ABS system. The controller recognizes the road surface to maintain energy efficient and safe braking performance for a specific road. Hence, the controller recuperates maximum possible kinetic energy from braking and simultaneously supports robust to various roads vehicle safety deceleration.

The paper is organized as follows. In next Section, the related to this studies works are analyzed and the current paper contribution is discussed. The 4WD EV powertrain modelling and parameterization are introduced in Section 3. The detailed explanation of the road detection algorithm as well as the control method description are presented in Section 4. In Section 5, the control results for different road adhesions are introduced. A comparative analysis of the controller performance for electric and hydraulic actuators is also reported. The research is discussed and concluded in Sections 6 and 7, respectively.

## 2. RELATED WORKS

Many different conventional control methods were proposed for EV energy regeneration. For instance, in (Long *et al.*, 2014), the sliding mode controller (SMC) and the proportional-integral-derivative (PID) controllers were compared. There, the SMC outperformed the PID. In Ye *et al.* (2010),  $H_2$  optimal control and  $H_\infty$  robust control were combined to guarantee EV recuperation performance and stability. Those methods require very complex numerical models. Mathematical models are computationally intensive and have complex stability problems. Moreover, models are often not accurate due to approximations, uncertainty, and lack of perfect knowledge. Fuzzy logic has an advantage over conventional control techniques (e.g. PID, SMC,  $H_\infty$ ), because it does not require a complex dynamic model development. Hereupon, it has a benefit in processing and mapping ill-defined and uncertain variables. Consequently, within few last decades, a fuzzy logic controller (FLC) deserved special attention in complex, imprecise nonlinear control (Passino and Yurkovich, 1998; Reznik, 1997).

One of the first EV regenerative antiskid braking and traction control system applying FLC with the tire-road adhesive characteristic estimation was proposed in Cikanek (1994). The controller was designed for a single-axle drive EV architecture. Since then, many other rule-based approaches were proposed for regenerative braking enhancement.

An FLC was applied to control an EV ABS with optimal wheel slip for varying road surfaces (Chen *et al.*, 2010; Khatun *et al.*, 2003). In addition to robust ABS, the authors in Pusca *et al.* (2004) and Tahami *et al.* (2003) also studied an ESP regulation. Although the controller showed precise road adhesive coefficient estimation, the authors did not investigate regenerative braking and torque blending.

Vehicle stability control for a 4WD hybrid EV was stressed in Kim *et al.* (2008). The FLC compensated the yaw dynamics control and recycled kinetic energy. Nevertheless, the simulation results are limited to the yaw rate and side slip angle compensation.

Fuzzy set theory also deserved an attention in kinetic energy recuperation. The scholars in Paterson and Ramsay (1993), Peng *et al.* (2006) and Li *et al.* (2008) proposed an electric motor and friction braking torque blending based on FLC. Furthermore, in Nian *et al.* (2014), the FLC and PID control were combined to distribute the mechanical and electrical braking forces. Even so, the authors neither consider braking torque between rear and front wheels distribution nor ABS control design.

On the contrary, in Zhang *et al.* (2016), Jianyao *et al.* (2015) and Xu *et al.* (2011), the authors examine both EV torque blending and braking force allocation between EV wheels. Nevertheless, the slip control and ABS safety investigation were not presented. Further, in Zhang *et al.* (2016), the researchers demonstrated effectiveness and

strong robustness in EV energy recuperation of the Takagi-Sugeno fuzzy SMC over conventional PID and Mamdani's type FLC. The results were verified in simulation and experimentation. Though, vehicle safety was not stressed. Optimal braking torque distribution with regenerative capability was examined on vehicle stability for a single line change in Kim *et al.* (2007) but an ABS controller was not designed there.

A regenerative ABS controller was built by combining FLC and SMC in Guo *et al.* (2014). The intelligent regulator requires a reference slip threshold, which likewise in modern industrial vehicles lead to energy losses on other than dry road surfaces.

Fuzzy set theory is also widely used as an estimator of vehicle states, for instance, linear velocity, battery performance, vehicle side slip angle, tire-road interaction parameters (Ivanov, 2015) and tire forces (Acosta and Kanarachos, 2017). Tire-road surface estimation with ABS control based on FLC was designed in Layne *et al.* (1993). The goal of the controllers was to keep the slip ratio to 20 % despite road friction characteristics.

In Paul *et al.* (2016), the researchers went further and offered, first, to estimate the road surface with fuzzy logic, and therefore to provide a braking torque distribution. The controller was tested on a single motor EV model. The wheel slip and vehicle steerability were not studied on different road surfaces, because the controller is designed with a fixed slip value.

Advanced FLCs for road type detection and thus optimal braking pressure generation were designed in Ivanov *et al.* (2006), Aly (2010) and Castillo *et al.* (2016). Although the experimental results showed perfect performance on varying road surfaces, the control algorithms are very complex. What is more, the FLCs were not tested on EV decoupled braking system, but only on conventional hydraulic brakes.

Other efficient techniques for vehicle states estimation were proposed before. Kalman filtering is widely used in vehicle longitudinal force estimation (Doumiati *et al.*, 2013). Lyapunov stability theory (Xia *et al.*, 2016), a combination of stiffness based estimation and least squares (Han *et al.*, 2015) and a combination of nonlinear Lipschitz observer and modified super-twisting algorithm (Rath *et al.*, 2015) were designed for road friction coefficient estimation. Those methods, however, require complicated nonlinear models or additional sensors, what multiply system's cost and complexity.

In this paper, a simple method for road surface recognition is presented. The estimation is based only on vehicle body maximum deceleration rate. The proposed technique is fulfilled with FLC and, unlike other methods mentioned in this Section, requires neither complicated mathematical model nor additional sensors, because the longitudinal acceleration measurement sensors are already in use in modern vehicles (Zabler, 2014). What is more, the FLC is able to compensate the lack of knowledge about

many other road surfaces that are not preliminary considered.

Previously, the road surface estimation strategy and ABS control were tested on hydraulic brake model (Aksjonov *et al.*, 2016). On the contrary, in this paper, the FLCs are designed for both electric and hydraulic actuators that are interacted together. The proposed controllers' task is to maximize energy recuperation from the vehicle deceleration maneuver. Hereupon, the same FLCs ensure the robustness to different road surfaces by maintaining an optimal wheel slip during the whole braking process and by avoiding a reference slip control. Therefore, an energy efficient torque blending and road surface estimation are implemented in the same controller without complex vehicle models.

In short, the following problems are solved:

- road surface detection from vehicle body longitudinal acceleration with vehicle energy efficient deceleration due to optimal wheel slip control and maximum energy regeneration capability using fuzzy set theory;
- controller implementation on ten degree of freedom (10DOF) 4WD EV model;
- control method robustness to different road surfaces demonstration and comparison with only friction and braking with blocked wheels.

### 3. VEHICLE MODELLING

#### 3.1. Dynamics of a Braked Wheel

The 3DOF single-wheel vehicle model for the EV longitudinal motion (Figure 1) is described by the following system of equations (Kiencke and Nielsen, 2005):

$$\begin{cases} I_w \cdot \dot{\omega} = T_d - T_t - T_b \\ F_x = m \cdot \dot{v}_{wx} \\ F_z = m \cdot g \end{cases} \quad (1)$$

where the tire torque  $T_t$  is expressed as:

$$T_t = r \cdot F_x \quad (2)$$

Due to its small influence comparing to the braking and friction forces during braking maneuvers, other forces, like aerodynamic drag and lateral wind force, are neglected.

A distinctive feature of the 4WD EV: total braking torque  $T_b$  is a sum of regenerative brake  $T_{RB}$  and friction brake  $T_{FB}$  torques:

$$T_b = T_{RB} + T_{FB} \quad (3)$$

where the friction brake torque is determined as (Kiencke and Nielsen, 2005):

$$T_{FB} = r \cdot k_b \cdot p_b \quad (4)$$

In turn, the friction braking coefficient  $k_b$  depends on brake disc friction area, mechanical efficiency of brake components, and braking factor. Tire deformation (change of the wheel radius  $r$ ) due to its small impact is neglected. Thus, both variables  $r$  and  $k_b$  are assumed as constants. The

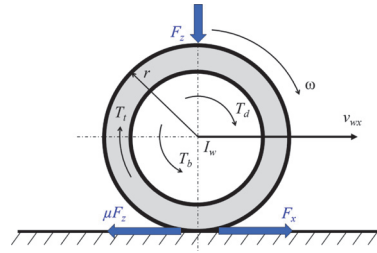


Figure 1. Vehicle single-wheel model of a braked wheel schematic drawing.

friction braking torque changes proportionally to the brake pressure  $p_b$ .

Finally, in case of a saturated phase, a torque  $T_j$  equation for switched reluctance motor (SRM) can be given as (Ehsani *et al.*, 2005):

$$T_j = \int_0^{I_j} \frac{\partial L(\theta, I_j)}{\partial \theta} I_j dI_j \quad (5)$$

The output torque of an SRM in traction or regenerative modes  $T_{d/RS}$  is the summation of torques in all the phases (Ehsani *et al.*, 2005):

$$T_{d/RS} = \sum_{j=1}^N T_j \quad (6)$$

The input to the SRM drive is direct current voltage. However, a converter controls phase current  $I_j$  flow. Therefore, control of the phase torque depends directly on  $I_j$  (Ehsani *et al.*, 2005).

In modern vehicles, the torque of the vehicle wheel cannot be measured, but only estimated. On the contrary, both  $p_b$  and  $I_j$  can be measured by appropriate sensors (Zabler, 2014). In this paper, the wheel torques are controlled by influencing on  $p_b$  and  $I_j$ . The variables serve as the controller correcting variables. Nevertheless, they will be directly expressed as the relevant torques.

For the braking maneuver the longitudinal wheel slip  $\lambda$  is expressed as (Kiencke and Nielsen, 2005):

$$\lambda = \frac{v_{wx} - v_{vwx}}{v_{vwx}} \cdot 100 \% \quad (7)$$

where the longitudinal wheel velocity  $v_{wx}$  is:

$$v_{wx} = r \cdot \omega \quad (8)$$

Tire deformation depends on a normal force  $F_z$  (Pacejka, 2006). The wheel radius  $r$  is assumed as constant.

Tire-road adhesive coefficient  $\mu$  is determined as a ratio between longitudinal  $F_x$  and vertical  $F_z$  forces applied on a wheel (Kiencke and Nielsen, 2005):

$$\mu = \frac{F_x}{F_z} \quad (9)$$

From the single-wheel dynamics, Equation (1),  $\mu$  can be simplified as:

$$\mu = \frac{F_x}{F_z} = \frac{m \cdot \dot{v}_{vx}}{m \cdot g} = \frac{\dot{v}_{vx}}{g} \quad (10)$$

Two main variables, the vehicle longitudinal acceleration  $a_{vx}$  and the wheel angular velocity  $\omega_i$ , serve as the controller inputs. The input signals are measured by the available on board sensors (Zabler, 2014). In this paper,  $\mu$  is connected to maximum vehicle acceleration rate  $a_{vx}$  (Equation (10)) for road surface recognition. The detected road surface is defined as  $\mu^*$ .

An overall motor power  $P_{d/b}$  with motor efficiency  $\eta_m$  expended on driving or braking is as follows (Ehsani *et al.*, 2005):

$$P_{d/b} = \eta_m \cdot T_{d/b} \cdot \omega_i \quad (11)$$

Electric motor net energy consumption  $E_C$  is described by an equation of power spent on driving and recycled during the regenerative braking, if the last one is applied (Ehsani *et al.*, 2005):

$$E_C = \int_{\text{traction}} P_d dt + \int_{\text{braking}} P_b dt \quad (12)$$

The index of performance  $ABS_{ip}$  is introduced to evaluate the effectiveness of the ABS control. It describes the ratio between vehicle deceleration with and without the applied controller:

$$ABS_{ip} = \frac{a_{ABS}}{a_{skid}} \quad (13)$$

### 3.2. Vehicle Modelling and Parametrization

Full 10DOF vehicle mathematical model Automotive Simulation Models™ (ASM) 2014-B (64-bit) is supplied by the dSPACE® GmbH (Paderborn, Germany). The ASM allow a vehicle model parameterization according to the user's needs. The ASM interaction with the MATLAB®/ Simulink® (Natick, MA, USA) R2013b (64 Bit) allows removing or substitution of the vehicle component models, if necessary. Furthermore, the control algorithm can be easily designed and simulated in MATLAB® environment without any supplementary software requirements. A multibody vehicle model simulation is accompanied with a visual interface, what help user to understand vehicle behavior in details. The EV and its powertrain system configurations are provided by a vehicle manufacturer and

Table 1. Electric vehicle configurations.

Components	Parameters	Description
Vehicle	Type	Sport utility vehicle
	Vehicle overall mass	2117 kg
	Front axle suspension spring constant stiffness	26700 N/m
	Rear axle suspension spring constant stiffness	23000 N/m
	Front axle suspension stabilizer stiffness	2851.4 N/m
	Rear axle suspension stabilizer stiffness	6833.5 N/m
	Tire type	235/55 R19
	Tire numerical model	Pacejka's Magic Formula
Electric motor	Type	Switched reluctance
	Peak torque at 800 V (+/- 10 %)	200 Nm (30 sec)
	Peak power at 800 V (+/- 10 %)	100 kW (30 sec)
	Nominal torque at 800 V (+/- 10 %)	125 Nm
	Nominal power at 800 V (+/- 10 %)	42 kW
	Maximum speed	1500 rpm
	Motor inertia (without gearbox)	21087 kgmm <sup>2</sup>
	Mass	50 kg
	Motor dimension	215 × 265 mm
	Liquid cooling system	Water 10 l/min, 50 °C max inlet
Transmission (in-wheel motor)	Type	Two stage reducer with helical gear and half-shaft
	Overall motor-gear ratio	1:10.5
	Estimated torsion stiffness of half-shaft	6500 Nm/rad
Battery pack	Voltage	400 V DC
	Peak power	160 kW
	Nominal power	80 kW
	Mass	274 kg
	Volume	0.235 m <sup>3</sup>
	Energy capacity	15 Ah (6 kWh)
	Module type	12 lithium-titanate oxide anode cells
	Modules number	15

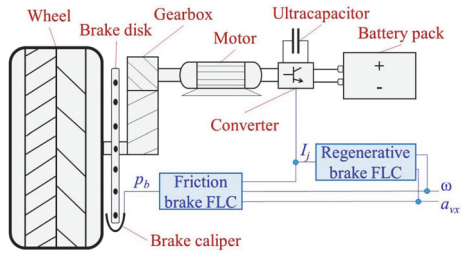


Figure 2. In-wheel motor architecture scheme: black – hardware; blue – software.

presented in Table 1.

The studied EV model was parametrized as a sport utility vehicle (SUV). Its total body weight is 2117 kg. Each 4WD powertrain motor is connected to the wheel through a gearbox and a half-shaft transmission. In Figure 2, a simplified in-wheel motor architecture and a controller are introduced. The EV has a decoupled electro-hydraulic brake system. Friction and electric motor brakes impacting on braking pressure and the motor phase current can be controlled independently.

Vehicle deceleration is a very fast process. In regenerative braking, huge amount of energy is released within a very short time. Most of the EV batteries are not able to save this energy. Despite, ultracapacitors are characterized by very high power, excellent life cycle, but represent a low-capacity energy storage. Consequently, most of the modern EVs are also equipped with ultracapacitors used in regenerative braking for fast energy storing (Bansal, 2005). The power electronics losses are neglected in the model.

Lithium-titanate battery is used as an energy storage device. Its maximum energy capacity is 6 kWh and a peak power reaches 160 kW. Wheels are equipped with a SRM. The SRM's maximum torque that can be applied during 30 seconds at 800 V voltage in both motor and generator modes is 200 Nm. The torque versus angular speed relation for the studied SRM is shown in Figure 3. Taking into consideration the in-wheel motor overall transmission gear ratio, the maximum torque applied directly to the wheel reaches 2100 Nm (Savitski *et al.*, 2016).

A first-order transfer function describes the electric motor dynamics as follows (Savitski *et al.*, 2014, 2016):

$$\frac{T_d^{\text{act}}}{T_d^{\text{ref}}} = \frac{1}{0,0022s + 1} e^{-0,002s} \quad (14)$$

whereas the motor transfer function in generator mode while braking is as follows:

$$\frac{T_b^{\text{act}}}{T_b^{\text{ref}}} = \frac{1}{0,02s + 1} e^{-0,025s} \quad (15)$$

The tires are modelled with the Pacejka's Magic Formula (Pacejka, 2006). Before designing the controller, the tire characteristics were studied. To this regard, the

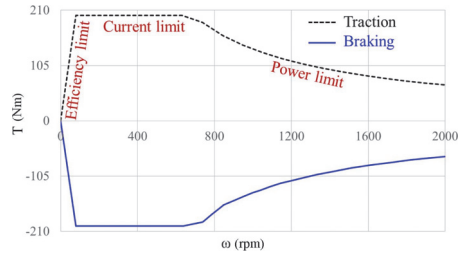


Figure 3. Torque – rotational speed characteristic for SRM in motoring and regeneration modes.

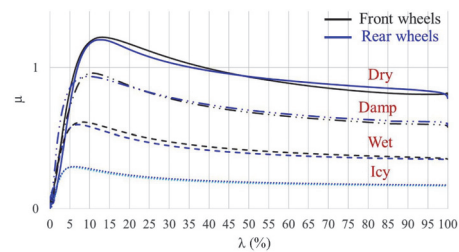


Figure 4. Tire-road friction – slip curves of the studied tire model for various road surfaces using Magic Formula model (Pacejka, 2006).

vehicle model was simulated on dry, damp, wet, and icy road surfaces. An ABS control was not applied. The vehicle decelerates under heavy braking conditions with locked wheels.

The tire-road friction  $\mu$  versus the wheel slip  $\lambda$  are plotted (Figure 4) to specify the stable working range for the given tire. Since the meaning of the vehicle body deceleration curves on different road surfaces is the same as the  $\mu - \lambda$  curves, they are not introduced in this paper. Only the straight road braking maneuver is studied, a slip angle effect on tire dynamics is omitted.

Tire dynamics have an exponential behavior (Figure 4). The optimal slip lays on the curve's peak, where the adhesive coefficient has its maximum rate. The plot region from 0 to optimal slip value is called stable for each road surface, where the vehicle maintains steerability. The rest of the curve from optimal to 100 % slip is called unstable

Table 2. Optimal wheel slip values and vehicle body maximum deceleration rate for different road surfaces.

	$\lambda$ (%)	Dry road	Damp road	Wet road	Icy road
Front wheels		13.18	10.66	8.34	6.14
Rear wheels		12.31	9.54	7.12	5.82
Peak deceleration (m/s <sup>2</sup> )		11.78	8.79	5.89	2.96

zone, where the vehicle lateral control (steerability) is impossible. Moreover, the vehicle maximum deceleration on a given road surface is achieved only with the optimal wheel slip. Braking with the slip ratios higher or lower than the optimum value leads to braking force reduction (Rajamani, 2012).

Although the vehicle velocity and tire models are the same for the front and rear wheels, the  $\mu - \lambda$  curves are slightly different (Figure 4). This can be explained by unequal body mass and, therefore, normal force distribution between the front and rear wheels (Rajamani, 2012). Vehicle vertical load has an impact on a tire dynamic behavior (Pacejka, 2006), because friction coefficient depends on a normal force, Equation (9).

Each road surface for the front and rear wheels of the EV has its own optimal slip. The optimal value maintenance leads to the most effective and energy efficient braking performance. Due to the forces balance, the vehicle decelerates as fast as feasible at the same time presuming the lateral control (Koch-Dücker and Papert, 2014). With the reference to the plots in Figure 4, the optimal slip values are concluded in Table 2. The peak vehicle deceleration values on different roads are also introduced in Table 2. The data are essential details for the control method design described in next Section.

#### 4. CONTROL METHOD

##### 4.1. Control Method Description

Regenerative ABS control algorithm has several requirements: (i) fast vehicle deceleration, (ii) vehicle steerability preservation, (iii) maximum energy recuperation rate. First two requirements are fulfilled with the wheel slip control. Efficiency of the ABS can be dramatically improved by holding an optimal wheel slip for a given tire on different road surfaces. The third requirement is satisfied by braking using the torque generated by an SRM only. This torque may not be enough to preserve the required slip and fast vehicle deceleration. Hence, the controller must involve a friction braking system in series while using the electric motor as a generator.

In this work, an improvement of ABS performance is proposed for the 4WD EV by keeping the wheel slip on its optimal level for various roads. For this, the algorithm uses vehicle body longitudinal deceleration to comprehend which kind of road is behind the tires. Additionally, the controller employs the electric motor for energy recuperation on its maximum power and therefore recycles as much energy as possible.

The regenerative-friction decoupled ABS control block scheme for a single wheel is presented in Figure 5. The idea is very simple: the controller uses electric motor torque and retains vehicle deceleration with an optimal slip ratio for a given road. The mechanical friction brake system is activated only when the generator's torque is not enough to maintain the optimal slip. In fact, the controlled

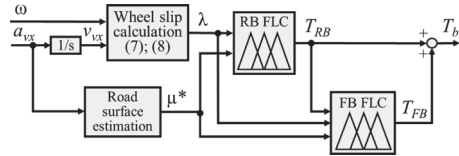


Figure 5. Single wheel controller block scheme: RB FLC – regenerative braking fuzzy logic controller; FB FLC – friction braking fuzzy logic controller; 1/s – integrational operation.

parameters are phase current for the regenerative brakes and the brake caliper pressure for the friction brakes. For better understanding, the outputs are expressed directly as appropriate torques.

Displacement of a braking pedal activates the ABS controller. The safety feature is deactivated when the braking pedal is released or vehicle velocity is smaller than 8 km/h, because a distance travelled with the locked wheels from 8 km/h is not critical for vehicle safety (Koch-Dücker and Papert, 2014).

An integrated signal transmitted from a vehicle longitudinal acceleration  $a_{vx}$  sensor and a signal from a wheel speed  $\omega_i$  sensor are used to estimate a tire slip for each wheel  $\lambda_i$ . The same estimation approach is used in modern vehicles (Koch-Dücker and Papert, 2014). The method is assumed to be enough accurate as the sensors offset, noise, and integration drift have no dramatic influence on  $\lambda$  calculation. A side slip influence can be also neglected, because only straight braking maneuver is performed (Pacejka, 2006).

The  $a_{vx}$  cannot provide the peak friction coefficient directly (Figure 4). However, if the maximum possible acceleration on a given road surface is known, the information may be utilized to understand the road surface  $\mu^*$  and to specify the optimal wheel slip accordingly (Table 2).

In heavy braking maneuver, the driver requests a peak braking torque by slamming on a brake pedal. During the first time lapse of the braking maneuver, the ABS is not yet

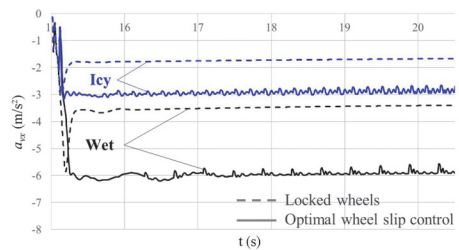


Figure 6. Vehicle longitudinal deceleration with locked wheels and with optimal slip control on wet and icy road surfaces.

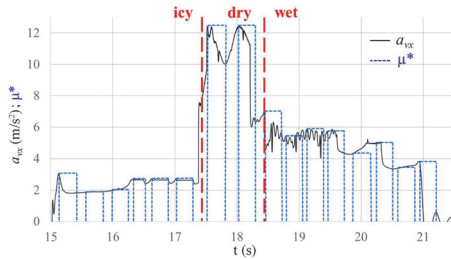


Figure 7. Example of road surface estimation in braking on varying road surfaces from icy, dry to wet profiles.

activated, and this interval is used for maximum  $a_{vx}$  detection. Therefore, the peak measured deceleration rate is referred to an appropriate road surface from Table 2. As soon as the road is estimated, the controller identifies an optimal wheel slip for a given road surface (Table 2), and the ABS control is running. A road surface detection example for wet and icy roads is presented in Figure 6. The controller detects a maximum deceleration rate and tries to maintain it during the whole braking maneuver by holding an optimal wheel slip.

Apart from this, to understand if the road surface has changed during the maneuver, the value of maximum  $a_{vx}$  resets to zero every 0.3 seconds. While  $\mu^*$  resets, a top braking torque is requested again. While the total torque grows, the algorithm records the new peak of  $a_{vx}$ . Thus, if the road surface has not been changed, approximately the same deceleration peak as in the previous step is fixed. However, if the road surface is different from the one in previous step, a new maximum value of  $a_{vx}$  is noted.

Figure 7 illustrates the principle of the proposed technique for braking performance. The black line represents vehicle  $a_{vx}$ . The blue dotted line indicates estimated road surface  $\mu^*$  for varying roads from icy to dry and to wet. More information about the controller performance on varying road surfaces can be found in Aksjonov *et al.* (2016). In next Section, where the simulation results are presented, it can be seen that the wheel slip do not rise significantly while the  $\mu^*$  resets. Consequently, the road surface estimation method has no effect on the vehicle lateral control maintenance.

To guarantee controller robustness to other roads, it is not enough to have the information about  $\lambda$  and  $\mu^*$  exclusively on dry, wet and icy surfaces. In reality, the drivers deal with a variety of different environment conditions. For instance, the optimal slips for dry concrete or snow roads are not the same as for the dry or icy surfaces, respectively (Doumiati *et al.*, 2013). Besides, the tire forces for the worn and new tire on the same road have different behavior (Pacejka, 2006).

In our case, it is not necessary to collect a huge amount of data for different road surfaces. It is enough to study the most common ones (e.g. dry, wet, icy). Based on their

tendency, the controller can be designed as an artificial decision making system using fuzzy logic. On the contrary, the conventional control applications are not suitable for nonlinear plant control with uncertain knowledge and measurement or without mathematical model (Passino and Yurkovich, 1998; Reznik, 1997).

The fuzzy set theory allows to cover the unknown workspace of the road surfaces and their optimal slip rates (Figures 4). For example, if the road surface is neither wet nor icy, but has a tire behavior somewhere in the middle, it is not efficient to maintain optimal slip exactly for wet or for icy roads. In this case, the amount of braking torque must be applied to hold the optimal slip value also somewhere between wet and icy surfaces.

The FLC, rather than conventional controllers, is capable to deal with the type of information that is partly true and partly false to any degree at the same time (partly icy and partly wet). It is easily understandable to human due to its attempt to model humans' sense of words, decision making and common sense (Negnevitsky, 2005). Its linguistic reasoning may be applied as follows: **IF** a vehicle peak deceleration rate is somewhere between wet and icy road, **THEN** hold an optimal wheels slip value somewhere between wet and icy road.

In this work, the FLC is chosen due to its ability to discern vague information about other possible road surfaces. The FLC is designed for both the friction and the regenerative ABS controllers with wheel slip  $\lambda$  and estimated road surface  $\mu^*$  as the input signals. The FLC design is described below.

#### 4.2. Fuzzy Logic Controller Design

An FLC may have multiple inputs and outputs. The input numerical signals are traditionally called "crisp" and translated into the fuzzy sets through the fuzzification process. The fuzzy set, in its turn, is a pair consisting of an element in universe of discourse (UOD) and a degree of membership function (MF). The rule-base block stores a

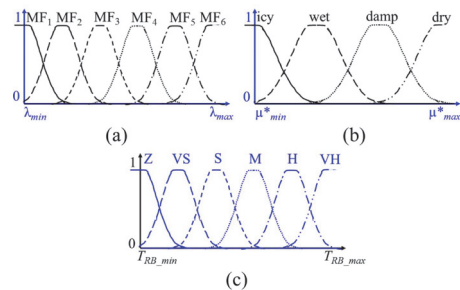


Figure 8. Regenerative braking fuzzy logic controller MFs: (a)  $\lambda$  input; (b)  $\mu^*$  input; (c)  $T_{RB}$  output with a set of MF values {zero (Z), very small (VS), small (S), medium (M), high (H), very high (VH)}.

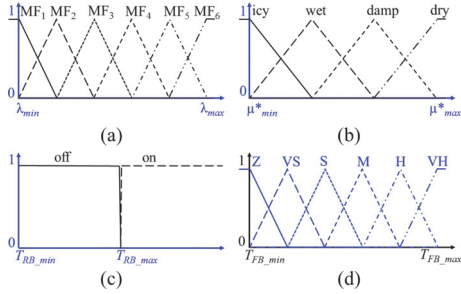


Figure 9. Friction braking FLC MFs: (a)  $\lambda$  input; (b)  $\mu^*$  input; (c)  $T_{RB}$  input; (d)  $T_{FB}$  output with a set of MF values {zero (Z), very small (VS), small (S), medium (M), high (H), very high (VH)}.

linguistic knowledge, which is used to convert the fuzzy input sets into the fuzzy output sets by the inference engine. The fuzzy set outputs are then turned back to the real numbers via defuzzification.

An electric motor is faster than a hydraulic actuator. Thus, for the electric motor FLC, Gaussian (exponential) shape MFs are applied. The regenerative braking control variables MFs are presented in Figure 8. The MFs overlap between each other over the whole UOD. A symmetric dispersion guarantees equal sensitivity of the controllers. The triangular MFs chosen for the mechanical system control are qualified by fast response because of their narrow shape (Figure 9).

In the FLC design, the input and output variables of the controllers must have a closed frontier  $[min, max]$  of the UOD. For the  $\lambda$  inputs the bounds for the front and rear wheels are chosen according to the tire stable region (Figure 4). This approach is valid because it affords an optimal slip control for almost every studied road surface. The road friction  $\mu^*$  UOD limitations obtained during the vehicle parameterization are described in Section 3.

The  $\mu^*$  input has 4 MFs (Figures 8 (b) and 9 (b)) with UOD restriction narrowed in [3, 12]. An additional input of the friction braking controller acquires an activation signal, which has only 2 MFs (Figure 9 (c)). This input turns on the friction braking system, when the regenerative braking FLC output signal reaches its maximum value.

The maximum pressure of the friction brake and the maximum torque of the generator are known from the EV datasheet. Thus, the UODs of the output variables lay between  $[0, 151]$  and  $[0, 200]$ , correspondingly. Each output variable has 6 MFs (Figures 8 (c) and 9 (d)).

The controllers have a multiple input, single output (MISO) structure. Taken from (Passino and Yurkovich, 1998) MISO pattern of the FLC linguistic rules in modus ponens form (**If-Then**) for the regenerative ABS is as follows:

Table 3. Fuzzy regenerative ABS control rule-base.

$\mu^*$ \ $\lambda$	MF <sub>1</sub>	MF <sub>2</sub>	MF <sub>3</sub>	MF <sub>4</sub>	MF <sub>5</sub>	MF <sub>6</sub>
Icy	VS	Z	Z	Z	Z	Z
Wet	M	S	VS	Z	Z	Z
Damp	VH	H	M	S	VS	Z
Dry	VH	VH	VH	H	S	Z

$$\text{If } u_1 \text{ is } A_1^i \text{ and } u_2 \text{ is } A_2^k \text{ Then } y_q \text{ is } B_q^p \quad (16)$$

where  $u_1$  and  $u_2$  denote the FLC inputs  $\lambda$  and  $\mu^*$ , respectively;  $y_q$  denotes the controller output torque;  $A_1^i$  and  $A_2^k$  relate to the  $j^{\text{th}}$  and  $k^{\text{th}}$  linguistic value related to wheel slip and road surface, respectively; and  $B_q^p$  is the linguistic value of the output torque.

Table 3 shows the linguistic relation between the controller inputs and output. The rules are true for both the friction and the regenerative braking FLCs. In total, 24 rules are used for regenerative braking control, while 25 rules are utilized for mechanical friction brake. A controller activation signal represents an additional rule in the friction actuator. The Mamdani's inference mechanism is applied.

The rule-base is designed to keep an optimal wheel slip by providing a necessary braking torque on every road surface. When the slip is higher than its optimal value, the torque diminishes. When the slip value is lower, the torque increases. For example, for the wet road the optimal wheel slip is between 7 ~ 8 %, which is somewhere between MF<sub>2</sub> and MF<sub>3</sub> depending on the front or rear wheels. A preliminary study (Section 3) has shown that to hold this value, approximately 1300 Nm and 750 Nm torques are required for front and rear wheels, respectively. The torque corresponds to “small (S)” and “very small (VS)” output MFs. When the slip value is higher, the torque decreases. When the slip value is lower, the torque rises. The same logic in linguistic rules is true for other road surfaces.

Fuzzy reasoning ends up with defuzzification procedure. The decoupled ABS controller defuzzification is calculated using the center-of-gravity approach. This method is

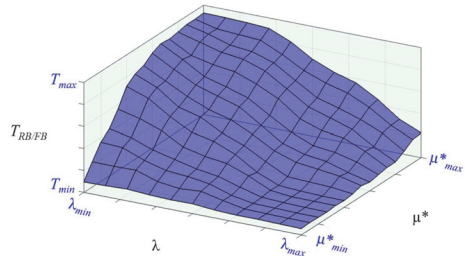


Figure 10. Regenerative ABS FLC surface.

Table 4. Fuzzy logic controller design outlook.

Parameter	Regenerative braking	Friction braking
Structure	MISO	MISO
Crisp input	Slip $\lambda$ (6 MFs) Road condition $\mu^*$ (4 MFs)	Slip $\lambda$ (6 MFs) Road condition $\mu^*$ (4 MFs) Regenerative brake torque $T_{RB}$ (2 MFs)
Crisp output	Regenerative brake torque $T_{RB}$ (6 MFs)	Friction brake torque $T_{FB}$ (6 MFs)
Fuzzy conjunction	AND = $\min(\lambda, \mu^*)$	AND = $\min(\lambda, \mu^*, T_{RB})$
MFs	Gaussian Symmetric	Linear Symmetric
Inference method	Mamdani's	Mamdani's
Rule-base	24 Modus Ponens	25 Modus Ponens
Implication operation	$\min(T_{RB})$	$\min(T_{FB})$
Aggregation method	$\max(T_{RB})$	$\max(T_{FB})$
Defuzzification	Geometric centre	Geometric centre

chosen based on the authors' experience and good continuity and plausibility. The three-dimensional surface of the designed FLC is expressed in Figure 10.

Each of the 4WDs is controlled independently. Altogether, four controllers are designed for the regenerative braking ABS: front and rear wheels regenerative braking, front and rear wheels friction braking FLCs. The outlook of the designed for the regenerative and friction braking ABS FLCs is summarized in Table 4.

## 5. RESULTS

Simulation results conducted on a straight road are presented in this section. The vehicle is accelerated to 100 km/h and then the heavy braking is applied. The results are introduced as a comparison between decoupled regenerative ABS control, only mechanical friction ABS control, and pure wheel blocking deceleration. Different road surfaces (i.e. dry, wet, icy) are examined to study the control method ability to maintain an optimal wheel slip ratio.

The regenerative ABS control simulation results on the straight dry asphalt road are studied in this section in details (Figure 11). The road surface estimation is introduced in Figure 11 (a). At around 15.1 seconds, the controller measures the first peak of  $a_{xx}$ . This value is almost 12 m/s<sup>2</sup>. Referring to Table 2 (peak  $a_{xx}$  for dry road is 11.78 m/s<sup>2</sup>), the controller reveals vehicle deceleration on a dry road. Herewith, the optimal slip value for each wheel for a dry asphalt is detected (Table 2). The road surface estimation procedure continues upon the fixed frequency until the ABS deactivation.

The wheels and vehicle speed curves are viewed in Figure 11 (b). At the time about 17.2 seconds the ABS control is turned off, because the vehicle speed reaches 8 km/h. The road estimation also stops. The maximum mechanical braking pressure is then applied and the wheels

are immediately locked for an insignificantly short period.

The wheel slip plots are shown in Figure 11 (c). The difference in the slip value for the front and the rear wheels can be easily recognized. Optimal slip deceleration on the dry surface is maintained during the whole braking process, because the road surface is uniform.

Braking torque curves for front and rear wheels are introduced in Figures 11 (d) and (e), accordingly. Both the regenerative and mechanical friction torque curves are shown in the same charts. At 15.1 seconds, the total braking torque (a sum of regenerative and mechanical torques) on both wheels is maximum, because the controller measures peak vehicle deceleration, and the ABS is not yet turned on.

For the front wheels, the torque generated by the SRMs is not enough to retain the optimal wheel slip value. As a result, the controller requests additional torque from the mechanical brakes to maintain optimal slip deceleration (Figure 11 (c)). Both regenerative and friction brakes work simultaneously. However, the electric motors do not supply constant torque within the whole braking maneuver. In around 16.7 seconds, the generators due to their efficiency limit (Figure 3) diminish the torque and the recuperation energy decreases. Contrariwise, the friction braking pressure rises to continue maintaining optimal wheel slip.

For the rear wheels, the mechanical friction braking torque is not actuated, because the SRM's one is enough to retain the optimal slip for the rear wheels on a dry road. Likewise, for the front wheels, the motor stops recycling kinetic energy on low speeds due to the SRM characteristics. Therefore, with low wheel velocities, the friction brakes are also activated.

An SRM power dissipation is performed in Figure 11 (f). The negative amount of power shown is the energy recuperated during the vehicle deceleration for only one rear or front wheel. The power saved by the front wheel is

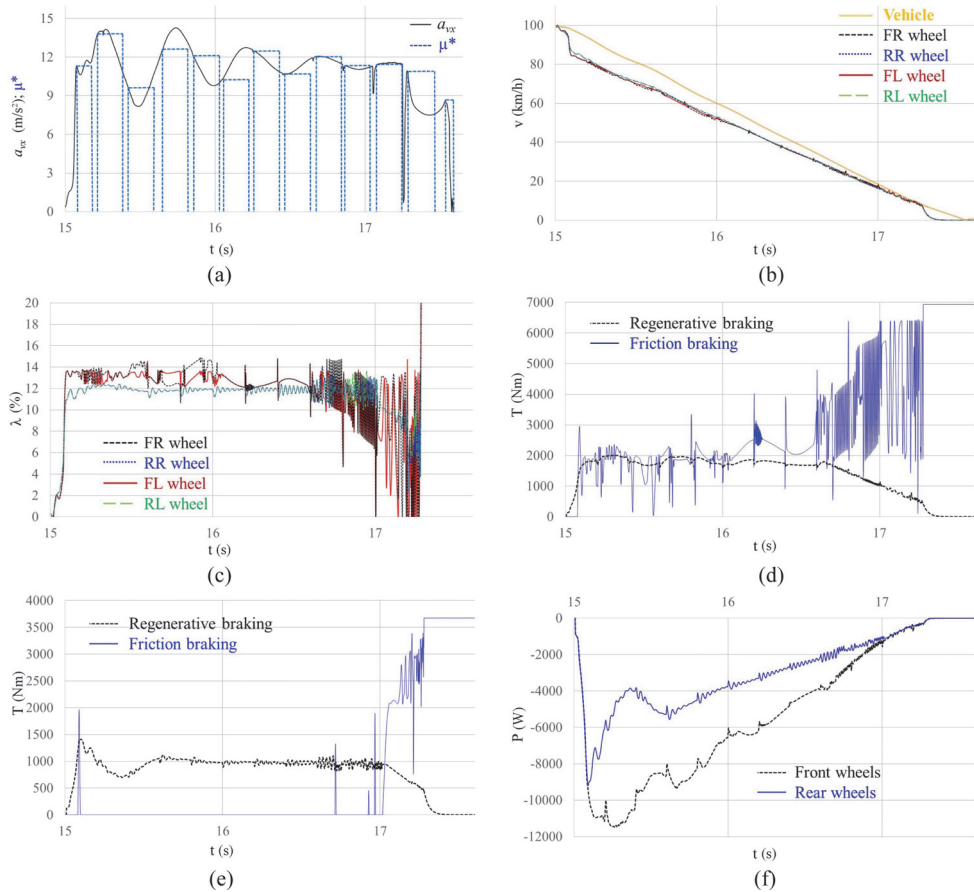


Figure 11. Regenerative braking on a straight dry asphalt road surface: (a) Road surface estimation; (b) Velocity curves; (c) Wheel longitudinal slip curves; (d) Front wheels braking torque curves; (e) Rear wheels braking torque curves; (f) Power dissipation curves.

greater than the one by the rear wheel.

A comparison between regenerative strategy and only friction braking on different road surfaces, including icy, wet and dry is shown in Table 5. The friction braking is also designed to retain the optimal wheel slip. For the dry road, the front wheels (9 %) do not recover as much energy as the rear wheels (6 %). This is due to the higher overall torque demand for required wheel slip braking. The rest of the necessary torque for front wheels is compensated by the friction brake, which is almost as high as the generator's one (Figure 11 (d)). Accordingly, the effectiveness of energy regeneration on the dry surface is not exalted as, for instance, braking on a wet or icy surfaces, where only motor torque is enough to decelerate the car with the optimal wheel slip.

For the icy and wet roads, front and rear wheels

recuperation is equal, because only the SRM is applied to stop the vehicle. Hence, the brake pads wear is minimum and the brakes particle emission is also belittled. Each wheel saves around 10 % of the whole energy spent on transport deceleration. Eventually, the control method maintains an optimal slip ratio for each studied road surface individually, what promises robust and energy efficient vehicle deceleration and lateral dynamics control preservation.

In modern vehicles, the controllers keep the slip around 20 %. This threshold is optimal individually for a dry asphalt surface. An optimal slip for icy road is usually more than two times smaller (Figure 4) and the threshold of 20 % consequently leads to more than 50 % energy losses. With the reference slip control, the energy losses are also true for other roads, like wet, snow or damp. As with the

Table 5. ABS braking performance comparison on different road surfaces.

Road	Criterion	Type	$s$ (m)	$a_{\text{average}}$ ( $\text{m/s}^2$ )	ABS <sub>IP</sub>	$i$	$\lambda_{\text{average}}$ (%)	$\lambda_e$ (%)	$P_{\text{reg}}$ (%)	$E_c$ (kJ)
Dry	Regenerative brake	32.99	- 11.40	1.50	FL	11.79	1.39	6.24	27.19	
					FR	11.79	1.39	6.10	27.19	
					RL	11.32	0.99	9.25	32.83	
					RR	11.32	0.99	9.26	32.83	
	Friction brake	33.15	- 11.37	1.49	FL	11.53	1.65	0	40.31	
					FR	11.52	1.65	0	40.31	
					RL	10.87	1.44	0	40.31	
					RR	10.94	1.37	0	40.31	
	Pure wheel blocking	51.30	- 7.62	-	FL	100	-	0	40.31	
					FR	100	-	0	40.31	
					RL	100	-	0	40.31	
					RR	100	-	0	40.31	
Wet	Regenerative brake	64.48	- 5.92	1.93	FL	8.70	0.36	9.47	22.57	
					FR	8.70	0.36	9.47	22.57	
					RL	8.13	1.01	9.52	29.45	
					RR	8.13	1.01	9.52	28.82	
	Friction brake	66.15	- 5.83	1.90	FL	9.04	0.70	0	40.31	
					FR	9.03	0.69	0	40.31	
					RL	8.51	1.39	0	40.31	
					RR	8.51	1.39	0	40.31	
	Pure wheel blocking	110.04	- 3.07	-	FL	100	-	0	40.31	
					FR	100	-	0	40.31	
					RL	100	-	0	40.31	
					RR	100	-	0	40.31	
Icy	Regenerative brake	130.97	- 2.85	1.74	FL	6.28	0.14	10.27	24.14	
					FR	6.28	0.14	10.27	24.14	
					RL	5.82	0	9.75	27.36	
					RR	5.82	0	9.75	27.36	
	Friction brake	132.29	- 2.80	1.70	FL	6.43	0.29	0	40.31	
					FR	6.43	0.29	0	40.31	
					RL	5.58	0.24	0	40.31	
					RR	5.59	0.23	0	40.31	
	Pure wheel blocking	226.03	- 1.64	-	FL	100	-	0	40.31	
					FR	100	-	0	40.31	
					RL	100	-	0	40.31	
					RR	100	-	0	40.31	

proposed control method, a wheel slip deceleration optimal for varying road surfaces guarantees an improvement of

energy efficiency. The studied in this paper decoupled regenerative and friction braking ABS FLC distributes

torque between 4WD powertrain wheels to maintain an optimal wheel slip for every road surface.

However, the average slip values are different, when comparing regenerative and friction brakes. The difference between theoretical (Table 2) and calculated during the simulation experiment slip  $\lambda_c$  for each wheel is presented in Table 5. The smaller the difference, the higher the accuracy in slip control is accomplished.

Although the controllers for electric and hydraulic systems are identical, the regenerative ABS FLC holds the wheel slip values closer to the optimal for a given tire model (Table 2), thus,  $\lambda_c$  is lower. It evidences that the electric actuators' reaction is faster than the mechanical one, what allows the precise wheel slip control. What is more, the smaller the error in wheel slip control, the shorter the braking distance is achieved (Table 5) due to higher braking force (Rajamani, 2012).

For the modelled SUV EV, the proposed control method allows to save around 10 % of the whole energy required for the fast and simultaneously safe deceleration, what is maximum for a given SRM. Thanks to the recuperative braking technology, energy consumption in each studied case is smaller for the decoupled system, comparing to the pure friction or braking with blocked wheels. Therefore, the regenerative ABS control method opens a possibility for energy improvement, what is an essential problem in environmental sustainability.

## 6. DISCUSSION

Electric mobility is a promising technology on a way to environmentally sustainable transportation. The EVs have a list of advantages over conventional ICE vehicles, such as quiet operation, cheap fuel, and zero emission. In addition, EVs architecture, like individual 4WD powertrain, opens a great opportunity to design accurate, efficient and fast dynamics control methods using different computational intelligence techniques. Nevertheless, EV mobility has also some disadvantages, such as a long recharging time and a short driving distance. The distance range may be increased using the kinetic energy recovery system.

Multiple researches studied in Section 2 show that scholars focused only on ABS (Chen *et al.*, 2010; Khatun *et al.*, 2003) and ESP control (Kim *et al.*, 2008; Pusca *et al.*, 2004; Tahami *et al.*, 2003) using FLC, or exclusively on regenerative braking algorithms (Li *et al.*, 2008; Nian *et al.*, 2014; Paterson and Ramsay, 1993; Peng *et al.*, 2006; Zhang *et al.*, 2016). Other authors merely dedicated the FLC approaches on electric and friction torque blending strategies (Jianyao *et al.*, 2015; Xu *et al.*, 2011; Zhang *et al.*, 2009). In Guo *et al.* (2014), the solution depends on a wheel slip threshold. In all these cases, unlike for the FLC described in this paper, the controller robustness and energy efficient deceleration are not proved.

The regenerative braking ABS control method proposed here is directed to illustrate both energy recuperation and

vehicle efficient safety fulfilments. The control method has the series architecture, in which electric motor torque is used maximally. The power gained from kinetic energy of the decelerated vehicle is directed to recycle the power back to the storage devices, such as ultracapacitors or directly to the battery cell.

Tire-road adhesive coefficient estimation was performed using fuzzy set theory in Layne *et al.* (1993) and Sharkavy (2006). The controllers were designed with the slip threshold of 20 %. In Paul *et al.* (2016), the ABS performance was not presented, hence, the vehicle safety is not demonstrated. In this paper, the recuperation braking control method is accompanied with ABS. The control method is designed to identify road adhesion and then to hold the optimal for various road surfaces wheel slip. The controller dependence on reference slip threshold is avoided.

The proposed controller has a certain advantage over earlier introduced similar methods. Namely, in Paul *et al.* (2016), likewise in this paper, the authors substituted a complex mathematical model for tire-road friction coefficient estimation with simple FLC. However, despite the high energy recuperation the controller did not hold an optimal for various road surfaces wheel slip. Thus, unlike inherent to the FLC described in this paper, a maximum possible efficient deceleration with steerability maintenance is not preserved.

In Castillo *et al.* (2016), a road type was detected by Kalman filter, FLC, and artificial neural network models combination. In Ivanov *et al.* (2006), road surface was estimated using eight variables applying three different FLCs. Lastly, another intelligent ABS FLC was described in Aly (2010), where three different FLCs (i.e. road identifier, optimal wheel slip estimator, and ABS controller) were connected in series. These controllers show good robustness to varying road surfaces. However, they are, unlike the controller proposed in this paper, where a road surface comprehension is accomplished referring to only single variable, vehicle body peak deceleration, very complex and computationally expensive. In addition, the algorithms were designed only for on a conventional hydraulic braking system. The appliance on the electric actuators and decoupled system were not stressed.

In suggested in this paper FLC, when the torque generated by the SRM is not enough to keep an optimal slip for a given surface, the controller runs the conventional friction brakes. Torque blending as well as regenerative energy capability are embodied based on fuzzy sets theory for each wheel separately. The controller outcomes are studied on a different road surfaces and are compared with the ABS control without regenerative possibility and with locked wheels deceleration.

A 10DOF vehicle model with a visual simulation interface helps to comprehend the vehicle behavior under various conditions. Analyzing the simulation outcomes in Section 5, it is concluded:

- the proposed solution recovers in average 8 % of power for each wheel, when on the wet and icy surfaces the energy consumption is lower;
- the control method maintains the optimal wheel slip value for varying road surfaces (Figure 4);
- electric actuators are faster than mechanical one, what enables them to maintain more accurate wheel slip control.

Additionally, the results have shown that with the designed control method the friction brakes are used less in EV. The time of friction between pads and discs is decreased, and thus the brake pads wear is minimized. It reduces at the same time the vehicle maintenance cost, brake components wear, and brake pads particles emission (El-Garhy *et al.*, 2013).

## 7. CONCLUSION

In short, the research innovations in recuperation ABS control stressed in this paper are listed as follows:

- Road surface recognition from vehicle longitudinal deceleration with optimal wheel slip for different road surface braking performance and high efficiency kinetic energy recovery based on FLC;
- Control method verification on 10DOF SUV EV mathematical model parametrized according to the vehicle manufacturer;
- Simulation comparison between decoupled regenerative, pure friction, and locked wheels braking performance on different road surfaces.

The results obtained in current research are limited with numerical simulation. Hence, the additional advantage of the present work is that it opens a great opportunity for further research. For instance, the controller could be tested on a hardware-in-the-loop system or on a real vehicle, because different behavior is expected for simulation and real world environments.

Due to missing information, state-of-charge, battery temperature, and some other aspects of power consumption are neglected in the model described in this paper. The future research will cover a study of the controller effectiveness on an extended model, where the mentioned characteristics have to be taken into consideration. Similarly, different maneuvers, for example, braking while cornering, may be also studied.

Finally, although the controller outputs are restricted by the system physical parameters (maximum motor current and maximum pressure), the controller nonlinear stability analysis may be performed, such as the Lyapunov's direct method proved to be very efficient in FLC stability analysis (Passino and Yurkovich, 1998).

**ACKNOWLEDGEMENT**—This work was supported by the European Community Horizon 2020 Framework Programme under the Marie Skłodowska-Curie grant agreement (grant number 675999); and the Deutschen Bundesstiftung Umwelt

(DBU) exchange scholarship.

## REFERENCES

- Acosta, M. and Kanarachos, S. (2017). Tire lateral force estimation and grip potential identification using neural networks, extended Kalman filter, and recursive least square. *Neural Computing and Applications*, 1–21.
- Aksjonov, A., Augsburg, K. and Vodovozov, V. (2016). Design and simulation of the robust ABS and ESP fuzzy logic controller on the complex braking maneuvers. *Applied Sciences* **6**, **12**, 382–390.
- Aly, A. A. (2010). Intelligent fuzzy control for antilock brake system with road-surfaces identifier. *Proc. IEEE Int. Conf. Mechatronics and Automation (ICMA)*, Xi'an, China.
- Bansal, R. C. (2005). *Electric Vehicles*, in: Emadi, A. (Ed.) *Handbook of Automotive Power Electronics and Motor Drives*. Taylor & Francis. Boca Raton, Florida, USA, 55–96.
- Castillo, J. J., Cabrera, J. A., Guerra, A. J. and Simon, A. A. (2016). Novel electrohydraulic brake system with tire-road friction estimation and continuous brake pressure control. *IEEE Trans. Industrial Electronics* **63**, **3**, 1863–1875.
- Chen, H., Yang, J., Du, Z. and Wang, W. (2010). Adhesion control method based on fuzzy logic control for four-wheel driven electric vehicle. *SAE Int. J. Passenger Cars - Mechanical Systems* **3**, **1**, 217–225.
- Cikanek, S. R. (1994). Fuzzy Logic Electric Vehicle Regenerative Antiskid Braking and Traction Control System. U.S. Patent 5,358,317.
- Dhameja, S. (2002). *Electric Vehicle Battery Systems*. Butterworth-Heinemann. Woburn, Massachusetts, USA, 1–42.
- Doumiati, M., Charara, A., Victorino, A. and Lechner, D. (2013). *Vehicle Dynamics Estimation Using Kalman Filtering: Experimental Validation*. 2nd edn. ISTE Ltd and John Wiley & Sons, Inc. Hoboken, UK, 37–61.
- Ehret, T. (2014). *Electronic Stability Program (ESP)*, in: Reif, K. (Ed.), *Brakes, Brake Control and Driver Assistance Systems: Function, Regulation and Components*. Springer, Friedrichshafen, Germany, 102–123.
- Ehsani, M., Gao, Y., Gay, S. E. and Emadi, A. (2005). *Modern Electric, Hybrid Electric, and Fuel Cell Vehicles*. CRC Press. Boca Raton, Florida, USA, 99–116, 204–232, 277–298.
- El-Garhy, A. M., El-Sheikh, G. A. and El-Saify, M. H. (2013). Fuzzy life-extending control of anti-lock braking system. *Ain Shams Engineering Journal* **4**, **4**, 735–751.
- Guo, J., Jian, X. and Lin, G. (2014). Performance evaluation of an anti-lock braking system for electric vehicles with a fuzzy sliding mode controller. *Energies* **7**, **10**, 6459–6476.
- Han, K., Hwang, Y., Lee, E. and Choi, S. (2015). Robust

- estimation of maximum tire-road friction coefficient considering road surface irregularity. *Int. J. Automotive Technology* **17**, **3**, 415–425.
- Ivanov, V. G., Algin, V. B. and Shyrokau, B. N. (2006). Intelligent control for ABS application with identification of road and environmental properties. *Int. J. Vehicle Autonomous Systems* **4**, **1**, 44–67.
- Ivanov, V. (2015). A review of fuzzy methods in automotive engineering applications. *European Transport Research Review* **7**, **29**, 19–29.
- Jianyao, H., Huawei, X., Zhiyuan, H., Linyi, H. and Qunxing, L. (2015). Study on braking force distribution based on fuzzy control algorithm. *Proc. IEEE Advanced Information Technology, Electronic and Automation Control Conf. (IAEAC)*, Chongqing, China.
- Khatun, P., Bingham, C. M., Schofield, N. and Mellor, P. H. (2003). Application of fuzzy control algorithm for electric vehicle antilock braking/traction control systems. *IEEE Trans. Vehicular Technology* **52**, **5**, 1356–1364.
- Kiencke, U. and Nielsen, L. (2005). *Automotive Control Systems: For Engine, Driveline, and Vehicle*. 2nd edn. Springer-Verlag Berlin Heidelberg, Berlin, Germany, 301–350.
- Kim, D., Hwang, S. and Kim, H. (2008). Vehicle stability enhancement of four-wheel-drive hybrid electric vehicle using rear motor control. *IEEE Trans. Vehicular Technology* **57**, **2**, 727–735.
- Kim, D.-H., Kim, J.-M., Hwang, S.-H. and Kim, H.-S. (2007). Optimal brake torque distribution for a four-wheel-drive hybrid electric vehicle stability enhancement. *Proc. Institution of Mechanical Engineers, Part D: J. Automobile Engineering* **221**, **11**, 1357–1366.
- Koch-Dücker, H.-J. and Papert, U. (2014). *Antilock Braking System (ABS)*, in: Reif, K. (Ed.), *Brakes, Brake Control and Driver Assistance Systems: Function, Regulation and Components*. Springer, Friedrichshafen, Germany, 74–93.
- Layne, J. R., Passino, K. M. and Yurkovich, S. (1993). Fuzzy learning control for antiskid braking systems. *IEEE Trans. Control Systems Technology* **1**, **2**, 122–129.
- Li, X., Xu, L., Hua, J., Li, J. and Ouyang M. (2008). Regenerative braking control strategy for fuel cell hybrid vehicle using fuzzy logic. *Proc. IEEE Int. Conf. Electrical Machines and Systems*, Wuhan, China.
- Long, B., Lim, S. T., Ryu, J. H. and Chong, K. T. (2014). Energy-regenerative braking control of electric vehicles using three-phase brushless direct-current motors. *Energies* **7**, **1**, 99–114.
- Miller, J. M. (2005). *Hybrid Electric Vehicles*, in: Emadi, A. (Ed.), *Handbook of Automotive Power Electronics and Motor Drives*. Taylor & Francis. Boca Raton, Florida, USA, 21–36.
- Negnevitsky, M. (2005). *Artificial Intelligence: A Guide to Intelligent Systems*. 2nd edn. Addison-Wesley. Harlow, UK, 87–131.
- Nian, X., Peng, F. and Zhang, H. (2014). Regenerative braking system of electric vehicle driven by brushless DC motor. *IEEE Trans. Industrial Electronics* **61**, **10**, 5798–5808.
- Pacejka, H. B. (2006). *Tyre and Vehicle Dynamics*. 2nd edn. Butterworth-Heinemann. Oxford, UK, 156–215.
- Passino, K. M. and Yurkovich, S. (1998). *Fuzzy Control*. Addison-Wesley. Menlo Park, California, USA, 1–22, 23–118, 187–232.
- Paterson, J. and Ramsay, M. (1993). Electric vehicle braking by fuzzy logic control. *Proc. Conf. Record of the IEEE Industry Applications Society Annual Meeting*, Toronto, Canada.
- Paul, D., Velenis, E., Cao, D. and Dobo, T. (2016). Optimal  $\mu$ -estimation based regenerative braking strategy for an AWD HEV. *IEEE Trans. Transportation Electrification* **3**, **1**, 249–258.
- Peng, D., Zhang, J. and Yin, C. (2006). Regenerative braking control system improvement for parallel hybrid electric vehicle. *Proc. IEEE Int. Technology and Innovation Conf.*, Hangzhou, China.
- Pusca, R., Ait-Amirat, Y., Berthon, A. and Kauffmann, J. M. (2004). Fuzzy-logic-based control applied to a hybrid electric vehicle with four separate wheel drives. *IEE Proc. - Control Theory and Applications* **151**, **1**, 73–81.
- Rajamani, R. (2012). *Vehicle Dynamics and Control*. 2nd edn. Springer. New York, USA, 87–112.
- Rath, J. J., Veluvolu, K. C. and Defoort, M. (2015). Simultaneous estimation of road profile and tire road friction for automotive vehicle. *IEEE Trans. Vehicular Technology* **64**, **10**, 4461–4471.
- Reznik, L. (1997). *Fuzzy Controllers*. Butterworth-Heinemann. Oxford, UK, 1–18.
- Savitski, D., Augsburg, K. and Ivanov, V. (2014). Enhancement of energy efficiency, vehicle safety and ride comfort for all-wheel drive full electric vehicles. *Proc. Eurobrake*, Lille, France.
- Savitski, D., Ivanov, V., Shyrokau, B., Pütz, T., De Smet, J. and Theunissen, J. (2016). Experimental investigations on continuous regenerative anti-lock braking system of full electric vehicle. *Int. J. Automotive Technology* **17**, **2**, 327–338.
- Sharkawy, A. B. (2006). Genetic fuzzy self-tuning PID controllers for antilock braking systems. *Alexandria Engineering Journal* **45**, **6**, 657–673.
- Tahami, F., Kazemi, R. and Farhanghi, S. (2003). A novel driver assist stability system for all-wheel-drive electric vehicles. *IEEE Trans. Vehicular Technology* **52**, **3**, 683–692.
- Xia, X., Xiong, L., Sun, K. and Yu, Z. P. (2016). Estimation of maximum road friction coefficient based on Lyapunov method. *Int. J. Automotive Technology* **17**, **6**, 991–1002.
- Xiong, L. and Yu, Z. (2011). *Vehicle Dynamics Control of 4 In-Wheel-Motor Driven Electric Vehicle*, in: Soylu, S., (Ed.) *Electric Vehicles – Modelling and Simulation*. InTech. Rijeka, Croatia, 67–106.
- Xu, G., Li, W., Xu, K. and Song, Z. (2011). An intelligent

- regenerative braking strategy for electric vehicles. *Energies* **4**, **9**, 1461–1477.
- Ye, M., Jiao, S. and Cao, B. (2010). Energy recovery for the main and auxiliary sources of electric vehicles. *Energies* **3**, **10**, 1673–1690.
- Zabler, E. (2014). *Sensors for Brake Control*, in: Reif, K. (Ed.), *Brakes, Brake Control and Driver Assistance Systems: Function, Regulation and Components*. Springer, Friedrichshafen, Germany, 142–153.
- Zhang, J., Song, B., Cui, S. and Ren, D. (2009). Fuzzy logic approach to regenerative braking system. *Proc. IEEE Int. Conf. Intelligent Human-Machine Systems and Cybernetics*, Hangzhou, Zhejiang, China.
- Zhang, X., Wang, Y., Liu, G. and Yuan, X. (2016). Robust regenerative charging control based on T-S fuzzy sliding-mode approach for advanced electric vehicle. *IEEE Trans. Transportation Electrification* **2**, **1**, 52–65.

**Publication VIII**

**Aksjonov, A.**, Nedoma, P., Vodovozov, V., & Petlenkov, E. (2018). A Method for Detection and Evaluation of Driver Distraction Induced by In-Vehicle Information Systems. *Proceedings of the 44th Annual Conference of the IEEE Industrial Electronics Society (IECON'18)* (pp. 4513–4518). Washington: IEEE. doi: 10.1109/IECON.2018.8591252



# A Method for Detection and Evaluation of Driver Distraction Induced by In-Vehicle Information Systems

Andrei Aksjonov, Pavel Nedoma

Innovation and Research

ŠKODA Auto a.s.

Mladá Boleslav, Czech Republic

{ andrei.aksjonov; pavel.nedoma }@skoda-auto.cz

Valery Vodovozov, Eduard Petlenkov

Department of Electrical Power Engineering and

Mechatronics

Tallinn University of Technology

Tallinn, Estonia

{ valery.vodovozov; eduard.petlenkov }@ttu.ee

**Abstract**—Steep improvement of an in-vehicle info- and entertainment systems has a positive impact on vehicle control, comfort, safety, etc. Nevertheless, it also leads to a multitasking load increase on the in-vehicle information system due to fundamental problems of driver distraction. In this paper, a method for detection and evaluation of driver distraction induced by the driver’s secondary activity is developed. The methodology is based on the machine learning and computation intelligence algorithms blend, which includes a driver model, a driver distraction detector, and a fuzzy logic evaluator. Several data fitting algorithms efficient for nonlinear regression are designed and are compared on the accuracy of the driver performance prediction. The method is verified by the driver-in-the-loop experiment with thirty participants on an advanced vehicle simulator. Driver’s interaction with the commercial in-vehicle information system is exploited as a secondary distractive task.

**Keywords**—Prediction methods; regression analysis; fuzzy logic; computational intelligence; vehicle safety; man-machine systems

## I. INTRODUCTION

With a rapid development of the in-vehicle information systems (IVIS), driver distraction (DD) becomes a new serious challenge for on-ground vehicle safety. DD is defined as “anything that delays the recognition of information necessary to safety maintain the lateral and longitudinal control of the vehicle (driver’s primary task) due to some event, activity, object or person (driver’s secondary activity), within or outside the vehicle that compels or tends to induce the driver’s shifting attention away from the fundamental driving task by compromising the driver’s auditory, biomechanical, cognitive or visual faculties or combinations thereof.” Almost 3500 people are killed and almost 400000 people are injured in the traffic accidents by distracted driving annually in the USA alone. In the EU, 20% of all fatalities on the road are due to DD. Unfortunately, this trend does not tend to decline [1], [2].

To improve vehicle safety, IVIS-induced DD detection and following minimization via human-machine interface (HMI)

design are the essential tasks for all vehicle manufacturers. The objective of this study is the development of a robust DD detection and evaluation methodology, which is capable not only to detect DD, but also to measure precisely its impact on safe vehicle operation for further DD minimization via vehicle cockpit design.

Some DD evaluation methods are based on subjective evaluation (e.g. questionnaire, survey) [3], [4], which depends on expert’s judgment and cannot be accepted as a fair evaluation. Therefore, scholars proposed different solutions for DD detection using modern practical machine learning and soft computing algorithms relying on behavioral (e.g. eye and head movement) attributes. For instance, in [5],  $k$ -nearest neighbor ( $k$ -NN), graph-regularized extreme learning machine and support vector machine (SVM) were compared on DD detection accuracy. Fuzzy logic (FL) [6], and artificial neural network (ANN) combined with gradient boosting machine [7] were also considered. Other researchers trusted the psychological attributes (e.g. electrocardio- and electroencephalographical signals). In [8], decision tree, random forest,  $k$ -NN, SVM, and Naïve Bayes algorithms were compared, while in [9] the Bayesian network and logic regression were used. The reliance on additional devices, such as cameras and neuroscan system, is the methods’ main drawback, because it rises the system price and complexity [10]. Moreover, this equipment is often considered as distractive.

Consequently, the performance-based attributes (e.g. vehicle lateral and longitudinal dynamics) are more feasible for practical application, because, in this case, DD detection and evaluation mechanism is supported by the signals transmitted from the sensors available in modern vehicles (e.g. vehicle speed, steering wheel rotation, vehicle acceleration, etc.). In [11], Gaussian mixture model was designed for DD detection. In [12], [13], the same algorithm was combined with ANN. Other computational intelligence and statistical learning theory approaches, like SVM [14], fuzzy logic [15], ANN with SVM [16], [17] were also applied for induced by secondary activity DD classification.

---

This research receives funding from the European Community Horizon 2020 Framework Programme under grant agreement No. 675999.

Although the accuracy of the proposed methods for DD detection is very high, all previously suggested approaches represent the binary logic classifiers, i.e. distracted/non-distracted. Thus, the methods are not applicable for precise measurement and evaluation of the secondary activity effect on the vehicle safe operation. Consequently, a new method for detecting and accurate measuring the secondary task impact on the DD level was developed by the authors [18].

In this paper, however, the method is enhanced with additional driver performance variable, namely steering wheel acceleration, and with one additional characteristic of the road segment. These innovations lead to the FL evaluator re-design that accordingly, provides more accurate DD evaluation. Hence, three performance-based variables are blended for DD detection and evaluation, instead of two in [18].

Furthermore, as the machine learning theory contains a vast variety of prediction algorithms [19], [20], different techniques for solving nonlinear regression problems, such as Gaussian process regression model (GPRM), ANN, layer-recurrent neural network (LRNN), adaptive neuro-fuzzy inference system (ANFIS), and  $k$ -NN are applied for driver modelling. The prediction models are compared in this study to determine the most accurate one. In [18], though, only the most commonly used prediction model ANN was applied. This paper tends to find the most accurate prediction model among the studied ones here. The algorithms are verified by the driver-in-the-loop experiment on an advanced driver decoy simulator, where DD is caused by various tasks from IVIS.

This paper is organized as follows. The DD detection and evaluation mechanism is described in the next section. In Section III, data collection is explained. Thereafter, the results of the drive-in-the-loop experiment are introduced. Finally, the studies are concluded in Section V.

## II. DRIVER DISTRACTION DETECTION AND EVALUATION METHOD

The block scheme of the DD detection and evaluation method is introduced in Fig. 1. The parameters description is presented in Table I. The method involves three steps.

First, the Driver model (Predictor) block predicts driver's performance on a road segment, which is described by three properties: speed limit  $v_l$ , road curvature  $c_r$ , and road curve direction  $c_d$ . The last feature may have three variables: -1 – the road leads to the left; 1 – to the right; or 0, when the road is

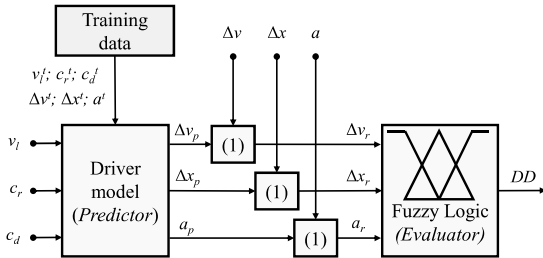


Fig. 1. Driver distraction detection and evaluation method block scheme.

straight. The predictor uses preliminary collected data and applies a machine learning algorithm for vehicle dynamic performance prediction (i.e. vehicle speed deviation  $\Delta v_p$ , lane keeping ability  $\Delta x_p$ , and steering wheel acceleration  $a_p$ ). The Driver model is unique for every person.

Next, the predicted vehicle longitudinal and lateral dynamics are compared with the same performance variables collected while driving under DD:  $\Delta v$ ,  $\Delta x$ , and  $a$ . In this phase the resultative performance, which is described by three parameters (i.e.  $\Delta v_r$ ,  $\Delta x_r$ ,  $a_r$ ) is calculated. The following rules are applied to each parameter (the example is shown only for  $\Delta v_r$  calculation):

$$\Delta v_r = \begin{cases} \Delta v - \Delta v_p, & \text{if } \Delta v > 0; \Delta v_p > 0; |\Delta v| > |\Delta v_p| \\ \Delta v - \Delta v_p, & \text{if } \Delta v < 0; \Delta v_p < 0; |\Delta v| > |\Delta v_p| \\ \Delta v + \Delta v_p, & \text{if } \Delta v > 0; \Delta v_p < 0; |\Delta v| > |\Delta v_p| \\ \Delta v + \Delta v_p, & \text{if } \Delta v < 0; \Delta v_p > 0; |\Delta v| > |\Delta v_p| \\ 0, & \text{if } |\Delta v| \leq |\Delta v_p| \end{cases} \quad (1)$$

In short, the block outputs zero, when the performance value under DD is smaller than the predicted one. If the DD performance value is greater than predicted value, the difference between two variables is calculated. Therefore, the difference symbolizes, how much does the secondary activity influence the vehicle dynamic performance from the safety point of view? Negative resultative performance,  $\Delta v_r$ ,  $\Delta x_r$ , and  $a_r$ , means driving slower its speed limit, driving on a right side from the road middle line, and turning a steering wheel to the right, correspondingly. Contrariwise, positive resultative values represent speeding, driving to the left from the center of the lane, and steering to the left, accordingly.

Finally, the resultative performance enters the Evaluator block. In this stage, the intelligent FL algorithm fuses three variables into a single output. The output represents DD in percentage and is utilized as a DD evaluation coefficient.

### A. Driver Model

Various practically used machine learning algorithms may be exploited in the Predictor model. In this paper, the prediction results of the most superb ones for solving nonlinear regression matter, namely GPRM, ANN, LRNN, ANFIS, and  $k$ -NN, are developed and are compared between each other.

TABLE I. PARAMETERS DESCRIPTION

Symbol	Description	Unit
$v_l$	Speed limit	km/h
$c_r$	Road curve radius	m
$c_d$	Road curve direction	Left/Right
$\Delta x$	Real lane keeping offset	m
$\Delta v$	Real vehicle speed deviation	km/h
$a$	Real steering wheel acceleration	$^\circ/s^2$
$\Delta x_p$	Predicted lane keeping offset	m
$\Delta v_p$	Predicted vehicle speed deviation	km/h
$a_p$	Predicted steering wheel acceleration	$^\circ/s^2$
$\Delta x_r$	Resultative lane keeping offset	m
$\Delta v_r$	Resultative vehicle speed deviation	km/h
$a_r$	Resultative steering wheel acceleration	$^\circ/s^2$
$DD$	Driver distraction level	%

Due to the software simplicity, all the algorithms were designed with MATLAB R2016b from MathWorks, Inc (Natick, Massachusetts, United States). In this sub-section, these algorithms are briefly described.

1) *Gaussian Process Regression Model*: Gaussian process methods are widely used for regression problem, where the predicted values are continuous quantities. The GPRM are nonparametric kernel-based probabilistic models with the main advantage of simplicity of implementation and interpretability. However, the algorithm has also a significant disadvantage, because its prediction accuracy degrades if the mapping between inputs and outputs cannot be approximated by a linear function. For more details about GPRM, the readers may refer to the Chapter 2 in [21]. In this work, the GPRM is trained using the linear basis function and exact prediction method.

2) *Artificial Neural Network*: ANN is the feedforward multilayer perceptron, while the multilayer perceptron is a mathematical function mapping the input-output values. The ANN contains an input layer, at least one hidden layer of computational neurons, and an output layer [20], [22]. In this work, the ANN with two hidden layers and 100 neurons in each hidden layer is trained with the Levenberg-Marquardt learning algorithm. The method is fast and efficient for the nonlinear regression problem. In this method, the gradients are computed by a backward propagation of errors, what makes it the most rapid and efficient algorithm. Thanks to their simplicity, the sigmoid activation functions were used in hidden layer neurons, while the output neuron transfer functions are linear. Number of neurons in the hidden layers is responsible for model exactness. At the same time, more neurons in the layers lead to network's computational cost growth [22]. In the designed ANN, an improvement of the network performance has not been noticed with more than 100 neurons. Initially the hyperparameters are set by default in the software, however, the training parameters, namely initial weights and threshold levels, are selected randomly.

3) *Layer-Recurrent Neural Network*: The difference between LRNN and ANN is that the first one has a feedback loops (with a delay) from its output to its next input. The network uses the hyperbolic tangent sigmoid transfer functions for the hidden layers and the linear transfer function in the output layer. More information about the recurrent and recursive nets can be found in Chapter 10 in [20]. In this work, the LRNN, as ANN, was trained with the Levenberg-Marquardt method. The network contains 15 neurons in the hidden layer. The input delay of the feedback signal from the hidden layer is 1:2.

4) *Adaptive Neuro-Fuzzy Inference System*: ANFIS is an equivalent to a first-order Sugeno's fuzzy model. The model is a combination of the two most popular computational intelligence algorithms: ANN and FL. The network is a six-layer feedforward ANN that uses a hybrid training method, which combines the back-propagation algorithm in the backward pass and least squares - in the forward pass, to

optimize both the antecedent and the consequent parameters [21], [23]. The greater number of membership functions (MFs), rather than their shape, improves the model efficiency. This is because the number of MFs directly influences the amount of linguistic links between inputs and outputs allowing more precise ANFIS tuning [21]. In this work, the ANFIS contains nine MFs for each input variable. They are symmetrically dispersed and overlapped between each other over the whole universe of discourse (UOD). The MFs have triangular shapes, because they are simple for programming. The output MFs are linear.

5) *k-Nearest Neighbor*:  $k$ -NN represents the last algorithm used as the Predictor. The algorithm for storing the input-output training set is enough simple. When requested, it searches the closest entry in the data set and returns the associated target. The main advantage of the algorithm is its ability to achieve the minimum possible training error on any regression data kit. Thus, it makes the algorithm one of the most accurate for prediction from a simple data sample. Nevertheless, at the same time it makes the method computationally expensive for real-time applications [19], [20]. In our case,  $k = 1$ . Hence, a new input ( $v_i, c_r, c_d$ ) representing the sample data from driving under DD, searches a nearest point from the preliminary gathered data ( $v_i^j, c_r^j, c_d^j$ ). As a result, the predicted performance is returned ( $\Delta y_p, \Delta x_p, a_p$ ), which corresponds to an appropriate point from the training data set ( $\Delta y^j, \Delta x^j, a^j$ ).

#### B. Fuzzy Logic Evaluator

The FL evaluator has three inputs (i.e.  $\Delta y_r, \Delta x_r, a_r$ ) and a single output, DD. In this work, a Sugeno's type inference mechanism based on simple matrix operation is applied [24], where the inputs are fuzzified into a 5x5x3 matrix. Due to its

TABLE II. FUZZY LOGIC EVALUATOR RULE-BASE

$a_r = \text{negative}$						
DD [%]		$\Delta x_r$				
		neg far	neg close	zero	pos close	pos far
$\Delta v_r$	neg high	100	85.8	42.9	85.8	100
	neg low	100	57.2	14.3	57.2	100
	zero	57.2	28.6	0	28.6	57.2
	pos low	85.8	42.9	14.3	42.9	85.8
	pos high	100	85.8	42.9	85.8	100
$a_r = \text{zero}$						
DD [%]		$\Delta x_r$				
		neg far	neg close	zero	pos close	pos far
$\Delta v_r$	neg high	100	71.5	42.9	71.5	100
	neg low	85.8	14.3	0	14.3	85.8
	zero	42.9	0	0	0	42.9
	pos low	71.5	14.3	0	14.3	71.5
	pos high	85.8	57.2	28.6	57.2	85.5
$a_r = \text{positive}$						
DD [%]		$\Delta x_r$				
		neg far	neg close	zero	pos close	pos far
$\Delta v_r$	neg high	100	85.8	42.9	85.8	100
	neg low	100	57.2	14.3	57.2	100
	zero	57.2	28.6	0	28.6	57.2
	pos low	85.8	42.9	14.3	42.9	85.8
	pos high	100	85.8	42.9	85.8	100

simplicity, all the input MFs have triangular shapes, where both  $\Delta v_r$  and  $\Delta x_r$  have five MFs and  $a_r$  – three MFs. The MFs are symmetrically dispersed and overlapped between each other over the whole UOD, what gives them equal sensitivity. The  $\Delta y_r$  is bounded in  $[-12, 12]$ , the  $\Delta x_r$  OUD is closed in  $[-1.5, 1.5]$ , and  $a_r$  - inside  $[-1500, 1500]$ .

The input and output mapping is done via 75 linguistic rules. The rule-base is lodged in Table II. As the fuzzified from the input matrix size is  $5 \times 5 \times 3$ , the rule-base has three different tables for each layer of the three-dimensional matrix. The UOD of the output is restricted in  $[0, 100]$ , because the final output represents the level of DD in percentage. Eight linear-form MFs are designed for the output. The output MFs are dissipated on equal step 14.3 between each other. An example of the modus-ponens-form rules connection is as follows: **IF** the steering wheel acceleration is “*positive*”, **AND** vehicle speed deviation is “*pos\_low*”, **AND** lane keeping offset is “*pos\_far*”, **THEN** driver distraction is 85.8 %.

### III. DATA COLLECTION

#### A. Participants

Thirty drivers without serious physical or mental health disorders, who use passenger vehicles daily contributed to the driver-in-the-loop experiment. Participants’ female – male ratio was 5 to 25. The contributors’ gender, age, and driving experience and statistical analysis on DD level were not under the scope of the studies. The participation was not voluntarily, but rewarded.

#### B. Apparatus

The real-time driver-in-the-loop experiment was conducted using the advanced driver decoy simulator provided by the ŠKODA Auto a.s. HMI laboratory (Mladá Boleslav, Czech Republic). The simulator is a fixed-base test rig with an identical to a commercial vehicle cockpit. The driver operates the simulator in the virtual world, which is displayed on the wall in front of the test bed. All the secondary activities are submitted via cockpit HMI. The data are collected with 10 Hz frequency. More information about the experiment facilities, including the simulator, software, vehicle modelling and parameterization, can be found in [18].

#### C. Procedure

The driver-in-the-loop experiment consisted of two phases. In the first phase, each driver was requested to drive the simulator in the virtual world staying in the middle of the road



Fig. 2. Driver-in-the-loop experiment procedure.

and holding the speed limit, as she/he would do in the real world. The data collected during this step were expended for the Predictor design. The two-lane road is identical to one of the road segments in Czech Republic, where each lane is 3.5 m width. The road shape has two main segments: 50 km/h speed limit with curvy shape, and almost straight road with 90 km/h speed limitation. There were no other dynamic objects (e.g. other vehicles, people or animals) modelled in the virtual world.

During the second stage, the participants were requested to continue driving in the virtual world as accurate as possible. Simultaneously, this time they were obliged to accomplish the secondary tasks by interacting with IVIS. The drivers got different commands (such as searching for a specific radio station, selecting the new city in the navigation system, making a call to a specific contact, etc.) from the experimenter. After the secondary task submission, the participants had to give a feedback via a windshield washer switch behind the steering wheel. If the secondary task is completed wrong, the drivers were asked to repeat the activity.

In Fig. 2, the photo taken during the second stage is shown. One of the experiment contributors interacts with the IVIS while piloting the simulator in the virtual world. The data gathered during this phase were applied for DD detection and IVIS-induced DD evaluation.

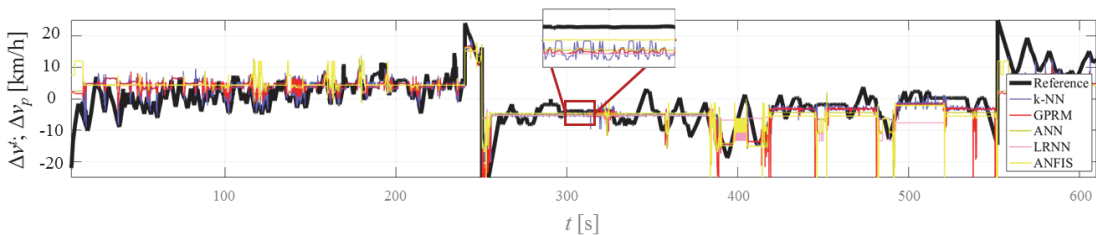


Fig. 3. Prediction algorithms comparison for  $\Delta y_p$  versus training reference data.

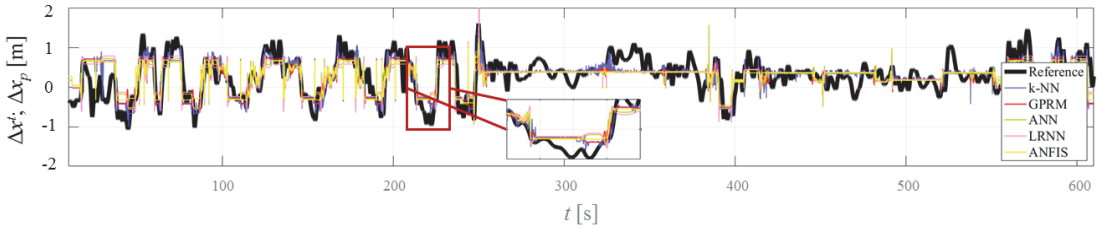


Fig. 4. Prediction algorithms comparison for  $\Delta x_p$  versus training reference data.

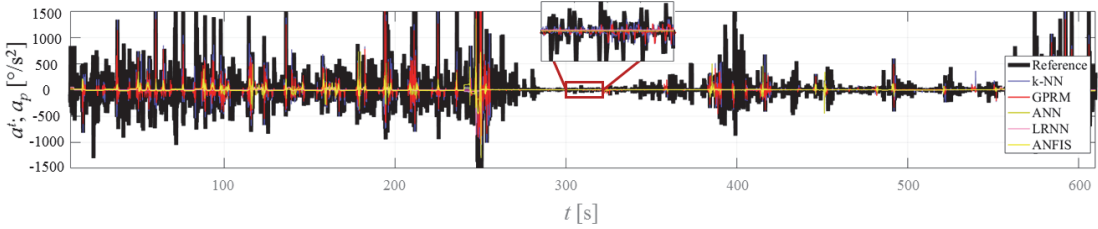


Fig. 5. Prediction algorithms comparison for  $a_p$  versus training reference data.

#### IV. RESULTS

In this section, the results of the driver-in-the-loop experiment are introduced. A random driver is selected from the experiment participants. Her/his performance is studied here in details. For the rest of the experiment participants the outcomes are very similar. For better observation, only 10 minutes of the DD experiment are presented.

Vehicle speed deviation (Fig. 3), lane keeping ability (Fig. 4), steering wheel acceleration (Fig. 5) along with the curve representing the reference data (black line in each plot) are delivered. It is hard to distinguish the optimization curves for all studied nonlinear regression algorithms (i.e.  $k$ -NN, ANN, ANFIS, GPRM, and LRNN). Therefore, in Table III the models' performance accuracies are presented.

In Table III, the sum of the squared error of prediction (SSE), which is a main parameter for regression accuracy [21], is calculated for every variable and each Predictor. In addition, the model training time  $t_{train}$  as another important parameter of the real-time application is tracked for every variable. It is concluded that, for our task, the  $k$ -NN outperforms other multidimensional mapping algorithms in both SSE and training

TABLE III. THE PREDICTORS' PREDICTION ACCURACY COMPARISON

$SSE$	$\Delta v_p$	$\Delta x_p$	$a_p$	$t_{train}$ [s]
<b>GPRM</b>	4.436	1.121	4.512	112.775
<b>ANN</b>	6.089	1.243	6.843	282.737
<b>LRNN</b>	1.243	1.340	6.890	231.515
<b>ANFIS</b>	6.843	1.216	6.678	155.720
<b><math>k</math>-NN</b>	5.941	0.918	4.137	50.39

time features. This judgment also confirms the statement from [20] that the nearest neighbor regression, depending of the data sample, is one of the most accurate predictors.

In Fig. 6, DD evaluation results are scoped, where due to its excellent performance the  $k$ -NN is applied as the Driver model (Fig. 1). The gray background symbolizes the period of the secondary task accomplishment. Though there were different IVIS-induced distractive tasks requested from the participants, an investigation of each single task's impact on vehicle safety was not under the scope of this study. The white background indicates free from distraction driving. The red curve represents the level of DD inferred by the FL Evaluator.

In short, it can be noticed that some secondary activities led to a significantly high level of DD. Moreover, the drivers

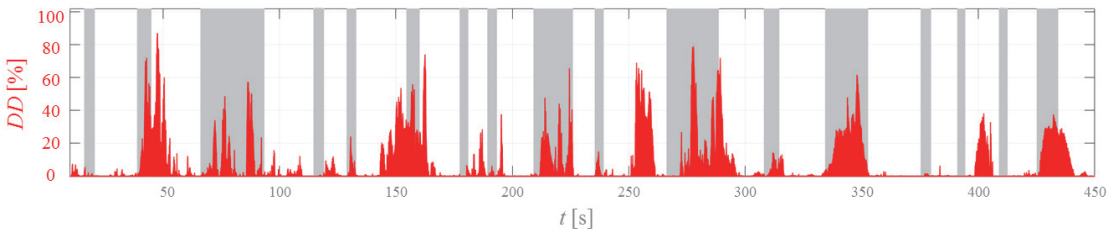


Fig. 6. Driver distraction evaluation by fuzzy logic.

require more time to complete these tasks, what can be addressed to the tasks' complexity and consequent humans' cognitive workload increase. On the contrary, some tasks do not cause DD at all, what makes them safe for multitasking vehicle operation.

## V. CONCLUSION

In this paper, a new IVIS-induced DD detection and evaluation method is described. The methodology concerns the Driver model designed with help of machine learning algorithms, the comparative rules for DD detection, and the FL Evaluator algorithm. The last one melts three performance-based attributes (i.e. vehicle lane and speed limit keeping abilities, as well as applied on a steering wheel force) into a single output, which expresses a level of DD in percentage.

Various nonlinear regression techniques are used for the Predictor development. Based on prediction accuracy and algorithm training time, the  $k$ -NN outperformed other approaches, namely ANN, ANFIS, GPRM, and LRNN. The methodology is tested in driver-in-the-loop experiment with thirty participants. Overall, the method can be applied as a practical tool for evaluation of the driver's secondary activity influence on vehicle safe piloting.

## REFERENCES

- [1] National Traffic Law Center. Investigation and prosecution of distracted driving cases. Report no. DOT HS 812 407. Washington, DC: National Highway Traffic Safety Administration, 2017.
- [2] European Commission, Directorate General for Mobility and Transport, Road safety newsletter, No 27, 2017. [Online] Available: [https://ec.europa.eu/transport/road\\_safety/sites/roadsafety/files/nl27\\_en.pdf](https://ec.europa.eu/transport/road_safety/sites/roadsafety/files/nl27_en.pdf)
- [3] M. R. Endsley, "Design and evaluation for situation awareness enhancement," *Proc. of the Hum. Fact. and Ergon. Soc. Annual Meeting*, vol. 32, no. 2, pp. 97 – 101, Oct. 1988.
- [4] H. Jander, J. Borgvall, and R. Ramberg, "Towards a methodological framework for HMI readiness evaluation," *Proc. of the Hum. Fact. and Ergon. Soc. Annual Meeting*, vol. 56, no. 1, pp. 2349 – 2353, Dec. 2016.
- [5] Y. Jiao, Y. Peng, B.-L. Lu, X. Chen, S. Chen, and C. Wang, "Recognizing slow eye movement for driver fatigue detection with machine learning approach," in 2014 Intern. Joint Conf. on Neural Netw. (IJCNN), Beijing, China, 2014, pp. 4035-4041.
- [6] M.-H. Sigari, M. Fathy, and M. Soryani, "A driver face monitoring system for fatigue and distraction detection," *Intern. Jour. of Vehic. Techn.*, vol. 2013, pp. 1-11, Jan. 2013.
- [7] X.-P. Huynh, S.-M. Park, and Y.-G. Kim, "Detection of driver drowsiness using 3D deep neural network and semi-supervised gradient boosting machine," in *Asian Conf. on Comp. Vision (ACCV)*, Lecture Notes in Computer Science, vol 10118. Springer, 2016, pp. 134-145.
- [8] V. Alizadeh and O. Dehzingi, "The impact of secondary tasks on drivers during naturalistic driving: Analysis of EEG dynamics," in 2016 IEEE 19th Intern. Conf. on Intell. Transp. Syst. (ITSC), Rio de Janeiro, Brazil, 2016, pp. 2493-2499.
- [9] M. Babaeian, N. Bhardwaj, B. Esquivel, and M. Mozumdar, "Real time driver drowsiness detection using a logistic-regression-based machine learning algorithm," in 2016 IEEE Green Ener. and Syst. Conf. (IGSEC), Long beach, CA, USA, 2016, pp. 1-6.
- [10] C. Ahlstrom, K. Kircher, and A. Kircher, "A gaze-based driver distraction warning system and its effect on visual behavior," *IEEE Trans. on Intel. Transp. Syst.*, vol. 14, no. 2, pp. 965-973, June 2013.
- [11] J. Yang, T. N. Chang, and E. Hou, "Driver distraction detection for vehicular monitoring," in *IECON 2010 - 36th Annual Conf. on IEEE Indust. Electron. Soc.*, Glendale, AZ, USA, 2010, pp. 108-113.
- [12] S.J. Choi, J.H. Kim, D.G. Kwak, P. Angkititrakul, and J. H. L. Hansen, "Analysis and classification of driver behavior using in-vehicle CAN-bus information," in 2011 IEEE Intern. Conf. on Multim. and Expo (ICME), Barcelona, Spain, 2011, pp. 1-6.
- [13] S. Im, C. Lee, S. Yang, J. Kim, and B. You, "Driver distraction detection by in-vehicle signal processing," in 2014 IEEE Symp. on Comput. Intell. in Vehic. and Transp. Syst. (CIVTS), Orlando, FL, USA, 2015, pp. 1-5.
- [14] T. Ersal, H. J. A. Fuller, O. Tsimhoni, J. L. Stein, and H. K. Fathy, "Model-based analysis and classification of driver distraction under secondary tasks," *IEEE Trans. on Intel. Transp. Syst.*, vol. 11, no. 3, pp. 692-701, Sept. 2010.
- [15] S. Qiu, R. McGee, and Y. L. Murphey, "Adaptive fuzzy prediction for automotive application usage," in 2015 IEEE 14th Intern. Conf. on Machine Learn. and Applic. (ICMLA), Miami, FL, USA, 2015, pp. 19-24.
- [16] V. Martínez, I. del Campo, J. Echanobe, and K. Basterretxea, "Driving behavior signals and machine learning: A personalized driver assistance system," 18th IEEE Intern. Conf. on Intel. Transp. Syst., Las Palmas, Spain, 2015, pp. 2933-1940.
- [17] S.M. Iranmanesh, H.N. Mahjoub, H. Kazemi, and Y.P. Fallah "An Adaptive Forward Collision Warning Framework Design Based on Driver Distraction," *IEEE Trans. on Intel. Transp. Syst.*, in press.
- [18] A. Aksjonov, P. Nedoma, V. Vodovozov, and E. Petlenkov, "Driver distraction detection and evaluation with artificial neural network and fuzzy logic," *The 15th IEEE Intern. Workshop on Advanced Motion Control (AMC)*, Tokyo, Japan, 2018, 523-528.
- [19] E. Alpaydin, *Introduction to Machine Learning*. Cambridge, Massachusetts: USA: The MIT Press, 2004.
- [20] I. Goodfellow, Y. Bengio, and A. Courville, *Deep Learning*. Cambridge, Massachusetts: USA: The MIT Press, 2016.
- [21] C.E. Rasmussen and C.K.I. Williams, *Gaussian Processes for Machine Learning*. Cambridge, Massachusetts: USA: The MIT Press, 2006.
- [22] M. Negnevitsky, *Artificial Intelligence: A Guide to Intelligent System*. 2nd ed. Harlow, England: Adison-Wesley, 2005.
- [23] L. Reznik, *Fuzzy Controllers*. Oxford, Great Britain: Newnes-Butterworth-Heinemann, 1997.
- [24] A. Aksjonov, P. Nedoma, V. Vodovozov, E. Petlenkov, and M. Herrmann, "A method of driver distraction evaluation using fuzzy logic," in 2017 XXVI Intern. Conf. on Inform., Commun. and Autom. Techn. (ICAT), Sarajevo, Bosnia & Herzegovina, 2017, pp. 23-28.

**Publication IX**

**Aksjonov, A.**, Vodovozov, V., Augsburg, K., & Petlenkov, E. (2019). Blended Antilock Braking System Control Method for All–Wheel Drive Electric Sport Utility Vehicle. *Proceedings of the 13th International Conference of the IMACS TC1 Committee (ELECTRIMACS 2019)*. Salerno: Springer.



# Blended antilock braking system control method for all-wheel drive electric sport utility vehicle

Andrei Aksjonov · Valery Vodovozov · Klaus Augsburg · Eduard Petlenkov

**Abstract** At least two different actuators work in cooperation in regenerative braking for electric and hybrid vehicles. Torque blending is an important area, which is responsible for better manoeuvrability, reduced braking distance, improved riding comfort, etc. In this paper, a control method for electric vehicle blended antilock braking system based on fuzzy logic is promoted. The principle prioritizes usage of electric motor actuators to maximize recuperation energy during deceleration process. Moreover, for supreme efficiency it considers battery's state of charge for switching between electric motor and conventional electrohydraulic brakes. To demonstrate the functionality of the controller under changing dynamic conditions a hardware-in-the-loop simulation with real electrohydraulic brakes test bed is utilized. In particular, the experiment is designed to exceed the state of charge threshold during braking operation, what leads to immediate switch between regenerative and friction brake modes.

## 1 Introduction

One of the advantageous features of the electric vehicles (EVs) is their ability to recuperated energy during a

deceleration process. In EVs, friction braking (FB) cooperates with regenerative braking (RB), what opens a need to efficient torque control between two separate actuators (i.e. torque blending), which are characterized by different dynamics. In some cases, RB is simply not enough to achieve requested braking torque, therefore, the FB system is activated in parallel or in series. In other case, the battery conditions (e.g. temperature, battery's state of charge (SOC), etc.) must be considered. For instance, when the battery is fully charged, the recuperation is no longer useful and even dangerous [1].

The SOC is a ratio of the remaining battery capacity to the full charged one. It is one of the most important parameters in EVs. Its feature is used not only in battery management to estimate potential driving range before the next recharge, but also in vehicle traction (e.g. hybrid EV) and braking (e.g. blended braking system) control strategies [1]. For example, to avoid electric battery overcharge, and consequent damage, the regeneration by electric motors is usually limited to a specific upper bound, 80–90% [2]. Therefore, the SOC must be always involved in a blended antilock braking system (ABS).

Nowadays, the fuzzy logic controllers (FLCs) are widely used in automotive engineering to solve various problems [3]. For instance, in [4], an effectiveness and strong robustness of a fuzzy sliding mode control over conventional proportional–integral–derivative (PID) and Mamdani's type FLC in energy recuperation for EV in simulation environment was demonstrated. Complexity of vehicle dynamics in deceleration process, especially during emergency braking, was not integrated in the study.

An FLC-based RB strategy integrated with series RB was developed in [5]. The FLC received driver's force command, vehicle speed, battery's SOC and temperature to determine distribution between FB and RB to improve

---

A. Aksjonov  
ŠKODA Auto a.s.  
Mladá Boleslav, Czech Republic  
E-mail: andrei.aksjonov@skoda-auto.cz

K. Augsburg  
Technische Universität Ilmenau  
Ilmenau, Germany  
E-mail: klaus.augsburg@tu-ilmenau.de

V. Vodovozov · E. Petlenkov  
Tallinn University of Technology  
Tallinn, Estonia  
E-mail: valery.vodovozov@taltech.ee, eduard.petlenkov@taltech.ee

energy recuperation efficiency. In [6], the FLC involved SOC and a ratio between brake torque and biggest brake torque to determine factual FB and RB brake torques. An RB control strategy applying FLC was presented in [7]. The simulation results demonstrated that the developed method is able to recover energy and distribute power flow to maintain SOC around target value. A PID in combination with FLC ensured efficient RB strategy of the EV [8]. The SOC was taken as an input of the FLC. Despite impressive results, all these works only focused on the base brake case. The ABS function was not considered.

In [9], the authors applied genetic algorithm in EV stability control logic using RB of the rear wheels motor and FB of electrohydraulic brake (EHB). The simulation results showed that the optimal recuperation strategy is able to provide an increase of recuperation energy. However, neither SOC in torque allocation nor ABS performance were under investigation. Brake force distribution strategy for EVs based on estimation of tire–road friction coefficient was provided in [10]. The road condition estimation was also based on fuzzy theory. An efficient torque blending was demonstrated in [11]. The experiment was conducted on a real vehicle braking on low–friction road surface. In [12], the FLC was used to adjust braking torque between RB and FB. However, in these works torque blending or force distribution did not consider SOC of a battery.

Scholars in [13] integrated sliding mode controller with FLC for an ABS control to maintain optimal wheel slip ratio deceleration. The SOC was reckoned in torque blending in this instant. Nevertheless, for the ABS control method the reference slip was fixed, thus, changing optimal slip for various road conditions was not involved. Advanced control allocation with energy recuperation for EV was introduced in [14]. The authors also involved battery's SOC. Both works did not study the situation, when SOC exceeds its bound during braking manoeuvre.

Earlier [15], the EV torque blending with recuperation capabilities with SOC taken into account was proposed by the authors. It was integrated with three types of controllers, namely PID, tabular, and FLC. In this paper, the attention is once again focused on SOC's influence on EV's blended ABS. To this aim, the intelligent FLC control method previously developed by the authors [16] is applied in hardware–in–the–loop (HIL) simulation with real EHB system. The HIL testbed accompanied with a hardware delay is exploited to represent actual EHB dynamics, making the simulation experiment more valued for real life application. The deceleration test is designed in a way that SOC reaches its maximum threshold in the middle of the braking process. Consequently, blended braking system rapidly switches from RB to FB.

In RB, the recovered energy is not stored directly in the battery, but in the ultracapacitor. From the latter, the recuperated energy is transmitted slowly to the battery or is used for vehicle acceleration. Thus, the SOC shall also consider capacity of an ultracapacitor. Furthermore, the

electronic power converters play an essential role in energy recuperation in EVs as they are an intermediate connection between energy sources and motors. In this paper, it is assumed that the energy is transferred directly to the battery, thus, the SOC may surpass its maximum limit during the EV deceleration. However, the power electronics losses are neglected in the powertrain model. Nevertheless, possible consideration of the SOC of ultracapacitor in torque blending was also proposed by the authors in [15].

This paper is organized as follows. The next section stresses the HIL simulation environment together with vehicle modeling. Section III describes the blended ABS control method. In Section IV, the HIL simulation results are delivered. The paper is briefly concluded in Section V.

## 2 Vehicle model and experimental setup

### 2.1. Single wheel model

A simplified schematic single wheel brake diagram is drawn in Fig. 1. The rolling resistance and lateral dynamics are neglected, because only the straight braking manoeuvre is studied in this work. The torque balance about a wheel axis is expressed as:

$$J_w \dot{\omega}_w = T_d - r_w \cdot F_x - T_b, \quad (1)$$

where  $J_w$  – moment of inertia of wheel;  $\omega_w$  – angular velocity of wheel;  $T_b$  – braking torque;  $T_d$  – driving torque;  $r_w$  – radius of deformed tire;  $F_x$  – longitudinal force of tire.

A distinctive feature of the EV: its braking torque  $T_b$  is a summation of the RB  $T_{RB}$  and FB  $T_{FB}$  braking torques [16]:

$$T_b = T_{FB} + T_{RB}. \quad (2)$$

In practice,  $T_{RB}$  and  $T_{FB}$  are not measured by the sensors directly. They change proportionally to phase current of a switched reluctance motor (SRM) and line pressure of an EHB, accordingly. Those states are measured by available on–board sensors in modern vehicles. In this paper, the variables are represented as torques directly.

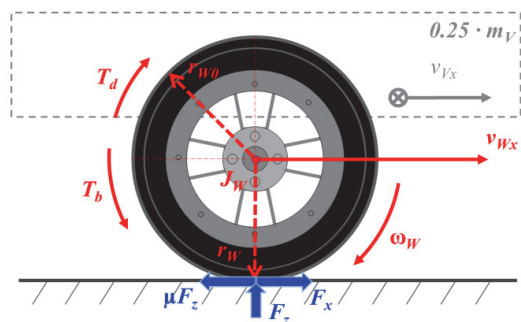


Fig. 1 A schematic drawing of a braked wheel for a single–wheel model.

## 2.2. State estimation

An essential characteristic of an ABS is tire–road friction coefficient  $\mu$ . Straight direction braking manoeuvre neglects lateral dynamics, hence,  $\mu$  is calculated as a ratio of longitudinal  $F_x$  and normal  $F_z$  forces:

$$\mu = \frac{F_x}{F_z}. \quad (3)$$

The proposed control method uses  $\mu$  to understand the road surface under the tires of the EV. In this regard,  $\mu$  is assumed to be proportional to the EV body deceleration rate [16]:

$$\mu^* = \frac{F_x}{F_z} = \frac{m_v \cdot a_{v_x}}{m_v \cdot g} = \frac{a_{v_x}}{g}, \quad (4)$$

where  $m_v$  – mass of vehicle;  $a_{v_x}$  – longitudinal acceleration of vehicle;  $g$  – gravitational acceleration.

Maximum achieved vehicle deceleration during the first period of heavy braking manoeuvre is related to road surface conditions and is used as the road recognizer in the proposed control method. The variable is expressed as  $\mu^*$  [16].

Another important state for the control method is longitudinal wheel slip  $\lambda$ , which is estimated from vehicle  $v_{v_x}$  and wheel  $v_{w_x}$  longitudinal velocities:

$$\lambda = \frac{v_{w_x} - v_{v_x}}{v_{v_x}} \cdot 100\%. \quad (5)$$

Vehicle longitudinal velocity is derived from the vehicle body deceleration signal:

$$v_{v_x} = \int a_{v_x} dt. \quad (6)$$

Wheel longitudinal speed is found as:

$$v_{w_x} = r_w \cdot \omega_w. \quad (7)$$

## 2.3. Electric vehicle model

The EV model is completed in IPG CarMaker<sup>®</sup> 6.0 (Germany) software. The 14 degrees-of-freedom model is interacted with MATLAB<sup>®</sup> from MathWorks, Inc. (USA) allowing users for rapid control algorithm development and testing. The software's integration in the HIL systems opens a great possibility for advance prototypes testing and concepts engineering, what sensitively saves development time and cost.

The sport utility EV model with all–wheel drive powertrain represents a vehicle under investigation. The specification of the vehicle parameterizations are provided by the EV's manufacturer (e.g. mass, dimensions, electric propulsion system, etc.) or are collected experimentally (e.g. suspension, tire model, etc.).

Each of four wheels is equipped with SRM. In–wheel motor transmission type is a two–stage reducer with helical gear and half–shaft. Considering SRM's peak torque (i.e. 200 Nm at 800 V) together with overall SRM–gear ration (i.e. 1:10.5), maximum torque achieved on single wheel reaches 2100 Nm. The motors behaviour is defined by the first–order transfer function. More information about vehicle model together with its parameters is available in [16].

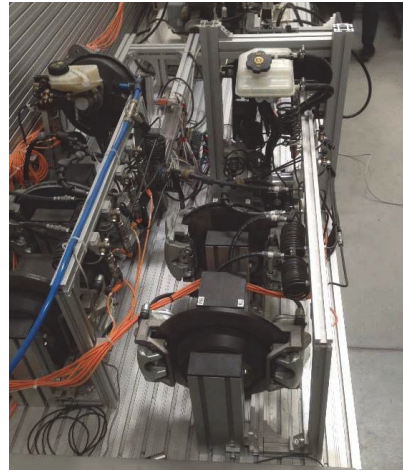


Fig. 2 Electrohydraulic brake system test bed.

The braking linings' coefficient of friction is modelled by means of a dynamic model, which was validated against data collected on the brake dynamometric test bed at Technische Universität Ilmenau (Germany). This model considers the influence of speed, pressure, and temperature on the brake linings' coefficient of friction [17].

The tire dynamics are approximated with Pacejka's "Magic Formula" with experimentally obtained coefficients. The tire–road model is a relevant element for the control method design. Particularly, it is important to know, what is the most efficient workspace for the  $\lambda$  with various road surfaces? Deceleration with the optimal  $\lambda$  results in maximum braking manoeuvre efficiency that impacts the deceleration distance. Moreover, when the wheel slip is equal or smaller than its corresponding peak (so-called stable region), the EV presumes steerability. On the contrary, deceleration with the  $\lambda$  exceeding its optimal one (i.e. unstable zone) leads to wheels' lockage and lateral control aggravation. The ABS's task is to avoid wheel slip unstable region.

## 2.4. Electrohydraulic brake system test bed

The EHB with control unit test bed (Fig. 2), was provided by Technische Universität Ilmenau. The test rig is developed by the ZF TRW Automotive GmbH (Germany). The EHB setup is used in vehicle braking dynamics studies for reproduction of the real pressure dynamics of the brake circuit.

The vehicle model sends demanded braking pressure for each wheel to the EHB control unit. The dSPACE<sup>®</sup> (Germany) platform is utilized as an intermediate connection between the vehicle numerical model and the EHB. The requested braking pressure received from the vehicle model activates the valves that generate corresponding braking pressure between the wheels and the

callipers. Finally, measured with the appropriate sensors line braking pressure on each wheel is returned back to the vehicle model.

### 3 Blended anti-lock braking system control method

#### 3.1. Control method

The ABS control method supplies an appropriate braking torque to decelerate the vehicle with optimal wheel slip for each wheel. Different road surfaces are taken into account in control method design. A detailed description of control method and its design can be found in [16]. Only brief introduction is delivered here.

The control area network bus provides vehicle longitudinal deceleration together with wheel velocity (Fig. 3). In the next steps, applying (4) – (7), two commanded variables,  $\lambda$  and  $\mu^*$ , are obtained. They are used by the FLCs to generate a required torque for the actuators.

Two FLCs are designed separately for SRM and EHB control for each wheel. The fuzzy system accepts the information about vehicle body deceleration during the first step of heavy braking. Its maximum value is fed as a constant crisp input to the FLC to recognize road surface. This crisp input is uncertain, hence, computational intelligence methods, such as a fuzzy set theory, are capable to deal with such ill-defined and vague data. Thanks to the methods robustness, precise mathematical modelling may be avoided. The second input is wheel slip, which is used to decide for the requested torque  $T^{req}$  increase or decrease.

Both FLC inputs have symmetrically dispersed over the whole universe of discourse triangular membership functions, five for  $\lambda$  and seven for  $\mu^*$ . Equal sensitivity of the inputs is ensured by membership functions overlapping. The  $\lambda$  is bounded in [0 18], and  $\mu^*$  – in [0 10]. Sugeno's inference method is exploited in this study. In Tab. 1, the rule base for the front and rear wheels in regenerative braking mode is provided. Considering motor's peak torque limits, the output torque for the SRM has eleven linguistic values from 0 to 200 Nm. The  $T_{FB}$  is between 0 and 150 bar and has the same design principle as the RB (Tab. 1). The FLCs are designed referring to given tire model and expert's knowledge concerning efficient plant control.

**Table 1** FLC rule base for front / rear wheels in regenerative mode

$T_{RB}$ [Nm]	$\mu^*$				
	Zero	Icy	Wet	Damp	Dry
$S_0$	60	80	160	200/120	200/140
$S_3$	40	60	140	200/100	200/120
$S_6$	20	40	120	200/80	200/100
$S_9$	0	20	100	180/40	200/80
$S_{12}$	0	0	60	160/20	200/40
$S_{15}$	0	0	20	140/0	180/20
$S_{18}$	0	0	0	120/0	160/0

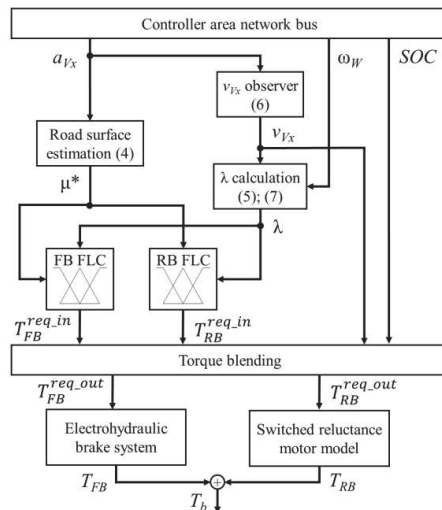


**Fig. 3** Control block scheme for a single wheel of the EV: superscript  $req$  stands for "requested"; RB FLC – regenerative braking fuzzy logic controller; FB FLC – friction braking fuzzy logic controller.

The modus ponens rules (**If** premise **Then** consequence) are the common expression of fuzzy input–output fit. Like in this work, the tabular representation is often acquired with trial and error method. The main criteria for Tab. 1 design is to achieve wheel slip for each tire as close as possible to the optimal one. An example of input–output linguistic mapping is as follows: **If** wheel "slip is 3 % ( $S_3$ )" and road surface is "Dry", **Then** request from the SRM "200" Nm for the front wheels and "120" Nm for the rear wheels. The final step is to translate the output linguistic variables back to crisp numbers. For this, centre of gravity is applied.

#### 3.2. Torque blending

Torque blending is realized with simple logic rules. It requires several inputs, in particular requested input RB and FB torques  $T_{RB}^{req,in}$  and  $T_{FB}^{req,in}$ , vehicle longitudinal velocity  $v_{vx}$ , and SOC of the battery  $SOC$ . Torque blending block outputs are requested RB torque  $T_{RB}^{req,out}$  for the SRM and requested FB torque  $T_{FB}^{req,out}$  for the EHB (Fig. 3). The approach flowchart is presented in Fig. 4. It is developed to prioritize the usage of the SRMs, yet without battery damage due to overcharge.

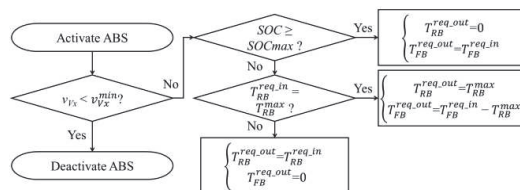


**Fig. 4** Control flowchart of torque blending for a single wheel.

Firstly, the algorithm checks the velocity of the vehicle. When vehicle longitudinal speed is slower than a desired minimum threshold  $v_{ix}^{min}$  (typically 15 – 8 km/h), the ABS control is deactivated, because the distance travelled with very low speed with locked wheels is not critical.

Secondly, when the SOC reaches maximum allowed threshold  $SOC_{max}$  (e.g. 90%), the braking switches to pure FB mode, where the torque for the SRM is equal to zero:

$$\begin{cases} T_{RB}^{req\_out} = 0 \\ T_{FB}^{req\_out} = T_{FB}^{req\_in} \end{cases} \quad (8)$$

Thirdly, the blended ABS considers the SRM's peak performance. Specifically, when peak torque  $T_{RB}^{max}$  of the SRM is requested by the FLC, the block supplies the peak torque request to the SRM and calculates additional torque for the FB actuator to ensure optimal  $\lambda$  deceleration as:

$$\begin{cases} T_{RB}^{req\_out} = T_{RB}^{max} \\ T_{FB}^{req\_out} = T_{FB}^{req\_in} - T_{RB}^{max} \end{cases} \quad (9)$$

Finally, when none of the previous conditions are true, the EV decelerates only with SRMs as the ABS actuators:

$$\begin{cases} T_{RB}^{req\_out} = T_{RB}^{req\_in} \\ T_{FB}^{req\_out} = 0 \end{cases} \quad (10)$$

## 4 Results

The results of the EV heavy braking with activated ABS on a dry asphalt road ( $\mu \approx 1$ ) is delivered in Fig. 5. At the experiment time 3.5 seconds, the SOC of the EV's battery is assumed to exceed its upper bound. At this moment, the torque blending control is easily noticeable, because the EV switches from RB to pure FB mode. Energy recuperation is no longer conducted. The vehicle speed together with the wheels' speeds are introduced in Fig. 5. (a).

Before the controller intervention, the wheels' slip rates grow due to exceeded torque requested by the driver (i.e. the braking pedal is instantly pressed to its maximum) (Fig. 5. (b)). Nevertheless, after the ABS activation, the wheel slip rates drop down to their optimal values for a given road surface. The optimal slips for every wheel are also depicted.

In Fig. 5. (c), the road surface estimation method is scoped. At the beginning of the braking manoeuvre, the controller measures the maximum deceleration rate of the EV body. Its peak value is mapped with an appropriate road surface. The blue line symbolizes the crisp input for the estimation road conditions. The variable together with wheel slip is therefore processed by the FLC to estimate a relevant braking torques.

In Fig. 5. (d), braking torques for each in-wheel SRM of the EV are presented. Until the SOC makes an impact on blended ABS, it is seen that the SRM supplies its maximum available torque for the front wheels. As a result, the torque blending requests additional torque from the EHB (Fig. 5. (e)) to lead  $\lambda$  as close as possible to their theoretical optimal

values in accordance to (9). For the rear wheels, however, the generated torques by the SRMs (Fig. 5. (d)) are enough to reach optimal rate. Thus, the FB torques are not required (Fig. 5. (e)) as stated by (10).

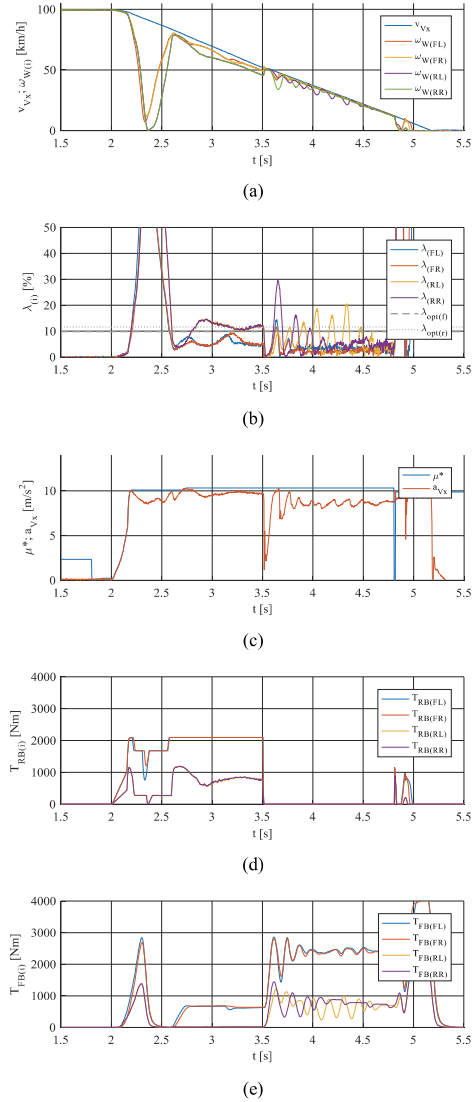


**Fig. 5** Experimental results from vehicle braking on a high- $\mu$  ( $\mu \approx 1$ ) road surface: (a) vehicle and wheels speeds; (b) wheels longitudinal slips; (c) road recognition with vehicle body deceleration rate (d) FB torques; (e) RB torques; [FL – front left, FR – front right, RL – rear left, RR – rear right].

When the SOC overshoot steps in (i.e.  $t = 3.5$  s), the energy recuperation stops, and the SRMs are not used as braking

actuators any more (Fig. 5. (d)). Consequently, the RB torques for all wheels drop to zero. On the contrary, the system moves to the pure FB mode. Now, only the EHB's torques are applied to decelerate the transport (Fig. 5. (e)), applying (8).

Moreover, the FB torques are not as smooth as RB ones. Furthermore, the optimal wheel slip achievability is not as precise as in the case, when the SRMs affect vehicle deceleration (Fig. 5. (b)). This phenomenon is mainly due to the EHB significant delay as well as the plant complexity (i.e. wheel tire highly nonlinear behaviour). It was also studied by the authors in the previous work [16].

The conclusion was made that thanks to the electric drives' fast response, the control method accomplishes fast and more accurate control. As a result, the EV's RB braking affords noticeably more efficient EV deceleration performance under the ABS operation. It allows for vehicle stopping distance diminishment. However, the electric motors are not always fully available as the braking systems, as for instance in the case of deceleration on high- $\mu$  surfaces or in case with the exceeded SOC threshold.

## 5 Conclusions

In this paper, the blended ABS control method for all-wheel drive sport utility EV is described. The SOC and the requested torques from both actuators, namely in-wheel SRMs and EHB, are taken into consideration for providing a sufficient braking torque to presume maximum deceleration efficiency for every wheel independently. The efficiency is guaranteed by the optimal wheel slip ratio braking for each separate wheel. In combination with the intelligent FLC, the blended ABS control method provides high efficiency and robustness against varying road conditions and changing system states.

The proposed solution is verified against HIL simulation, where the experimentally validated EV is coupled with EHB test bed, which provides real brakes dynamics followed by significant hardware delay. The presented experimental results are dedicated to heavy braking conditions on a high- $\mu$  road surface, during which the upper SOC threshold is achieved. As a result, the blended ABS switches from the RB mode to the pure FB, and the vehicle continues the deceleration process with optimal slip ratio without motors' impact and performance degradation.

Despite good optimal slip control for various road surfaces, the proposed FLC-based control method has several limitations. Firstly, the method depends on tire model, whose behaviour is also different for other types of vehicle characterized by different centres of gravity, masses, etc. Hence, for other vehicle and tire types the control method must be slightly modified. Secondly, to design an FLC for complex control system, like ABS, expert's multidisciplinary knowledge is essential.

**Acknowledgements** This project has received funding from the European Union's Horizon 2020 research and innovation program under grant agreement No. 675999.

## References

1. M. Ehsani, Y. Gao, S. E. Gay, and A. Emadi, *Modern Electric, Hybrid Electric, and Fuel Cell Vehicles*, Boca Raton, Florida, USA: CRC Press, 2005.
2. A. Emadi, *Handbook of Automotive Power Electronics and Motor Drives*, Boca Raton, Florida, USA: Taylor and Francis Group, 2005.
3. V. Ivanov, "A review of fuzzy methods in automotive engineering applications," *Eur. Transp. Res. Rev.*, Vol. 7, pp. 1–10, 2015.
4. X. Zhang, Y. Wang, G. Liu, and X. Yuan, "Robust regenerative charging control based on T-S fuzzy sliding-mode approach for advanced electric vehicle," *IEEE Trans. on Transp. Electrification*, Vol. 2, pp. 52–65, 2016.
5. G. Xu, W. Li, K. Xu, and Z. Song, "An intelligent regenerative braking strategy for electric vehicles," *Energies*, Vol. 4, pp. 1461–1477, 2011.
6. J. Zhang, B. Song, S. Cui, J. Zhang, and D. Ren, "Fuzzy logic approach to regenerative braking system," 2009 Intern. Conf. on Intel. Human–Machine Syst. And Cybern., pp. 451–454, 2009.
7. X. Li, L. Xu, L. Hua, J. Li, and M. Ouyang, "Regenerative braking control strategy for fuel cell hybrid vehicles using fuzzy logic," 2008 Intern. Conf. on Elect. Machines and Syst., pp. 2712–2716, 2008.
8. X. Nian, F. Peng, and H. Zhang, "Regenerative braking system of electric vehicle driven by brushless DC motor," *IEEE Trans. on Indust. Elect.*, Vol. 61, pp. 5798–5808, 2014.
9. D.–H. Kim, J.–M. Kim, S.–H. Hwang, and H.–S. Kim, "Optimal brake torque distribution for a four-wheel-drive hybrid electric vehicle stability enhancement," *Proc. IMechE Part D: J. Automobile Engineering*, Vol. 221, pp. 1357–1366, 2007.
10. D. Paul, E. Velenis, D. Cao, and T. Dobo, "Optimal  $\mu$ -estimation based regenerative braking strategy for an AWD HEV," *IEEE Trans. on Transp. Electrification*, Vol. 3, pp. 249–258, 2017.
11. D. Savitski, V. Ivanov, B. Shyrokau, T. Pütz, J. de Smet, and J. Theunissen, "Experimental investigation on continuous regenerative anti-lock braking system of full electric vehicle," *Int. J. Automotive Technology*, Vol. 17, pp. 327–338, 2016.
12. P. Dong, Z. Jianwu, and Y. Chengliang, "Regenerative braking control system improvement for parallel hybrid electric vehicle," *Intern. Tech. and Innov. Conf. 2016 (ITIC 2016)*, pp. 1902–1908, 2006.
13. J. Guo, X. Jian, and G. Lin, "Performance evaluation of an anti-lock braking system for electric vehicles with a fuzzy sliding mode controller," *Energies*, vol. 7, pp. 6459–6476, 2014.
14. B. Shyrokau, D. Wang, D. Savitskiy, and V. Ivanov, "Vehicle dynamics control with energy recuperation based on control allocation for independent wheel motors and brake system," *Int. J. Powertrain*, Vol. 2, pp. 153–181, 2013.
15. A. Aksjonov, V. Vodovozov, and Z. Raud, "Improving energy recovery in blended antilock braking systems of electric vehicles," 16th Inter. Conf. of Indust. Informat. (INDIN'2018), pp. 589–594, 2018.
16. A. Aksjonov, V. Vodovozov, K. Augsburg, and E. Petlenkov, "Design of regenerative anti-lock braking system controller for 4-in-wheel-motor drive electric vehicle with road surface estimation," *Int. J. Automotive Technology*, Vol. 19, pp. 727–742, 2018.
17. V. Ricciardi, D. Savitski, K. Augsburg, and V. Ivanov, "Estimation of brake friction coefficient for blending function of base braking control," *SAE Int. J. Passeng. Cars – Mech. Syst.*, Vol. 10, pp. 774–785, 2017.

**Publication X**

**Aksjonov, A.**, Ricciardi, V., Vodovozov, V., Augsburg, K., & Petlenkov, E. (–) Hardware–in–the–Loop Test of a Fuzzy–Logic–Based Control Method for Antilock Braking System on All–Wheel Drive Electric Vehicle. *In review*.



# Hardware-in-the-Loop Test of a Fuzzy Logic-Based Control Method for Anti-Lock Braking System on All-Wheel Drive Electric Vehicle

Andrei Aksjonov, Vincenzo Ricciardi, Valery Vodovozov, and Klaus Augsburg

**Abstract**—An anti-lock braking system aims to maximize braking effectiveness and to maintain vehicle steerability during emergency braking maneuvers. However, unexpected road conditions might lead to a degradation of the system performance. To cope with this problem an intelligent fuzzy logic-based anti-lock braking system control method for 4-on-board-motor drive sport utility electric vehicle was developed. It features a very simple and at the same time effective and robust road recognition tool with estimation of the best braking conditions for a specific road surface. In this paper, the functionality of the developed control method is tested in hardware-in-the-loop simulation on the equipment available at Technische Universität Ilmenau (Germany). It includes the test bed, which is capable of reproducing the real pressure dynamics of the brake circuit allowing simulation of various tire-road adhesions conditions and brake blending scenarios. The results indicate that fuzzy logic-based control method manages highly nonlinear and time-variant dynamics of the braking system and offers significant feasibility for optimal slip control at regenerative braking. Hence, the experimental results ensure its potentiality for practical application.

**Index Terms** — Anti-lock braking system, brake blending, electric vehicle, fuzzy control, intelligent control, vehicle dynamics

## I. INTRODUCTION

IN addition to its fundamental purpose of people and goods transportation, safety in vehicle technology (i.e. marine, air, and ground vehicles) plays a considerable role, which has higher priority than time or cost. To improve vehicle safety, advanced driver assistance systems are developed by scientists and vehicle manufacturers from all over the world. One of the oldest advanced driver assistance systems is an active safety element, namely the anti-lock braking system (ABS). It was first used in a volume-production ground vehicle 40 years ago,

in 1978 [1]. Since then, a constant development of ABS components and control methods together with other vehicle safety systems has taken place. Nowadays, ABS is a mandatory safe feature for all passenger vehicles.

An excessive braking torque applied to the wheels leads to wheels' lockage, which, in turn, deteriorates vehicle steerability and significantly reduces braking force. Therefore, the vehicle is able to neither turn and avoid collision nor decelerate as fast as practicable. To solve this problem, the ABS was applied to ground vehicles inspired by the aerospace industry, where the wheel lockage during the braking was excluded several decades before [1]. ABS aims at decelerating a vehicle as fast as possible along with simultaneous maintaining steerability during an emergency braking maneuver. Its superior goal is to enhance the braking, steering, and driving stability.

Development and further verification of safety systems on real vehicle is often very expensive and time consuming. On the other hand, computer simulation does not always allow a realistic environment for testing such complex vehicle active safety technologies as ABS, traction control systems, or electronic stability program. As a consequence, in recent years the researchers have extensively used hardware-in-the-loop (HIL) simulation techniques that replicate vehicle subsystems such as braking system, suspension, and steering rack while the rest of the vehicle is represented as a numerical model. HIL testing provides real behavior of the studied vehicle system and enables significant cost and time reduction of testing and development [2].

This work belongs to a development of an intelligent ABS control method based on fuzzy set theory and designed for 4-on-board-motor drive (4WD) electric vehicle (EV). The contribution of this paper is functionality verification of previously proposed ABS control method [3] against HIL platform, which is available at Technische Universität Ilmenau (Germany). The HIL consists of an electro-hydraulic brake system (EHB) interfaced with the vehicle dynamics simulator IPG CarMaker<sup>®</sup> (Karlsruhe, Germany). Experimentally validated model of a full electric sport utility vehicle (SUV)

This project has received funding from the European Union's Horizon 2020 research and innovation program under grant agreement No. 675999.

A. Aksjonov is with ŠKODA AUTO a.s., Mladá Boleslav, 29301 Czech Republic (e-mails: [andrei.aksjonov@skoda-auto.cz](mailto:andrei.aksjonov@skoda-auto.cz)).

V. Ricciardi and K. Augsburg are with the Department of Automotive Engineering, Technische Universität Ilmenau, Ilmenau, 98693 Germany (e-mails: [vincenzo.ricciardi@tu-ilmenau.de](mailto:vincenzo.ricciardi@tu-ilmenau.de); [klaus.augsburg@tu-ilmenau.de](mailto:klaus.augsburg@tu-ilmenau.de)).

V. Vodovozov is with the Department of Electrical Power Engineering and Mechatronics, Tallinn University of Technology, Tallinn, 19086 Estonia (e-mail: [valery.vodovozov@taltech.ee](mailto:valery.vodovozov@taltech.ee)).

equipped with four on-board motors was used for the simulation task. Moreover, data collected from the brake dynamometric test rig at Technische Universität Ilmenau (Germany) are used to identify the Ostermeyer's model to reproduce the real behavior of the brake linings coefficient of friction [4].

The paper is structured as follows. In the next Section, an analysis of related works and problem statement are presented. Section III is devoted to the 4WD EV model. In Section IV, the ABS control method based on fuzzy logic is explained in details. The HIL experimental results at low- $\mu$  and varying road conditions are presented and compared in Section V. Finally, the paper is concluded in Section VI.

## II. RELATED WORKS AND PROBLEM STATEMENT

The fuzzy set theory [5] found a wide range of practical and theoretical applications in automotive area, in particular artificial decision making systems (e.g. vehicle-environment interaction, driver modeling, and driver assistance systems) and control methods for both conventional and electric vehicles (e.g. vehicle dynamics control and ride comfort) [6]. Most of the related works are limited with numerical simulation. Hence, practical applicability of the algorithm is not certain.

Among the first patent applications, it is worth mentioning the ABS control based on fuzzy logic for friction braking (FB) by Nissan Motor Co., Ltd. (Yokohama, Japan) [7] and for regenerative braking (RB) by Ford Motor Company (Dearborn, Michigan, USA) [8]. Afterwards, many different control approaches exploiting a fuzzy logic controller (FLC) were developed for different vehicles, including EV with 4WD powertrain. For instance, in [9], an FLC was proposed for FB to maintain the wheel slip to a desired road surface. In [10], a self-learning fuzzy sliding-mode control was designed for conventional ABS. Later, the scholars improved the proposed control method introducing a self-organized function-link fuzzy cerebellar model articulation controller [11]. For EV, a fuzzy sliding mode controller with braking force distribution between RB and FB was proposed in [12]. In [13], an ABS and electronic stability program controller for 4WD EV was presented.

It is worth noting that mentioned controllers were all designed to keep a fixed optimal slip for specific tire-road adhesion conditions (i.e. 20% - optimal for dry asphalt). Nonetheless, physical behavior of the tire is very different for various road surfaces as well as tire conditions (i.e. worn, seasonal, depressurized, etc.). Thus, braking with optimal slip for dry asphalt on an icy or wet road, where ABS function is extremely important, leads to up to 50% braking force losses and consequent efficiency deterioration [14]. Moreover, they were only verified against computer simulation, which does not ensure their correct operation on a real vehicle.

Both the computer and HIL simulations were conducted for a Mamdani's FLC applied to EV [15], for an FLC combined with proportional-integral-derivative controller [16] and for a quasi-sliding mode controller accompanied with fuzzy-neural network estimator applied to a conventional passenger car [17]. Although the experiments showed promising results, the controllers were again limited to reference slip input.

As a reference slip control does not solve the problem of efficient and robust ABS performance, the scholars devised several methods to recognize the road surface or estimate road-

adhesion coefficient, which allowed for an optimal slip control of each wheel separately [18] – [20]. Unfortunately, again only computer simulations were performed for a simple single wheel model [18] or a full vehicle [19], [20].

In [21], authors went further and developed ABS FLC that provides optimal slip for varying road conditions. Recently, another solution consisting of sliding mode control and FLC cooperation was presented [22]. The developed methodologies were validated on a quarter-car HIL test bench. Although optimal slip was maintained for changing road conditions, namely vehicle braking on road surfaces from icy to dry [21] and from wet to dry [22], a single wheel HIL simulation is not enough to verify the whole vehicle performance. Due to the weight transfer during a braking process, front and rear wheels have different optimal slips. Moreover, due to the mechanical connection offered by the suspensions, the wheels have a significant influence on each other [23].

Another approach used fuzzy logic for road surface detection, and additional FLC for pressure control that keeps optimal wheels slip. The control method was first tested against a quarter-car HIL simulation [24]. Later, road type recognition was enhanced by the authors with artificial neural network and validated in simulation and testing on a real vehicle [25]. Based on these results, fuzzy logic performs very well in road recognition (i.e. from high- $\mu$ , to low- $\mu$ , to high- $\mu$ ).

In [26], fuzzy logic was again used for road adhesion estimation. The method was simulated and tested on prototype EV. However, an ABS controller was not considered at this stage. Finally, a complex control method based on fuzzy logic for 4WD EV was developed in [27]. The FLC required three inputs and a state observer to detect road friction coefficient and to decide upon an optimal wheel slip. The control method was tested in simulation and experiment with a real car.

Bearing in mind drawbacks and complexity of the proposed FLC-based control methods, the authors, first, developed a control method for both electric motor with energy recuperation priority [3] and conventional FB [28]. The method used a single FLC as estimator and controller simultaneously. Therefore, it recognized road surface and held optimal wheel slip deceleration on various road adhesions as well as in complex braking maneuvers. The controllers were previously verified in simulation only, what does not guaranty its functionality on a under real braking system dynamics. Therefore, in this paper, the control strategy proposed by the authors in [3] is tested via HIL experiments with real EHB system.

In addition, several dynamics, which were neglected in the previous studies [3], [28], are now taken into consideration. Particularly: (i) the Magic Tire Formula 6.1 [29] identified against experimental data on a wet surface is used; (ii) front and rear tire deformations are now accounted [23], [30] to achieve a more accurate estimation of the wheel slip; (iii) the dynamics of the brake linings coefficient of friction is herein modelled based on experimental data collected at Technische Universität Ilmenau (Germany). The FLC-based control method is tested on low- $\mu$  and on varying road conditions (from high- $\mu$  to low- $\mu$ ). In short, the main contribution of this study lies in verification of the ABS control method based on fuzzy logic under HIL simulation consisting of an EHB integrated with an experimentally validated model of a full electric SUV in IPG CarMaker<sup>®</sup> environment.

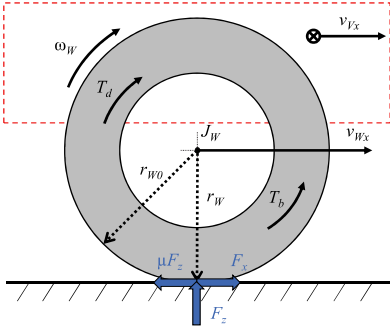


Fig. 1. Simplified drawing of a braked wheel: single-wheel model.

### III. VEHICLE MODEL

#### A. Dynamics of a Braked Wheel

A simplified schematic drawing of a braked wheel is depicted in Fig. 1. The variables used in the paper are listed in alphabetic order in Appendix in Table A.I. During straight braking, lateral force mostly has no impact on braking. Thus, torque balance about a wheel axis is described as [30]:

$$J_W \dot{\omega}_W = T_d - r_W \cdot F_x - T_b. \quad (1)$$

Owing to its small impact, rolling resistance is neglected.

The braking torque of a 4WD EV is a sum of regenerative  $T_{RB}$  and friction  $T_{FB}$  brake torques:

$$T_b = T_{RB} + T_{FB}, \quad (2)$$

where the  $T_{FB}$  is calculated as [30]:

$$T_{FB} = 2 \cdot \mu_b \cdot A_p \cdot p_b \cdot r_b. \quad (3)$$

A wide range of phenomena occurs between the brake pad and disc causing a remarkable variation in the brake linings coefficient of friction, such as increase of brake disc temperature [31]. To this effect, the Ostermeyer's model [4] is validated against brake dynamometric data collected at Technische Universität Ilmenau to render the dynamics of the brake linings coefficient of friction [31].

In case of saturated phase, the torque  $T_{RB}^j$  of a switch reluctance motor (SRM) is calculated as [32]:

$$T_{RB}^j = \int_0^{i_j} \frac{\partial L(\theta, i_j)}{\partial \theta} i_j di_j, \quad (4)$$

therefore, the output torque of the SRM is a sum of all phase torques:

$$T_{RB} = \sum_{j=1}^N T_{RB}^j(i_j, \theta), \quad (5)$$

where  $N$  is phase number of motor. A converter of a SRM controls the flow of the phase current  $i_j$ , which is proportional to phase torque [32].

Although the  $T_{RB}$  and  $T_{FB}$  cannot be measured directly, pertinent sensors available in modern cars measure  $p_b$  and  $i_j$  [33]. Hence, in this paper, the controller's corrective variables are RB torque for SRM and braking pressure – for FB.

#### B. States Estimation

The tire-road adhesion coefficient  $\mu$  is a ratio of the applied forces on a wheel. Considering uniform adhesion among the wheels, the tire-road friction can be approximated as [30]:

$$\mu = \frac{F_x}{F_z} = \frac{m_V \cdot a_{Vx}}{m_V \cdot g} = \frac{a_{Vx}}{g}. \quad (6)$$

In this paper, a maximum value of vehicle body deceleration during braking maneuver  $a_{Vx}$  is utilized for road surface estimation. Thanks to the robustness and simplicity offered by the fuzzy set theory, this approach proved to be effective in ABS control without the need of sophisticated road surface algorithms [3]. An estimate of the maximum adhesion potential, according to eq. (6), is defined as  $\mu^*$ .

During braking, the longitudinal wheel slip expressed in percentage is calculated as [30]:

$$\lambda = \frac{v_{Vx} - v_{Wx}}{v_{Vx}} \cdot 100\%, \quad (7)$$

where longitudinal vehicle velocity is an integration of the vehicle longitudinal acceleration [30], [33]:

$$v_{Vx} = \int a_{Vx} dt, \quad (8)$$

and longitudinal wheel velocity is derived from the measured wheel speed:

$$v_{Wx} = r_W \cdot \omega_W. \quad (9)$$

Accurate wheel slip calculation (7) must also consider tire radius deformation (9). The radius of deformed tire is a relation of the stationary wheel ground contact force to the tire stiffness in accordance with [30]:

$$r_W = r_{W0} - \frac{(F_z - F_{z0})}{k_T}. \quad (10)$$

The wheel vertical load  $F_z$  is approximated using a quasi-static longitudinal weight transfer approach [30]. In the case of pure longitudinal driving without lateral acceleration, tire vertical forces can be computed as:

$$\begin{cases} F_{z(f)} = m_V \left( \frac{l_f}{l} g - \frac{h_c}{l} a_{Vx} \right) \\ F_{z(r)} = m_V \left( \frac{l_r}{l} g + \frac{h_c}{l} a_{Vx} \right) \end{cases} \quad (11)$$

#### C. Vehicle Configuration

The vehicle under investigation is a full electric SUV equipped with EHB. Each wheel is equipped with an SRM drive connected through a half-shaft transmission that enables independent wheels control. The 4WD SUV parameters are listed in Table A.II located in the Appendix.

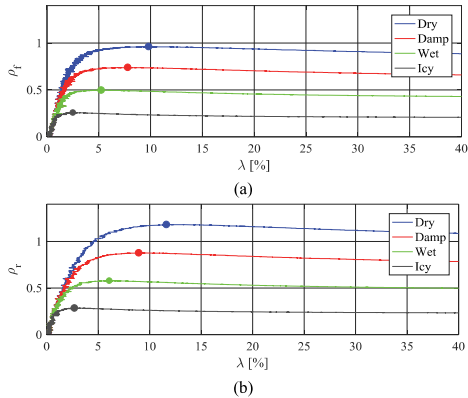


Fig. 2. Tire-road friction-slip curves of a studied tire model for various road surfaces modelled with Pacejka’s Magic Formula 6.1 [29]: (a) front wheels; (b) rear wheels.

TABLE I  
OPTIMAL WHEELS’ SLIP RATES AND VEHICLE’S BODY PEAK DECELERATION  
VALUES FOR COMMON ROAD SURFACES

	Icy	Wet	Damp	Dry
Font wheels $\lambda$ [%]	2.51	5.25	7.81	9.83
Rear wheels $\lambda$ [%]	2.71	6.09	8.95	11.64
Peak $a_{ix}$ [ $m/s^2$ ]	2.66	5.12	7.66	10.03

An experimentally validated 14 degree-of-freedom vehicle model is provided by the proprietary software IPG CarMaker<sup>®</sup> 6.0. The model is fully integrated with MATLAB<sup>®</sup>/Simulink<sup>®</sup> (Natick, MA, USA) R2015a (64 Bit) enabling fast controller development and simulation. A fixed time step of 1 ms was set during the simulations and the signals required by the observers were acquired from the high-speed control area network frame with a sampling time of 3 ms (100Hz). An additive noise was employed to incorporate white Gaussian noise into the simulation signals. The standard deviation values of the noise were extracted from real test data available at Technische Universität Ilmenau:  $\sigma_{\omega_W} = 0.1 \text{ rad s}^{-1}$ ;  $\sigma_{a_{ix}} = 0.05 \text{ m s}^{-2}$ .

#### D. Tire Model

The Pacejka’s “Magic Formula” 6.1 is applied for tire modelling [29]. In case of only longitudinal motion, for longitudinal  $F_x$ , and normal  $F_z$  forces acting on a tire, the normalized longitudinal force  $\rho$  is calculated as [23]:

$$\rho = \frac{F_x}{F_z} \quad (12)$$

The normalized longitudinal forces vs longitudinal wheel slip for common road surfaces (i.e. icy, wet, damp, dry) are scoped in Fig. 2 for front and rear wheels. The curves are obtained from a simulation of the parametrized SUV on different road surfaces. The ABS controller was deactivated, and a straight lane heavy braking maneuver was performed starting from 100 km/h.

The peak of each curve is emphasized with a dot where the tire exhibits the optimal slip ratio for a given road surface. The region from zero to peak is called stable. Here, because of the



Fig. 3. Different views of the EHB hardware-in-the-loop testbed.

positive force-slip gradient, the vehicle is easy to control and to maintain steerability. The rest of the curve is referred to as unstable zone, because in this working space, the wheels rapidly lock and steerability is compromised. The main task of the ABS controller is to decelerate a vehicle with a slip rate as close as possible to the peak for a given road surface. Deviation from this optimal slip leads to braking force degradation [23].

The optimal wheel slips are reported in Table I along with the corresponding peak vehicle body deceleration values for different road surfaces. Optimal slips and maximum vehicle deceleration rates for various roads represent essential information for the proposed FLC design. It must be mentioned that the number of passengers and their positioning in the vehicle might have an effect on the tire-road characteristics. Indeed, an asymmetric load produces a shift in the optimal wheel slip ratios for left and right sides. However, such a difference is very small [29] and, for the sake of simplicity, is neglected in this work.

#### E. Brake Disk Model

Data from the brake dynamometric test rig at Technische Universität Ilmenau were used to identify the Ostermeyer’s model [4], [31] to reproduce the real dynamics of the brake linings coefficient of friction. Such a model allows for an improved fidelity of the HIL platform, because it accounts for the brake linings’ coefficient of friction dependence against speed, pressure, and temperature. The model relies on two differential equations in the friction  $\mu_b$  and temperature  $\tau$  states:

$$\begin{cases} \dot{\mu}_b = -\alpha \cdot \{\mu_b \cdot (r_b \cdot \omega_W \cdot F_{cl} + \beta) - \gamma \cdot \tau\} \\ \dot{\tau} = \varepsilon \cdot r_b \cdot \omega_W \cdot F_{cl} - \delta \cdot (\tau - \tau_0) \end{cases}, \quad (13)$$

where the brake clamping force  $F_{cl}$  is found as:

$$F_{cl} = A_p \cdot p_b. \quad (14)$$

Such a model assumes that the friction coefficient is proportional to the total area of contact patches [4]. The resulting patches area is determined by the equilibrium between the flow of growth (temperature related) and destruction (wear related). It is worth noticing that the term  $r_b \cdot \omega_W \cdot F_{cl}$  embeds the combined effect of clamping force and sliding speed, whilst the constant parameters  $\alpha$ ,  $\beta$ ,  $\gamma$ ,  $\delta$ , and  $\varepsilon$  are attributable to the pad chemical formulation. Namely: (i)  $\alpha$  is a time constant

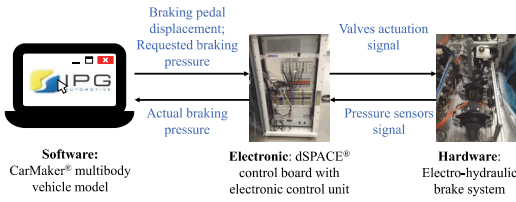


Fig. 4. Hardware and software communication.

ruling the growth/destruction rate of the contact area and its current value; (ii)  $\beta$  is the correlation parameter between the change rate of the contact area and its current value; (iii)  $\gamma$  correlates the change rate of the contact area to the temperature; (iv)  $\varepsilon$  rules the frictional power dissipated as heat on the contact patches; (v)  $\delta$  is herein referred to as brake cooling factor and rules the convection effect. Based on the collected experimental data, the parametrization used for the simulations is presented in Appendix (Table A.III). The initial brake temperature  $\tau_0$  must be specified before the simulation starts to account for the initial brake thermal state. For the present analysis an initial temperature  $\tau_0 = 298$  K was considered. The detailed explanation of the Ostermeyer's model is provided in [4].

#### F. Blended Braking System

##### 1) Hardware-in-the-loop testbed: EHB system

The employed EHB system shown in Fig. 3 is based on the slip control boost technology developed by ZF TRW Automotive (Koblenz, Germany). The EHB system finds wide use in EV, because it ensures smooth coordination between FB and RB without the driver noticing it. Such a system also ensures faster response time, more flexible packaging, and better integration with other chassis and powertrain control systems.

The hardware setup consists of the EHB and the EHB control unit. The brake calipers are mounted on two discs, fixed with respect to the structure frame. The main task of the HIL is to reproduce the real pressure dynamics of the brake circuit, which is demonstrated to have a remarkable impact on the ABS performance.

The HIL is connected to a host personal computer (PC) through the dSPACE® (Paderborn, Germany) electronic platform. The PC runs the IPG CarMaker® multibody SUV model parameterized according to experimental data. The dSPACE® unit serves as an intermediate connection between the vehicle numerical model and the real EHB (Fig. 4). Its task is to convert signals from analogue to digital form and vice versa for real-time experiments.

The dSPACE® platform receives signals (i.e. brake pedal displacement, wheel speed, vehicle speed, demanded braking pressure, etc.) from IPG CarMaker® 4WD EV model for the EHB actuation. The HIL is provided with sensors to measure the brake line pressure in the four brake calipers in a range from 0 to 20 MPa with cut-off frequency of 1 kHz. The signals are fed back to the PC through dSPACE® equipment, where they are taken into consideration in vehicle model [34].

##### 2) Four on-board-motor powertrain model

The SRM's drive torque versus angular speed relation characteristics are presented in Fig. 5. These curves are

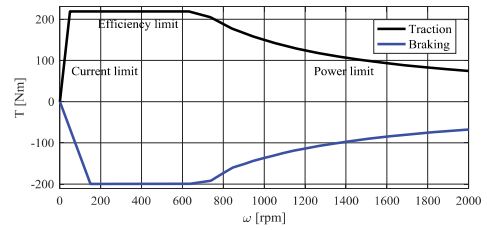


Fig. 5. SRM's torque-rotational speed characteristic in traction and braking modes.

obtained from experimental measurements of the studied SRM. Considering transmission gear ratio, the maximum torque applied directly to the wheel achieves 2100 Nm. The SRM dynamics are described by the first-order transfer function [35]:

$$\frac{T_{RB}}{T_{RB}^{REQ}} = \frac{1}{0.0022s+1} e^{-0.002s}. \quad (15)$$

## IV. ANTI-LOCK BRAKING SYSTEM CONTROL METHOD

### A. Control Method Description

The main task of the ABS controller is fast vehicle deceleration by keeping vehicle handling stability and steerability. Additionally, for the EVs, the ABS must guarantee the maximum energy recuperation from the braking process. The main tasks are ensured by holding the optimal wheel slip value. Efficient regenerative braking is provided by applying the maximum possible braking torque from the electric motors, and adding braking torque from a conventional EHB only when the torque generated by the electric motors is not sufficient to attain an optimal wheel slip.

The control method under investigation in this paper is designed to keep optimal wheel slip for each wheel on different road surfaces. A peak longitudinal deceleration is utilized to recognize the road surface under the tires. The control scheme for a single wheel is presented in Fig. 6. The scheme is identical for each individual wheel. In the State Observation stage, a wheel slip is calculated using the signals from the available sensors (e.g. longitudinal deceleration  $a_{Vx}$  and wheel velocity  $\omega_W$ ). In this regard, tire deformation is estimated using (10) and (11). Integrated signal from  $a_{Vx}$  is used for vehicle speed estimation (8). Finally, applying (7)-(9),  $\lambda$  is calculated, which serves as a first input to the FLCs.

To recognize road surface  $\mu^*$ , the peak deceleration value of the sensor is fixed during the first phase of heavy braking. When the driver steps on the brake pedal, the ABS is not yet activated and the EHB operates in the base brake mode. The controller switches on as soon as the slip value exceeds a fixed threshold. During this term, the road surface estimation (Fig. 6) is able to recognize the maximum vehicle body deceleration. Thereafter, the controller avails itself of the variable for road surface estimation by mapping its value against the ones in Table I. During the braking process,  $\mu^*$  is reset with a certain frequency. While the variable is reset, the ABS is turned off allowing maximum requested braking torque on the wheels. In this period, a peak  $a_{Vx}$  is measured again. If the road surface remains

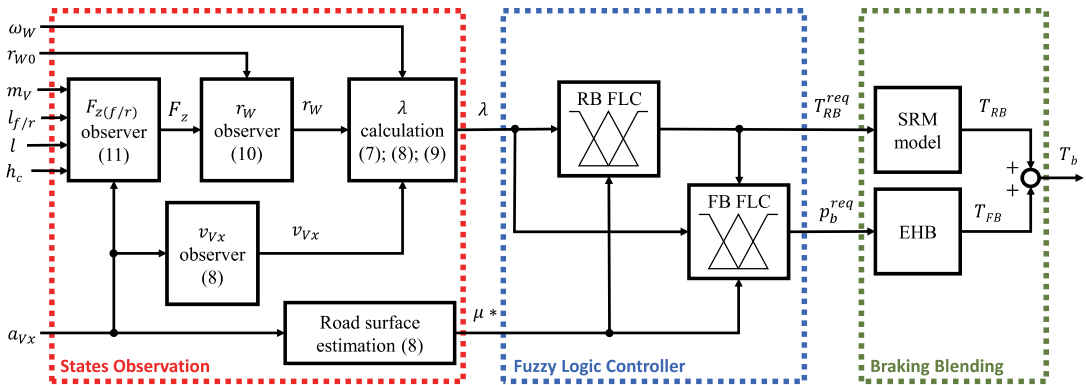


Fig. 6. Control method block scheme for a single wheel: RB FLC – regenerative braking fuzzy logic controller; FB FLC – friction braking fuzzy logic controller.

unchanged, the same peak  $a_{Vx}$  is detected as in the previous step. However, if the road surface changes, the value of  $\mu^*$  is updated according to the road profile. More details on the principle of the used road recognition technique are explained in [3].

The method of road estimation proved to be very efficient in combination with fuzzy logic. In this case, it is necessary to know neither the peak deceleration rates nor the wheel optimal slips for every possible road surface. As to the limited available data about the wheel slip curves, computational intelligence methods based on fuzzy set theory, artificial neural networks, etc. can be used as an artificial decision making system to approximate the SUV behavior for varying road surfaces. Conventional controllers, unlike soft computing methods, are not suitable for dealing with this type of stochastic and ill-defined information [5].

For instance, when the peak vehicle body deceleration is somewhere between wet and damp to any degree of certainty, it is efficient to hold the optimal slip precisely neither for wet nor for damp road. The optimal slip ratio, according to the tendency (Fig. 2) lays somewhere between those two road surfaces. Fuzzy logic processes this type of vague information using linguistic reasoning understandable for human. For example, fuzzy inference may be expressed in the *modus ponens* (If premise Then consequence) form as follows: **If** the road surface value is between wet and damp **and** wheel slip ratio is high for damp road, **then** decrease torque to obtain wheel slip ratio between optimal for wet and damp roads. In this example, a premise part consists of two elements.

In the Fuzzy Control stage, both RB and FB FLCs receive  $\lambda$  and  $\mu^*$  as inputs. The regenerative torques or pressure are generated to keep an optimal slip for each wheel. The FB FLC also receives information about the requested braking torque from the electric motor. The FB controller activates the conventional EHB only if the maximum possible torque of the SRM (Fig. 5) for a given speed is requested, and the slip value is lower than its optimal one for a given road (Table I).

Finally, the requested RB torque  $T_{RB}^{req}$  and FB pressure  $p_b^{req}$  proceed to the electric motor model and the EHB, respectively. As a result, actual torques from both systems (i.e.  $T_{RB}$  and  $T_{FB}$ ) are generated. Their sum is a total braking torque  $T_b$  (2).

### B. Fuzzy Logic Controller

An FLC is composed of four main elements: fuzzification interface, inference engine, rule base, and defuzzification interface. It may have multiple inputs and multiple outputs. FLC takes a numerical value (“crisp”) and transforms it into a linguistic variable in the fuzzification interface. Using a pre-defined rule-based (a set of “If-Then” rules), the mapping between input and output linguistic values is conducted by the inference engine. Finally, defuzzification interface turns consequent linguistic output back into its crisp value [5].

#### 1) Fuzzification

The first FLC input is the wheel slip  $\lambda$ . It has seven symmetrically dispersed and overlapping membership functions (MFs) over the whole universe of discourse (UOD) with a set of linguistic values {“slip equal to 0” ( $S_0$ ); “slip equal to 3” ( $S_3$ ); “slip equal to 6” ( $S_6$ ); “slip equal to 9” ( $S_9$ ); “slip equal to 12” ( $S_{12}$ ); “slip equal to 15” ( $S_{15}$ ); “slip equal to 18” ( $S_{18}$ )}. Its UOD is bounded inside [0 18] limit, which provides the range of values the  $\lambda$  can assume.

The second crisp input is the road surface estimate  $\mu^*$ . The input has five symmetrically dispersed and overlapping MFs.

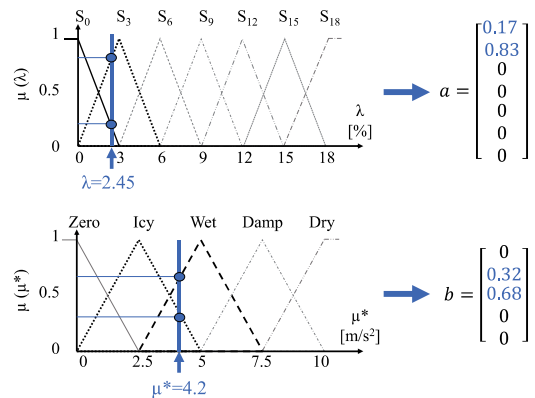


Fig. 7. FLC MFs and fuzzification procedure for randomly picked  $\lambda = 2.45$  and  $\mu^* = 4.2$ :  $\mu$  ( $\lambda / \mu^*$ ) – degree of certainty of an FLC input.

$T_{RB(f)}^{req}$ [Nm]	$\mu^*$ [m/s <sup>2</sup> ]				
	Zero	Icy	Wet	Damp	Dry
$S_0$	60	80	160	200	200
$S_3$	40	60	140	200	200
$S_6$	20	40	120	200	200
$S_9$	0	20	100	180	200
$S_{12}$	0	0	60	160	200
$S_{15}$	0	0	20	140	180
$S_{18}$	0	0	0	120	160

 $\rightarrow R = \begin{bmatrix} 60 & 80 & 160 & 200 & 200 \\ 40 & 60 & 140 & 200 & 200 \\ 20 & 40 & 120 & 200 & 200 \\ 0 & 20 & 100 & 180 & 200 \\ 0 & 0 & 60 & 160 & 200 \\ 0 & 0 & 20 & 140 & 180 \\ 0 & 0 & 0 & 120 & 160 \end{bmatrix}$ 

Fig. 8. Front wheel RB FLC rule base (Table V) expression as a matrix  $R$ .

The set of MF values is {"Zero"; "Icy"; "Wet"; "Damp"; "Dry"}. The UOD is restricted inside [0 10].

Symmetrical dispersion of the MFs over the UOD is responsible for equal MFs' sensitivity. Due to simplicity and fast response, all the inputs' MFs have triangular shape. The UOD limits are chosen based on the information about the plant (Table I) obtained during the parameterization (Section III).

In Fig. 7, a fuzzification process for the designed MFs for the FLC inputs is presented. The crisp inputs are fuzzified with a singleton (blue) function. As a result, two arrays  $a$  and  $b$  are obtained. Each position of the array corresponds to an appropriate MF linguistic value, and it contains a rate of its degree of membership (value between 0 and 1) for a given input. When the input singleton does not intersect a MF, its array position value is equal to zero. Thereafter, a dyadic product of two arrays is calculated resulting in matrix  $C$  [36]:

$$C = a \otimes b = ab^T. \quad (16)$$

## 2) Rule base and inference mechanism

A rule base captures the expert's knowledge about how to control the plant. Because a finite number of input MFs are designed, there is only a finite number of fuzzy rules. When there are not more than three inputs, a conventional way to list all possible sets of linguistic relations is to use a tabular representation [5].

The output of the RB FLC is the requested torque  $T_{RB}^{req}$ . In total, it has eleven possible values starting from 0 to 200 with equal step of 20 between each variable. Its fuzzy rule base is presented in Table II for front and rear wheels. The requested FB pressure  $p_b^{req}$  is limited to 150 bar. Therefore, its consequent values from 0 to 150 form sixteen output options with a fixed step of 10 between each other. Input-output mapping of the FB FLC for front and rear wheels is introduced in Table III. Each FLC has 35 rules.

All the rule bases were obtained with a trial and error method, where the main criterion was to keep wheel slip as close as possible to its optimal rate. A linguistic quantification for one of the front wheels in regenerative braking may be expressed,

TABLE II

FLC RULE BASE FOR REGENERATIVE BRAKING FOR FRONT / REAR WHEELS

$T_{RB}^{req}$ [Nm]	$\mu^*$ [m/s <sup>2</sup> ]				
	Zero	Icy	Wet	Damp	Dry
$S_0$	60	80	160	200 / 120	200 / 140
$S_3$	40	60	140	200 / 100	200 / 120
$S_6$	20	40	120	200 / 60	200 / 100
$S_9$	0	20	100	180 / 40	200 / 80
$S_{12}$	0	0	60	160 / 20	200 / 40
$S_{15}$	0	0	20	140 / 0	180 / 20
$S_{18}$	0	0	0	120 / 0	160 / 0

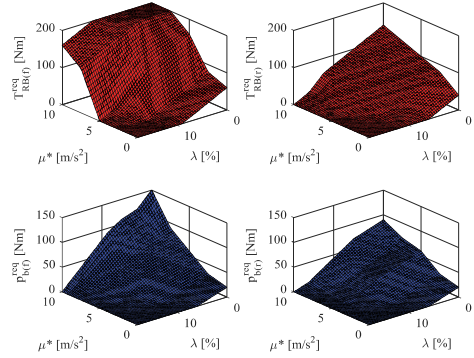


Fig. 9. FLC three-dimensional surfaces for regenerative braking and friction braking front (subscript 'f') and rear wheels (subscript 'r').

for example, as follows: **If** wheel "slip equals to 9" **and** road surface is "Wet" **then** request from the SRM regenerative braking torque equal to "100" Nm.

For inference engine, every rule base is converted into a matrix  $R$ . In our case, every matrix  $R$  for each rule base has 7×5 size. In Fig. 8 the transformation for RB front wheels FLC is shown. The same principle is applied to other rule bases.

Finally, fuzzy inference is done via Hadamard product of two matrices of the same dimensions:  $C$  from the fuzzification interface, and  $R$  from the rule base [36]:

$$D = C \circ R. \quad (17)$$

## 3) Defuzzification

The final element of every FLC is a defuzzification interface, where a resultative crisp output is obtained. In this step, the derived matrices  $C$  and  $D$  are converted into a single number, which is, thus, supplied in a plant. In this paper, a weighted average of the matrix elements is found. To this effect, a sum of elements in matrix  $D$  is divided by a sum of the elements in matrix  $C$ . The calculation is shown for the RB requested torque on the front wheels [36]:

$$T_{RB(f)}^{req} = \frac{\sum_{i=1}^M \sum_{j=1}^N d_{ij}}{\sum_{i=1}^M \sum_{j=1}^N c_{ij}}, \quad \begin{matrix} i=1,2,\dots,N; \\ j=1,2,\dots,M, \end{matrix} \quad (18)$$

where  $d_{ij}$  is an element of  $i^{th}$  row and  $j^{th}$  column of matrix  $D$  and  $c_{ij}$  is an element of  $i^{th}$  row and  $j^{th}$  column of matrix  $C$ .

At last, the nonlinear three-dimensional surfaces for every FLC are generated (Fig. 9). The surfaces plots represent the outputs of the FLCs against their own inputs  $\lambda$  and  $\mu^*$  [5].

TABLE III

FLC RULE BASE FOR FRICTION BRAKING FOR FRONT / REAR WHEELS

$p_b^{req}$ [bar]	$\mu^*$ [m/s <sup>2</sup> ]				
	Zero	Icy	Wet	Damp	Dry
$S_0$	20	30	60	90 / 70	150 / 90
$S_3$	10	20	50	80 / 50	130 / 80
$S_6$	0	10	30	70 / 30	110 / 70
$S_9$	0	0	10	50 / 10	90 / 50
$S_{12}$	0	0	0	30 / 0	60 / 30
$S_{15}$	0	0	0	10 / 0	30 / 10
$S_{18}$	0	0	0	0 / 0	0 / 0

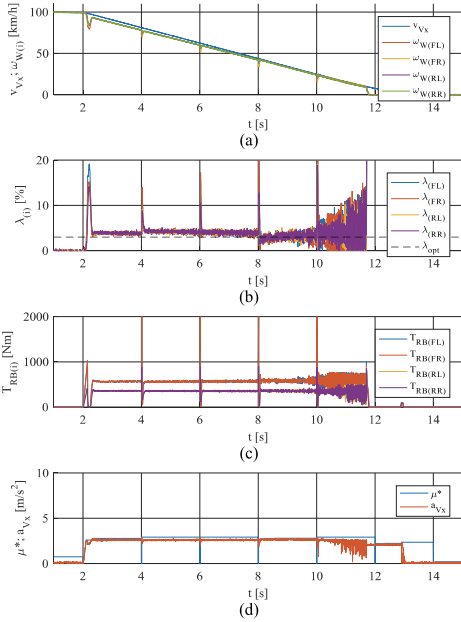


Fig. 10. Experimental results from braking on a low- $\mu$  ( $\mu \approx 0.25$ ) road surface for regenerative braking: (a) vehicle and wheels speeds (b) wheels longitudinal slips; (c) RB torques; (d) road detection with vehicle body deceleration.

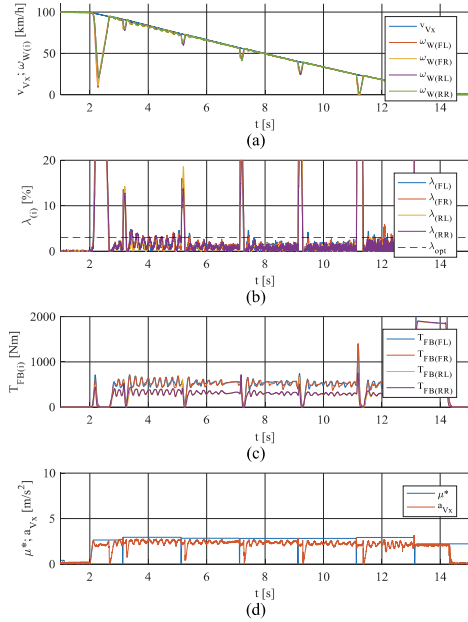


Fig. 11. Experimental results from braking on a low- $\mu$  ( $\mu \approx 0.25$ ) road surface for friction braking: (a) vehicle and wheels speeds (b) wheels longitudinal slips; (c) FB torques; (d) road detection with vehicle body deceleration.

## V. HARDWARE-IN-THE-LOOP EXPERIMENTAL RESULTS

### A. Low- $\mu$ Surface Experiment

High-performance ABS is essential on low- $\mu$  surfaces (e.g. icy, dry), because on a slippery road the vehicle can very quickly become uncontrollable [14]. In this subsection, the results of heavy braking on a low- $\mu$  road surface ( $\mu \approx 0.25$ ) are presented (Fig. 10, Fig. 11). The vehicle is accelerated to 100 km/h, and then the maximum braking torque is requested. The experiment is conducted with blended braking control (Fig. 10), and compared to the conventional FB (Fig. 11). It must be noticed that the experiment has been conducted with many different road friction coefficients. In addition, various HIL tests on changing road surfaces were performed. Nevertheless, due to paper limitation, only experimental testing results for low- $\mu$  road surface are reported here.

#### 1) Regenerative braking

In Fig. 10.a, wheel speeds and vehicle longitudinal velocity diagrams for RB are plotted. The braking torques are generated by the electric motors only. Thus, the vehicle decelerates in full regenerative mode, as the FBs are not applied. Each wheel rotates almost with the same speed because the optimal wheel slip ratios are approximately the same for both the front and the rear wheels, roughly equal to 3 % (Table I). Thanks to its fast dynamics, the controller is able to maintain the optimal slip value for each wheel (Fig. 10.b).

In Fig. 10.b, the optimal wheel slip is also depicted as a black dashed line. Every two seconds peaks in the slip signals are observable. These are the results of the reset, which is used to understand whether the road surface is changed or not during

the braking maneuver. As already mentioned, within this time period, the road surface estimator applies the maximum braking torque (Fig. 10.c) and concurrently the road recognition is reset to null (Fig. 10.d). The road recognition strategy was previously also tested on vehicle stability, and the results have shown no dramatic impacts on ABS performance [3].

In Fig. 10.c, wheel RB torques are represented. The SRMs respond very fast allowing precise and smooth control of the vehicle. Finally, in Fig. 10.d, the vehicle longitudinal deceleration  $a_{Vx}$  curve is shown along with a road recognition variable  $\mu^*$ , which represents the maximum braking potential. At the beginning of the heavy braking maneuver (i.e. at around 2 seconds), the controller detects maximum possible deceleration rate. Thereafter, the FLC addresses this variable to an appropriate road surface (Table I), whose linguistic value is “Icy”. As a result, thanks to optimal wheel slip control, a constant vehicle deceleration is maintained during the whole braking process. Therefore, high efficiency of a braking process is deemed with an enabled steerability.

#### 2) Friction braking

In Fig. 11.a, wheels speed and vehicle velocity are presented for the conventional FB case. In this experiment, the vehicle decelerates by only applying the FB torques supplied by the EHB. The difference between RB and FB results is easily noticeable. The wheel slip tracking of the FB (Fig. 11.b) has significant lower performance than the RB (Fig. 10.b). This phenomenon is attributable to the EHB slower dynamics compared to the SRM model. Indeed, the FLC for the FB was tuned to optimize the optimal slip tracking performance (Table I) and avoid controller output oscillation detrimental to the EHB

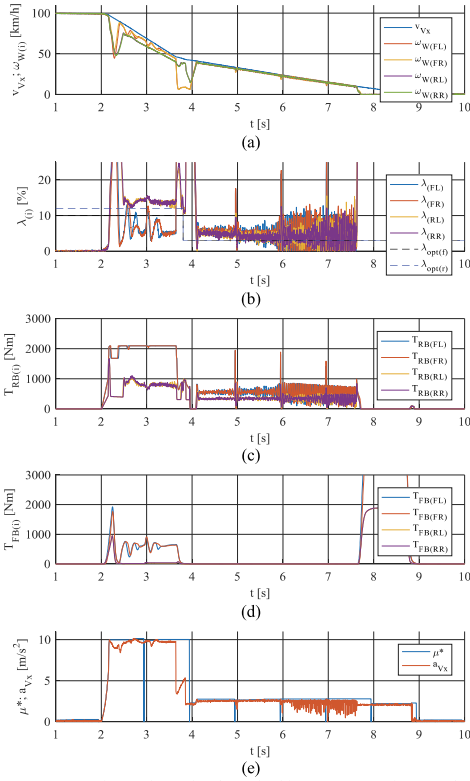


Fig. 12. Experimental results from braking on a transient road surface condition (from high- $\mu$  ( $\mu \approx 1$ ) to low- $\mu$  ( $\mu \approx 0.25$ )) for regenerative braking: (a) vehicle and wheels speeds (b) wheels longitudinal slips; (c) RB torques; (d) FB torques; (e) road detection with vehicle body deceleration.

actuators. Therefore, the FLC FB efficiency is sensibly decreased.

In Fig. 11.c, the FB torques for each wheel are revealed. Comparing to RB (Fig. 10.c), HIL system entails a slower but markedly oscillating dynamics that take a toll on the driving comfort. Nevertheless, both FLCs are requesting similar torque values for the front and rear wheels.

In Fig. 11.d, road detection together with vehicle body deceleration curve are presented. The vehicle deceleration rate is considerably lower than for the full RB scenario (Fig. 10.e). The tracking of a slip value lower than its optimal value still ensures steerability but to the detriment of the braking force (Fig. 2), which accordingly leads to efficiency losses [29].

### 3) Regenerative and friction braking performance comparison

Although the difference between the FLCs' performance for RB and FB is clearly visible in Fig. 10 and 11, the main ABS performance indexes are presented in Table IV. The average deceleration rate for RB braking is higher comparing to the FB.

TABLE IV

RB AND FB ABS PERFORMANCE BENCHMARKING ON ICE ROAD SURFACE			
Mode	Mean $a_{yx}$ [ $m/s^2$ ]	$S_{braking}$ [m]	$ABS_{IP}$
RB	2.6033	149.0047	1.2535
FB	2.3611	169.0679	1.1369

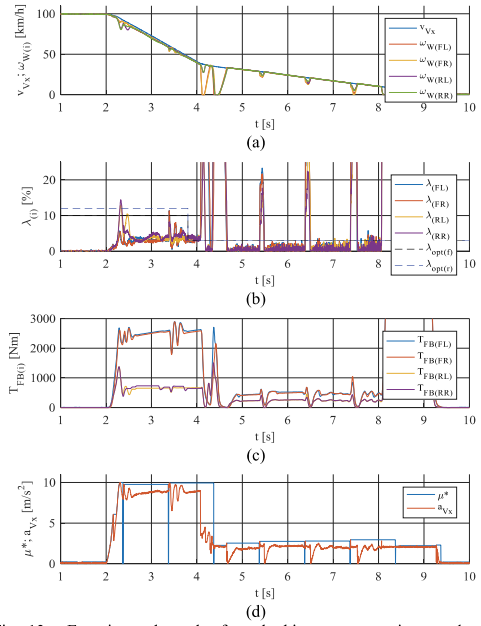


Fig. 13. Experimental results from braking on a transient road surface condition (from high- $\mu$  ( $\mu \approx 1$ ) to low- $\mu$  ( $\mu \approx 0.25$ )) for friction braking: (a) vehicle and wheels speeds (b) wheels longitudinal slips; (c) FB torques; (d) road detection with vehicle body deceleration.

Accordingly, the braking distance of the RB is smaller than FB by almost 20 m, which is a significant result in vehicle safety.

Furthermore, ABS index of performance  $ABS_{IP}$  is considered to evaluate the system's efficiency. The variable is a ratio between the mean vehicle body decelerations achieved respectively with enabled controller and with locked wheels when no ABS control is applied [3]:

$$ABS_{IP} = \frac{a_{vx}^{ABS}}{a_{vx}^{lock}}. \quad (19)$$

### B. Varying Road Conditions (From High- $\mu$ to Low- $\mu$ )

Despite ABS's functionality is extremely important on low- $\mu$  (i.e. icy, wet) surfaces, the road conditions are rarely homogeneous. In addition to this, the wheels may be also easily locked under emergency braking on high- $\mu$  surfaces, such as dry or damp asphalt. In this Subsection, the results stemming from a heavy braking maneuver on changing road surface are reported. Particularly, the vehicle starts decelerating on a high- $\mu$  ( $\mu \approx 1$ ) surface and continues towards low- $\mu$  ( $\mu \approx 0.25$ ). For this test, the RB requires additional torque from the EHB, as the torque generated by the SRMs is not enough to reach optimal wheel slip.

#### 1) Regenerative braking (blended)

In Fig. 12, vehicle braking results in regenerative mode on a changing road surface are presented. The vehicle decelerates with higher wheel slip values at the beginning of the maneuver. Whilst the slip of the rear wheels is close to its optimal value (Table I), for the front wheels the value is much lower. This

TABLE V  
RB AND FB ABS PERFORMANCE BENCHMARKING ON TRANSIENT SURFACE

Mode	Mean $a_{rx}$ on high- $\mu$ [m/s <sup>2</sup> ]	Mean $a_{rx}$ on low- $\mu$ [m/s <sup>2</sup> ]	$s_{braking}$ [m]	$ABS_{fp}$ on high- $\mu$	$ABS_{fp}$ on low- $\mu$
RB	9.6368	2.4896	66.3462	1.0863	1.1988
FB	8.5675	1.9674	69.2806	1.0776	1.0473

phenomenon is due to the fact that the peak brake torque for the front wheels exceeds the SRMs limits (Fig. 12.c). Consequently, the controller activates the FB to supply the brake torque gap (Fig. 12.d). The slow EHB dynamics deteriorates the wheel slip tracking performance on the front wheels causing efficiency losses.

The road estimator successfully detects transient road conditions (Fig. 12.e). At the beginning, the peak deceleration is around 10 m/s<sup>2</sup>, which refers to high- $\mu$  surface (Table I). After 4 seconds, the vehicle drives on a low- $\mu$  road, the control method resets  $\mu^*$  and measures peak  $a_{rx}$  again. As the road surface has changed, a new value of  $\mu^*$  is recognized. Thereafter, the controller reduces the braking torques (Fig. 12.c, d) to maintain the wheel slip rates close to their optimal values for a low- $\mu$  road surface (Table I).

### 2) Friction braking

Friction braking performance results are presented in Fig. 13. The difference in optimal slip control is easily noticeable (Fig. 13.b): the EHB is not able to reach optimal slip for high- $\mu$  surface and keeps its value on significantly lower percentage for all wheels. The road estimation (Fig. 13.d) worked similar to the RB experiment. However, this time the vehicle deceleration rate is much lower.

### 3) Regenerative and friction braking performance comparison

A comparison of the main ABS performance indexes in the case of transient road surface conditions for regenerative and friction braking experiments is reported in Table V. Based on Fig. 12.e and Fig. 13.d, it is worth noticing that the mean vehicle decelerations in the regenerative mode are higher in comparison with the FB for both the high- $\mu$  and low- $\mu$  phases. As a result, the controller requires around 3 m shorter distance with electric motors to bring the vehicle to a full stop. Furthermore, the ABS index of performance is higher for the RB as compared to the FB for all changing road conditions tested in this experiment.

## VI. CONCLUSION

This research deals with development and testing of an intelligent FLC-based ABS control method designed for 4WD electric SUV. In this paper, the functionality of the previously developed FLC-based control method is tested on HIL platform at Technische Universität Ilmenau (Germany). The platform consists of a real EHB connected to a host PC through the dSPACE® electronic platform. The PC runs the IPG CarMaker® software containing the experimentally validated model of a full 4WD electric SUV. The HIL system is capable of reproducing the real pressure dynamics in the brake circuit, whereas the vehicle dynamics are rendered by a numerical model. Thus, successful implementation of the proposed control method in HIL simulation increases its potential applicability on industrial passenger vehicle.

The data from the brake dynamometric test rig at Technische Universität Ilmenau were exploited to identify the Ostermeyer's model [4] to capture the real behavior of the brake linings coefficient of friction. The adopted fuzzy inference system, characterizing the developed approach, is reported in a dedicated section. Particularly, the control information content is represented under the form of surfaces plots of the FLC input/output. The developed controller is provided with a road surface recognition feature based on the estimation of the maximum braking potential for a specific road.

Numerous sets of experiments are conducted to test the functionality of the developed control method against different road and brake blending scenarios. Presented experimental results on low- $\mu$  surface and changing road conditions prove that the controller is able to track the optimal slip values for each wheel and recognize the road surface conditions. Nevertheless, the EHB slower dynamics compared to the SRM model takes a toll on the controller tracking performance: in the case of pure conventional FB utilization, the controller exhibits significant lower performance. The fast dynamics of the SRM allows an accurate tracking of the optimal wheel slip.

As a result, the mean vehicle decelerations in full RB mode are higher in comparison with conventional FB for both high- $\mu$  and low- $\mu$  surfaces. Furthermore, the ABS index of performance also proves that the controller in case of full braking regeneration performs better than in the case of pure FB utilization. In the future, the FLC-based ABS control method will be tested on a real SUV with 4WD powertrain in presence of different road surfaces (i.e. dry and wet asphalt).

APPENDIX

TABLE A.I  
NOMENCLATURE

Symbol <sup>a</sup>	Quantity	Unit
$a_{yx}$	Longitudinal acceleration of vehicle	m/s <sup>2</sup>
$ABS_{IP}$	Index of performance of ABS controller	-
$A_p$	Piston area of caliper	m <sup>2</sup>
$F_{cl}$	Clamping force of brake	N
$F_x$	Longitudinal force of tire	N
$F_y$	Lateral force of tire	N
$F_z$	Vertical force of tire	N
$F_{z0}$	Normal force of tire at rest	N
$g$	Gravitational acceleration	m/s <sup>2</sup>
$h_c$	Centre-of-gravity height	m
$i_j$	Phase current of SRM	A
$J_W$	Moment of inertia of wheel	kg m <sup>2</sup>
$k_T$	Equivalent stiffness of tire	N/m
$l$	Wheel base	m
$l_f$	Semi-wheelbase of front	m
$l_r$	Semi-wheelbase of rear	m
$L$	Phase bulk inductance of SRM	H
$m_V$	Mass of vehicle	kg
$p_b$	Line pressure of brake	Pa
$r_b$	Effective braking radius	m
$r_W$	Radius of deformed tire	m
$r_{W0}$	Radius of undeformed tire	m
$s_{braking}$	Braking distance	m
$T_b$	Braking torque of wheel	N m
$T_d$	Driving torque of wheel	N m
$T_{FB}$	Friction braking torque	N m
$T_{RB}^b$	Regenerative braking torque	N m
$v_{Vx}$	Longitudinal velocity of vehicle	m/s
$v_{Wx}$	Longitudinal velocity of wheel	m/s
$\alpha$	Time constant of $\mu_b$	W <sup>-1</sup> s <sup>-1</sup>
$\beta$	Change rate vs real contact area of $\mu_b$	W
$\gamma$	Change rate vs $\tau$ of $\mu_b$	W K <sup>-1</sup>
$\delta$	Cooling factor of brake	s <sup>-1</sup>
$\epsilon$	Correlation between brake friction power and heat generated on the patch	K W <sup>-1</sup> s <sup>-1</sup>
$\theta$	Rotor aligned position of SRM	rad
$\lambda$	Longitudinal slip of wheel	-
$\lambda_{opt}$	Optimal longitudinal slip of wheel	-
$\mu$	Tire-road adhesion coefficient	-
$\mu_b$	Lining coefficient of friction of brake	-
$\mu^*$	Estimated road surface	-
$\rho$	Normalized longitudinal force	-
$\sigma_{aVx}$	Noise standard deviation of $a_{Vx}$	m/s <sup>2</sup>
$\sigma_{\omega W}$	Noise standard deviation of $\omega_W$	rad/s
$\tau$	Temperature of brake disk	K
$\tau_0$	Initial temperature of brake disc	K
$\omega_W$	Angular speed of wheel	rad/s

<sup>a</sup> Subscript “i” is for each wheel: [front left (FL), front right (FR), rear left (RL), rear right (RR), f – front, r – rear].

<sup>b</sup> Superscript “j” is a phase number of SRM.

TABLE A.II  
VEHICLE CONFIGURATION

Component	Parameters	Description
Vehicle	Type	Sport utility vehicle
	Vehicle overall mass	1963 kg
	Front / rear axle suspension spring constant stiffness	25000 / 30000 N/m
	Front / rear axle suspension stabilizer stiffness	17326.8 / 10843.6 N/m
	Wheelbase	2.665 m
	Track width	1.625 m
	Centre of gravity height	0.673 m
	Drag coefficient	0.35
	Frontal surface	2.323 m <sup>2</sup>
	Tire type	235/55 R19
Battery pack	Tire model	Pacejka’s Magic Formula
	Front wheels tire stiffness	2.647·10 <sup>6</sup> N/m
	Rear wheels tire stiffness	1.273·10 <sup>6</sup> N/m
	Voltage	400 V DC
	Peak / nominal power	160 / 80 kW
	Mass	274 kg
	Volume	0.235 m <sup>3</sup>
	Cell capacity	15 Ah (6 kWh)
	Driving range	> 40 km
	Module type	12 lithium-titanic oxide anode cells
Electric motor	Operation temperature	0 – 55 °C
	Type	Switch reluctance
	Peak torque / power at 800 V (+/- 10%)	200 Nm / 100 kW (30 sec)
	Nominal torque / power at 800 V (+/- 10%)	135 Nm / 42 kW
	Maximum speed	15000 min <sup>-1</sup>
	Motor inertia (without gearbox)	21087 kg mm <sup>2</sup>
	Mass	50 kg
	Dimensions	495 x 155 x 282 mm
	Liquid cooling system	Water 10 l/min, 55 °C max inlet
	Operation temperature	-40 – 85 °C
Transmission (on-board motor)	Type	Two-stage reducer with helical gear and half-shaft
	Overall motor-gear ratio	1:10.56
	Estimated torsion stiffness on half-shaft	6500 Nm/rad

TABLE A.III  
BRAKE DISK MODEL PARAMETERIZATION

Parameter	Value for front wheels	Unit
$A_p$	2.5·10 <sup>-3</sup>	m <sup>2</sup>
$r_b$	0.140	m
$\alpha$	5.560·10 <sup>-4</sup>	W <sup>-1</sup> s <sup>-1</sup>
$\beta$	1.645·10 <sup>6</sup>	W
$\gamma$	1.051·10 <sup>3</sup>	W K <sup>-1</sup>
$\delta$	3.298·10 <sup>-2</sup>	s <sup>-1</sup>
$\epsilon$	3.166·10 <sup>-5</sup>	K W <sup>-1</sup> s <sup>-1</sup>

ACKNOWLEDGMENT

The authors would also like to express their sincere gratitude to Dzmitry Savitski from Arrival Ltd. (Oxfordshire, England) for HIL operation consultation.

## REFERENCES

- [1] W. Post, "Car braking systems," in K. Reif (Ed.), *Brakes, Brake Control and Driver Assistance Systems: Function, Regulation and Components*, Wiesbaden, Germany: Springer Vieweg, 2014, pp. 28–39.
- [2] V. Schreiber, V. Ivanov, K. Augsburg, M. Noack, B. Shyrokau, C. Sandu, and P. S. Els, "Shared and distributed X-in-the-loop tests for automotive systems: Feasibility study," *IEEE Access*, vol. 6, pp. 4017–4026, Jan. 2018.
- [3] A. Aksjonov, V. Vodovozov, K. Augsburg, and E. Petlenkov, "Design of regenerative anti-lock braking system controller for 4-in-wheel-motor drive electric vehicle with road surface estimation," *Int. J. Automotive Technology*, vol. 19, no. 4, pp. 727–742, Aug. 2018.
- [4] G. P. Ostermeyer and K. Bode, "On dynamic friction phenomena in brake systems," *Friction, Wear and Wear Protection*, pp. 301–306, June 2009.
- [5] K. M. Passino and S. Yurkovich, *Fuzzy Control*, Menlo Park, California, USA: Addison-Wesley Longman, Inc., 1998, pp. 1–22, 23–118.
- [6] V. Ivanov, "A review of fuzzy methods in automotive engineering applications," *Eur. Transp. Res. Rev.*, vol. 7, no. 29, pp. 1–10, Sep. 2015.
- [7] H. Takahashi and Y. Ishikawa, "Antiskid brake control system based on fuzzy inference," U.S. Patent 4 842 342, Jun. 27, 1989.
- [8] S. R. Cikanek, "Fuzzy logic electric vehicle regenerative antiskid braking and traction control system," U.S. Patent 5 358 317, Oct. 25, 1994.
- [9] A. Mirzaei, M. Moallem, B. M. Dehkordi, and B. Fahimi, "Design of an optimal fuzzy controller for antilock braking system," in *IEEE Veh. Power and Propuls. Conf.*, Chicago, IL, USA, 2005, pp. 1725–1730.
- [10] C.-M. Lin and C.-F. Hsu, "Self-Learning fuzzy sliding-mode control for antilock braking systems," *IEEE Trans. on Cont. Syst. Tech.*, vol. 11, no. 2, pp. 273–278, Mar. 2003.
- [11] C.-M. Lin and H.-Y. Li, "Intelligent hybrid control system design for antilock braking systems using self-organizing function-link fuzzy cerebellar model articulation controller," *IEEE Trans. on Fuzzy Syst.*, vol. 21, no. 6, pp. 1044–1055, Jan. 2013.
- [12] J. Guo, X. Jian, and G. Lin, "Performance evaluation of an anti-lock braking system for electric vehicle with fuzzy sliding mode controller," *Energies*, vol. 7, no. 10, pp. 6459–6476, Aug. 2014.
- [13] R. Pusca, Y. Ait-Amirat, A. Berthon, and J.-M. Kauffmann, "Fuzzy-logic-based control applied to a hybrid electric vehicle with four separate wheel drives," *IEE Proc. - Control Theory and Applic.*, vol. 151, no. 1, pp. 73–81, Jan. 2004.
- [14] H.-J. Koch-Dücker and U. Papert, "Antilock braking systems (ABS)," in K. Reif (Ed.), *Brakes, Brake Control and Driver Assistance Systems: Function, Regulation and Components*, Wiesbaden, Germany: Springer Vieweg, 2014, pp. 74–93.
- [15] K. Jalali, T. Uchida, J. McPhee, and S. Lambert, "Development of a fuzzy slip control system for electric vehicles with in-wheel motors," *SAE Int. J. of Alternative Powertrains*, vol. 1, no. 1, pp. 46–64, June 2012.
- [16] H.-Z. Li, L. Li, L. He, M.-X. Kang, J. Song, L.-Y. Yu, and C. Wu, "PID plus fuzzy logic method for torque control in traction control system," *Int. J. Automotive Technology*, vol. 13, no. 3, pp. 441–450, Apr. 2012.
- [17] S. Lj. Peric, D. S. Antic, M. B. Milovanovic, D. B. Mitic, M. T. Milojkovic, and S. S. Nikolic, "Quasi-sliding mode control with orthogonal endocrine neural network-based estimator applied in anti-lock braking system," *IEEE/ASME Trans. on Mechatronics*, vol. 21, no. 2, pp. 754–764, Apr. 2016.
- [18] G. F. Mauer, "A fuzzy logic controller for an ABS braking system," *IEEE Trans. on Fuzzy Syst.*, vol. 3, no. 4, pp. 381–388, Nov. 1995.
- [19] V. G. Ivanov, V. B. Algin, and B. N. Shyrokau, "Intelligent control for ABS application with identification of road and environmental properties," *Int. J. of Veh. Autonom. Syst.*, vol. 4, no. 1, pp. 44–67, 2006.
- [20] D.-H. Kim, J.-M. Kim, S.-H. Hwang, and H.-S. Kim, "Optimal brake torque distribution for a four-wheel-drive hybrid electric vehicle stability enhancement," *Proc. of the Institution of Mech. Engin., Part D: J. of Autom. Engin.*, vol. 221, no. 11, pp. 1357–1366, Nov. 2007.
- [21] P. Khatun, C. M. Bingham, N. Schofield, and P. H. Mellor, "Application of fuzzy control algorithms for electric vehicle antilock braking/traction control systems," *IEEE Trans. on Veh. Tech.*, vol. 52, no. 5, pp. 1356–1364, Sep. 2013.
- [22] X. Peng, M. Jia, L. He, X. Yu, and Y. Lv, "Fuzzy sliding mode control based on longitudinal force estimation for electro-mechanical braking systems using BLDC motor," *CES Trans. on Elect. Machines and Syst.*, vol. 2, no. 1, pp. 142–151, Mar. 2018.
- [23] R. Rajamani, *Vehicle Dynamics and Control*, 2nd ed., New York, NY, USA: Springer, 2012, pp. 87–112, 397–400.
- [24] J. A. Cabrera, A. Ortiz, J. J. Castillo, and A. Simón, "A fuzzy logic control for antilock braking system integrated in the IMMA tire test bench," *IEEE Trans. on Veh. Tech.*, vol. 54, no. 6, pp. 1937–1949, Nov. 2005.
- [25] J. J. Castillo, J. A. Cabrera, A. J. Guerra, and A. Simón, "A novel electrohydraulic brake system with tire-road friction estimation and continuous brake pressure control," *IEEE Trans. on Indust. Electr.*, vol. 63, no. 3, pp. 1863–1875, Mar. 2016.
- [26] D. Paul, E. Velenis, D. Cao, and T. Dobo, "Optimal  $\mu$ -estimation based regenerative braking strategy for an AWD HEV," *IEEE Trans. on Transp. Electrif.*, vol. 63, no. 3, pp. 1863–1875, Mar. 2016.
- [27] H. Chen, J. Yang, Z. Du, and W. Wang, "Adhesion control method based on fuzzy logic control for four-wheel-driven electric vehicle," *SAE Int. J. Passeng. Cars – Mech. Syst.*, vol. 3, no. 1, pp. 217–225, Apr. 2010.
- [28] A. Aksjonov, K. Augsburg, V. Vodovozov, "Design and simulation of the robust ABS and ESP fuzzy logic controller on the complex braking maneuvers," *Appl. Sci.*, vol. 6, no. 12, pp. 1–18, Dec. 2016.
- [29] H. B. Pacejka, *Tyre and Vehicle Dynamics*, 3rd ed., Oxford, UK: Butterworth-Heinemann, 2012.
- [30] U. Kiencke and L. Nielsen, *Automotive Control Systems: For Engine, Driveline, and Vehicle*, 2nd ed., Berlin, Germany: Springer-Verlag Berlin Heidelberg, 2005, pp. 301–350, 351–408, 409–424.
- [31] V. Ricciardi, D. Savitski, K. Augsburg, and V. Ivanov, "Estimation of brake friction coefficient for blending function of base braking control," *SAE Int. J. Passeng. Cars – Mech. Syst.*, vol. 10, no. 3, pp. 774–785, 2017.
- [32] M. Ehsani, Y. Gao, S. E. Gay, and A. Emadi, *Modern Electric, Hybrid Electric, and Fuel Cell Vehicles*, Boca Raton, Florida, USA: CRC Press, 2005, pp. 204–232.
- [33] E. Zabler, "Sensors for Brake Control," in K. Reif (Ed.), *Brakes, Brake Control and Driver Assistance Systems: Function, Regulation and Components*, Wiesbaden, Germany: Springer Vieweg, 2014, pp. 142–153.
- [34] B. Shyrokau, D. Wang, D. Savitski, K. Hoepfing, and V. Ivanov, "Vehicle motion control with subsystem prioritization," *Mechatronics*, vol. 30, pp. 297–315, Sep. 2015.
- [35] D. Savitski, V. Ivanov, B. Shyrokau, T. Pütz, J. De Smet, and J. Theunissen, "Experimental investigations on continuous regenerative anti-lock braking system of full electric vehicle," *Int. J. Automotive Technology*, vol. 17, no. 2, pp. 327–338, Apr. 2016.
- [36] A. Aksjonov, P. Nedoma, V. Vodovozov, E. Petlenkov, and M. Herrmann, "A method of driver distraction evaluation using fuzzy logic," in *26th Intern. Conf. on Inform., Commun. and Autom. Techn. (ICAT)*, Sarajevo, Bosnia & Herzegovina, 2017, pp. 23–28.



**Andrei Aksjonov** received his M.Sc. in electrical engineering and electrical drives and power electronics with automation specialization from Tallinn University of Technology in 2015. He is currently a Marie Skłodowska-Curie research fellow hosted by Škoda Auto a.s. His research topic is development of driver distraction

detection and human-machine interface evaluation methods for multi-actuated ground vehicles. His research interests include driver distraction, human-machine interface, fuzzy systems, machine learning, and vehicle safety.



**Vincenzo Ricciardi** received in 2014 the Master's degree in Mechanical Engineering from the University of Salerno. He was employed at eProLab (UNISA) by taking care of waste heat recovery systems for internal combustion engines. He is currently employed as Ph.D. – Marie Skłodowska-Curie fellow at the

Technische Universität Ilmenau under the framework of the ITEAM Project. His research interests include advanced vehicle controllers, state estimators and analysis of brake-related emissions.



**Valery Vodovozov** (M<sup>2</sup>-) received the Candidate of Science degree from Saint Petersburg Electrotechnical University, Russia. He was an Associate Professor and a Senior Researcher in electrical engineering with Saint Petersburg Electrotechnical University. He is currently a Professor with Tallinn

University of Technology, Estonia. His research interests include power electronics and electrical drives areas. He is a member of the International Institute of Informatics and Systemics and the Global Research Alliance of Texas Institute of Science.



**Klaus Augsburg** received the Dr.-Ing. Degree from Technische Universität Dresden, Germany, in 1985. From 1984 to 1993, he was with industry on leading engineer positions and then from 1993 to 1999 as a Senior Assistant with Technische Universität Dresden. In 1999, he was a Full Professor and the Chair of

Automotive Engineering Group, Technische Universität Ilmenau, Germany. In 2011, he founded Thuringian Centre of Innovation in Mobility, where he is coordinating many industrial and public research projects. He has authored over 100 research papers, guest lectures, and patents. He is a member of the Association of German Engineers, the Chairman of Workgroup Automotive Engineering VDI Thüringen, and the CEO of Steinbeis-Transferzentrum Fahrzeugtechnik.



## Appendix 2

Table A2.1. Electric sport utility vehicle configuration.

Component	Parameters	Description
Vehicle	Type	Sport utility vehicle
	Vehicle overall mass	1963 kg
	Front / rear axle suspension spring constant stiffness	25000 / 30000 N/m
	Front / rear axle suspension stabilizer stiffness	17326.8 / 10843.6 N/m
	Wheelbase	2.665 m
	Track width	1.625 m
	Centre of gravity height	0.673 m
	Drag coefficient	0.35
	Frontal surface	2.323 m <sup>2</sup>
	Tire type	235/55 R19
	Tire model	Pacejka's Magic Formula
	Front wheels tire stiffness	2.647·10 <sup>6</sup> N/m
	Rear wheels tire stiffness	1.273·10 <sup>6</sup> N/m
Battery pack	Voltage	400 V DC
	Peak / nominal power	160 / 80 kW
	Mass	274 kg
	Volume	0.235 m <sup>3</sup>
	Cell capacity	15 Ah (6 kWh)
	Driving range	> 40 km
	Module type	12 lithium–titanic oxide anode cells
	Operation temperature	0 – 55 °C
Electric motor	Type	Switch reluctance
	Peak torque / power (30 sec)	200 Nm / 100 kW
	Nominal torque / power	135 Nm / 42 kW
	Maximum speed	15000 min <sup>-1</sup>
	Motor inertia (without gearbox)	21087 kg mm <sup>2</sup>
	Mass	50 kg
	Dimensions	495 x 155 x 282 mm
	Liquid cooling system	Water 10 l/min, 55 °C max inlet
Operation temperature	-40 – 85 °C	
Transmission (on-board motor)	Type	Two-stage reducer with helical gear and half-shaft
	Overall motor–gear ratio	1:10.56
	Estimated torsion stiffness on half-shaft	6500 Nm/rad

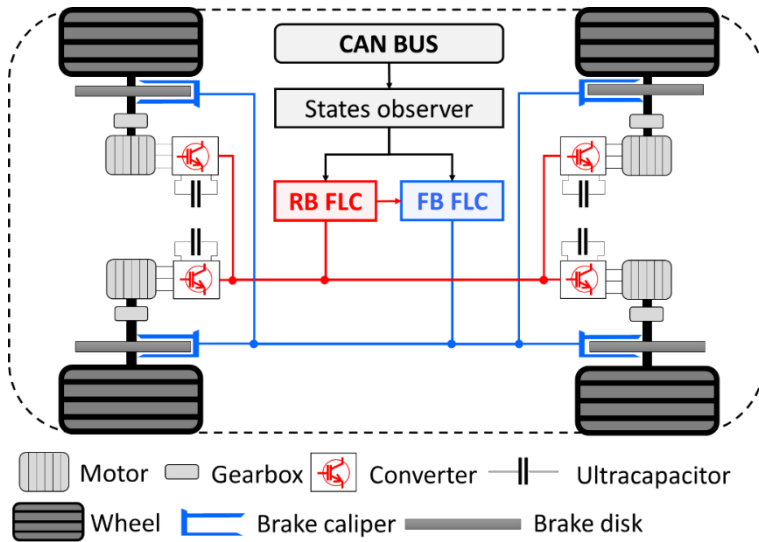


Figure A2.1. Simplified scheme of four on-board motor powertrain electric vehicle architecture with control links: CAN BUS – controller area network bus; RB FLC – regenerative braking fuzzy logic controller; FB FLC – friction braking fuzzy logic controller.

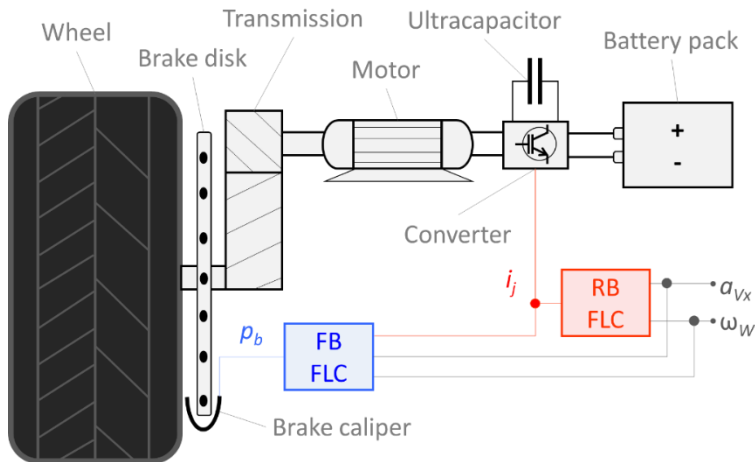


Figure A2.2. Simplified scheme of on-board motor architecture with control links: RB FLC – regenerative braking fuzzy logic controller; FB FLC – friction braking fuzzy logic controller;  $a_{vx}$  – longitudinal acceleration of vehicle;  $\omega_w$  – angular velocity of wheel;  $i_j$  – current of  $j^{\text{th}}$  phase of motor;  $p_b$  – line pressure of brake.

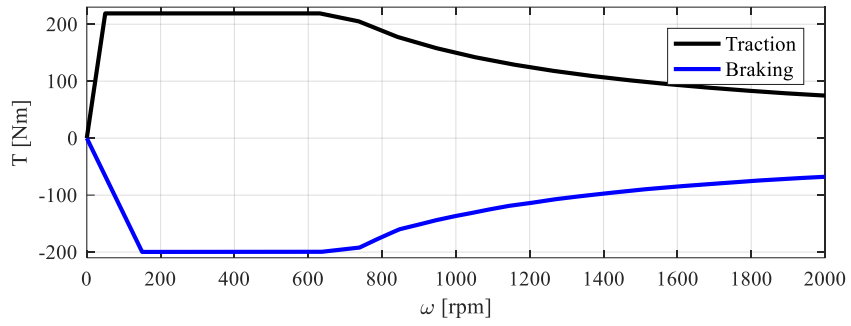


Figure A2.3. Switched reluctance motor drive torque versus angular speed relation characteristic in traction and braking modes.



## Appendix 3

Table A3.1. List of the in-vehicle secondary tasks.

#	In-vehicle secondary task	
1.	Volume	Volume regulation
2.	Context selection	Radio
3.		Media
4.		Telephone
5.		Navigation
6.	Radio	Radio station selection from a primary list
7.		Radio station selection from an overall list
8.	Media	Media source selection (e.g. CD, SD-card)
9.		Media item selection
10.		Song shuffle
11.	Telephone	Call a number from a favourite contact list
12.		Call a number from an overall contact list
13.	Navigation	Insert location
14.		Insert next target
15.		Zoom

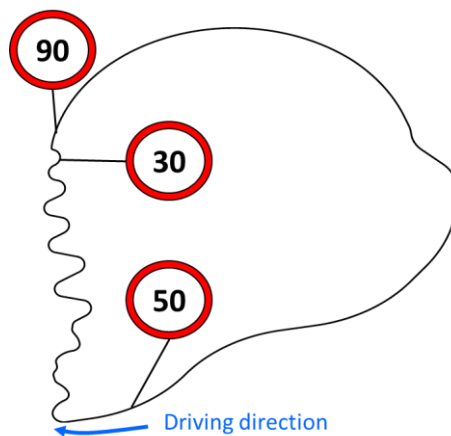


Figure A3.1. Road shape with segments speed limits.

# Curriculum vitae

## Personal data

Name: Andrei Aksjonov  
Date of birth: 05.12.1989  
Place of birth: Tallinn, Estonia  
Citizenship: Estonian

## Contact data

E-mail: andrei.aksjonov@taltech.ee

## Education

2015–2019 Tallinn University of Technology – PhD  
2013–2015 Tallinn University of Technology – MSC  
2010–2013 Tallinn University of Technology – BSC  
1997–2009 High school

## Language competence

English – Fluent  
Estonian – Fluent  
Russian – Fluent  
German – Beginner  
French – Beginner

## Professional employment

2016–... ŠKODA AUTO a.s. (Czech Republic), Development Engineer  
09.2018–11.2018 Virtual Vehicle Research Center (Austria), Visiting Researcher  
04.2018–06.2018 Technische Universität Ilmenau (Germany), Visiting Researcher  
03.2017–06.2017 IPG Automotive GmbH (Germany), Visiting Researcher  
03.2016–12.2016 Technische Universität Ilmenau (Germany), Visiting Researcher  
08.2014–02.2016 Vertex Estonia AS (Estonia), Project manager  
06.2012–09.2013 Vertex Estonia AS (Estonia), Department manager  
05.2009–06.2012 Sportland Eesti AS (Estonia), Customer Service Representative

## Elulookirjeldus

### Isikuandmed

Nimi: Andrei Aksjonov  
Sünniaeg: 05.12.1989  
Sünnikoht: Tallinn, Eesti  
Kodakondsus: Eesti

### Kontaktandmed

E-post: andrei.aksjonov@taltech.ee

### Hariduskäik

2015–2019 Tallinna Tehnikaülikool – PhD  
2013–2015 Tallinna Tehnikaülikool – MSC  
2010–2013 Tallinna Tehnikaülikool – BSC  
1997–2009 Keskkharidus

### Keelteoskus

Inglise keel – Kõrgtase  
Eesti keel – Kõrgtase  
Vene keel – Kõrgtase  
Saksa keel – Algtase  
Prantsuse keel – Algtase

### Teenistuskäik

2016–... ŠKODA AUTO a.s. (Tšehhi), Arendusinsener  
09.2018–11.2018 Virtual Vehicle Teaduskeskus (Austria), Külalisteadur  
04.2018–06.2018 Ilmenau Tehnikaülikool (Saksamaa), Külalisteadur  
03.2017–06.2017 IPG Automotive GmbH (Saksamaa), Külalisteadur  
03.2016–12.2016 Ilmenau Tehnikaülikool (Saksamaa), Külalisteadur  
08.2014–02.2016 Vertex Estonia AS (Eesti), Projektijuht  
06.2012–09.2013 Vertex Estonia AS (Eesti), Jaoskonna juht  
05.2009–06.2012 Sportland Eesti AS (Eesti), Klienditeenindaja

